BIOTOXINS FROM NEW ZEALAND SHELLFISH

A thesis submitted

under the requirements

for the Degree of

Doctor of Philosophy in Chemistry

at the

University of Canterbury

by

Michael Stewart

University of Canterbury

Christchurch

New Zealand

1997

CONTENTS

Chapter Two

Investigation of Toxicity In Coromandel Mussels 35

Chapter Three

Yessotoxin 56

Abstract

New Zealand experienced its first recognised outbreak of shellfish poisoning around Northland in early 1993. The poisoning symdrome was characterised as neurotoxic shellfish poisoning (NSP) from the observed symptoms. The major causative toxins were isolated and characterised by the Japanese research groups of Professor Ishida[a] (University of Shizuoka) and Professor Yasumoto[b,c] (Tohoku University). The toxins were identified as brevetoxin B derivatives.

Diarrhetic shellfish poisoning (DSP) was suspected as responsible for further poisoning around this area. Yessotoxin (YTX), a suspect DSP toxin, was isolated as part of this research and is the first reported instance of YTX in New Zealand.

A stereochemical study was carried out on a desulfated YTX derivative. The results suggested anomalies in the reported conformation of YTX. Attempted synthesis of haptens of YTX for development of an ELISA is outlined in this thesis.

Another incident of shellfish contamination occurred around Foveaux Strait in early 1994. The toxicity was characterised by NSP symptoms in mice. The causative toxin, gymnodimine, was first reported by a Japanese research group, although independent parallel structure elucidation was carried out as part of this research.

---

a Ishida, H.; Nozawa, A.; Totoribe, K.; Muramatsu, N.; Nukaya, H.; Tsuji, K.; Yamaguchi, K.; Yasumoto, T.; Kaspar, H.; Berkett, N.; Kosuge, T. *Tetrahedron Lett.*, **1995**, *36*, 725-728.

b Yasumoto, T. Marine Toxins Occurring in the Oceanian Waters. *Symposium On Oceanian-Japanese Organic Chemistry Synthesis and Natural Products: Socs 12 - Tokushima*, **1996**. Tokushima Bunri University, Japan.

c Morohashi, A.; Satake, M.; Murata, K.; Naoki, H.; Kaspar, H.F.; Yasumoto, T. *Tetrahedron Lett.*, **1995**, *36*, 8995-8998.

The absolute stereochemistry of gymnodimine was solved by X-ray analysis of a synthetically modified derivative. Gymnodimine haptens were prepared for development of an ELISA. A chromatography based assay has been developed for the specific detection of gymnodimine in shellfish and alga. This work was modified from the extremely efficient isolation procedure for gymnodimine developed as part of this research.

Acknowledgements

I would like to express gratitude to my supervisors Drs John Blunt and Murray Munro for their expert guidance throughout my time in the marine chemistry group at Canterbury.

I would also like to give thanks to my associate supervisor, Dr Donald Hannah of ESR in Wellington, who has "led from afar" and shown unwavering enthusiasm.

The technical staff at Canterbury have been excellent. I would like to thank especially Bruce Clark (mass spectrometry) and Gill Ellis (P388 assays).

For assistance outside of Canterbury I would like to thank Dr Penny Truman from CDC in Porirua for analysing shellfish extracts, and Dr Lewis Pannell, NIDDK, NIH, U.S.A., for additional mass spectrometry work.

Throughout my time in the marine chemistry group I have seen many faces come and go. It would take at least two pages to acknowledge them all and so I would like to thank everyone who has had a positive influence on my time here.

Finally I would like to thank my partner Sally who has shown amazing support. You have been the perfect companion, editor and shown enormous patience throughout.

Chapter One

Shellfish Toxins

1.1 Introduction

1.1.1 Phytoplankton[1]

Phytoplankton are a diverse group of unicellular and colonial organisms, most of which are classified as algae. These microscopic plants form the base of the food chains in aquatic environments and support the bivalve and fin fisheries. Under favourable environmental conditions, phytoplankton populations multiply rapidly (or bloom) to reach high cell densities (10^5-10^8 cells per litre) and discolour the water, hence the term red tide.

The majority of phytoplankton species are harmless. However, some can be noxious or toxic, for example the dinoflagellates *Gymnodinium* cf. *breve* and *Alexandrium minutum* (Fig 1.1.1). Dense blooms of algae may deplete oxygen levels through nocturnal respiration or decay, leading to massive fish and shellfish mortalities. Some species of algae may kill fish through gill damage, whereas others produce toxins that pass through the food chain and may kill vertebrate predators. It is estimated that world-wide there are 2000 cases of shellfish poisoning caused by algal toxins each year, of which about 15% are fatal.

In addition to human health problems, considerable economic losses result from the presence of algal toxins. These losses stem from closure of bivalve farms and fisheries, through deaths of fish in sea cages and from consumer resistance to seafood products.

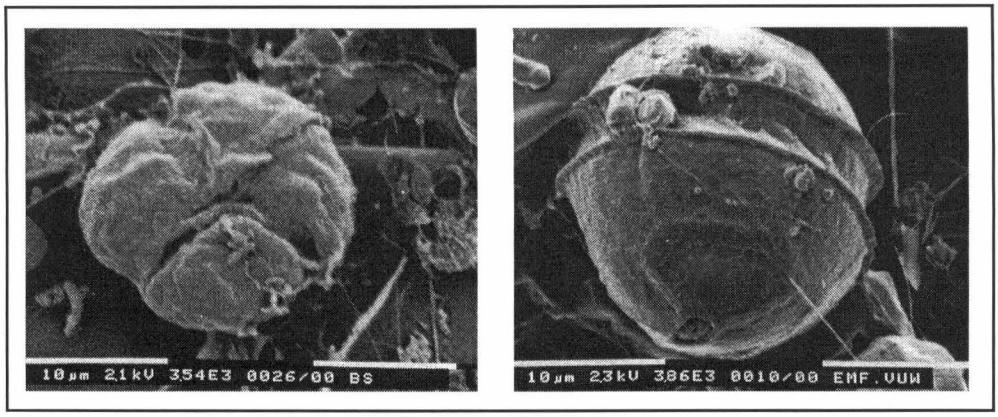

Fig 1.1.1 *Scanning Electron Micrographs of Gymnodinium cf. breve (left) and Alexandrium minutum (right)*

1.1.2 Shellfish Toxins

Shellfish toxins are generally classed in groups with reference to their physiological effects produced. The main groups are detailed in the following sections: Paralytic Shellfish Poisoning (PSP, Section 1.2), Neurotoxic Shellfish Poisoning (NSP, Section 1.4), Diarrhetic Shellfish Poisoning (DSP, Section 1.5), Amnesic Shellfish Poisoning (ASP, Section 1.6), and Ciguatera Poisoning (Section 1.7). As ciguatera poisoning is prevalent in tropical fish and hence is not strictly a shellfish toxin, the similar symptoms and mode of action to NSP warrant its inclusion in this chapter. Tetrodotoxin poisoning (Section 1.3), although caused by a symbiotic bacterium, shows similar action to PSP, and so is included for completeness. Various miscellaneous toxins (Section 1.8), not within these groups, but possibly implicated in poisoning are also discussed. Finally, Section 1.9 reveals current methods used in detection of shellfish toxins.

1.2 Paralytic Shellfish Poisoning

Numerous dinoflagellate species are known to produce the toxins causing PSP: *Alexandrium* spp. (formerly *Gonyaulax* or *Protogonyaulax*), *Gymnodinium catenatum* and *Pyrodinium bahamense* var. *compressum*.[2] The toxins responsible have been named the saxitoxins.

PSP is by far the most lethal form of shellfish toxicity. It has been documented for over 50 years as a cause of deaths in North America and during the last 10 years has killed more than 40 people in the Philippines. In a single outbreak in Guatemala some years ago, 26 people were killed by eating PSP contaminated shellfish.[3]

The symptoms of PSP are numbness, or hypersensitivity of the mouth and skin, a floating sensation and motor signs including ataxia, muscle weakness, paralysis and death, due to respiratory failure. The symptoms are usually rapid in onset (hours), but can vary from being acute, resulting in death, to prolonged, with less severe symptoms.[4]

1.2.1 Saxitoxins

Structurally the saxitoxins can be divided into two major groups: represented by saxitoxin (STX, **1**) and neosaxitoxin (NEO, **7**), depending on the functionality on N1. The compounds in both groups

are further distinguished by the presence of 11-*O*-sulfates (eg. GTX2, **3**) and 21-*N*-sulfates (eg. B1, **2**).[5,6]

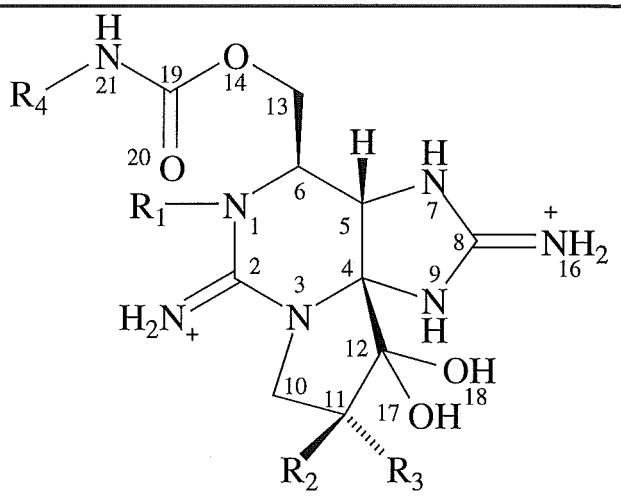

	R_1	R_2	R_3	R_4
STX (**1**)	H	H	H	H
B1 (**2**)	H	H	H	SO_3^-
GTX2 (**3**)	H	H	OSO_3^-	H
C1 (**4**)	H	H	OSO_3^-	SO_3^-
GTX3 (**5**)	H	OSO_3^-	H	H
C2 (**6**)	H	OSO_3^-	H	SO_3^-
NEO (**7**)	OH	H	H	H
B2 (**8**)	OH	H	H	SO_3^-
GTX1 (**9**)	OH	H	OSO_3^-	H
C3 (**10**)	OH	H	OSO_3^-	SO_3^-
GTX4 (**11**)	OH	OSO_3^-	H	H
C4 (**12**)	OH	OSO_3^-	H	SO_3^-

Other members of the saxitoxin family, eg. dcSTX (**13**),[7] do not possess the carbamoyl moiety of saxitoxin (**1**).

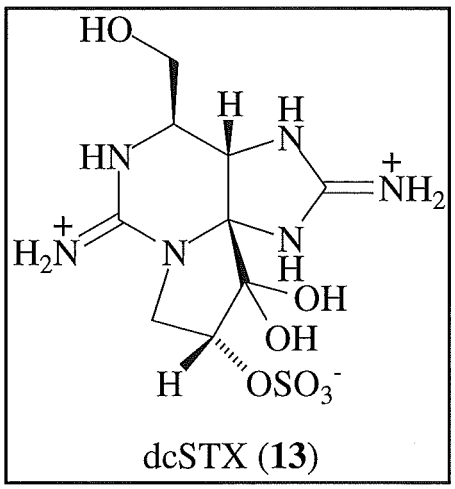

dcSTX (**13**)

1.2.2 Mode of Action of Saxitoxins

Saxitoxins alter the function of sodium channels, which are essential for the production of action potentials in excitable cells such as neurons. Normally, a change in membrane potential causes sodium channels to open, allowing sodium ions to flow through and rapidly depolarise the nerve membrane. The result is that a wave of depolarisation is propagated along the nerve. Saxitoxin binds to the outside of the sodium channel, blocking the ion flow, thus slowing, or even abolishing, the propagation of the action potential (Fig 1.2.1.).

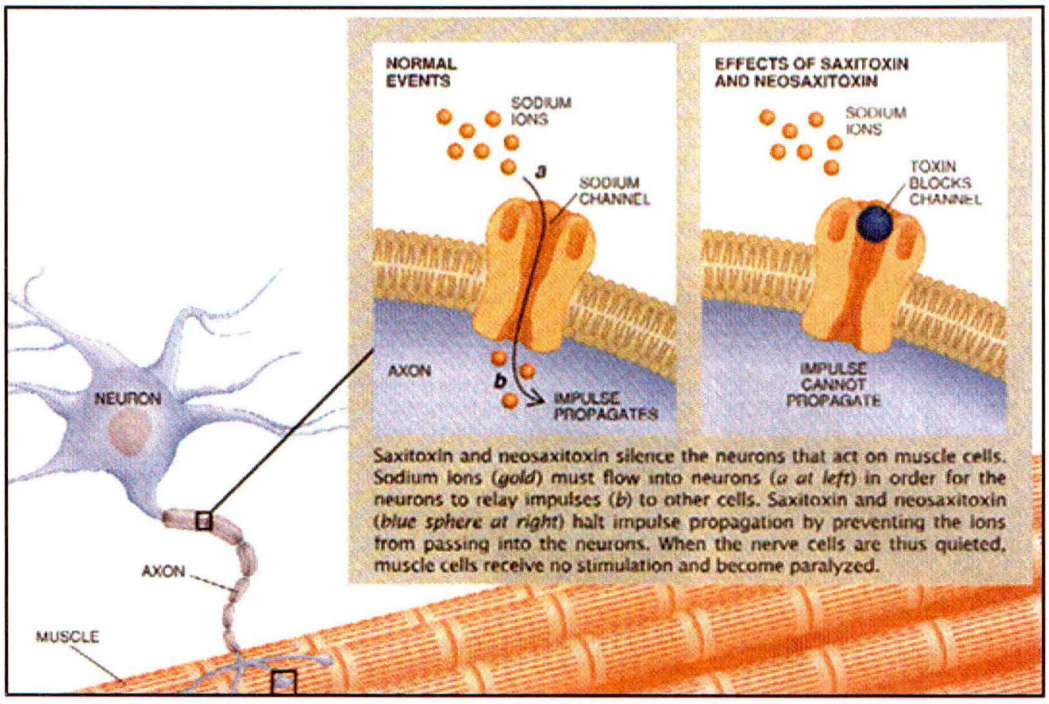

Fig 1.2.1 *Mode of Action of Saxitoxin and Neosaxitoxin*[8]

Since saxitoxins are charged, water soluble molecules, it is probable that they do not penetrate the blood-brain barrier well and the majority of their effects are on peripheral nerves.[9]

1.3 Tetrodotoxin Poisoning

The primary source of tetrodotoxin (TTX, **14**) was traced to a dietary alga and finally to a symbiotic bacterium.[10] The bacterium was first assigned as a *Pseudomonas* sp., then changed to *Alteromonas* sp. and finally described as a new species, *Shewanella alga*.[11] Subsequently, a broad spectrum of bacteria have been reported to produce the toxin.[12,13,14]

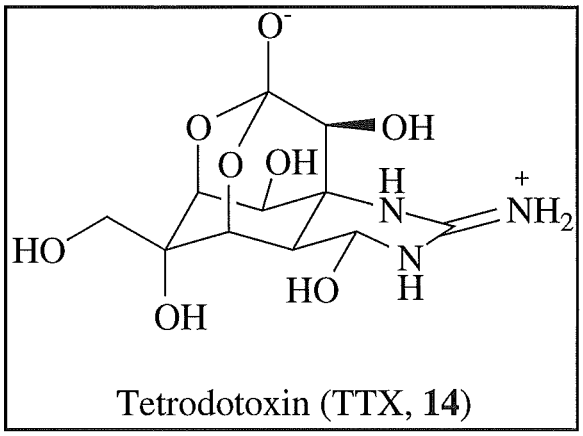

Tetrodotoxin (TTX, **14**)

TTX derives its name from the puffer fish family (Tetraodontidae) and is frequently involved in fatal food poisoning. The toxin has a unique structure and a similar mode of action to saxitoxin (**1**), causing the blockage of sodium channels of excitable membranes.

Analogues of TTX have been reported occurring in puffer fish, newts and a frog. Their presence was determined by the use of pre-column derivatisation with sodium hydroxide and detection of products by HPLC (*H*igh *P*erformance *L*iquid *C*hromatography) fluorescence.[15,16]

1.4 Neurotoxic Shellfish Poisoning

The dinoflagellate that is responsible for NSP is *Gymnodinium breve* and the causative toxins have been named the brevetoxins.

Brevetoxins are potent fish toxins and have been responsible for mass fish mortalities along the Florida coast.[17]

NSP is characterised by a range of neurological and gastrointestinal symptoms, including paraesthesia, changes in thermoreception, muscle weakness, incoordination, headache, muscle and joint pains, malaise, chills, diarrhoea, nausea and vomiting. One distinct feature of brevetoxin-containing blooms is their ability to trigger respiratory distress when involved in sea spray.

In terms of symptoms, NSP overlaps significantly with PSP. However, time of onset and duration of illness are generally longer for NSP. Also, NSP is more likely to cause muscle weakness, rather than the paralysis associated with PSP. Importantly, NSP has never been recorded as causing death.[18]

A distinctive neurosensory feature of NSP is a change in thermoreception, such as reversal of this sensation. This has never been reported for PSP, although it also occurs with ciguatera poisoning (Section 1.7).

1.4.1 Brevetoxins

Brevetoxin B (BTX-B, **15**) was the first member of this class of compounds. Its structure was established by X-ray crystallography in 1980, and has a ladder-like skeleton consisting of *trans*-fused polyether rings.[19] All brevetoxins found subsequently have the same backbone as BTX-B.

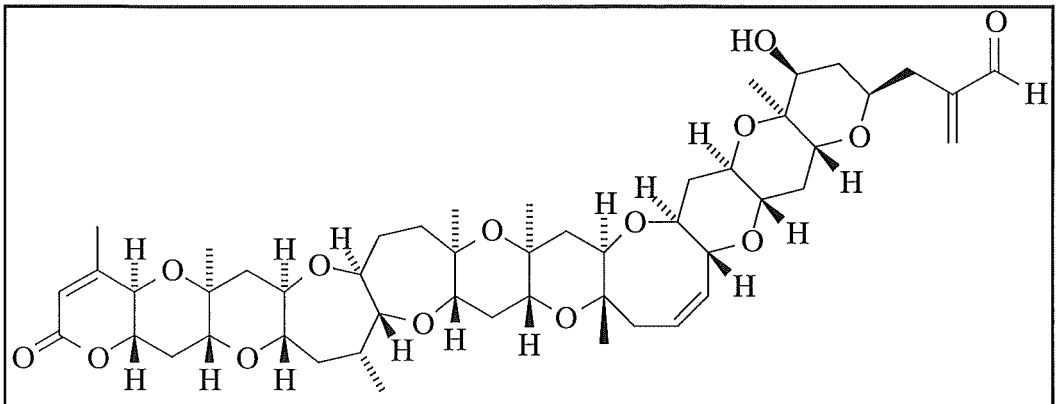

Brevetoxin B (**15**)

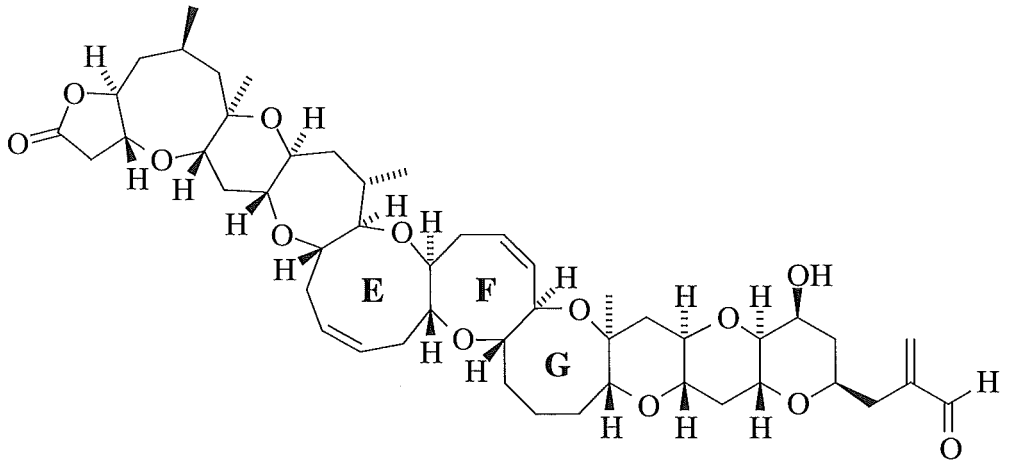

Brevetoxin A (**16**)

Brevetoxin A (BTX-A, **16**) is the most potent of the toxins produced by *G. breve*. Its lethality against zebra fish is reportedly 3 ppb. The

structure was elucidated by X-ray crystallography and the most unusual structural feature of BTX-A is its fused central rings (EFG), which have been shown to undergo slow conformational changes.[5]

1.4.2 Mode of Action of Brevetoxins

Brevetoxins act on the sodium channel at a site distinct from that affected by the saxitoxins. They cause the channel to remain open longer and stabilise the pre-open and open states. This then allows greater sodium ion inflow to occur, leading to neuronal membrane depolarisation and eventually causing nervous system failure.[20]

In addition to neurotoxicity, cardiac and respiratory toxicity also occur. The former is caused by increased sodium influx allowing greater sodium-calcium exchange, thus inducing increased catecholamine release. The latter is due to both peripheral effects on respiratory reflexes and muscle function There are also central effects on respiratory and cardiovascular control.[21]

Brevetoxins, being lipid soluble, should penetrate the blood-brain barrier easily and affect the central nervous system.[9]

1.5 Diarrhetic Shellfish Poisoning

The causative organisms of DSP have been identified as several dinoflagellates in the genus *Dinophysis*.[22] These algae produce okadaic acid (**17**) and the closely related dinophysis toxins, eg. DTX-1 (**18**). Other toxins, suspected of being involved in DSP, eg. the pectenotoxins[23] and yessotoxin (YTX, **19**),[24] have been isolated from Japanese scallops. However, the causative algae were of unknown origin. The dinoflagellate *Protoceratium reticulatum* has recently been established as the organism responsible for production of YTX.[25] DSP has wide distribution around the world and the poisoning is a serious problem, both to public health and to the shellfish industry. DSP was first recognised in 1976, when a mussel poisoning case occurred in Northeastern Japan.[26]

The prominent human symptoms of DSP are gastrointestinal disorders such as diarrhoea, nausea, vomiting, and abdominal pain. Histopathological investigations have revealed that pectenotoxin-1 (**20**) is hepatotoxic by inducing rapid necrosis of hepatocytes.[27]

1.5.1 Okadaic Acid

Okadaic acid (**17**) and the closely related dinophysis toxins, eg. DTX-1 (**18**) are the major causative agents of DSP. Okadaic acid was first isolated from the sponge *Halichondria okadai*[28] and subsequently was found in dinoflagellates *Prorocentrum lima*[29] and *Dinophysis* sp.[30]

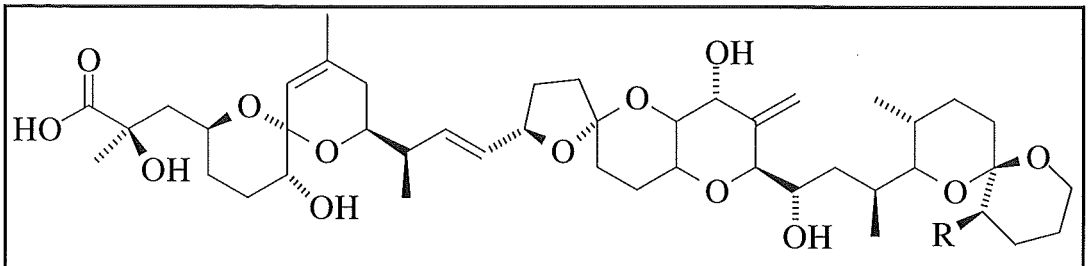

R = H Okadaic acid (**17**)
R = Me DTX-1 (**18**)

1.5.2 Mode of Action of Okadaic Acid

Aside from causing symptoms of diarrhoea, okadaic acid is known to be a potent carcinogen and to cause neuronal cell damage in cultured neurons.[9] The cause of diarrhoea and carcinogenicity are a result of a potent and specific inhibition of the serine/threonine protein phosphatases, PP1 and PP2A. This inhibition allows the build-up of phosphorylated proteins in cells that leads to pronounced "second messenger" production, eg. calcium influx, cyclic AMP and prostaglandin production.

1.5.3 Pectenotoxins and Yessotoxin

Pectenotoxin-1 (**20**) was isolated as one of the diarrhetic shellfish toxins from the digestive glands of the scallop *Patinopecten yessoensis* found in Northeastern Japan. The structure was revealed to be a novel polyether lactone by X-ray crystallography.[23]

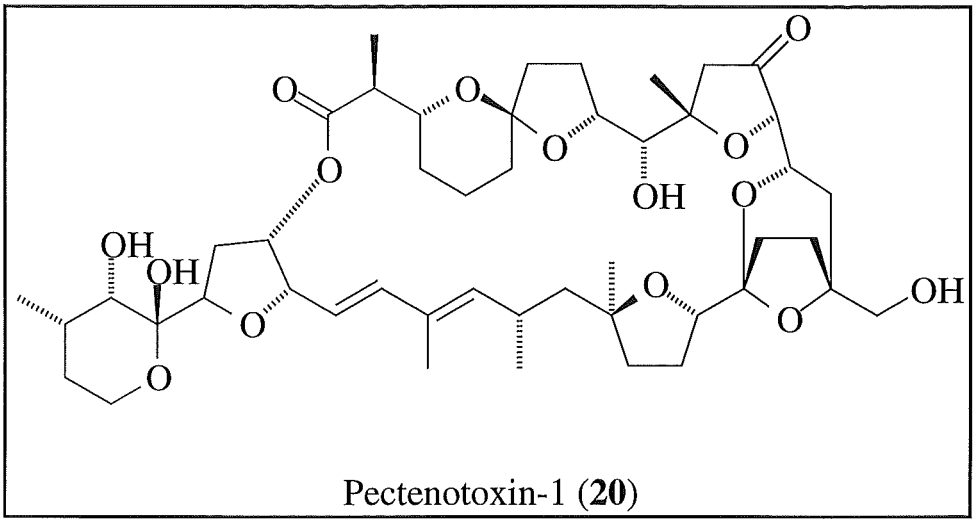

Pectenotoxin-1 (**20**)

Yessotoxin (YTX, **19**) was first isolated from Japanese scallops and the structure elucidated to be a brevetoxin-like polyether.[24] Its structural features include two sulfate groups and an olefinic C9 side chain. The relative[31] and absolute[32] stereochemistry of YTX has only recently been determined. Three new analogues of YTX have recently been discovered from shellfish, *viz* homo YTX (**21**), 45-hydroxy YTX (**22**) and 45,46,47-trinor YTX (**23**).[31,33] YTX has since been discovered in New Zealand shellfish, around the Coromandel Peninsula (Fig 2.1.1) and Wedge Point, Marlborough Sounds (Fig 4.1.1).[34,35]

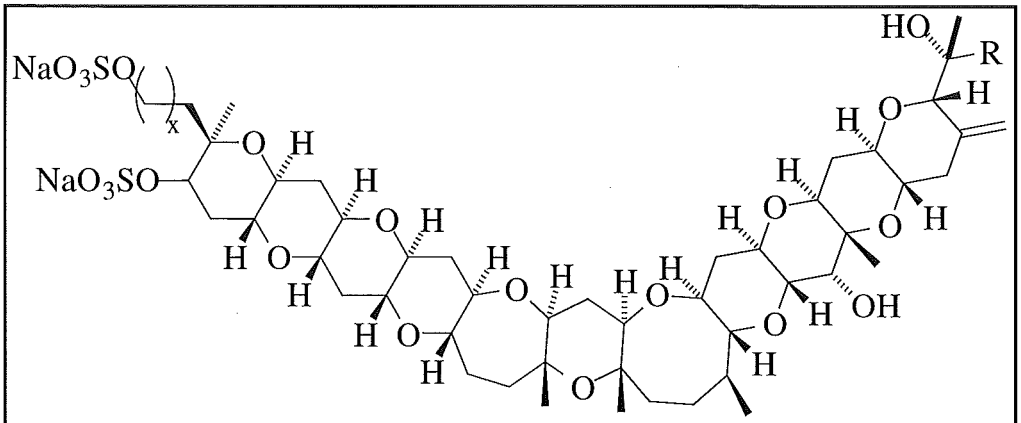

	R	x
YTX (**19**)	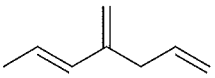	1
homo YTX (**21**)	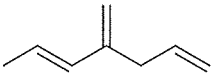	2
45-OH YTX (**22**)	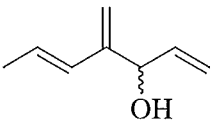	1
45,46,47-trinor YTX (**23**)	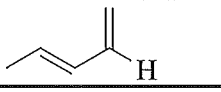	1

1.6 Amnesic Shellfish Poisoning

In late 1987 a mysterious and serious outbreak of food poisoning occurred in Canada. Symptoms of the poisoning included vomiting and diarrhoea. In some cases, this was followed by confusion, memory loss, disorientation and coma. Three elderly patients died and other victims still suffer from neurological problems.[36] The compound was identified as domoic acid (**24**) a compound first identified in crude extracts of certain seaweed found in the waters around Japan.[37] The Japanese used it as a folk medicine remedy for intestinal worm infestation. This argues against domoic acid as a toxin, however the higher doses found in the shellfish showed the obvious difference between therapeutic and toxic doses.

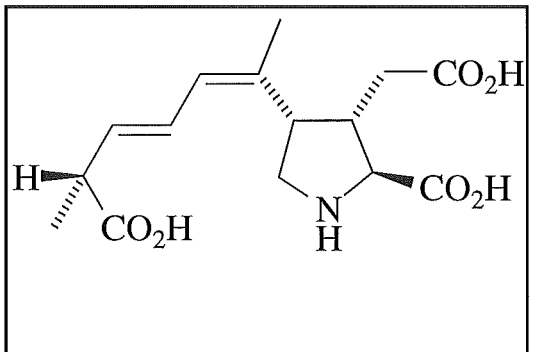

Domoic acid (**24**)

Further research showed that domoic acid was produced by a diatom *Nitzschia pungens* forma *multiseries*.[38,39]

1.6.1 Mode of Action of Domoic Acid

Domoic acid stimulates the kainate-sensitive type of glutamate receptor on nerves, causing depolarisation, influx of calcium and eventual cell death. Extracts may be more lethal because of synergism between domoate and other excitatory amino acids such as glutamate.[9]

1.7 Ciguatera Poisoning

There are two groups of compounds implicated in ciguatera poisoning: the main responsible toxins are ciguatoxin (CTX, **25**) and its congeners, and the other is maitotoxin (MTX, **26**). Both groups are produced by the epiphytic dinoflagellate *Gambierdiscus toxicus*,[40,41] transferred to herbivorous fish and subsequently to carnivores.

Ciguatera is a seafood poisoning prevalent in circumtropical areas. The poisoning is caused by ingestion of coral reef fish that have become toxic through their diet.

The clinical symptoms are diverse.[42] Neurological disturbances are prominent. For example, reversal of thermoreception (as in NSP), called "dry ice sensation", is one of the most characteristic symptoms of ciguatera poisoning. Other symptoms include joint pain, miosis, erethism, cyanosis and prostration. Gastrointestinal disorders are nausea, vomiting, and diarrhoea. Cardiovascular disturbances are low blood pressure and bradycardia.

1.7.1 Ciguatoxin

Ciguatoxin (**25**) was first isolated in 1980 by Scheuer *et al* and characterised as a polyether compound.[43] Insufficient material prevented the structural elucidation. In 1989, Murata *et al* elucidated the full structure of CTX and its congener, CTX-4B (**27**).[44] Since

1989, ciguatoxin congeners have been isolated, either from toxic fish,[45] or from cultured *G. toxicus*.[46]

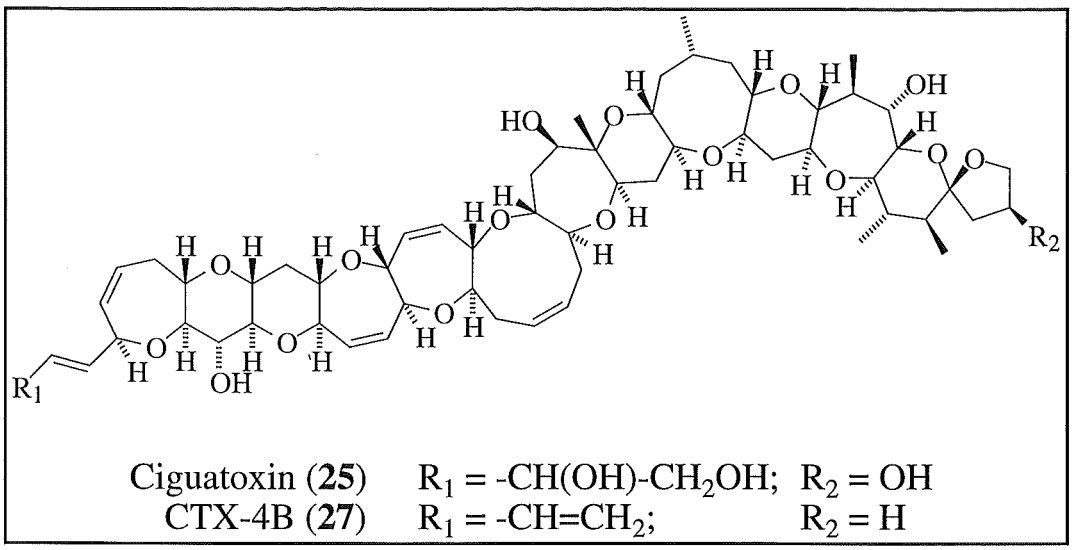

Ciguatoxin (**25**) R_1 = -CH(OH)-CH_2OH; R_2 = OH
CTX-4B (**27**) R_1 = -CH=CH_2; R_2 = H

An interesting aspect is that the moray eel, which is at the top of the coral ecosystem, tends to contain more polar (more oxygenated) congeners, while the dinoflagellate produces less polar ones. Ciguatoxin itself, the most oxygenated member of this class of toxins is absent in the dinoflagellates. These data suggest that the less polar congeners produced by the dinoflagellate are precursors to the more polar toxins found in fish, the latter toxins formed by oxidative enzyme systems in the fish. The toxicity is also increased in the oxidised metabolites, with CTX being 11 times more toxic than its plausible precursor CTX-4B.[5]

1.7.2 Mode of Action of Ciguatoxin

Many studies have been carried out on the pharmacological and toxicological actions of CTX. In earlier studies, the primary action of

CTX was thought to be inhibition of choline esterase,[47] until Rayner *et al* revealed that it stimulated the sodium ion influx into cells.[48]

1.7.3 Maitotoxin

Maitotoxin (MTX, **26**) is suspected of diversifying the ciguatera symptoms and is found particularly in herbivorous fish. MTX is an extremely potent polyether compound (LD_{50} against mice is *ca.* 50 ng/kg, ip)[49] constructed from a C142 carbon chain containing 32 ether rings, 28 hydroxyl groups, and two sulfate esters. With a molecular weight of 3422 Da, MTX is the largest non-peptidic natural product elucidated. The relative[50,51] and absolute[51] stereochemistry of MTX have recently been elucidated.

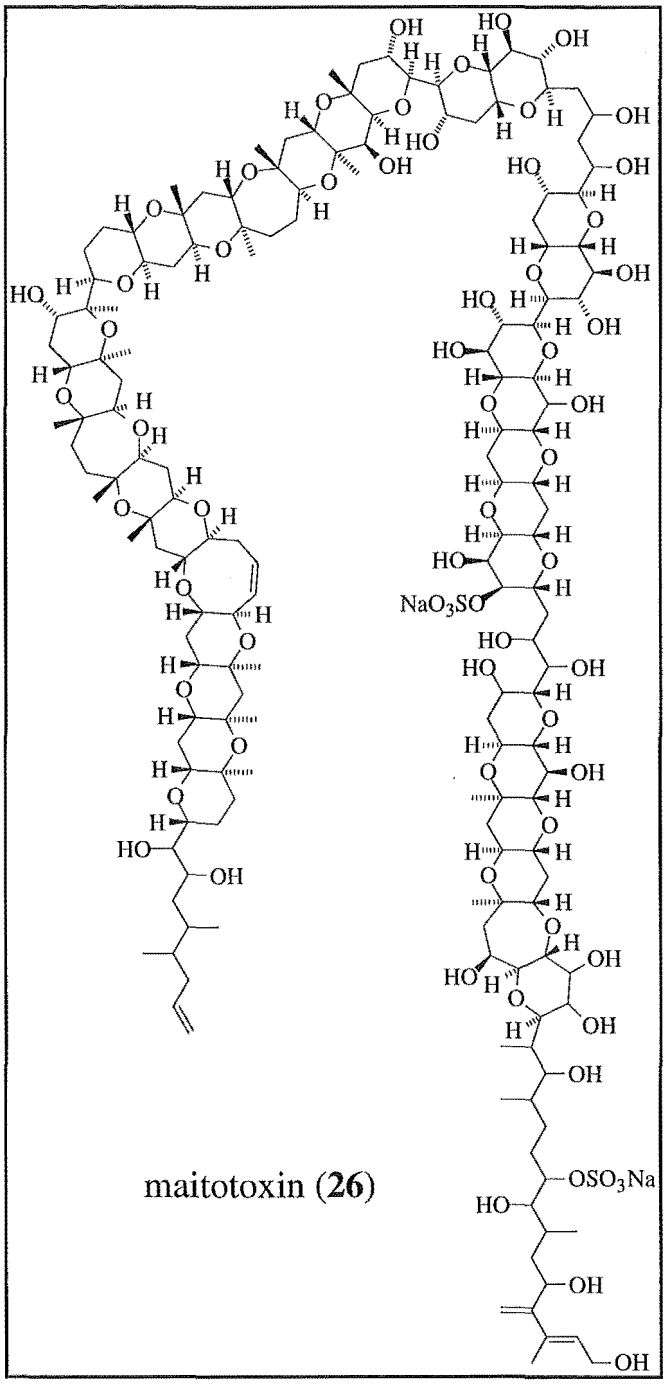

maitotoxin (**26**)

1.8 Miscellaneous Toxins

1.8.1 Neosurugatoxin and Prosurugatoxin

In 1965, there were 26 reported cases of intoxication after ingestion of the Japanese ivory shell, *Babylonia japonica*. Reported symptoms were visual defects, thirst, numbness of lips, constipation and dysuria. The toxins responsible were isolated from the digestive glands of the ivory shell and named neosurugatoxin (**28**) and prosurugatoxin (**29**).[52,53,54]

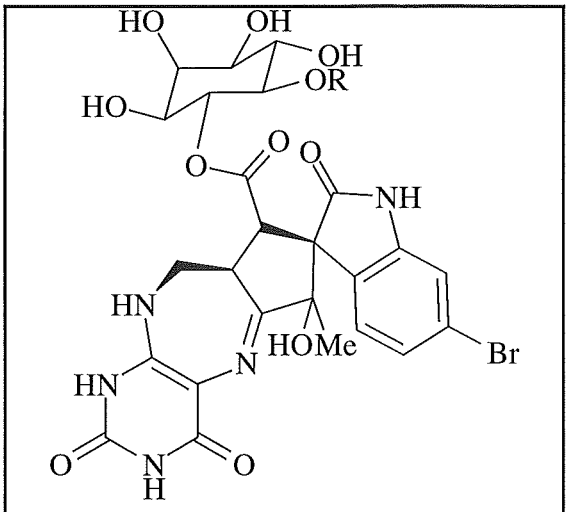

Neosurugatoxin (**28**) R = β-xylose
Prosurugatoxin (**29**) R = H

1.8.2 Polyoxygenated Compounds

The group of polyoxygenated compounds, named the amphidinolides eg. amphidinolide B (**30**), were isolated from the dinoflagellate *Amphidinium* sp., which is symbiotic to the flatworm *Amphiscolops*

breviviridis.[55] The number of compounds in this series has recently been extended to include up to amphidinolide Q.[56] The majority of the macrolides in this group exhibit extremely potent cytotoxicity against the L1210 and KB cell lines.[56]

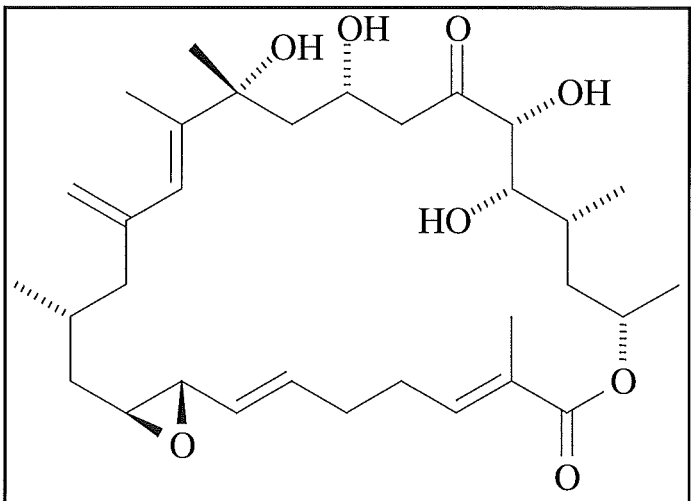

amphidinolide B (**30**)

The dinoflagellate, *Amphidinium klebsii*, was found to produce amphidinol (**31**), which belongs to a new class of polyhydroxypolyene compounds, showing potent antifungal and haemolytic activity.[57] A new member of this class, amphidinol 2, has recently been reported.[58]

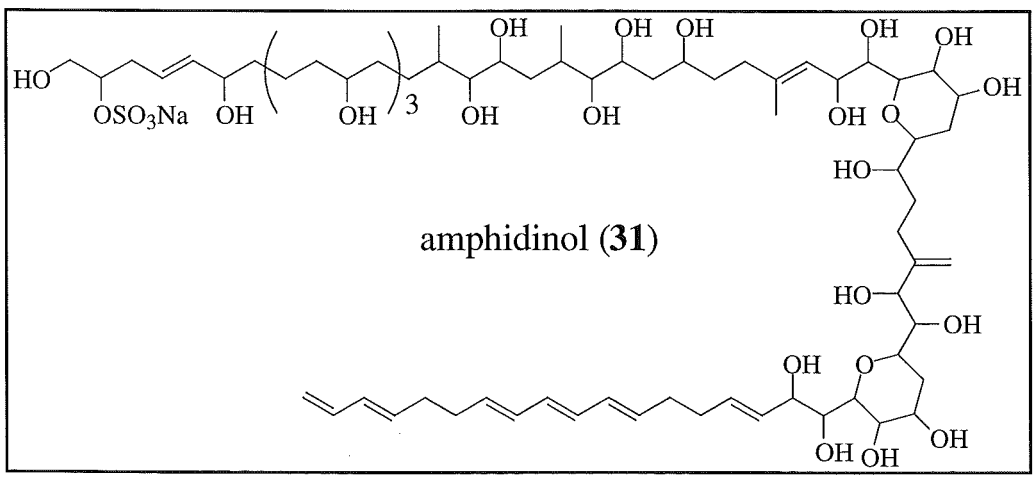

amphidinol (**31**)

The antifungal compound, goniodomin A (**32**) has been isolated from the tide pool dinoflagellate, *Gonyaudoma pseudogonyaulax* and elucidated as a novel polyether lactone.[59]

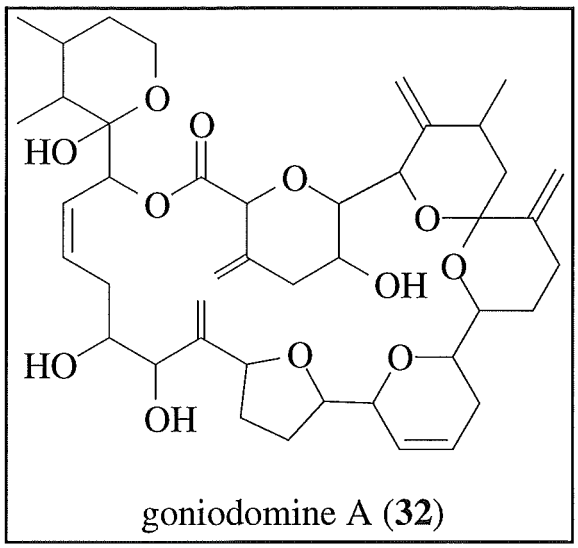

goniodomine A (**32**)

1.8.3 Nitrogen Containing Macrocycles

Prorocentrolide (**33**) has been isolated from the ciguatera-associated dinoflagellate, *Prorocentrum lima*. The structure was elucidated as a new type of nitrogenous polyether lactone.[60] The closely related congener, prorocentrolide B has recently been isolated from the tropical dinoflagellate, *Prorocentrum maculosum* Faust.[61]

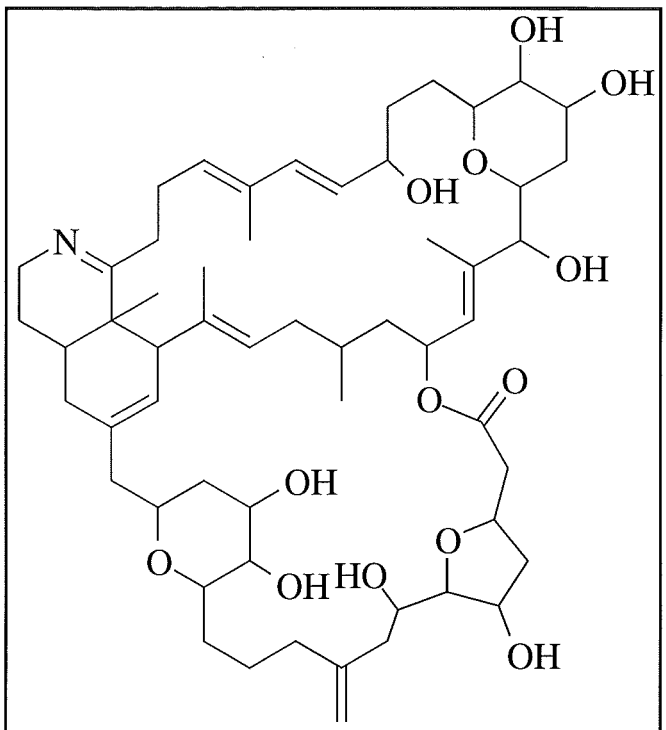

prorocentrolide (**33**)

The imine moiety, seen in prorocentrolide, is also found in a suite of recently isolated toxins. These compounds are further distinguished by the inclusion of a spiro-centre. The biological properties of these toxins are unique and characterised by the rapid onset of symptoms in the mouse bioassay.[62]

Pinnatoxin A (**34**) was isolated from the Okinawan bivalve, *Pinna muricata*.[63] The relative stereochemistry of pinnatoxin A was elucidated[64] along with a second analogue, pinnatoxin D (**35**).[65]

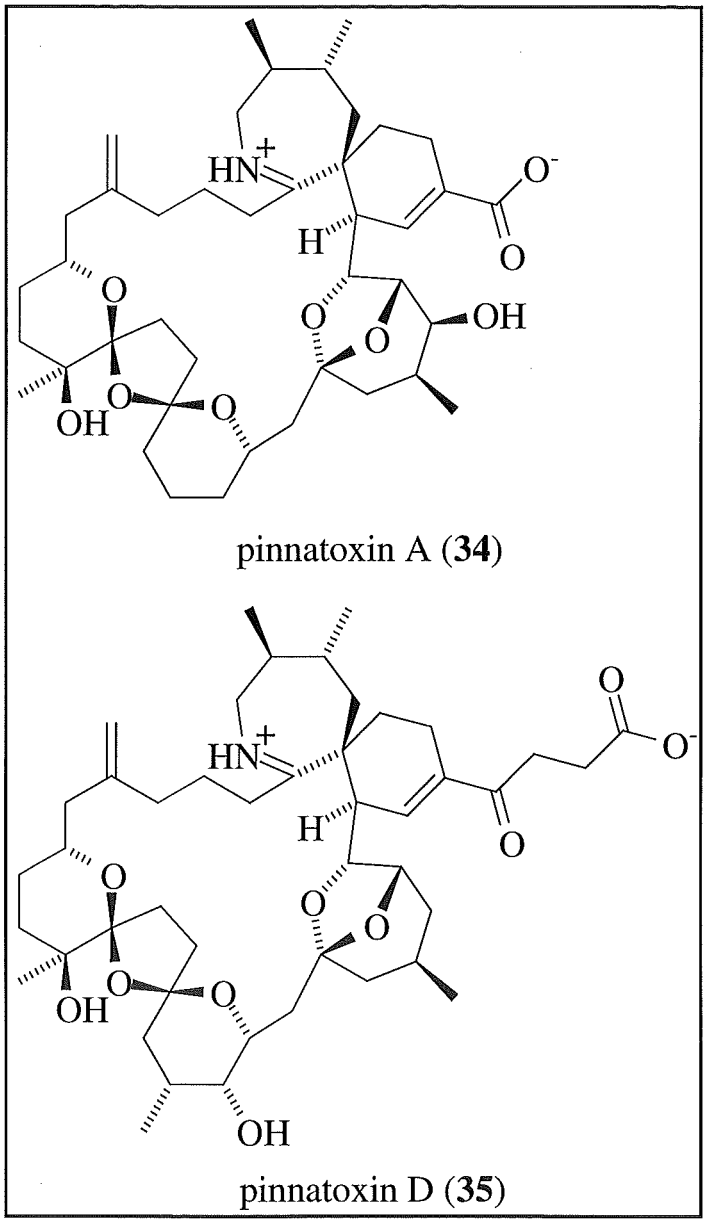

Spirolide B (**36**) and spirolide D (**37**) were isolated from the digestive glands of mussels, (*Mytilus edulis*) and scallops, (*Placopecten magellanicus*).[66] Subsequently, spirolide E (**38**) and spirolide F (**39**) were isolated as biologically inactive keto amines from the same shellfish extracts.[62] The biological inactivity of spirolides E and F suggests the common pharmacophore, in this class of compounds, is the cyclic imine/iminium moiety.

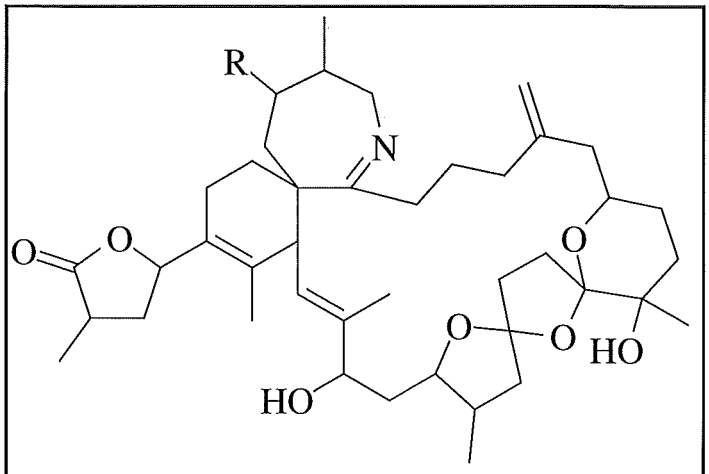

spirolide B (**36**) R = H
spirolide D (**37**) R = Me

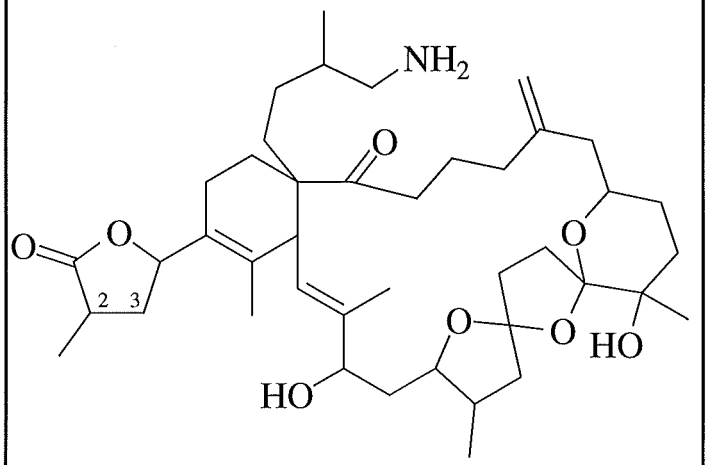

spirolide E (**38**) $\Delta^{2,3}$
spirolide F (**39**)

Gymnodimine (**40**) is a nitrogen containing macrolide isolated from oysters *Tiostrea chilensis*, from Foveaux Strait in New Zealand,[67] and is toxic to mice when administered intraperitoneally. The absolute stereochemistry of gymnodimine was elucidated as part of this research and is described in Section 5.3.

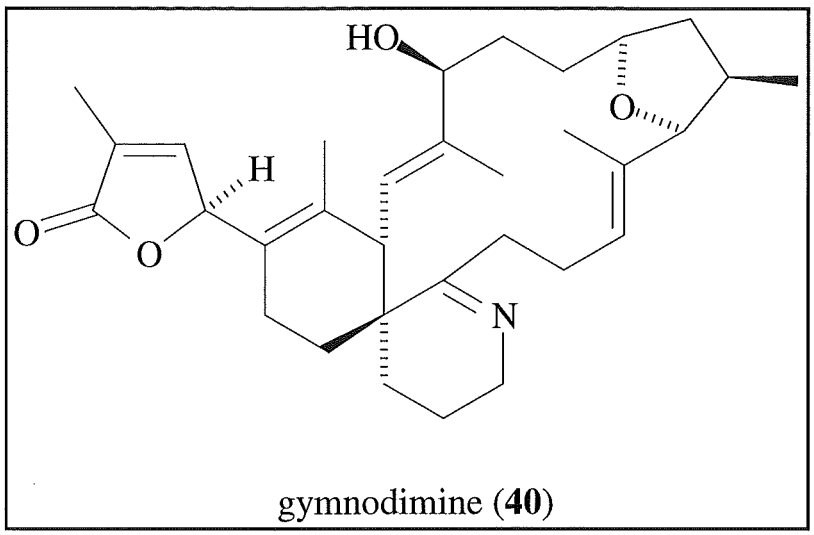

gymnodimine (**40**)

1.9 Detection Methods for Shellfish Toxins

Assay techniques for the toxicity testing of shellfish are dependent on the type of poisoning under consideration. Each poisoning syndrome is caused by one or more toxins, either multi-component (eg. PSP, DSP, NSP) or single component (eg. ASP). The contribution of each component to overall toxicity, within a multi-component toxic shellfish poisoning (TSP), is variable. The testing and monitoring for TSP requires knowledge of the range and levels of each contributing component.[68]

An excellent example is the multi-component PSP toxin class. Toxicities of each member in the class vary substantially (Fig 1.9.1),[69] providing evidence that specific toxin testing is essential for accurate toxicity determination.

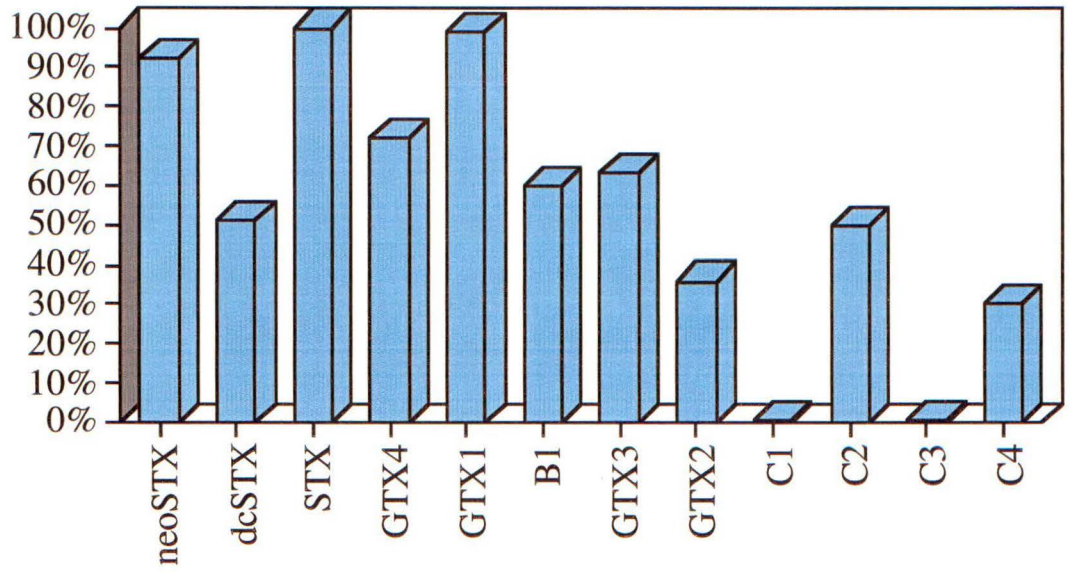

Fig 1.9.1 *PSP Profile: Relative Toxicity*[69]

A suitable toxicity test must be accurate, specific and reliable towards the type of toxin(s) assayed against. In addition, the test must provide quantitative measurements of toxicity for relating observed public health effects to toxicity. From this knowledge regulatory thresholds may be set.[68]

Shellfish biotoxin toxicity testing is most often performed using the mouse bioassay.[70,71] Extracts for testing are assayed by performing inoculations into the peritoneal cavities of mice and observing symptoms and death times. This approach suffers from poor reproducibility, low sensitivity and interference from certain matrices.[72]

The mouse bioassay is relatively non-specific, except in the case of NSP and PSP testing. The extraction method can also give some indication of the type of TSP toxicity (Table 1.9.1).

Table 1.9.1 *Shellfish Toxins, Extraction Methods and Mouse Bioassay*[68]

TSP	Extraction Method	Observation In Mouse Bioassay
ASP	Aqueous extraction	Non-specific behaviour
DSP	Lipid extraction	Non-specific behaviour
NSP	Lipid extraction	Characteristic behaviour
PSP	Aqueous acid extraction	Characteristic behaviour

Furthermore, the barbaric nature of the mouse bioassay is causing world-wide intolerance of this as an acceptable method for routine monitoring. Much current research is focused on the identification and

confirmation of the toxins responsible for each TSP, by specific, humane methods.

The testing for specific toxins (or groups of toxins, in the case of multi-component systems) can occur in a variety of ways. The most common assays include: the ELISA (*E*nzyme *L*inked *I*mmuno*S*orbent *A*ssay) , currently under investigation for most TSP, RIA (*R*adio *I*mmuno*A*ssay) , for NSP analysis, and PPA (*P*rotein *P*hosphatase enzyme *A*ssay) for DSP testing (Table 1.9.2). In addition, highly specific chemical assays, such as HPLC with specific detection, are being developed for the major TSP incidents encountered (Table 1.9.2).

Table 1.9.2 *Chemical Assay Techniques for Shellfish Toxin Testing*[68]

TSP	Specific Techniques
ASP	HPLC with UV
DSP	HPLC/Fluorescence with pre-column derivatisation
	Enzyme Immunoassays (ELISA)
	Phosphatase enzymes
NSP	HPLC with UV
	Sodium channel binding assays (N2A)
	Radio immunoassays (RIA)
PSP	HPLC/Fluorescence with post-column reaction
	Enzyme Immunoassays (ELISA)

At present, most of the above techniques are "in-house" developed or research techniques. Few have been subjected to inter-laboratory collaborative trials and, for each TSP category, there is no specific toxin assay that is "officially recognised" world-wide.

Chapter Two

Investigation of Toxicity In Coromandel Mussels

2.1 Introduction

On 4 January 1993 the initial indications of New Zealand's first recognised outbreak of shellfish toxicity became apparent. In Whangarei, several cats were diagnosed by local veterinary surgeons as having been poisoned after consuming shellfish. Owners of the affected animals were also found to have experienced toxic symptoms after consuming shellfish. Publicity led to further notifications of human illness following shellfish consumption. In addition, respiratory irritation was reported by people present near Orewa beach.[18] These reports were consistent with reported incidents of a syndrome associated with red tides of *Gymnodinium breve* in Florida.[73] The illness is caused by an aerosol containing particles of *G. breve*, a particularly fragile species, which is broken up by the pounding action of surf. As a result, the New Zealand coastline was progressively closed for shellfish harvesting. The entire coastline was closed from 22 January 1993, and was progressively re-opened as the levels of biotoxins dropped below the regulatory limit.[18]

Four specific toxin groups were detected in shellfish from different localities around New Zealand. For three of the toxin groups, the specific toxin was identified by bioassay or chemical means. These were the saxitoxins (PSP), domoic acid (ASP) and okadaic acid (DSP).

The fourth group were the brevetoxins (BTX), which are responsible for neurotoxic shellfish poisoning (NSP). The majority of NSP cases reported were from the upper NE coast of New Zealand's North

Island, between North Cape and East Cape, and could be related to shellfish collected from coastline between Northland and Bay of Plenty. However, mouse bioassays indicated that the area where shellfish were affected with lipid soluble toxins was between Bay of Islands and Bay of Plenty, hence around the Coromandel Peninsula (Fig 2.1.1).[18]

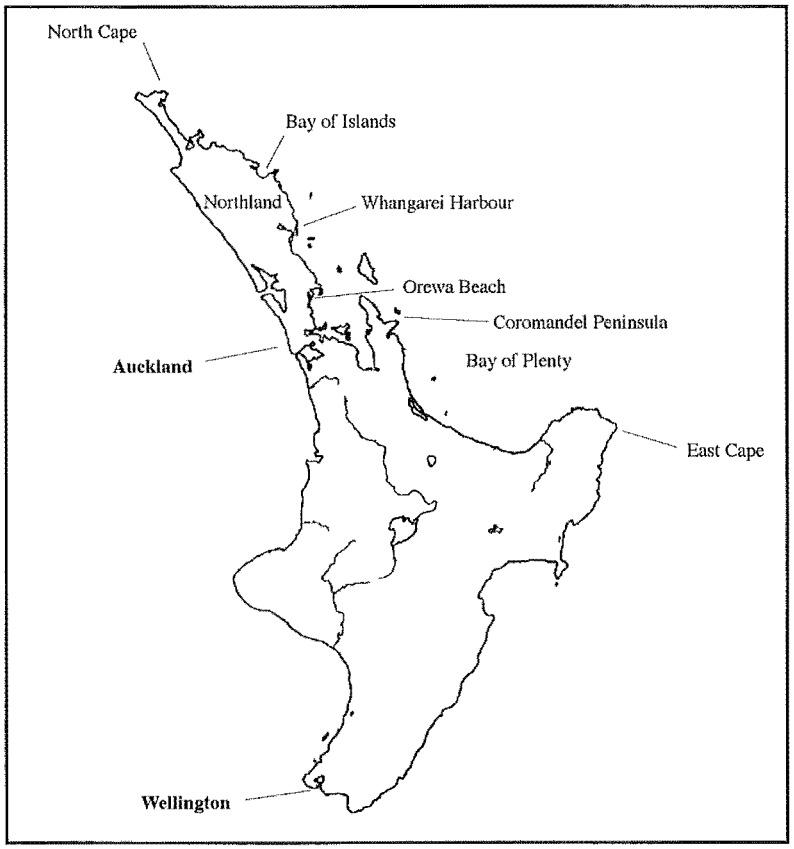

Fig 2.1.1 *New Zealand's North Island*

It was initially thought that the onset of characteristic NSP symptoms ie. respiratory irritation, had been caused by brevetoxins. This was supported by cross-reaction with antibodies specific to brevetoxins, positive results against neuroblastoma cell lines[74] and the identification of *Gymnodinium* species in the areas.[1] These findings are summarised in Table 2.1.1.

Table 2.1.1 *Summary of the Clinical Symptoms Observed and Biotoxins Demonstrated During the 1993 Crisis*

Prototype Clinical Syndrome	Causative Toxins	Clinical Syndrome Observed	Phytoplankton Observed	Toxin Demonstrated By
PSP	Saxitoxins	Doubtful	*Alexandrium minutum* *A. tamarense*	Mouse bioassay
NSP	Brevetoxins	Yes	*Gymnodinium breve*	Mouse bioassay
Respiratory irritation	Brevetoxins	Yes	*G. breve*	
DSP	Okadaic acid and related compounds	Probable	*Dinophysis* sp.	Chemical assay
ASP	Domoic acid	Doubtful	*Nitzschia pungens*	Chemical assay

However, subsequent work at the Institute of Environmental and Scientific Research (ESR) laboratories in New Zealand, as well as research findings from the USA and in Japan, suggested that the toxins involved were not any of the known brevetoxins. Differences in chromatographic behaviour and in mode of action suggested that the toxic reaction was caused by a compound (or compounds) that might have some relationship to the brevetoxins, but may be in a unique class.

Tonne quantities of commercial green shell mussels (*Perna canaliculus*) were contaminated by the NSP toxins. As a result, an investigation into the chemical nature of the toxins contained in these mussels was carried out as part of this research. Particular emphasis was placed on the determination of their structure and stereochemistry. The investigation into the toxic component(s) of the shellfish is described in Section 2.2.

2.2 Investigation of Toxicity

The establishment of a mouse bioassay was deemed as essential for the isolation of the toxic components in the shellfish. The mouse bioassay (Appendix 1) shows total toxicity in the extracts although it had three limitations. The assay was run at the Communicable Diseases Centre (CDC) in Porirua, where samples were sent for analysis. This made for long turn-around times between sending the samples off and receiving the results, slowing progress measurably. The infancy of the mouse bioassay in New Zealand and the lack of experienced technicians at the time, meant that major problems existed while the assay was being run. The most important problem was the difficulty in dissolving highly lipid soluble samples in a detergent/saline solution.

The slow turn around times and handling problems forced alternative ways of detecting the toxicity in the extracts. The marine group at the University of Canterbury has an "in house" P388 murine leukaemia assay (Appendix 1). The P388 assay is a very sensitive, cytotoxicity based assay that is used extensively for following biological activity in natural product isolation. The advantages of the P388 assay over the mouse bioassay were threefold. First, the P388 assay is a well established procedure. Second, it has a turn around time of 3 days. Third, solvents such as methanol and mixtures of up to 50% dichloromethane may be used, hence facilitating the management of highly lipid soluble fractions.

A total lipid extract, prepared by the NZ acetone extraction method[75] and supplied by ESR, was assayed and the result was an IC_{50} value of 50 μg/mL. This result, although only showing mild cytotoxicity, prompted further investigation of the suitability of the P388 assay to detect the toxicity in the shellfish.

The total lipid extract was partitioned between 80% methanol/water and petroleum ether (b.p. range 50-70 °C). The P388 assay revealed that all the cytotoxicity was in the aqueous methanol phase, with an IC_{50} value of 20 μg/mL. Mouse bioassays were then run on both fractions. Mouse toxicity occurred in the aqueous/methanol phase only, hence supporting a likely correlation between the two assays.

Following this, reverse phase C18 column chromatography of the aqueous phase was performed with a gradient solvent system. The results of the P388 assay are shown in Fig 2.2.1. The column concentrated the cytotoxicity into three adjacent fractions, designated 2.A3 - 2.A5. The cytotoxicity of these fractions was very strong, with P388 IC_{50} values of < 975 ng/mL. An aliquot of 2.A4 was sent for mouse bioassays and proved very toxic, with 100% mouse deaths in 20 minutes. As the correlation between P388 cytotoxicity and mouse toxicity was convincing, the P388 assay was adopted as the more appropriate assay for further research.

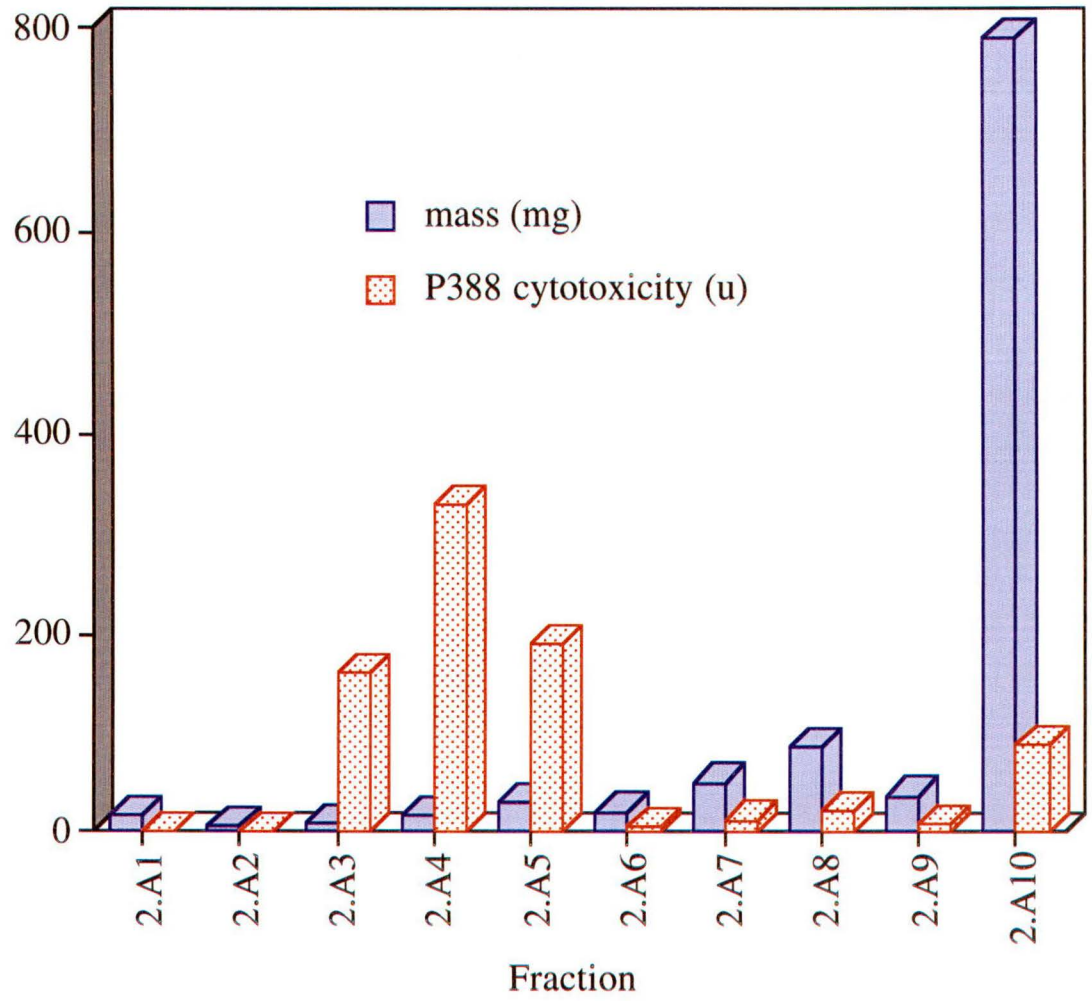

Fig 2.2.1 *Graph Showing Cytotoxicity and Mass of Fractions off C18 Reverse Phase Column*

P388 cytotoxicity (u) = mass (mg)/IC_{50} (ng/mL) x 10^4

Further purification was performed on fractions 2.A3 - 2.A4 by LH-20 gel permeation chromatography. The column was run in dichloromethane and then stripped with dichloromethane/methanol to clean the column. All the observed cytotoxicity eluted in the methanol strips (2.B7 - 2.B8), as shown in Fig 2.2.2.

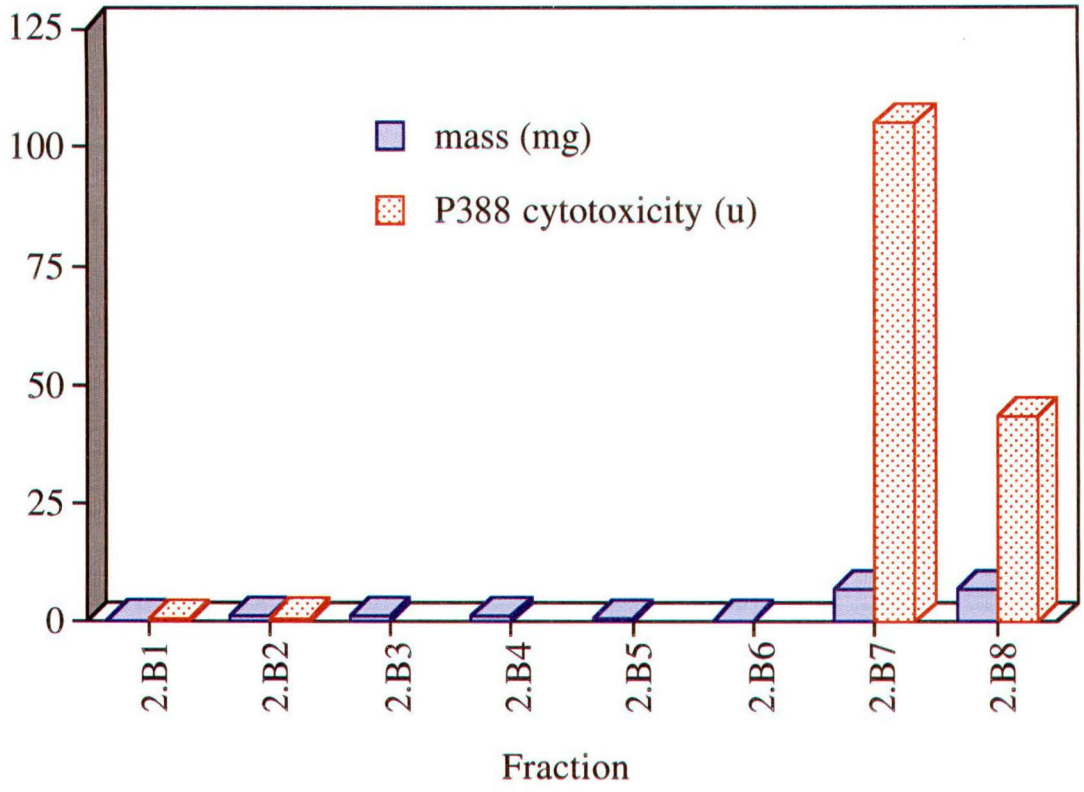

Fig 2.2.2 *Graph Showing Cytotoxicity and Mass of Fractions off LH-20 Gel Permeation Column*

P388 cytotoxicity (u) = mass (mg)/IC_{50} (ng/mL) x 10^4

Fractions 2.B7 and 2.B8 were then re-chromatographed on LH-20 using 10% methanol in dichloromethane as eluting solvent. The cytotoxic compound(s) streaked badly on this column. Consequently, most of the cytotoxicity was lost. The behaviour on LH-20 suggested toxin solubility problems in both dichloromethane and 10% methanol in dichloromethane. These results suggested that the compound(s) showing cytotoxicity are more polar than the known brevetoxins.

This prompted an alternative method of extraction to be sought to replace the total lipid extraction method used for detecting NSP toxicity.

2.2.1 Alternative Extraction Method

The new method involved freeze drying the frozen mussel tissue to remove the water (80% by weight). The dried shellfish were then crushed to release the contents of the cells and extracted with a succession of solvents from water, methanol, ethyl acetate through to dichloromethane.

The water and methanol extracts were toxic in the mouse bioassay. This was consistent with the toxin solubility problems encountered earlier on LH-20. The use of highly polar extraction solvents has an advantage over a total lipid extraction. Shellfish have a high lipid content, of which only a minimal amount will be extracted by using water or methanol/water mixtures below 80% methanol/water.

A method was developed based on this theory. Frozen mussels were freeze dried and extracted with water, 40% methanol/water and 70% methanol/water. The extracts, all of which showed mild P388 cytotoxicity, were combined and concentrated to an aqueous solution. The resulting extract was partitioned against hexane and the water phase was kept. This was then desalted on a large C18 reverse phase column and passed through a smaller C18 column, from which six fractions (2.C1 - 2.C6) were collected (Scheme 2.2.1). The cytotoxicity was contained predominantly in 2.C2 -2.C4. These fractions were combined and chromatographed on diol phase, from which fractions 2.D1 - 2.D10 were collected (Scheme 2.2.1). The P388 cytotoxicity was observed in two bands; early eluting 2.D1 and late eluting 2.D8 and 2.D9.

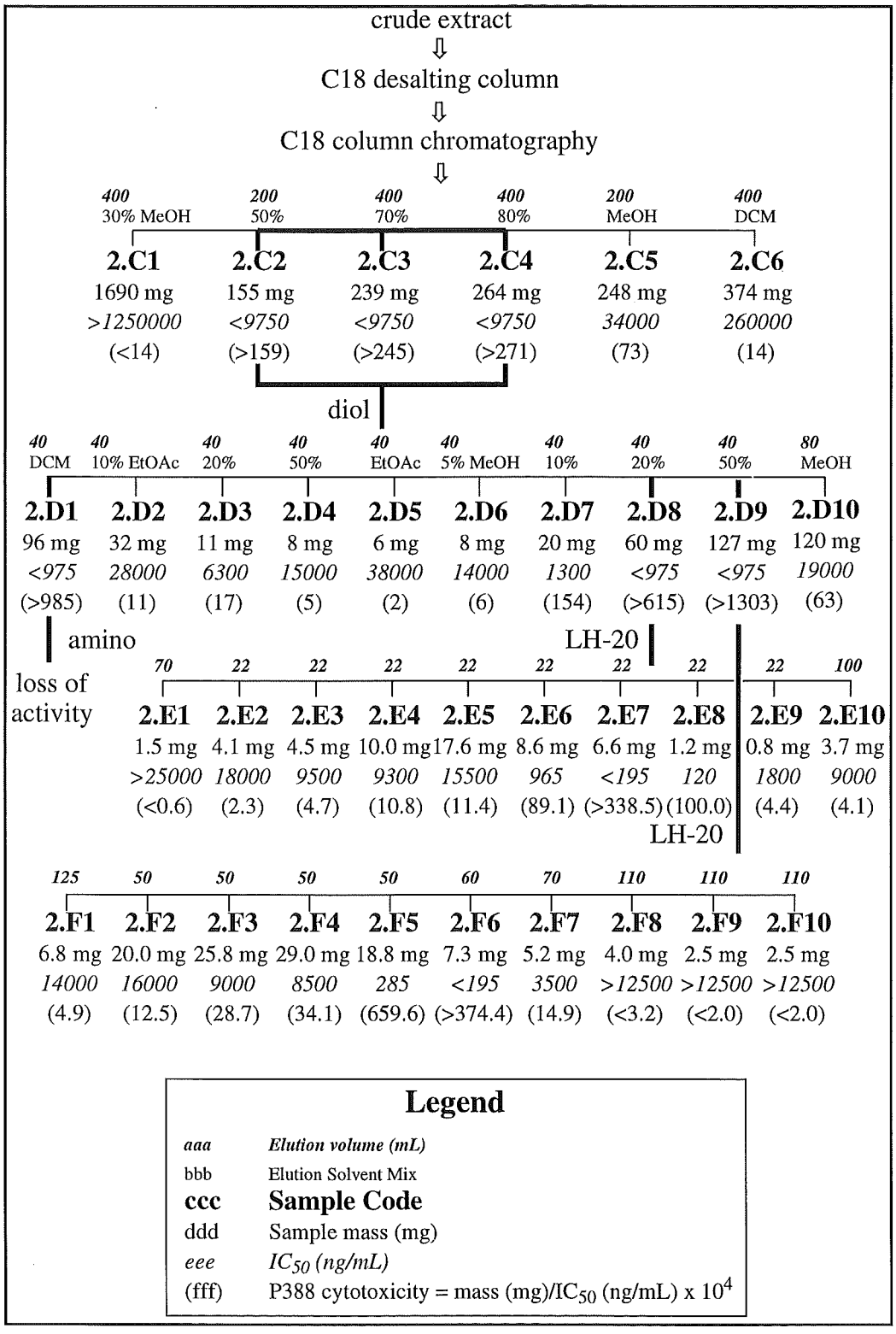

Scheme 2.2.1 *Isolation Scheme for P388 Cytotoxic Compound from Coromandel Mussels*

Fractions 2.D8 and 2.D9 exhibited the strongest total cytotoxicity and were chromatographed separately on LH-20 gel permeation columns. Fraction 2.D8 was fractionated into 2.E1 - 2.E10, with the majority of the cytotoxicity contained in 2.E6 - 2.E8 (Scheme 2.2.1). Fraction 2.D9 was fractionated further into 2.F1 - 2.F10 with the cytotoxicity concentrated in 2.F5 - 2.F6 (Scheme 2.2.1).

Early promise for purification of fraction 2.D1 on amino phase chromatographic sorbent was shown. However, when the full amount was passed through a column containing this phase, almost all cytotoxicity was lost. The acidic nature of the compound (hence strong binding to amino phase chromatographic material) was also observed for subsamples of 2.D8 and 2.D9. The large difference in chromatographic behaviour (as exhibited on diol phase chromatographic material) was unexplained but could be due to residual methanol still present, which was used to clean the diol material, before use. Thus, it was believed that the cytotoxic compound contained in 2.D1 was the same as that exhibiting the major cytotoxicity in 2.D8 and 2.D9.

At this stage a sodium channel sensitive assay using a neuroblastoma (N2A) cell line (Appendix 1) was setup at CDC, in Porirua. This assay was designed for analysis of BTX and STX containing samples. Fractions 2.E1 - 2.E10 and 2.F1 - 2.F10 were sent for analysis and the results are shown in Fig 2.2.3 and Fig 2.2.4.

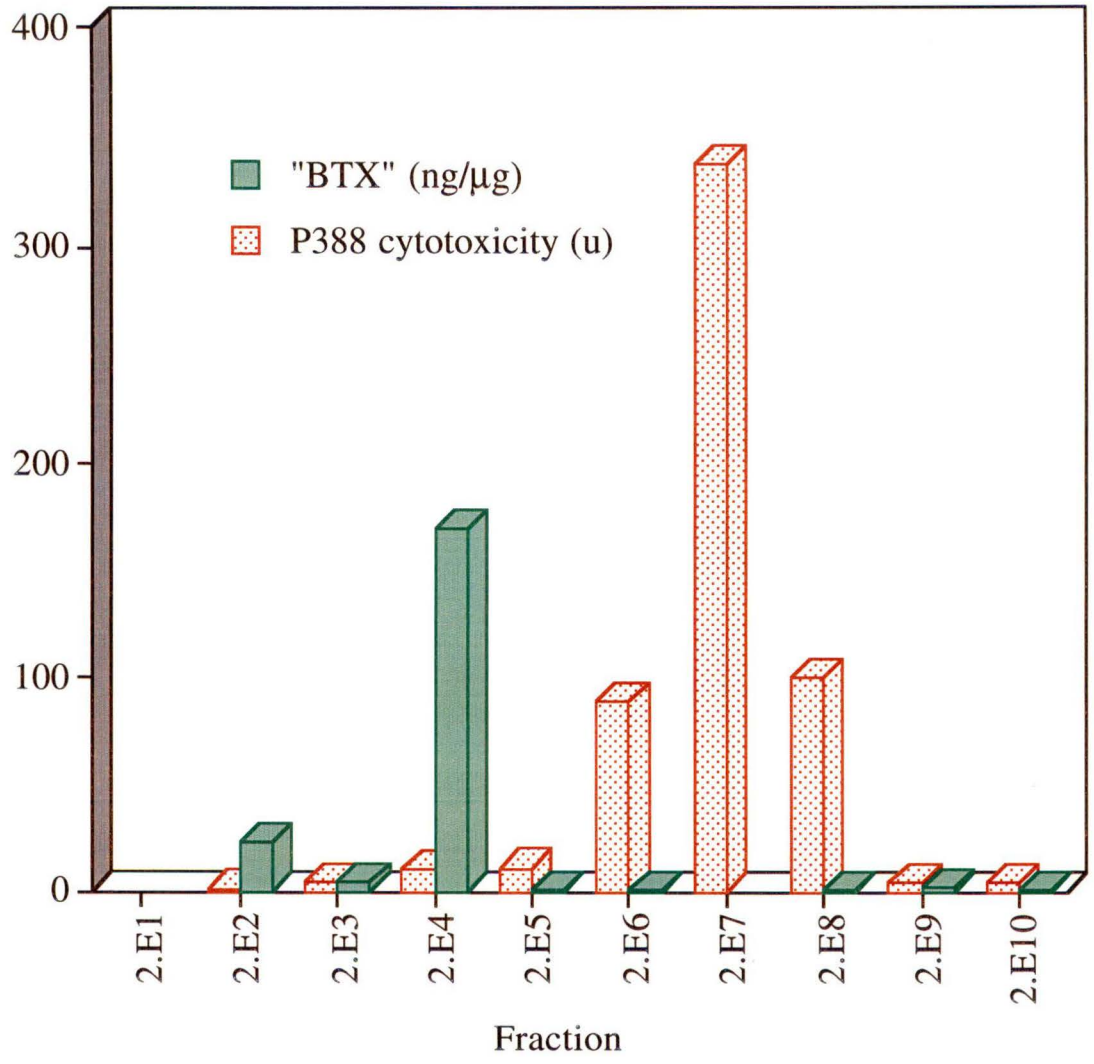

Fig 2.2.3 *Graph Showing Cytotoxicity and "BTX" of Fractions off LH-20 Gel Permeation Column*

"BTX" = brevetoxin B equivalents from N2A assay

P388 cytotoxicity (u) = mass (mg)/IC_{50} (ng/mL) x 10^4

The results revealed an anomaly between the P388 cytotoxicity and the N2A activity. As shown in Fig 2.2.3, 2.E4 is the only fraction containing appreciable amounts of BTX-like material, whereas the P388 cytotoxicity is concentrated in 2.E6 - 2.E8.

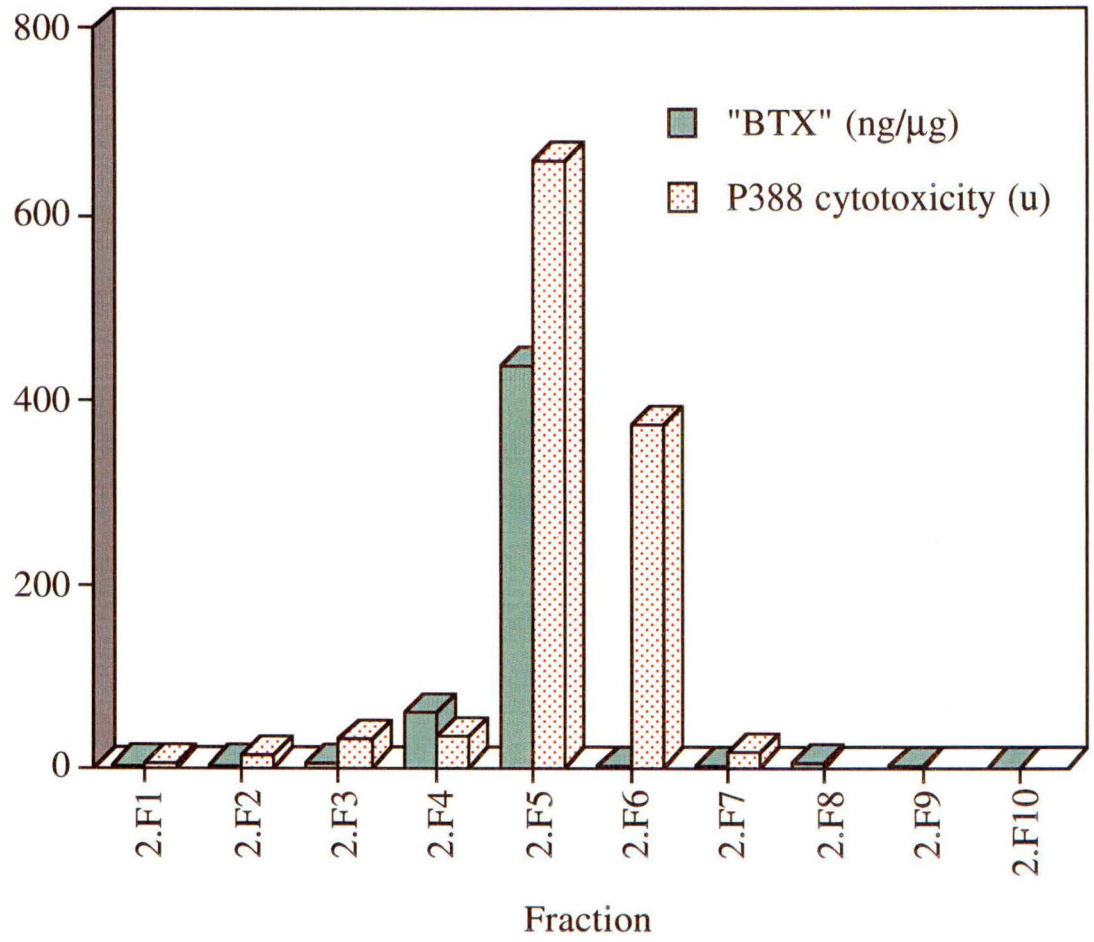

Fig 2.2.4 *Graph Showing Cytotoxicity and "BTX" of Fractions off LH-20 Gel Permeation Column*

"BTX" = brevetoxin B equivalents from N2A assay

P388 cytotoxicity (u) = mass (mg)/IC_{50} (ng/mL) x 10^4

Fig 2.2.4 does not show such an obvious result, with BTX activity in 2.F4 and 2.F5, but P388 cytotoxicity in 2.F5 and 2.F6. These data suggest overlapping areas of activity.

As confirmation, a pure sample of BTX-A (supplied by ESR laboratories) was assayed against the P388 cell line. The result was an IC_{50} value >812.5 ng/mL, evidently demonstrating no cytotoxicity.

From these data it became apparent that the P388 cytotoxicity was not caused by BTX-like compounds, but possibly a unique compound which has no effect on the sodium channel.

2.2.2 Brevetoxins

While this work was in progress, it was discovered that a large amount of toxic shellfish had been sent to two research groups in Japan. A personal communication with Dr Ishida of University of Shizuoka in Japan, resulted in the notification of the isolation and identification of the major causative toxin in this same 1993 New Zealand outbreak. A following publication of the results unveiled a BTX-B conjugate, named BTX-B1 (**41**), isolated from cockles, which were collected during the 1993 outbreak.[76] BTX-B1 differs from BTX-B only in the side chain, where a taurine group is conjugated at the aldehyde position.

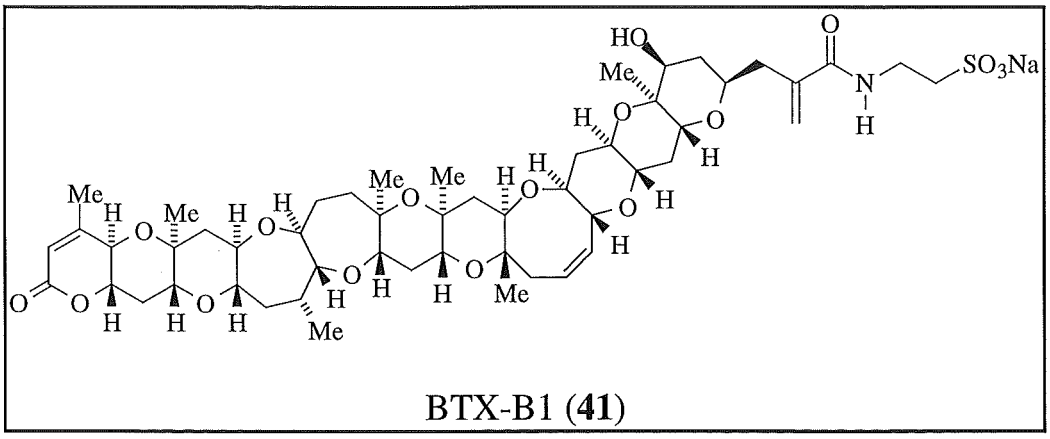

BTX-B1 (**41**)

Communication with Professor Yasumoto of Tohoku University in Japan, revealed that his group had isolated and identified similar

conjugates, BTX-B2, BTX-B3 and BTX-B4, from mussels collected during the 1993 New Zealand outbreak of shellfish poisoning. It was not until recently, however, that the chemical structures of BTX-B2 (**42**)[77] and BTX-B3 (**43**)[78] were published.

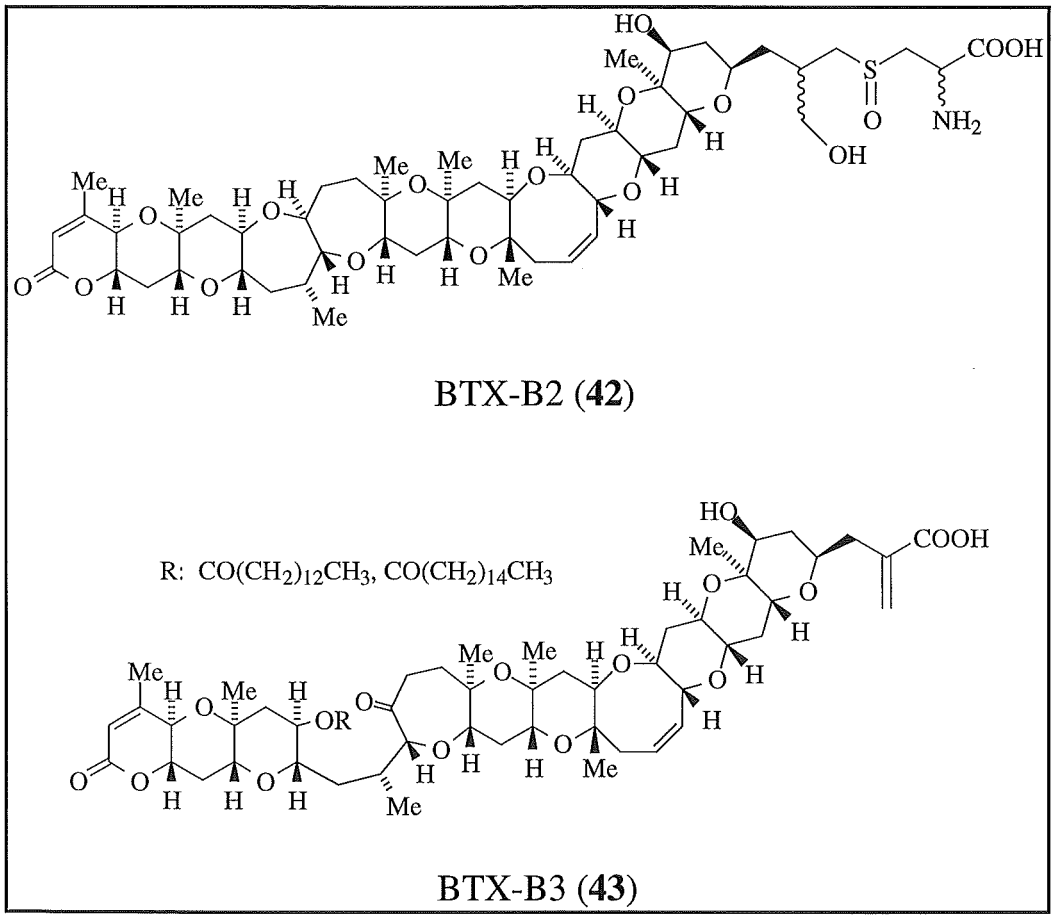

All the new BTX conjugates contain functional groups, which enhance the polarity of each molecule. In particular, each contains acidic and/or basic groups, eg. BTX-B1 (SO_3Na/NH), BTX-B2 ($COOH/NH_2$) and BTX-B3 (COOH).

The nature of the molecules explains the predominantly polar chromatographic profiles observed in the preliminary examination.

This lead to the assumption of the possibility of an entirely new class of compound.

None of the BTX conjugates have ever been isolated from the algae. It is postulated that the shellfish modify the toxins to less toxic, water soluble conjugates, which are able to be excreted.[79]

The similar chromatographic profile of the compound(s) exhibiting P388 cytotoxicity, suggested certain common characteristics to the newly discovered conjugated brevetoxins.

2.2.3 Isolation of Cytotoxic Compound

Although the causative NSP toxins had been identified from the mussels, the potent P388 cytotoxicity observed was of considerable interest. The priority of this research was then directed at elucidating the structure of the compound(s) which exhibited this activity.

Fractions 2.E6 - 2.E8 and 2.F6 were all analysed by ^{1}H NMR (*N*uclear *M*agnetic *R*esosnance) spectroscopy. The ^{1}H NMR spectrum of fractions 2.E6 and 2.E7 contained fatty acids as their major component, with other peaks appearing with only baseline intensity. The ^{1}H NMR spectrum of 2.E8 contained sharp isolated resonances in the region of 4 - 6 ppm, with a broad mass of resonances between 3 - 4 ppm, indicative of a glycoside structure. The ^{1}H NMR spectrum of 2.F6 revealed the same broad resonances as seen in 2.E8, however, sharp aromatic signals between 7 - 9 ppm suggested different structural features. Due

to the low mass of the active fractions, combined with no clear common peaks observed by ^{1}H NMR spectroscopy, these fractions were kept as reference samples for a larger scale extraction.

A larger extraction was undertaken by ESR laboratories in Lower Hutt (using the protocol described in Section 6.2.3) on 6.5 kg of frozen mussels.

The extract was sent to University of Canterbury as a methanol/water solution. The methanol was evaporated off and the resulting water solution run through a large C18 column. The resulting fractions 2.H1 - 2.H7 (Scheme 2.2.2) were assayed in both the P388 and N2A assays. The majority of the P388 cytotoxicity was concentrated in fractions 2.H5 and 2.H6, while the BTX activity was in 2.H6.

Fraction 2.H5 was further chromatographed on diol, from which fractions 2.I1 - 2.I11 (Scheme 2.2.2) were collected. Two distinct bands of activity eluted off the column and concentrated in 2.I5 - 2.I7 and 2.I9. LH-20 gel permeation chromatography of 2.I5 - 2.I7 afforded fractions 2.J1 - 2.J7 (Scheme 2.2.2), of which 2.J6 had a very potent P388 cytotoxicity with an IC_{50} value of 70 ng/mL. A ^{1}H NMR spectrum of fraction 2.J6 showed virtually 100% fatty acid material however minor baseline peaks were also present. Fraction 2.J6 was kept as reference until examination of fraction 2.I9 was complete. Upon resuming this work, a P388 assay revealed the activity in fraction 2.J6 had diminished. This suggested that probable degradation of the active component in this fraction had occurred.

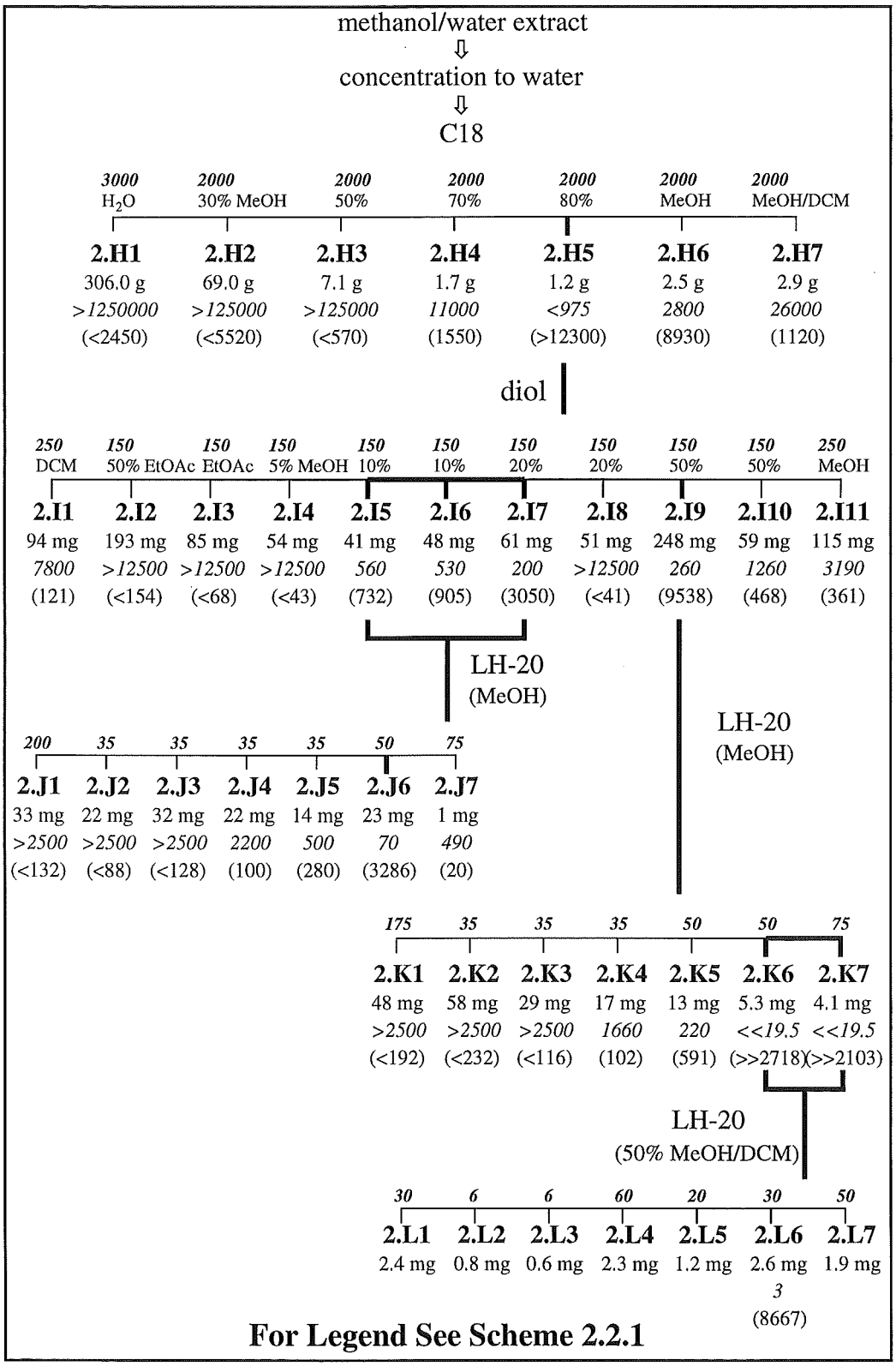

Scheme 2.2.2 *Isolation Scheme for The P388 Cytotoxic Component of Coromandel Mussels*

Fraction 2.I9 was separated into 2.K1 - 2.K7 on LH-20 gel permeation chromatography (Scheme 2.2.2). Fractions 2.K6 and 2.K7 exhibited very potent P388 cytotoxicity with IC_{50} values of << 19.5 ng/mL.

The ^1H NMR spectra of 2.K6 and 2.K7 illustrated many well defined peaks, common to both fractions. Multiple signals in the 3 - 4 ppm region were characteristic of a polyether compound. This confirmed the earlier assumption that the compound(s) exhibiting P388 cytotoxicity had similar characteristics to those of the conjugated brevetoxins.

Final purification was achieved by fractionating 2.K6 and 2.K7 on a second LH-20 column to give 2.L6 (Scheme 2.2.2) as 2.6 mg of pure toxin, exhibiting a very potent P388 cytotoxicity, with an IC_{50} value of 3 ng/mL.

The ^1H NMR spectrum of 2.L6 demonstrated signals different from BTX with olefinic resonances at δ 6.35, 5.91, 5.86, 5.12, 5.10 and 4.84 ppm, suggesting an entirely different compound.

Examination of the literature revealed that the potent cytotoxic compound was most likely yessotoxin (YTX, **19**), a suspect DSP causing toxin isolated previously from Japanese scallops in 1987.[24]

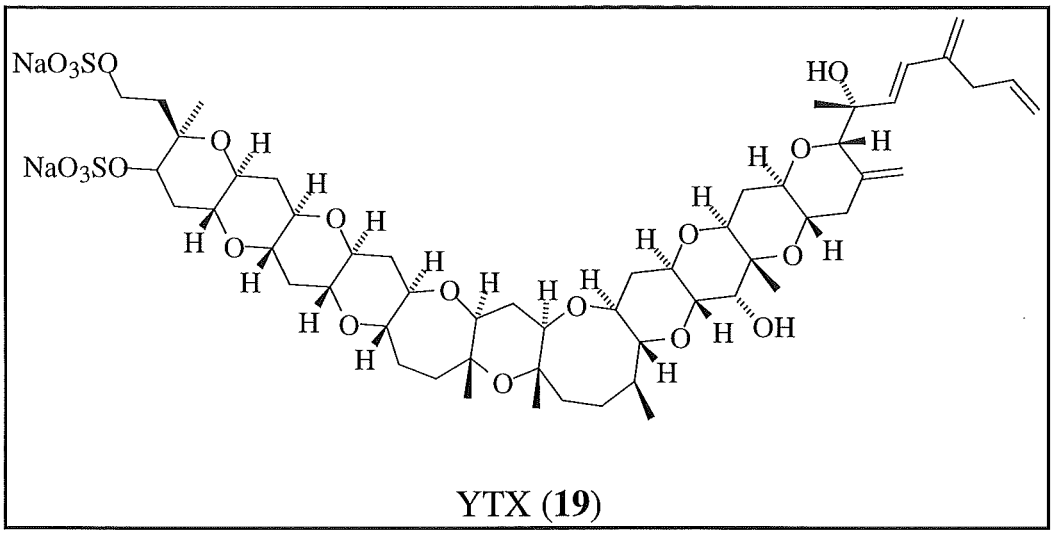

YTX (**19**)

An examination of the structure of YTX is described in chapter 3.

2.3 Conclusions

The toxins responsible for the outbreak in seafood poisoning and respiratory irritation, around Coromandel Peninsula, in early 1993, were isolated and characterised by two Japanese research groups. These compounds were identified as polar brevetoxin-B conjugates, *viz* BTX-B1 - BTX-B4.[76,77,78]

Yessotoxin (YTX) was isolated as the major P388 cytotoxic compound from these shellfish as part of this research. The extremely low levels of YTX in the shellfish suggested that the toxin was probably not a public health concern. However, this research was the first to identify YTX in New Zealand.

A further cytotoxic component in the mussels was detected using a P388 cytotoxicity guided purification. Likely degradation of this compound occurred during examination suggesting that it was unstable. Subsequent research into the large scale isolation procedure of YTX (Section 3.5) was unsuccessful in detecting more of this compound.

Chapter Three

Yessotoxin

3.1 Introduction

Yessotoxin (YTX, **19**) was isolated from the New Zealand green lipped mussel, *Perna canaliculus*, harvested from the Coromandel Peninsula during the toxic shellfish outbreak in early 1993. YTX is a previously isolated shellfish toxin from Japan[24] and the confirmation of its structure is detailed in Section 3.2.

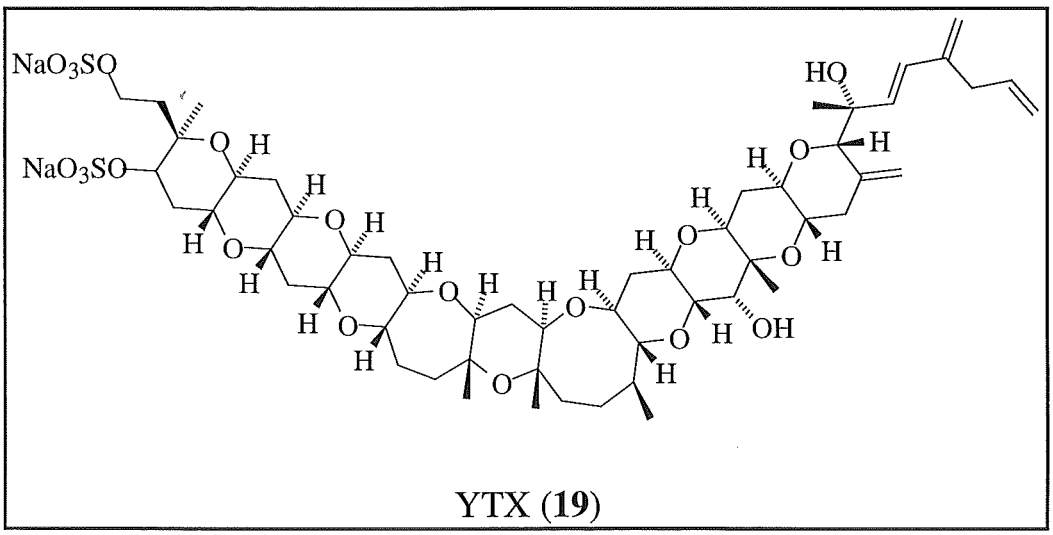

YTX (**19**)

The relative[31] and absolute[32] stereochemistry of YTX has only recently been published. However partial elucidation of the relative stereochemistry of YTX was performed independently as part of this research topic. This work is described in Section 3.3.

YTX exhibits potent cytotoxicity against the P388 murine leukaemia cell line (IC_{50} = 3 ng/mL) and shows cytotoxicity towards rat hepatocytes.[80] Other studies revealed that YTX induces acute heart failure in mice when administered intra-peritoneally (i.p.) (LD_{50} = 286 μg/kg). However, YTX shows no toxic effects when given orally.[27]

For multi-component toxin systems, such as the "DSP shellfish poison complex", the mouse bioassay is unable to distinguish between the individual toxins in the system. The toxicity of YTX, observed in the mouse bioassay, requires the development of a more selective support assay to quantify the toxin in commercial shellfish samples. The rat hepatocyte assay,[80] used in conjunction with the mouse bioassay, for DSP toxins, is reasonably selective, although it provides no quantitative measure of the individual toxins. The most promising assay for detection of YTX is likely to be a YTX-specific ELISA. The development of an ELISA requires modification of the target compound. The modification of YTX for development of a YTX-specific ELISA is described in Section 3.4.

To enable future research on YTX to be undertaken, sufficient quantities of the pure toxin must be available. The very low level of YTX in the shellfish makes this an arduous exercise. The development of a large scale isolation procedure is detailed in Section 3.5.

3.2 Spectroscopic Assignment of YTX

Negative ion LRFABMS (*L*ow *R*esolution *F*ast *A*tom *B*ombardment *M*ass *S*pectrometry) on a pure sample of YTX revealed an ion at *m/z* 1163.5. This ion corresponded closely to the published value of *m/z* 1163 $(M-Na)^-$ for YTX. Subsequent positive ion HRFABMS (*H*igh *R*esolution *F*ast *A*tom *B*ombardment *M*ass *S*pectrometry) was performed on the *m/z* 1163.5 ion for accurate mass measurement. Acceptable high resolution mass determination was achieved, with the caesium adduct of YTX, which gave an ion with *m/z* 1539.1680 corresponding to $[M-2Na+3Cs]^+$ ($C_{55}H_{80}O_{21}S_2Cs_3$).

A full spectroscopic NMR assignment of YTX was essential for conclusive proof of chemical structure. This was achieved by ^1H, ^{13}C, COSY (*CO*rrelation *S*pectroscop*Y*) and HMQC (*H*eteronuclear *M*ultiple *Q*uantum *C*oherence) NMR experiments.

The ^{13}C NMR spectrum of the isolated YTX was compared with the published values of YTX (Table 3.2.1). The data collated extremely well, with no value differing by more than 0.1 ppm.

Table 3.2.1 *Comparisons Between Published* $(C_p)^{24}$ *and Observed* (C_o) ^{13}C *NMR Data for YTX*

Position	δ C_p	δ C_o	Position	δ C_p	δ C_o	Position	δ C_p	δ C_o
1	65.1	65.1	**20**	82.4	82.5	**38**	39.0	39.0
2	40.1	40.2	**21**	33.2	33.1	**39**	143.1	143.1
3	76.5	76.6	**22**	87.3	87.4	**40**	85.1	85.2
4	78.4	78.4	**23**	77.0	77.0	**41**	78.4	78.4
5	32.8	32.8	**24**	47.0	47.0	**42**	136.7	136.7
6	78.4	78.4	**25**	32.8	32.8	**43**	130.6	130.6
7	70.6	70.6	**26**	40.8	40.8	**44**	145.4	145.5
8	36.5	36.5	**27**	89.4	89.5	**45**	37.8	37.8
9	78.3	78.3	**28**	84.1	84.1	**46**	137.5	137.6
10	78.3	78.3	**29**	40.0	40.0	**47**	116.6	116.5
11	36.2	36.2	**30**	73.2	73.3	**48**	16.4	16.3
12	77.6	77.6	**31**	79.6	79.6	**49**	23.9	23.9
13	78.1	78.1	**32**	73.8	73.8	**50**	20.7	20.7
14	38.0	38.0	**33**	76.7	76.8	**51**	22.4	22.3
15	81.1	81.1	**34**	73.2	73.2	**52**	15.4	15.3
16	82.2	82.2	**35**	31.7	31.7	**53**	115.7	115.7
17	30.3	30.3	**36**	73.1	73.0	**54**	26.2	26.2
18	41.1	41.1	**37**	73.0	73.0	**55**	116.6	116.5
19	78.4	78.4						

All δ values expressed in ppm. Solvent (CD_3OD) referenced to δ 49.0 ppm

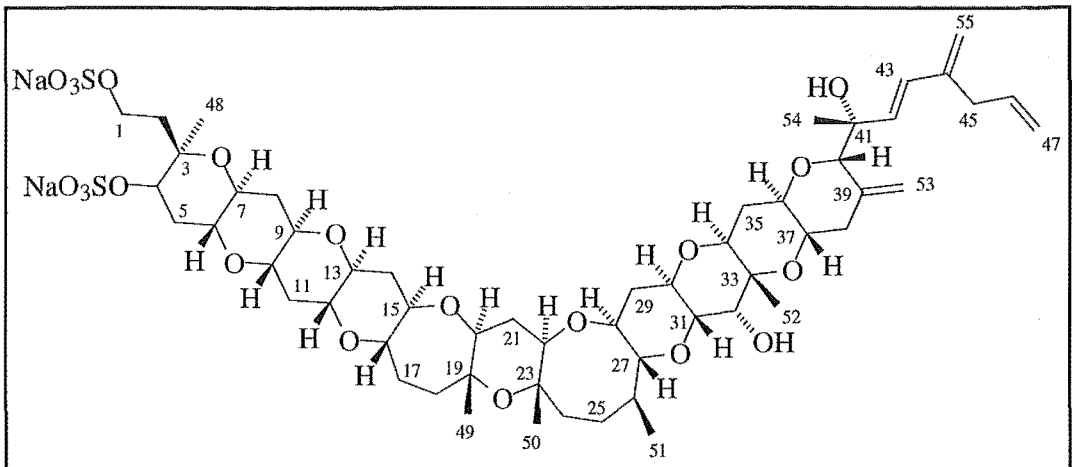

YTX (**19**)

The ^{1}H NMR spectrum of YTX (Fig 3.2.1) contained many overlapping peaks, especially in the ether and aliphatic regions. This required the use of COSY and HMQC experiments to elucidate some proton data assignments.

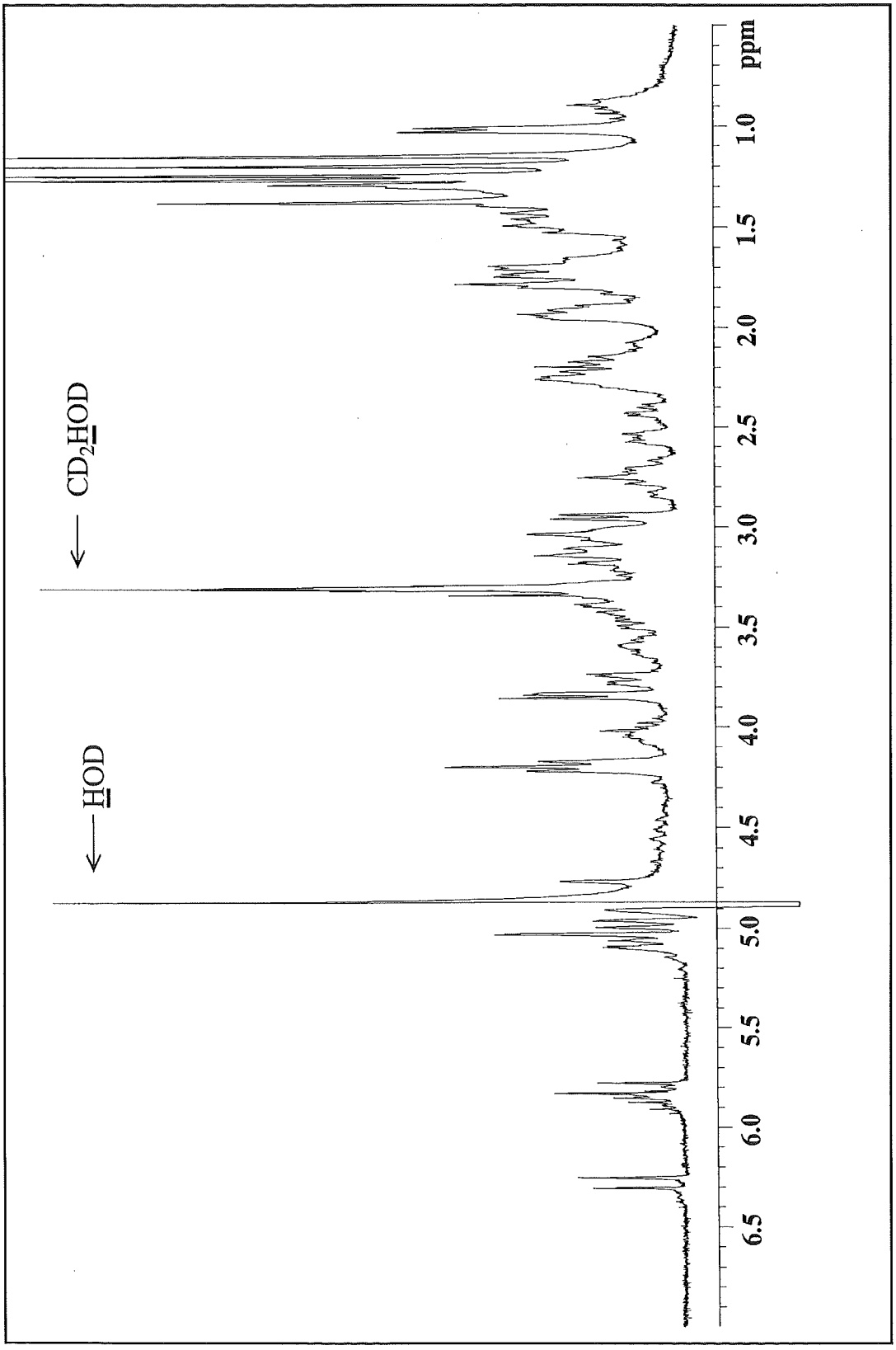

Fig 3.2.1 *^1H NMR Spectrum of Yessotoxin*

(CD_3OD)

The olefinic resonances δ 5.85 (H46), δ 6.27 (H43) and δ 5.81 (H42) ppm were well isolated and assigned by direct comparison with published data. The COSY spectrum showed correlations from δ 5.85 (H46) to two further resonances at δ 5.03 and 2.95 ppm, completing the H45-H47 spin system and allowing the assignment of both H47 as δ 5.03/5.03 and H45 as δ 2.95/2.95 ppm.

All six methyl resonances in the ^{1}H NMR spectrum were assigned conclusively by observation of $^{1}J_{CH}$ couplings, from their respective carbon atoms, in an HMQC experiment.

Geminal coupling between proton resonances at δ 5.07 and 4.96 ppm in the COSY spectrum suggested their assignment as an olefinic methylene. Assignment of these resonances as H55 was achieved by observation of an allylic COSY correlation to δ 2.95 (H45). The remaining olefinic resonances at δ 5.00 and 4.77 ppm, exhibited geminal coupling to each other and were assigned as H53.

Proton resonances at δ 4.05, 3.86, 3.84 and 3.76 ppm were well removed from other signals in the ^{1}H NMR spectrum. Consequently they were assigned by direct comparison with literature values as H36, H40, H32 and H34 respectively. Similarly, the proton resonances, belonging to the H38 methylene (δ 2.73/2.42 ppm), were well removed and assigned by direct comparison with the published data. The spin system H38-H34 was defined by the COSY spectrum, allowing the assignment of protons H37 (δ 3.40), H36 (δ 4.05), H35 (δ 2.07/1.47 ppm) and H34 (δ 3.80). The spin system H32-H24 was also unravelled by the COSY spectrum, in conjunction with comparisons with

published proton chemical shift data, leading to the assignment of all protons in that system (Table 3.2.2).

Resonances at δ 4.19 (H1) and δ 4.22 (H4) were well removed from other resonances in the ^{1}H NMR spectrum and were assigned by direct comparison with published data. COSY correlations from δ 4.19 (H1) to two other resonances at δ 2.30/1.90 ppm, were observed and assigned as the methylene protons belonging to H2. COSY correlations from δ 4.22 (H4) established the spin system only as far as H6 (Table 3.2.2). This was due to inadequate resolution of signals, close in chemical shift, which lay further along the spin system. An attempt at solving the spin system by the use of an HMBC (*H*eteronuclear *M*ulti*B*ond *C*oherence) NMR experiment was unsuccessful. The small amount of toxin was the major contributing factor as poor quality data was obtained in the HMBC experiment. This made further structural assignments by this method impossible.

The proton resonances that could be assigned, are summarised in Table 3.2.2. The small differences, between the observed and published data, are presumably a result of concentration or temperature effects.

Table 3.2.2 *Comparisons Between Published* $(H_p)^{24}$ *and Observed* (H_o) ^1H *NMR Data for YTX*

Position	δ Hp	δ Ho	Position	δ Hp	δ Ho	Position	δ Hp	δ Ho
1	4.24	4.19	**17**	1.84		**36**	4.09	4.05
1	4.24	4.19	**18**	1.89		**37**	3.43	3.40
2	2.21	2.30	**18**	1.83		**38**	2.75	2.73
2	1.99	1.90	**20**	3.46		**38**	2.47	2.42
4	4.26	4.22	**21**	1.97		**40**	3.92	3.86
5	1.77	1.70	**21**	1.79		**42**	5.86	5.81
5	2.60	2.55	**22**	3.53		**43**	6.35	6.27
6	3.09	3.10	**24**	1.77	1.75	**45**	3.00	2.95
7	3.36		**24**	1.54	1.50	**45**	3.00	2.95
8	2.22		**25**	1.75	1.75	**46**	5.91	5.85
8	1.44		**25**	1.51	1.50	**47**	5.12	5.03
9	3.18		**26**	1.74	1.65	**47**	5.10	5.03
10	3.16		**27**	2.81	2.75	**48**	1.31	1.25
11	2.30		**28**	3.34	3.30	**49**	1.29	1.24
11	1.45		**29**	2.32	2.25	**50**	1.20	1.14
12	3.06		**29**	1.58	1.49	**51**	1.74	1.01
13	3.12		**30**	3.64	3.61	**52**	1.25	1.19
14	2.34		**31**	3.22	3.25	**53**	5.05	5.00
14	1.47		**32**	3.89	3.84	**53**	4.84	4.77
15	3.37		**34**	3.80	3.76	**54**	1.43	1.37
16	3.26		**35**	2.14	2.07	**55**	5.09	5.07
17	1.99		**35**	1.53	1.47	**55**	5.01	4.96

All δ values expressed in ppm. Solvent (CD_3OD) referenced to δ 3.30 ppm

3.3 Stereochemical Assignment of YTX

3.3.1 Desulfation of YTX

The quality of the NMR data acquired on YTX was insufficient to carry out a stereochemical study. In addition to dealing with small amounts of sample, the data quality was affected by the need to use CD_3OD as the NMR solvent. This was a consequence of the insolubility of YTX in $CDCl_3$. The insolubility of YTX in $CDCl_3$ is an inevitable result of the two sulfate functional groups at C1 and C4.

Removal of the sulfate groups was achieved by refluxing YTX in a solution of 50% pyridine/1,4-dioxane. After work-up, 0.8 mg of pure desulfated YTX, was achieved. The desulfated YTX used in this study is hereafter referred to as D-YTX (**44**).

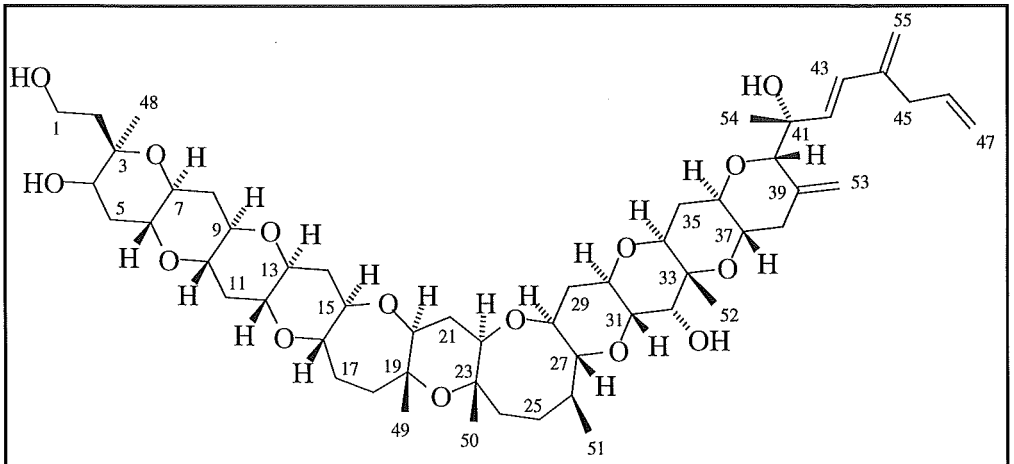

D-YTX (**44**)

3.3.2 Spectroscopic Assignment of D-YTX

Positive ion LRFABMS on D-YTX revealed a base peak at *m/z* 965.5, assigned as $[M\text{-}H_2O+H]^+$. Subsequent HRFABMS was performed on this ion, (accurate mass 965.5619 corresponding to $C_{55}H_{81}O_{14}$, $[M\text{-}H_2O+H]^+$). From this, a molecular formula of $C_{55}H_{82}O_{15}$ was confirmed for D-YTX.

The low sample mass restricted the use of NMR experiments solely to ^1H nuclei. As a result, a multitude of ^1H based NMR experiments were carried out on D-YTX, including; ^1H, TOCSY (*TO*tal *C*orrelation *S*pectroscop*Y*), NOESY (*N*uclear *O*verhauser and *E*xchange *S*pectroscop*Y*) and selective 1D-TOCSY and NOE (*N*uclear *O*verhauser *E*ffect) experiments.

Proton assignments were made for rings G-K in the following manner:

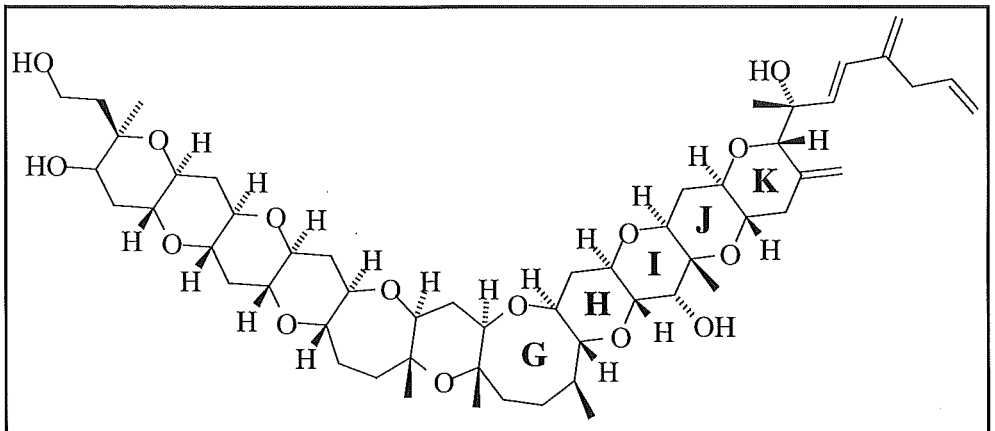

D-YTX (**44**)

The ^1H NMR spectrum of D-YTX showed slightly different chemical shifts, compared with those of YTX. The methyl peaks of D-YTX

were virtually identical in chemical shifts to those in YTX and, as such, were assigned by direct comparison. The olefinic region of D-YTX was also assigned predominantly by comparison with that of YTX (Fig 3.3.1). However, a TOCSY experiment was needed to locate H53 (δ 5.09), which was concealed by the H47 resonances (δ 5.09). The TOCSY spectrum was also used to assign both H55 methylene protons at δ 5.04/5.01.

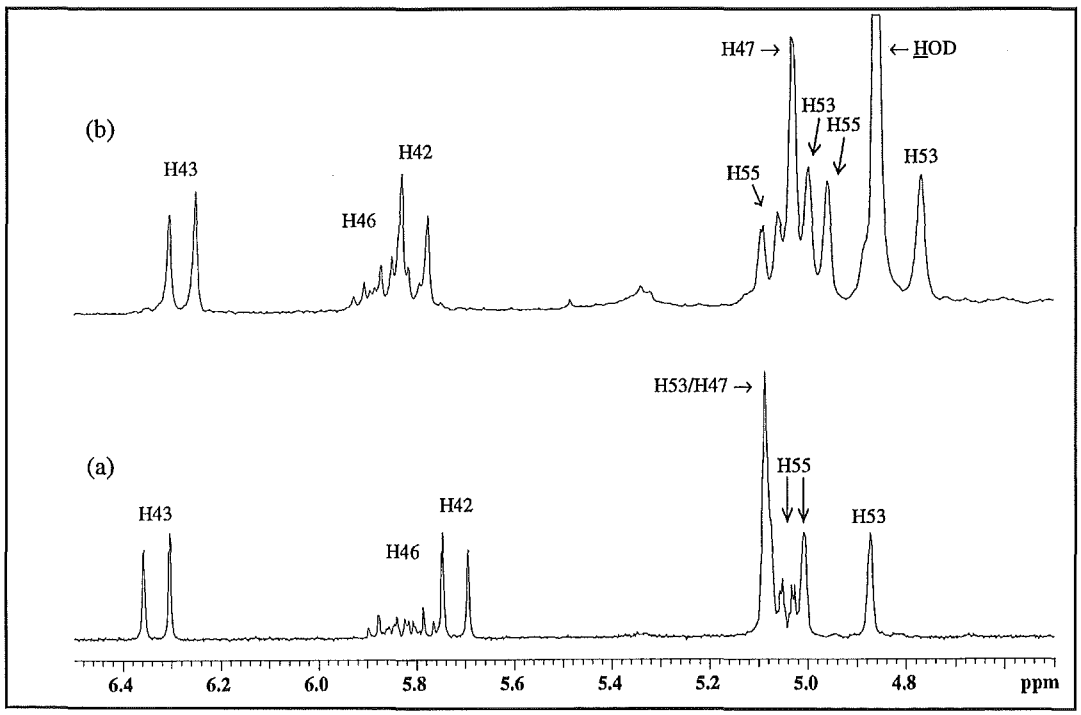

Fig 3.3.1 *^{1}H NMR Spectra of Olefinic Regions of (a) D-YTX and (b) YTX*

The major difference between the ^{1}H NMR spectra of D-YTX and YTX, was in the region 4.5-1.5 ppm (Fig 3.3.2). In the spectrum of D-YTX, the resonances H1 and H4 had moved substantially upfield to around δ 3.8. These upfield chemical shifts are consistent for the cleavage of the sulfate groups and comply with previously published data.[24] The proton resonances δ 3.94 (H40), δ 3.90 (H32), δ 2.73

(H27) and δ 2.49 (H38), were well resolved and able to be assigned by direct comparison with those in YTX (Fig 3.3.2). The latter three proton positions served as ideal entry points for both 2D and 1D TOCSY NMR experiments, allowing the assignment of the other resonances in rings G-K.

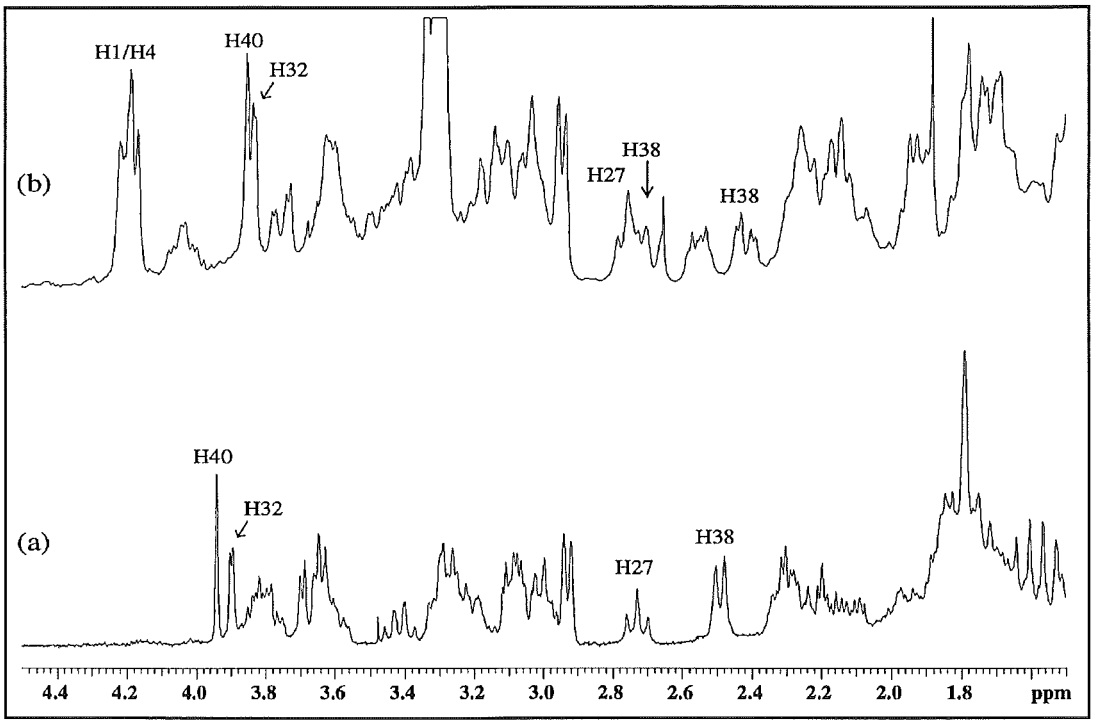

Fig 3.3.2 *^{1}H NMR Spectra of Ether Regions of (a) D-YTX and (b) YTX*

Long range allylic coupling was observed in the 2D TOCSY spectrum from the exocyclic methylene at δ 5.09/4.87 (H53), to the methylene at δ 2.49 (H38). A trace through the resonance at δ 2.49 (H38), revealed correlations to δ 5.09, 4.87 (H53) and further unassigned resonances δ 3.80, 3.68, 3.42, 2.11 and 1.57. A 1D TOCSY experiment, using excitation at δ 2.49 (H38) and different mixing times (Fig 3.3.3), was used to solve the sequence of resonances in the spin system H38-H34.

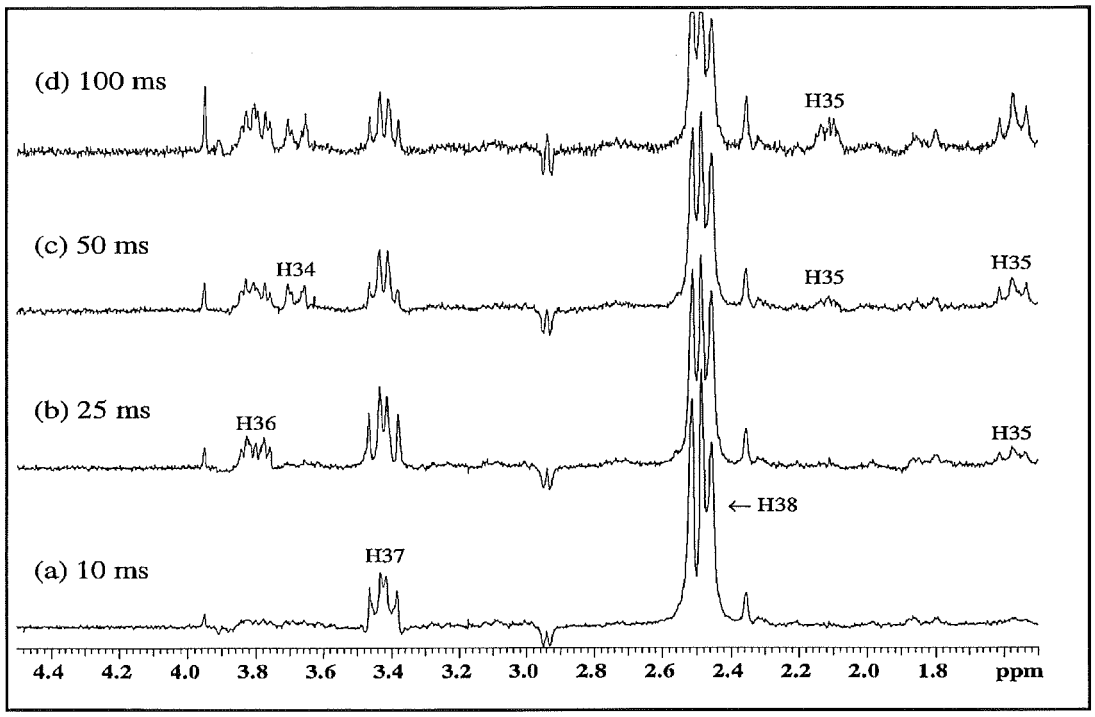

Fig 3.3.3 *1D TOCSY Spectrum of D-YTX With Excitation At H38 and Mixing Times of (a) 10 ms, (b) 25 ms, (c) 50 ms and (d) 100 ms*

At a mixing time of 10 ms (Fig 3.3.3(a)), one strong correlation to δ 3.42 was observed and assigned as H37. At 25 ms (Fig 3.3.3(b)), additional strong correlations could be seen for δ 3.80 and weak correlations for δ 1.57. These were assigned as H36 methine and one diastereotopic H35 methylene proton respectively. At 50 ms (Fig 3.3.3(c)), a further correlation appeared at δ 3.68 (H34). In addition, the resonance at δ 1.57 (H35) was of increased strength and a weak signal, at δ 2.11 (H35), was observed. The trace, at a mixing time of 100 ms (Fig 3.3.3(d)), confirmed the correlation to δ 2.11 (H35). This completed the assignment of the spin system H38-H34.

The doublet at δ 3.90 was assigned as H32 by direct comparison with YTX (Fig 3.3.2). The 2D TOCSY spectrum revealed correlations from this resonance to δ 3.61, 3.23, 3.11, 2.31 and 1.56 ppm. A

second 1D TOCSY, using excitation at δ 3.90 (H32), was used to assign the sequence of resonances along the spin system (Fig 3.3.4).

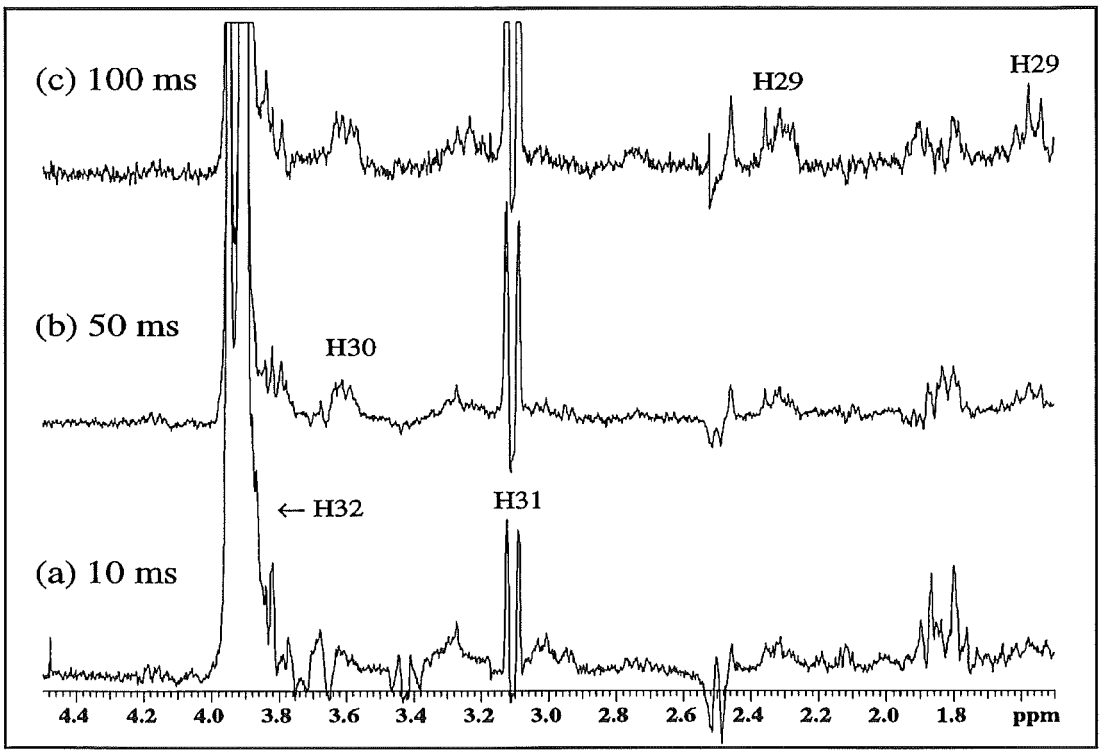

Fig 3.3.4 *1D TOCSY Spectrum of D-YTX, With Excitation At H32 and Mixing Times of (a) 10 ms, (b) 50 ms and (c) 100 ms*

At a mixing time of 10 ms (Fig 3.3.4(a)), a strong correlation was observed to δ 3.11 and assigned as H31. At 50 ms (Fig 3.3.4(b)) an additional correlation was observed to δ 3.61, accordingly assigned as H30. At 100 ms (Fig 3.3.4(c)), further correlations were observed to δ 2.31/1.56 (H29). No further correlations were observed from H32.

The triplet at δ 2.73 was assigned as H27, by direct comparison with YTX (Fig 3.3.2). The 2D TOCSY spectrum showed correlations from this resonance to δ 3.61, 3.23, 3.11, 2.31, 1.83, 1.71, 1.57 and 1.01 ppm. The sequence of resonances within the spin system were solved

by a third 1D TOCSY experiment, using excitation at δ 2.73 (H27) (Fig 3.3.5) and various mixing times.

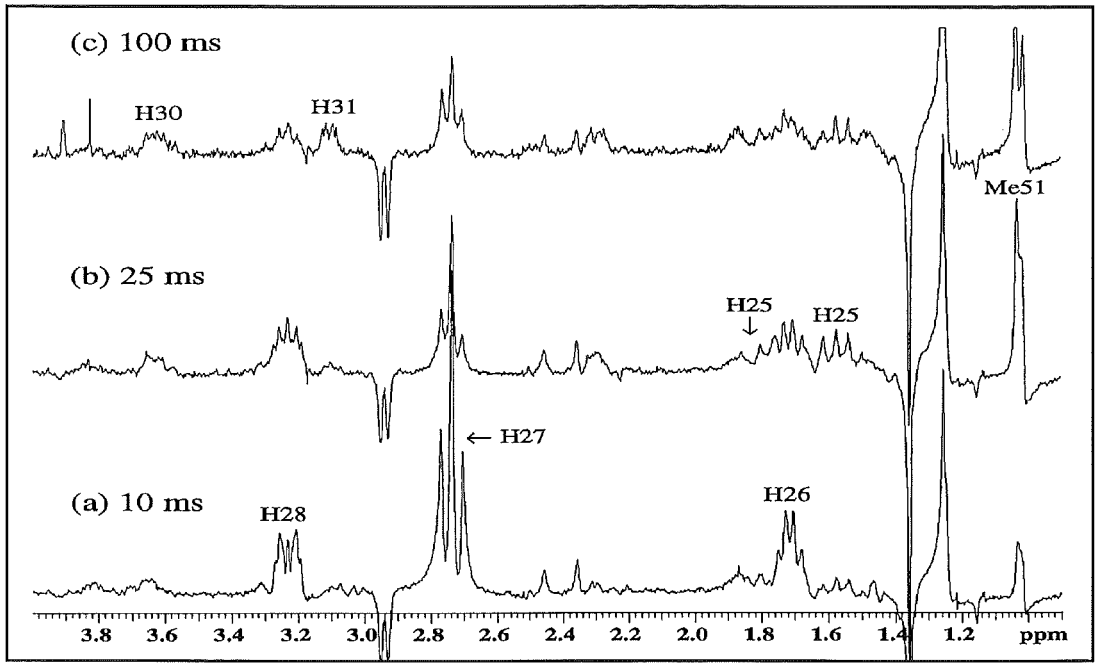

Fig 3.3.5 *1D TOCSY Spectrum of D-YTX, With Excitation At H27 and Mixing Times of (a) 10 ms, (b) 25 ms and (c) 100 ms*

At a mixing time of 10 ms (Fig 3.3.5(a)), strong correlations were observed to δ 3.23 and 1.71 ppm, hence assigned as H28 and H26 respectively. The experiment at 25 ms (Fig 3.3.5(b)), showed additional correlations to δ 1.57, 1.83 (H25) and 1.01 ppm, the doublet Me51. At 100 ms (Fig 3.3.5(c)), additional correlations were observed to δ 3.61 (H30) and δ 3.11 (H31). Collation of the above data assigned the complete spin system, H32-H25.

3.3.3 Conformations of Rings G-K In D-YTX

Conformational elucidation for rings G-K of D-YTX was made by measurement of observed coupling constants. Estimation of dihedral angles, from coupling constants, was achieved by consideration of the Karplus equation.[81]

Analysis of the coupling constants between protons on rings G-K, was achieved by direct measurement of well resolved signals in the ^{1}H NMR spectra and by measurement of signals, resolved by 1D TOCSY traces. In addition, various couplings were "removed" in 1D TOCSY experiments, by the decoupling of selected resonances during the acquisition of data. This simplified some multiplets and allowed assessment of coupling patterns. The measurement of coupling constants could then be achieved both for the simplified multiplet and, by subtraction, the coupling removed.

The conformation of ring K was proposed in the following manner: The resonance at δ 3.42 (H37) was well resolved in the ^{1}H NMR spectrum of D-YTX (Fig 3.3.2). The vicinal $^3J_{HH}$ couplings were measured as 8.9, 7.2 and 9.4 Hz. A 1D TOCSY experiment was run with excitation at δ 2.49 (H38) and selective decoupling at δ 3.80 (H36) (Fig 3.3.6(a)), 3.42 (H37) (Fig 3.3.6(b)), 2.11 (H35) (Fig 3.3.6(c)) and 1.57 (H35) (Fig 3.3.6(d)).

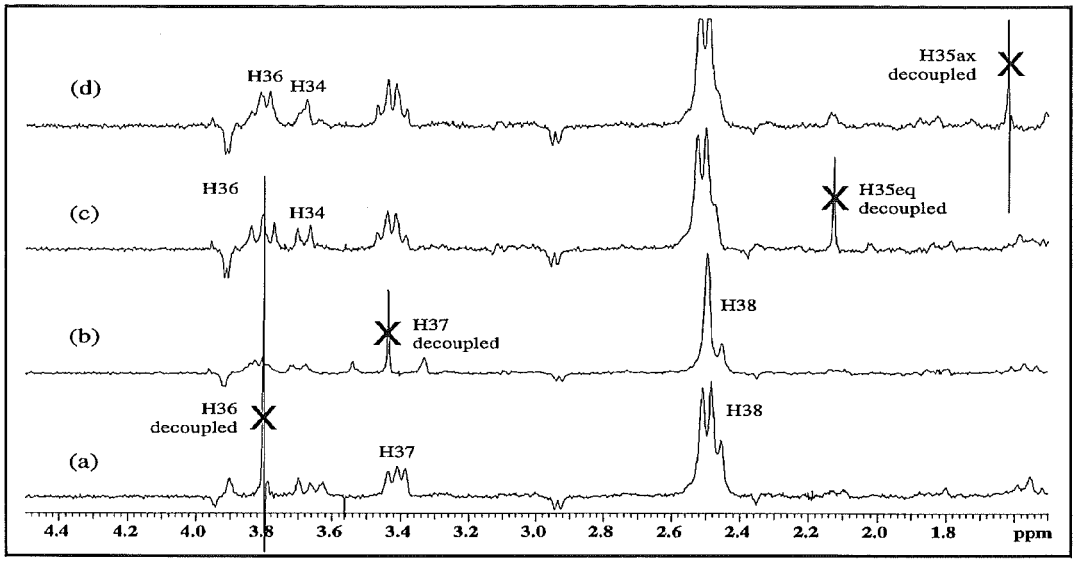

Fig 3.3.6 *1D TOCSY Spectrum of D-YTX With Excitation At H38 and Decoupling At (a) H36, (b) H37, (c), H35eq and (d) H35ax*

Decoupling at δ 3.80 (H36) (Fig 3.3.6(a)) collapsed δ 3.42 (H37) to a triplet (J = 7.9, 7.6), with the couplings assigned as $^3J_{H37H38ax}$ and $^3J_{H37H38eq}$. By subtraction, the coupling of $^3J_{H37/H36}$ was shown as large and approximately 8.5 Hz. This corresponds most closely to a dihedral angle of *ca.* 180° and, consequently, a *trans*-linked ring junction at H36/H37. The approximately equal couplings, of *ca.* 8 Hz for both $^3J_{H37H38ax}$ and $^3J_{H37H38eq}$, are not consistent with a chair conformation for ring K. In particular, the $^3J_{H37H38eq}$ coupling constant would be expected to be small due to the dihedral angle being close to 90° for these protons. A more plausible explanation would be if ring K adopted a twisted chair conformation as shown in Fig 3.3.7.

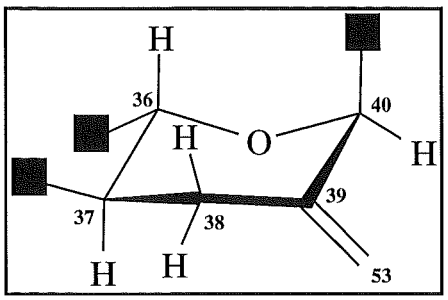

Fig 3.3.7 *Proposed Conformation of Ring K of D-YTX*

The dihedral angles of the H37/H38 protons are more clearly shown by the Newman projections (Fig 3.3.8) of both the chair (Fig 3.3.8(a)) and twisted chair (Fig 3.3.8(b)) conformations for ring K. The dihedral angle of H37/H38eq is close to 90° for the chair conformation, however is close to 0° for the twisted chair conformation.

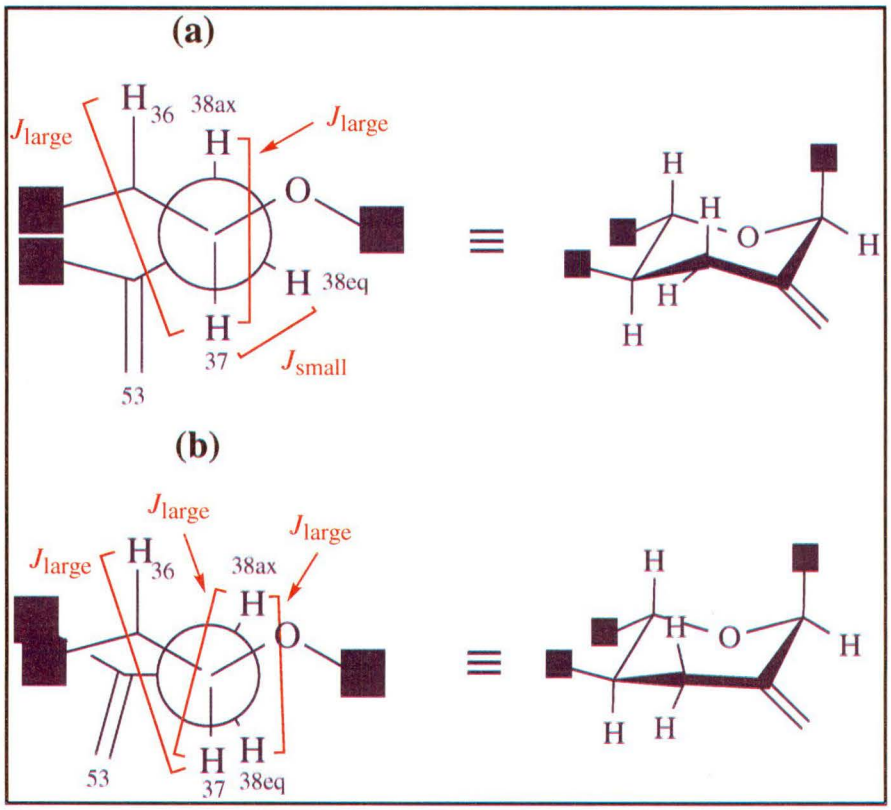

Fig 3.3.8 *Newman Projections for (a) Chair and (b) Twisted Chair Conformations for Ring K of D-YTX*

Decoupling at δ 3.42 (H37) (Fig 3.3.6(b)) collapsed δ 2.49 (H38) to a singlet, revealing the vicinal $^3J_{H38H37}$ coupling of 7.3 Hz.

The conformation of ring J was proposed as follows:
Decoupling at δ 2.11 (one diastereotopic H35) (Fig 3.3.6(c)), gave rise to no significant changes in the appearance of multiplets δ 3.80 (H36)

and δ 3.68 (H34). This showed small couplings from H36 and H34 to δ 2.11, assigning this resonance as equatorial H35. This was supported by decoupling at the other H35 resonance (1.57 ppm) (Fig 3.3.6(d)), which led to the collapse of δ 3.80 (H36) to a doublet and δ 3.68 (H34) to a singlet, assigning δ 1.57 as axial H35. The coupling seen in the doublet δ 3.80 J = 8.0, could only be explained by a *trans* orientation from H37 to H36, further supporting the *trans*-linked ring junction at this position. The collapse of the multiplet δ 3.68 (H34) to a singlet, revealed the coupling of $^{3}J_{H34H35ax}$ was 11.5 Hz and hence H34 as axial. The conformation best fitting the above data for ring J, is a chair conformation.

The conformation of ring I was proposed as follows:
A second 1D TOCSY experiment was run, using excitation at δ 3.90 (H32), with decoupling at δ 3.61 (H30) (Fig 3.3.9). The decoupling led to the collapse of δ 3.11 (H31) to a non resolvable doublet ($^{3}J_{H31H32}$ *ca.* 1 Hz). This revealed a large $^{3}J_{H30H31}$ coupling and, consequently, a *trans* ring junction between H30 and H31. This $^{3}J_{H31H32}$ requires H32 to be in an equatorial orientation, with the hydroxyl group axial. The conformation best fitting the above data for ring I, is a chair conformation.

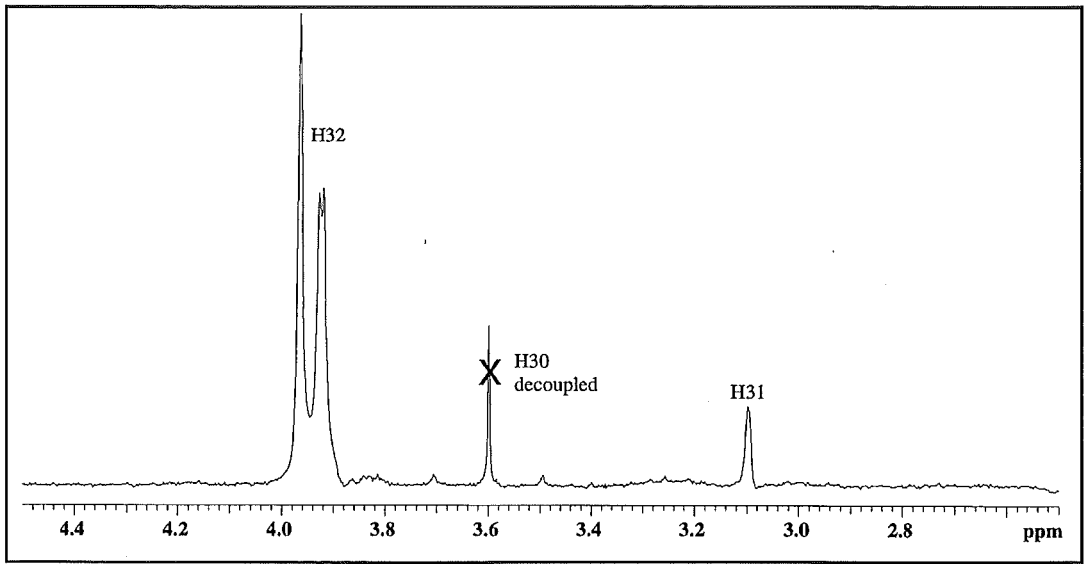

Fig 3.3.9 *1D TOCSY Spectrum of D-YTX, With Excitation At H32 and Decoupling of H30*

The conformation of ring H was proposed in the following way:
A 1D TOCSY experiment, using excitation at δ 2.73 (H27) and decoupling at δ 1.56 (one diastereotopic H29) (Fig 3.3.10), led to the collapse of δ 3.23 (H28) to a doublet, revealing large coupling of $^{3}J_{H27H28}$ and, consequently, a *trans* ring junction between H27 and H28. The coupling from H28 to H29 was large and removed by decoupling of δ 1.56. This lead to the assignment of δ 1.56 as the axial proton at C29 and, consequently, δ 2.31 as equatorial H29.

Again, the data best fits a chair conformation for ring H.

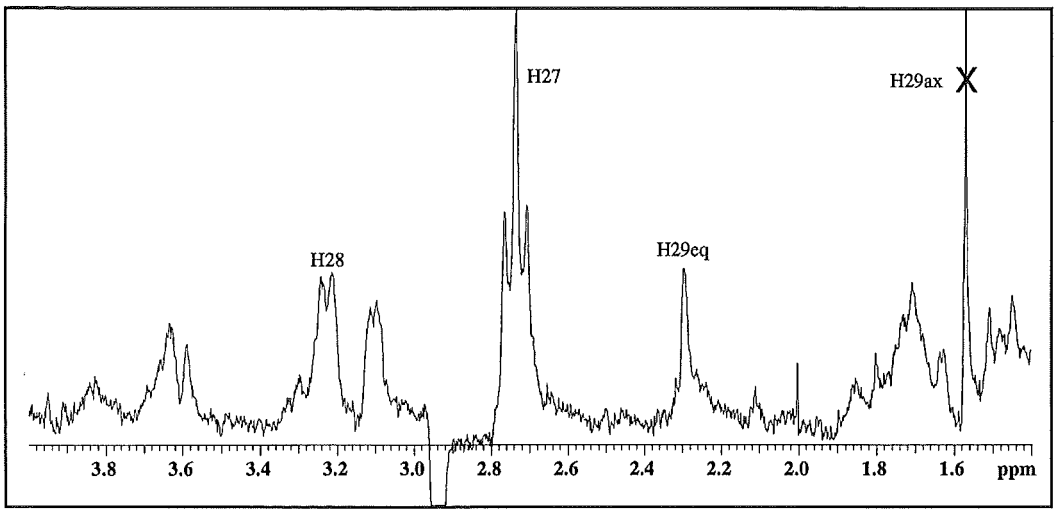

Fig 3.3.10 *1D TOCSY Spectrum of D-YTX, With Excitation At H27 and Decoupling of H29ax*

This implies that the three *trans*-linked rings all have chair conformations, as shown in Fig 3.3.11.

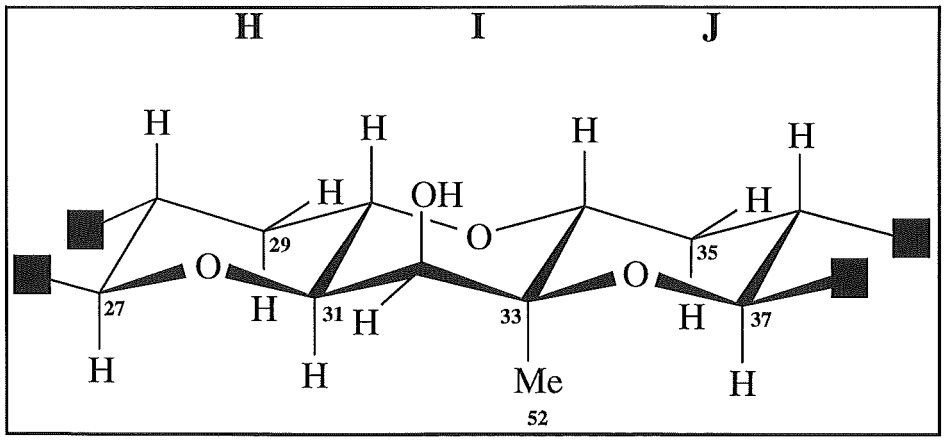

Fig 3.3.11 *Proposed Conformations of Rings H-J of D-YTX*

The assignment of the conformation of ring G is more complex, as it is an 8 membered ring and the chemical shift values of the methylenes H24 and H25 are identical. The resonance at δ 2.73 (H27) showed two large couplings, J = 9.3, 8.8. One of the couplings was previously assigned as arising from the $^{3}J_{H27H28}$ trans-ring junction. The other is

best explained by an approximate 180° orientation to δ 1.71 (H26), assigning H26 as *pseudo*-trans. No other useful data from ring G could be obtained from 1D TOCSY experiments, due to the proximity of the chemical shifts of the key protons.

The coupling constants, revealed by decoupled 1D TOCSY experiments, are summarised in Fig 3.3.12. These show large coupling (7-11 Hz) and small coupling (1-2.5 Hz).

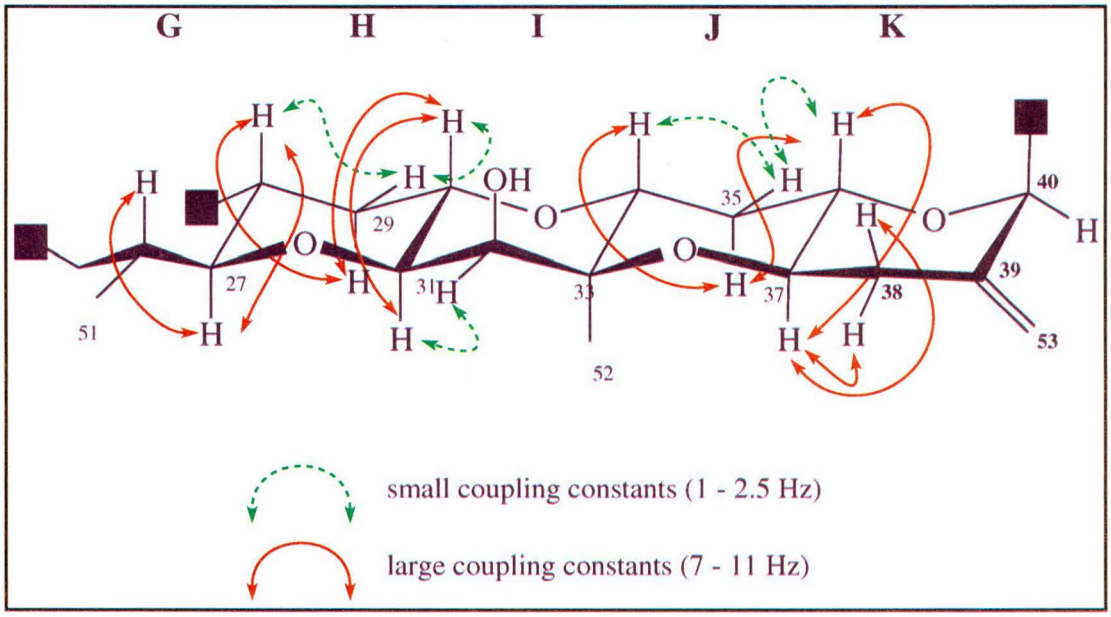

Fig 3.3.12 *Coupling Constants of Protons on Rings G-K*

The conformations of rings H-K were verified by selective NOE experiments on isolated resonances (Table 3.3.1). In addition, a 2D NOESY experiment was used to examine enhancements over the whole chemical shift range and, in particular, between signals that were not well separated (Table 3.3.2).

Table 3.3.1 *Selected Difference NOE Enhancements (%) for D-YTX*

From/To					
Me54	H53† (1.23)	H43 (4.01)	H42 (3.42)	H40 (5.89)	
Me52	H37 (6.60)	H32 (4.34)	H31 (1.28)		
H53†	H53° (4.39)	H40 (2.86)			
H45	H55˅ (2.00)	H47 (*)	H46 (4.62)	H42 (5.14)	
H43	Me54 (0.38)	H47 (*)			
H42	Me54 (0.41)	H45 (2.57)	H40 (1.78)	H38 (0.76)	H36 (0.81)
H40	Me54 (0.72)	H53 (1.27)	H42 (1.74)		
H38	H55^ (1.20)	H53 (*)	H43 (1.98)	H42 (2.09)	H37 (3.79)
H32	Me52 (0.96)	H31 (1.34)			
H27	H31 (1.41)				

* % enhancement unknown
† H53 at δ 4.87 ppm only
° H53 at δ 5.09 ppm only
˅ H55 at δ 5.01 ppm only
^ H55 at δ 5.04 ppm only

Selective irradiation at δ 1.20 (Me52), in an NOE experiment, enhanced signals at δ 3.11 (H31) and 3.42 ppm (H37) (Table 3.3.1), supporting an all axial arrangement for these protons and, consequently, chair conformations for rings I and J. Enhancement of the signal at δ 3.90 (H32) (Table 3.3.1), in the same experiment, showed further evidence for the placement of this proton as equatorial and the hydroxyl group as axial. A trace through the same resonance in a NOESY experiment, revealed an extra enhancement to δ 1.57 ($H35_{ax}$) (Table 3.3.2), further supporting the assignment of this proton as axial.

Table 3.3.2 *2D NOESY Correlations for D-YTX*

From/To						
H55	H46	H45				
Me54	H53†	H43	H42	H40	H36	
H53†	Me54	H53°	H40			
Me52	H37	H35˅	H32	H31		
Me51	H27	H26	H25^			
H47/H53°	H53†	H38				
H46	H47	H45				
H45	H55	H42				
H43	Me54	H47	H42			
H42	Me54	H45	H43	H40	H38	H36
H40	H53†	H42				
H38	H37					
H37	Me52	H38				
H32	Me52	H31	H29			
H31	Me52	H32	H27			
H27	Me51	H31				

† H53 at δ 4.87 ppm only
° H53 at δ 5.09 ppm only
˅ H35 at δ 1.57 ppm only
^ H25 at δ 1.57 ppm only

The enhancement of δ 3.11 (H31), by selective irradiation of δ 2.73 (H27) (Table 3.3.1) in an NOE experiment, further supported the all chair conformation of rings H, I and J. Additionally, the NOESY spectrum showed correlations between δ 2.73 (H27) and δ 1.01 (Me51) (Table 3.3.2), supporting the placement of Me51 as equatorial in ring G.

The orientation around C41 was solved by use of NOE and NOESY experiments. Selective irradiation at δ 1.35 (Me54), in an NOE

experiment, gave enhancements to δ 6.33 (H43), 5.72 (H42) and 3.94 (H40) (Table 3.3.1) and a correlation to δ 3.85 (H36) (Table 3.3.2) was observed in the NOESY spectrum. Similarly, selective irradiation from δ 5.72 (H42), in another NOE experiment, revealed enhancements to δ 3.94 (H40) and 3.85 (H36) (Table 3.3.1). These data indicated that Me54, H40 and the H42/H43 double bond all lie in one plane of the C41/C40 bond, with the hydroxyl group in the opposite (Fig 3.3.13).

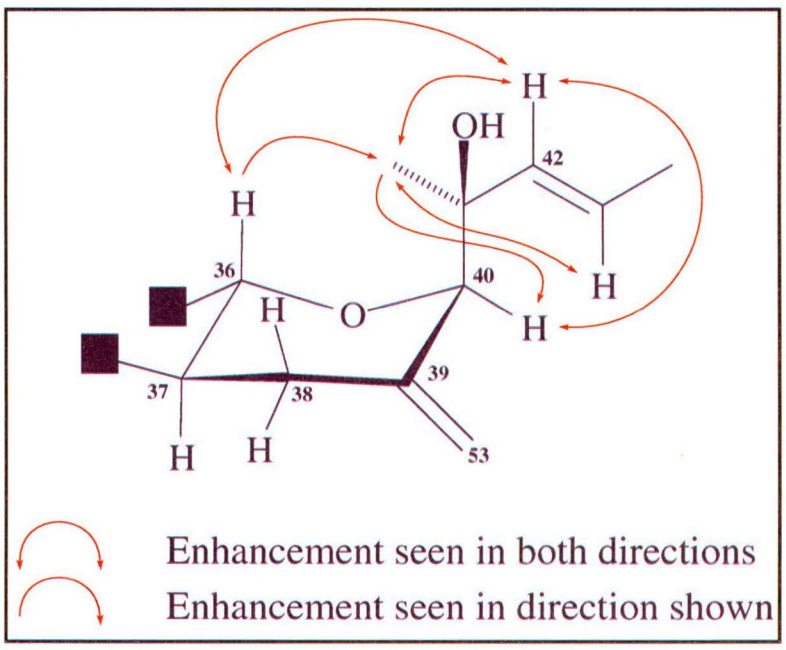

Fig 3.3.13 *Orientation around C41 of D-YTX as Described by NOE and NOESY Enhancements*

The recent publication of the relative stereochemistry of YTX by Sataki *et al*,[31] provided data complementary to that obtained in this research.

The all-*trans* conformation of rings G-K, proposed in this thesis, was consistent with published data. Furthermore, the all-*trans* relationship

was shown to be present in all rings, a phenomena consistent with the brevetoxin backbone.

However, one inconsistency arose from the comparison of observed and published data. A chair conformation for ring K is not in accordance with the apparent quartet observed for H37. The three large vicinal couplings (*ca.* 8 Hz) of H37 are best explained by a twisted chair conformation proposed here.

It was necessary to consider whether there was a conformational change upon desulfation. This was addressed by a trace through the 2D TOCSY spectrum of YTX at δ 2.70 (H38) (Fig 3.3.14). This trace revealed the apparent quartet of H37, seen for D-YTX. Hence these data provided evidence for the twisted chair conformation of ring K in YTX.

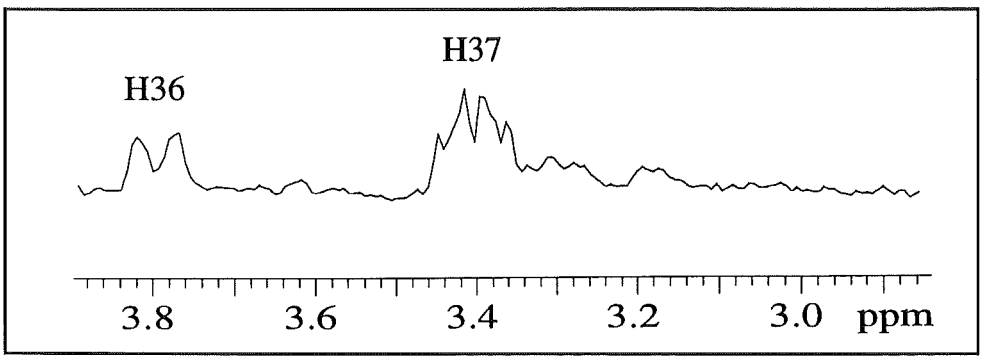

Fig 3.3.14 *Trace Through 2D TOCSY Spectrum of YTX Revealing Resonances for H36 and H37*

3.4 Design and Synthesis of YTX Haptens

3.4.1 Design

Yessotoxin (YTX, **19**) contains two likely positions for the attachment of linker groups suitable for the synthesis of haptens. The sulfate groups provide indirect positions for attachment. Attachment may be achieved through the hydroxyl groups formed by desulfation or amino groups formed by aminolysis. The olefinic "tail" on YTX is amenable to cleavage by ozone. The product(s) formed provide useful linker sites at this end.

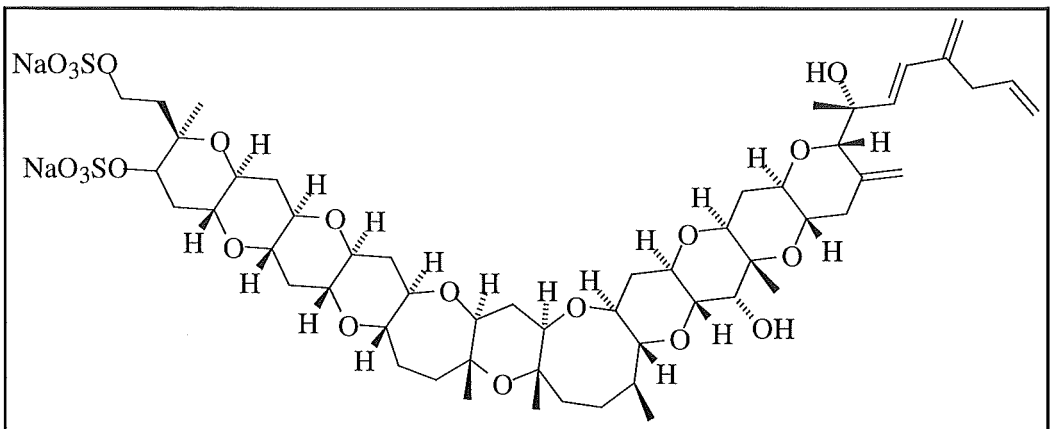

YTX (**19**)

Desulfation of YTX is an established procedure and had already been achieved as part of this research (Section 3.3.1). The linker group chosen was *p*-maleimidophenyl isocyanate (PMPI, **45**).

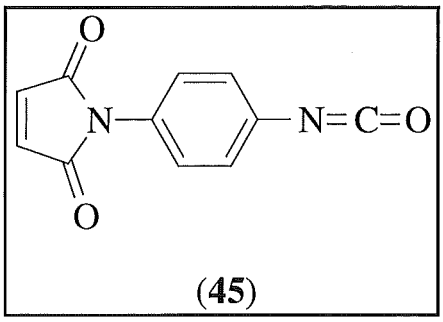

(45)

PMPI was selected as the linker group because the maleimide provides a linker for selective attachment to sulfhydryl (S-H) residues on proteins.

Substitution of the sulfate groups can be achieved with an appropriate nucleophile. An amine provides an ideal nucleophile as the product formed is an amino group (Fig 3.4.1). Due to this amino group, coupling to the carboxylic acid terminus of a protein then becomes possible.

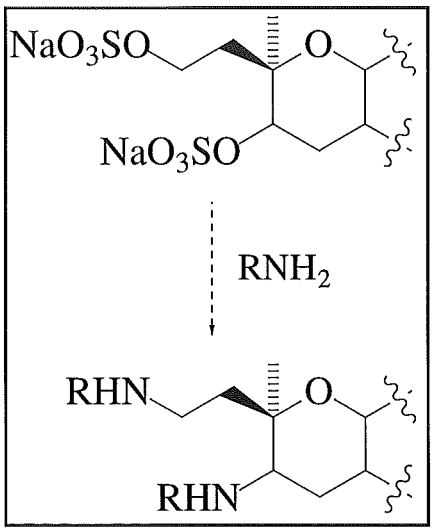

Fig 3.4.1 *Proposed Aminolysis of Sulfate Groups On YTX*

Ammonia was selected for aminolysis as the probable product would be either a mono or di primary amine. In addition, glycine provides a

mono/di carboxylic acid for linkage and was also selected for this reason.

Ozonolysis is a commonly used procedure for cleavage of carbon-carbon double bonds.[82] The product(s) formed are dictated by the work-up procedure. A reductive work-up typically yields ketones and aldehydes, whereas an oxidative work-up usually produces carboxylic acids. The likely aldehyde produced after reductive work-up (Fig 3.4.2) can be conjugated in high yields to the amino terminus of a protein.[83]

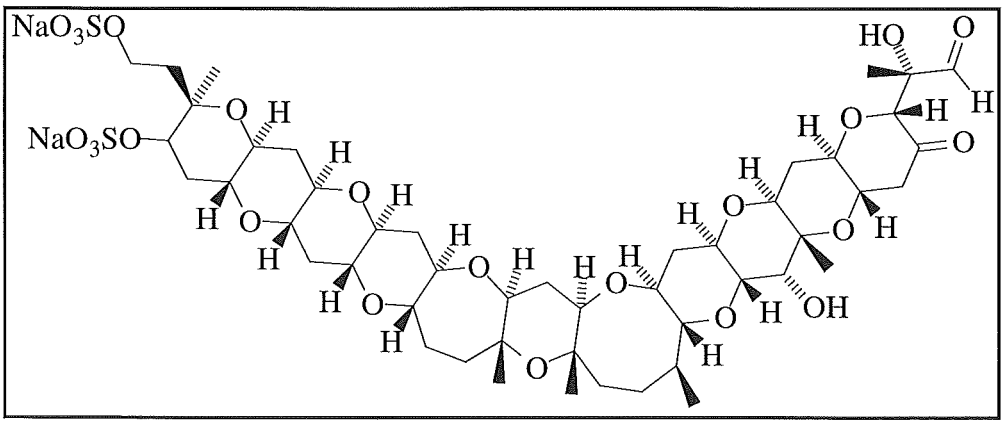

Fig 3.4.2 *Likely Product from Ozonolysis of YTX*

3.4.2 Syntheses

PMPI

Desulfation of YTX was carried out previously and is described in Section 3.3.1. The product formed, D-YTX (**44**) was reacted with PMPI, under anhydrous conditions, in a sealed glass NMR tube.

Analysis of the reaction progress was made by ^{1}H NMR spectroscopy, with particular examination of the emergence of signals around 4 ppm, which are indicative of protons adjacent to carbamate moieties. After 24 hours, baseline resonances were observed in the region 4.2 - 4.4 ppm. The intensities of these resonances increased slowly over time and after 167 hours no further apparent change was observed in the spectrum.

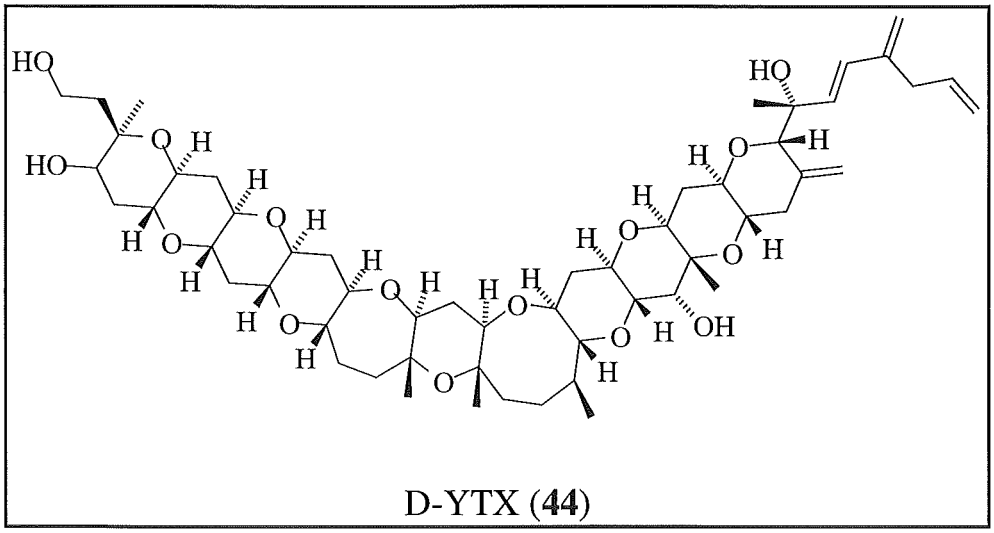

D-YTX (**44**)

The dichloromethane soluble products were purified on reverse phase C8 HPLC, using acetonitrile/water gradient elution. Eleven fractions were collected and those showing UV absorbance at above 250 nm were analysed by ^{1}H NMR spectroscopy.

The NMR spectra all showed degradation of the olefinic side chain. Fraction 5 showed aromatic peaks consistent with one PMPI moiety. However, fractions 6, 7 and 8 all showed indiscernible multiples of these resonances. This gave evidence for the attachment of the PMPI linker at multiple hydroxyl groups.

The degraded olefinic side chain would probably provide significant effects for the recognition by an immunogen. Hence this degradation was considered disadvantageous for the success of these haptens in an immunoassay.

Aminolysis

The reaction between YTX and 50% ammonia/MeOH was carried out at room temperature, in a sealed vial for 1 hour and all solvents removed. The ^{1}H NMR spectrum of the reaction product revealed that the resonances for H1 & H4 were still at δ 4.2. These data demonstrated that at least one sulfate group was still intact. However, the low sample mass prevented accurate integrals from being measured, hence not allowing the number of attached sulfate groups to be determined.

Analysis of this sample by reverse phase C18 TLC (*T*hin *L*ayer *C*hromatography) was undertaken. Spraying of these plates separately with Dragendorff's reagent and ninhydrin (Section 6.1.5) gave negative results. These data suggested that no amine group had been formed.

It was postulated that the aminolysis was slow at room temperature, based on the requirement of high temperatures (120 °C) for the hydrolysis of YTX. The incorporation of heat into the aminolysis could not be accompanied by the use of ammonia, due to its low boiling point. Hence, glycine was used.

Glycine was reacted with YTX at 60 °C (64 hours). After removal of solvents the reaction mixture was analysed by ^{1}H NMR spectroscopy. The spectrum showed the presence of at least one sulfate group indicated by the resonance at δ 4.2. The olefinic resonances of the molecule were diminished in intensity, giving evidence for degradation of the side chain.

The failure of the PMPI and aminolysis syntheses was attributed largely to the instability of the olefinic side chain. The success of using different reagents or conditions to achieve a linker at the sulfate end of the molecule was low.

Ozonolysis

An initial reaction of ozone and YTX was undertaken. Analysis of the reaction mixture by ^{1}H NMR spectroscopy revealed the complete cleavage of the carbon-carbon double bonds in YTX. This revelation was due to the absence of the olefinic proton resonances. The absence of an aldehyde peak and the presence of new resonances around 5.1 ppm was observed in the spectrum. In addition, a singlet at δ 3.60 was suggestive of a methoxy group. These data indicated that the aldehyde formed (**46**) had undergone acetal formation with methanol to form the hemiacetal (**47**). This hemiacetal may have then undergone intramolecular acetal formation to form the acetal (**48**) (Fig 3.4.3).

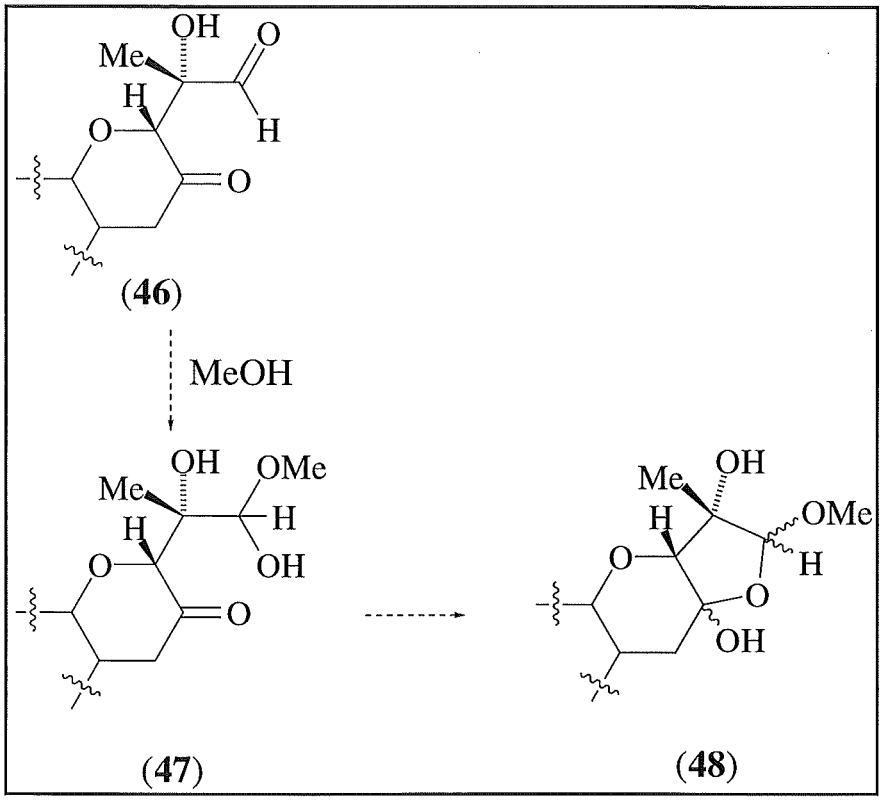

Fig 3.4.3 *Proposed Formation of The Hemiacetal (47) and Cyclic Acetal (48) from The Ozonolysis Product (46)*

Attempts at formation of the desired aldehyde (**46**) from the proposed acetal (**48**) were made with acetic acid. This proved unsuccessful with complete loss of material.

A second ozonolysis reaction was carried out on a "year old sample" of YTX. The reaction product formed was analysed by ^{1}H NMR spectroscopy. The spectrum did not show the expected resonances at around 5.1 ppm, suggesting that the hemiacetal/acetal had not been formed. The chance of the acetal proton coinciding with the HOD solvent peak was addressed. Consequently, the sample was analysed by mass spectrometry.

LRFABMS was performed on the sample. Negative ion FABMS and positive ion FABMS, with the addition of CsI was used. A molecular ion at *m/z* 1150 was postulated from these data. The negative ion FABMS spectra afforded a peak at *m/z* 1127, corresponding to $[M-Na]^-$. This data was supported by the positive ion CsI FABMS spectrum, which afforded a peak at *m/z* 1503, corresponding to $[M-2Na+3Cs]^+$.

The presence of doublets (2 mass units apart with a 1:1 intensity ratio) of the highest mass peaks, was observed in all spectra, characteristic of the presence of bromine (Br) in the molecule. This data was supported by the loss of 80 mass units (HBr) from *m/z* 1503 in the CsI spectrum, with a corresponding removal of the bromine pattern.

The incorporation of Br into the molecule was presumably a result of degradation over time. The YTX sample used for ozonolysis had been isolated 1 year previously. It was probable that the incorporation of Br over that time was due to a contaminant in the sample. The presence of Br rendered the molecule unsuitable for immuno-assay development. Consequently, the ozonolysis was repeated a third time on a newly isolated YTX sample.

The product formed from the third ozonolysis of YTX was analysed by ^1H NMR spectroscopy. The spectrum was similar to that of the second ozonolysis reaction, with no apparent acetal or aldehyde peaks observed.

LRFABMS (with the addition of CsI) on this sample did not reveal a molecular ion for the compound.

Although not characterised, the third ozonolysis sample was sent to AgResearch, at Hamilton, New Zealand for direct conjugation to a protein.

3.4.3 Results

At the time of writing, the preparation of a protein conjugate with the ozonolysis product was being carried out at AgResearch. An immunisation schedule will involve inoculation of the conjugate into sheep and mice for the development of a competitive ELISA.

3.5 Development of a Large Scale Isolation Method for YTX

3.5.1 Strategy

The strategy for the large scale extraction and isolation of YTX from shellfish revolved around the unexpected chromatographic behaviour of the toxin on LH-20 gel. A compound the size of YTX (1186 Da) would be expected to elute off the LH-20 gel very early, however preliminary work on the initial isolation of YTX revealed that the majority of the toxin eluted very late (Scheme 2.2.2). The late elution of YTX, on LH-20 gel, is presumably a result of reversible absorption effects of the two terminal sulfate groups with the gel, hence retarding the toxin (K_D >1).

The retardation of YTX on LH-20 was advantageous for quick isolation in two ways: first, much "unwanted" mass is removed from the YTX containing sample (95% is removed from fraction 2.I9, Scheme 2.2.2), while the toxin is concentrated, predominantly, in the remaining mass. The second advantage is that loss of the toxin on the gel is less than for any other chromatographic phase examined.

With the strategy centred on LH-20 gel permeation chromatography, it was essential that the remainder of the extraction and isolation procedure prepared the extract for this phase. The criteria for the protocol was; maximum extraction followed by efficient removal of unwanted mass, with concurrent minimal loss of toxin.

3.5.2 Extraction Methodology

The aim of the extraction methodology for YTX was to develop a procedure that extracted the toxin yet gave a readily manageable extract. As mentioned in Section 2.2.1, the high lipid content of shellfish, which causes handling problems, can be controlled by the use of highly polar extraction solvent mixtures. The polarity of YTX is favourable to the use of polar extraction solvents.

Freeze drying the mussels aided handling, while extraction with 70% methanol/water was effective in extracting minimal amounts of lipid material. However, the cytotoxicity of the extract was not as high as seen previously for other crude extractions. Re-extraction of a small amount of the shellfish, with methanol, revealed that substantial amounts of toxin had not been extracted by the first method.

Extraction under reflux conditions was a method previously used by Ishida *et al*, for extraction of BTX-B_1 from shellfish.[76] Re-extraction of a small portion of the shellfish, by refluxing in methanol, afforded an extract with a 2-fold increased cytotoxicity, compared with that of the cold methanol extraction.

The reflux extraction was established as a superior method and accordingly applied on a larger scale.

3.5.3 Preliminary Isolation

The extract from the initial 70% methanol/water extraction, was partitioned against petroleum ether, to remove unwanted, non-polar material. After removal of the methanol, the aqueous phase was partitioned against ethyl acetate. P388 assays of all partitions revealed that the total cytotoxicity was spread evenly among the ethyl acetate and water phases. For this reason, this particular partition sequence was deemed highly unsuccessful and eliminated from future protocols.

The utilisation of reverse phase C18 chromatographic material, for removal of unwanted mass, was attempted. The results proved to be mixed. Separation was poor for samples containing predominantly lipid soluble material (eg. the ethyl acetate phase) (Fig 3.5.1), but improved for samples containing predominantly polar material (eg. aqueous methanol partitions) (Fig 3.5.2). For the C18 phases used, there was always a loss of toxin (as demonstrated by diminishing of total cytotoxicity recovered off the columns), presumably by irreversible absorption onto the solid support.

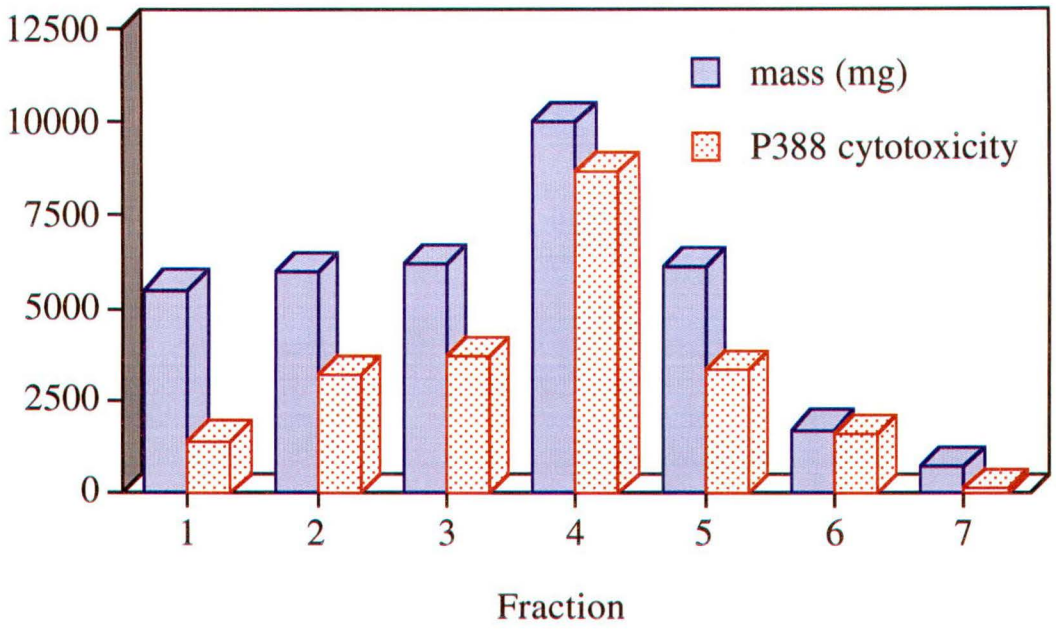

Fig 3.5.1 *Graph Showing Cytotoxicity and Mass of Fractions off C18 Reverse Phase Column*

P388 cytotoxicity (u) = mass (mg)/IC_{50} (ng/mL) x 10^4

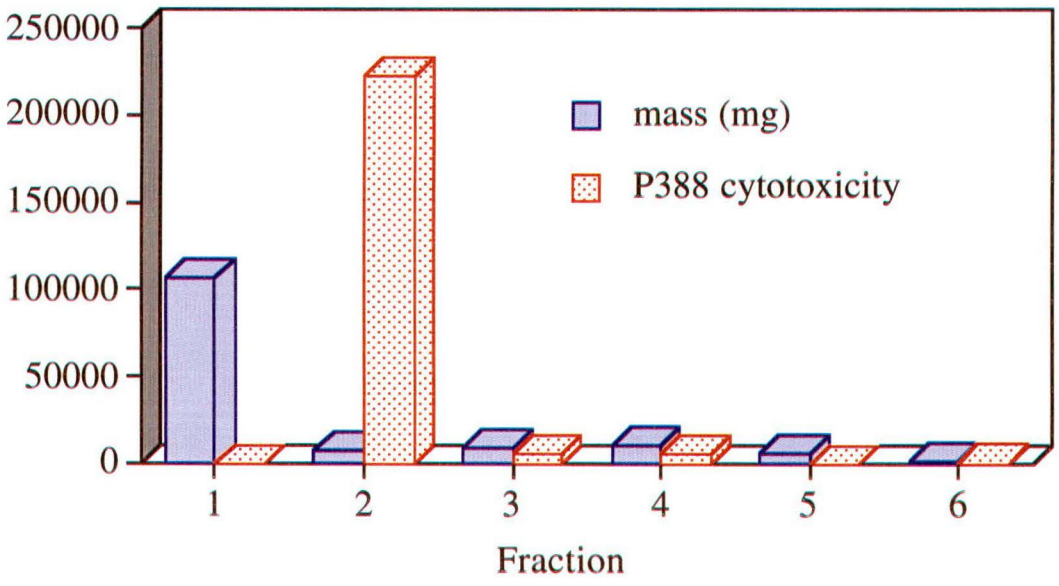

Fig 3.5.2 *Graph Showing Cytotoxicity and Mass of Fractions off C18 Reverse Phase Column*

P388 cytotoxicity (u) = mass (mg)/IC_{50} (ng/mL) x 10^4

For samples of predominantly high lipid content, silica chromatographic material was tried as an alternative phase. The exploratory trial of silica was unsuccessful, due to "streaking" of the toxin. Almost every fraction contained amounts of the toxin.

The elimination of the water *vs* ethyl acetate partition and the unsuitability of silica as a first solid-phase purification step, placed the emphasis back on C18 as the primary solid-phase purification process. The combination of large volumes of aqueous extracts and large amounts of C18 material (*ca.* 1 kg), created problems.

Large volumes required large columns, which in turn led to increased difficulties in sample handling and consequently time required to complete the operation. The published isolation scheme for YTX utilised an n-butanol *vs* water partition, followed by primary solid phase chromatography on alumina material.[24]

Exploratory use of this method was promising. The total measurable amount of toxin was partitioned into the n-butanol phase, from which good separation and toxin recovery were exhibited by the alumina phase. This method was adopted as the primary isolation procedure for the further extraction/isolation of shellfish (Scheme 3.5.1).

3.5.4 Final Purification Methodology

The design of a "custom made" column, suitable for purification of large quantities of sample on LH-20 gel permeation chromatography,

was fundamental to the overall isolation. A column, of length 2 metres and internal diameter of 25 millimetres was of appropriate size to contain *ca.* 200 grams of LH-20 gel. This amount of gel was pertinent for processing large quantities of extract (a weight ratio of 50:1 gel:sample, *cf* 1000:1 normally required). Being a gel filtration technique, the length of column was of major importance. Overloading of the column was tolerated due to the absorption effects, exhibited by YTX on the gel. Generally, use of this column removed 97-98% of unwanted mass from the YTX containing samples.

With efficient concentration of the toxin by LH-20 gel permeation chromatography (Scheme 3.5.1), final purification could be achieved on a reverse phase C18 lobar column. The C18 lobar column proved successful in near completion of the purification.

Early work had shown that diol phase was successful in isolations, however the low amount available and vulnerability of this phase, made it practical only as a final purification step. After the C18 lobar column, the diol phase proved successful in purifying YTX to an acceptable level of purity (Scheme 3.5.1).

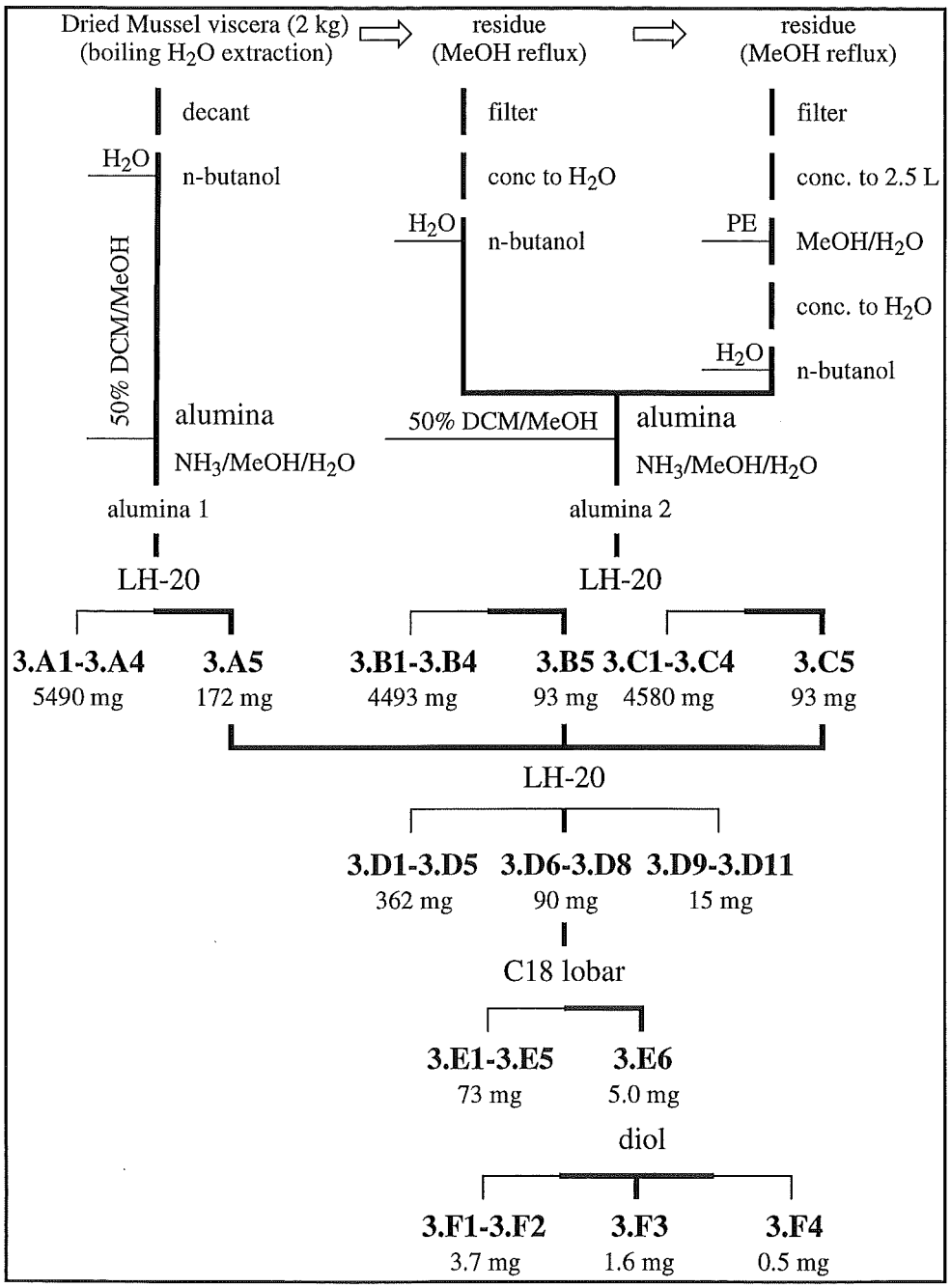

Scheme 3.5.1 *Large Scale Isolation Scheme for YTX*

The yield of YTX purified by this protocol (fraction 3.F3, 1.6 mg, $1.6x10^{-5}$% yield, wet/weight) was lower than initially expected. However, the mussels extracted were from a different batch than those examined earlier. It is possible that the levels of YTX in the mussels were variable and were lower in the batch extracted on a large scale.

3.6 Conclusions

3.6.2 Spectroscopic Assignment of YTX

Close NMR and MS data correlations between published[24] and observed data for YTX proved the presence of this toxin in the shellfish.

3.6.3 Stereochemical Assignment of YTX

Partial stereochemical assignment of YTX was carried out on the desulfated derivative D-YTX (**44**) as part of this research. However, the relative[31] and absolute[32] stereochemistry was subsequently published by Professor Yasumoto's research group.

The data obtained during this research suggested the published chair conformation of ring K[31] was incorrect, with the likely conformation for this ring being a twist boat.

3.6.4 Design and Synthesis of YTX Haptens

Attempted synthesis of YTX haptens was carried out. The syntheses were largely unsuccessful, with the most promise shown by ozonolysis. The product of the ozonolysis reaction was sent to AgResearch at Ruakura, Hamilton for immunisation in sheep. At the time of writing this immunisation is in the early stages and so no results are available.

3.6.5 Development of a Large Scale Isolation Method for YTX

A large scale isolation procedure for YTX has been developed. The method centres on the use of LH-20 gel permeation chromatography, a phase effective in rapid concentration of the toxin and successful in the quick removal of unwanted mass. The overall success of the method could not be accurately gauged due to the unknown YTX content in the mussels.

Accurate evaluation of the success of the method (and hence possible improvements) can only be made after a quantitative, YTX-specific assay is implemented.

A fluorescence HPLC assay, for the determination of YTX and 45-hydroxy YTX in shellfish, has been developed by Professor Yasumoto's research group in Japan. The assay is not yet available for outside use, although with a reported detection limit of 1 ng it is very sensitive.[79]

The assay has been used to determine low levels of YTX and 45-hydroxy YTX in contaminated mussels, harvested in early 1993 from Coromandel peninsula. In addition, the assay has proven instrumental in the determination of YTX, as the major contaminant of shellfish at Wedge point, in the Marlborough Sounds (Fig 2.1.1). Levels of 7.5 mg/kg shellfish have been reported in these shellfish.

Once the assay technique is revealed, accurate analysis of the success of the methodology, developed here, can be made.

Chapter Four

Investigation of Toxicity in Foveaux Strait Oysters

4.1 Introduction

On 14 January 1994, as part of the biotoxin monitoring program, the routine testing of shellfish using the mouse bioassay led to the discovery of a lipid soluble toxin in oysters, harvested from Foveaux Strait area. The initial levels of 39 mouse units (MU)/100 g shellfish, were above the regulatory limit of 20 MU/100 g. Over the following weeks the levels increased until, by 25 February, values greater than 650 MU/100 g were observed. As a result, a large part of the Southland coast was closed. Over a period of two months, the toxicity spread up the East coast of the South Island, to reach northern Marlborough Sounds in early May (Fig 4.1.1).[84]

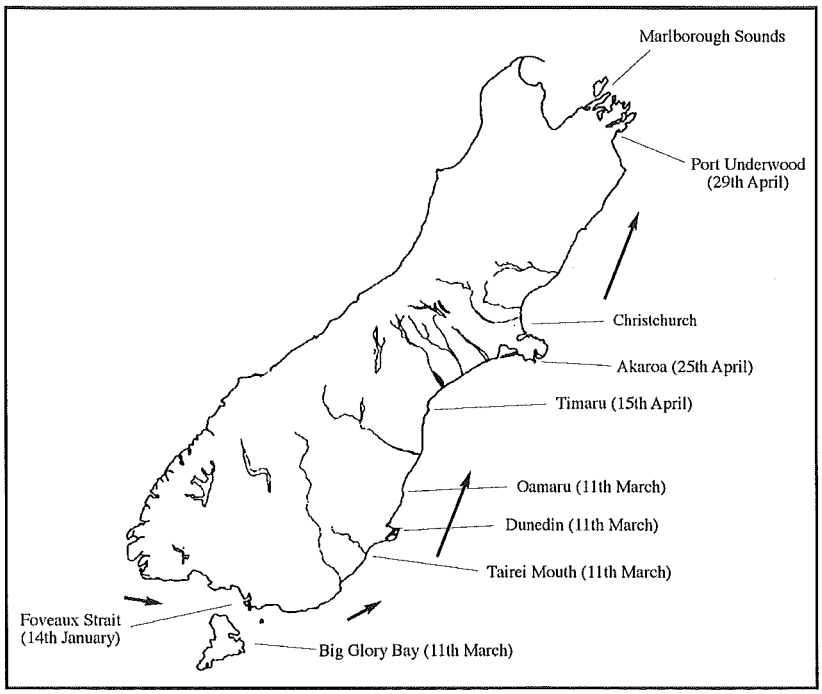

Fig 4.1.1 *Map of New Zealand's South Island Showing the Location and Dates of the Detection of Toxic Shellfish. Large Arrows Indicate the Direction of the Sea Current*

High algal counts of a *Gymnodinium* species of dinoflagellate were found in the vicinity of the toxic shellfish.[84] The spread of contamination up the East coast of the South Island was accompanied by the presence of these algae. Confirmation that this *Gymnodinium* sp. was responsible for the shellfish contamination was made after the establishment of the dinoflagellate in culture. The dinoflagellate shares many characteristics with *Gymnodinium mikimotoi* and was consequently named *Gymnodinium* cf *mikimotoi*, (Fig 4.1.2).[84]

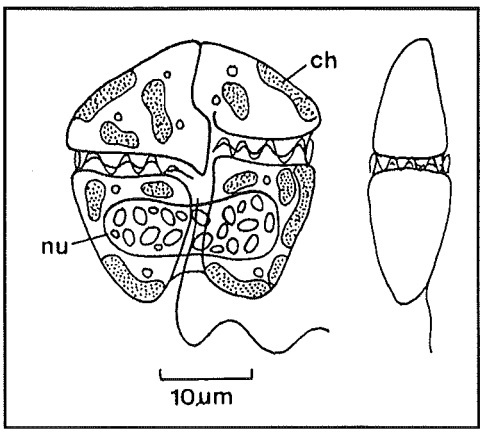

Fig 4.1.2 *Schematic Drawing of Ventral and Lateral Views of Gymnodinium cf. mikimotoi*

ch = chloroplast, nu = nucleus

The results from the mouse bioassay suggested NSP toxicity. Due to the NSP toxicity and the presence of the dinoflagellate *G.* cf. *mikimotoi*, brevetoxins (BTX) were assumed to be the cause of the toxicity. However, the observed symptoms of the mice were unlike those normally observed for BTX containing samples. The key observation was that, on dilution, these samples did not show the proportional reduction in toxicity, observed for BTX containing extracts. A gradual increase in death time was observed until a

"critical" dilution of *ca* 1:5 was reached where no mouse deaths occurred.

An investigation of the toxicity in the oysters was undertaken as part of this research and is described in Section 4.2. At the time at which this work commenced, it was not known that on 21 February 1994, twenty kilograms of toxic oysters had been sent to Professor Yasumoto's research group at Tohoku University, Japan. This material had been sent by the Cawthron Institute for chemical analysis in order to determine the identity of the toxin which has been the subject of this present research.[84]

4.2 Investigation of Toxicity

Due to the slow turn around times of the mouse bioassay and difficulties in handling highly lipid soluble samples (Section 2.2) an alternative method of detecting toxicity was required. Again, the P388 murine leukaemia assay (Appendix 1) was used.

An exploratory test of the polarity of the cytotoxic component(s) was made by extracting the oysters with various solvents. Frozen oyster flesh was freeze dried and extracted twice with water and once with 50% methanol/water, methanol, ethyl acetate, and dichloromethane. The P388 assay showed a low level of cytotoxicity in the water extract, however the vast majority appeared in the ethyl acetate and dichloromethane extracts (Scheme 4.2.1). These results suggested that the cytotoxin was a non-polar, lipid soluble compound.

An elaborate P388 cytotoxicity directed isolation was carried out on the extracts. The isolation is summarised in Schemes 4.2.1, 4.2.2, 4.2.3 and is detailed in Section 6.4.

The extract was concentrated into three samples of high cytotoxicity: fractions 4.J3 (0.3 mg, P388 IC_{50} value 230 ng/mL, Scheme 4.2.2), 4.M10 (1.7 mg, P388 IC_{50} value <487 ng/mL, Scheme 4.2.3) and 4.O1 (0.8 mg, P388 IC_{50} value 310 ng/mL, Scheme 4.2.3).

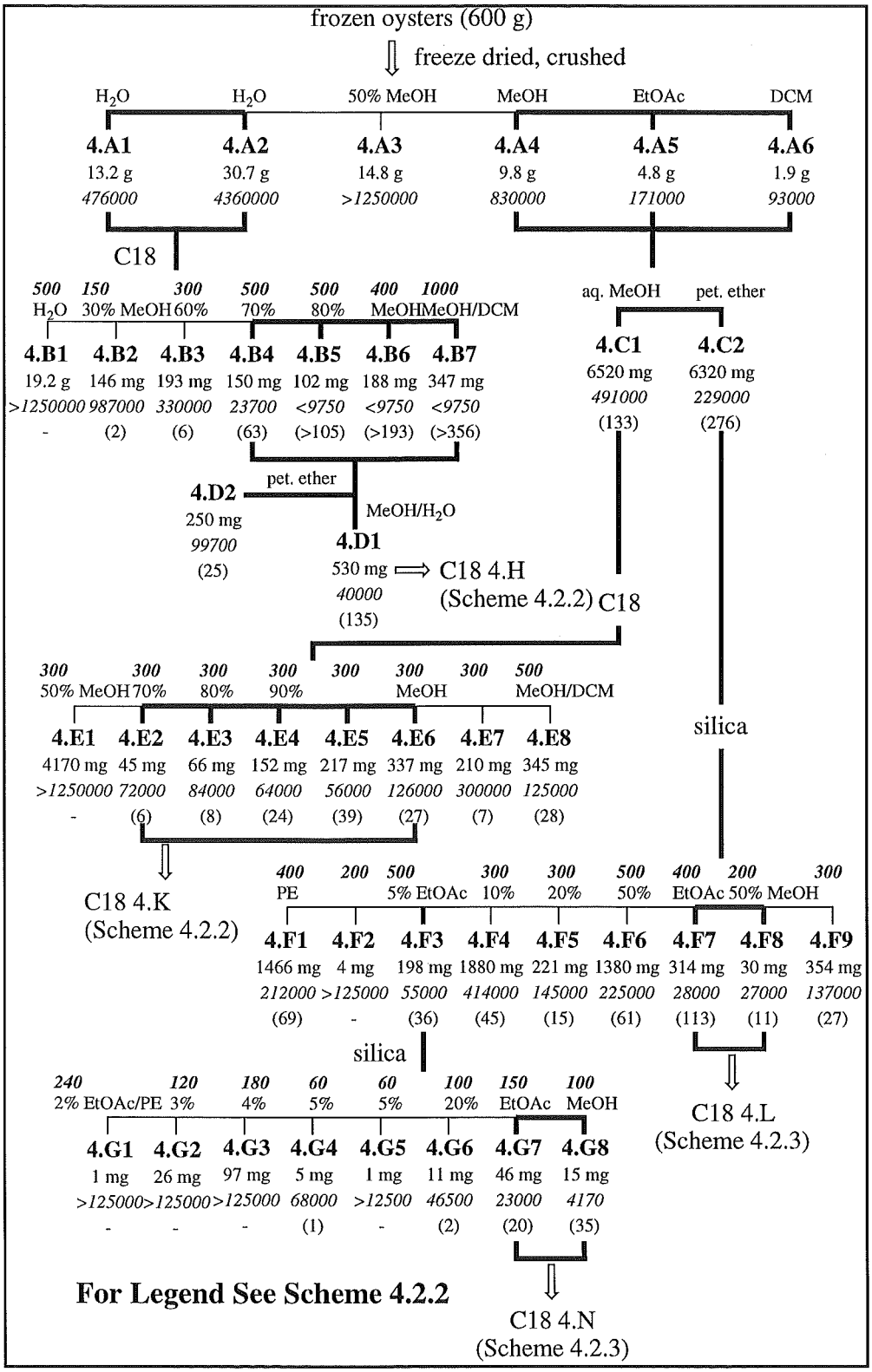

Scheme 4.2.1 *Concentration of P388 Cytotoxicity in Foveaux Strait Oysters*

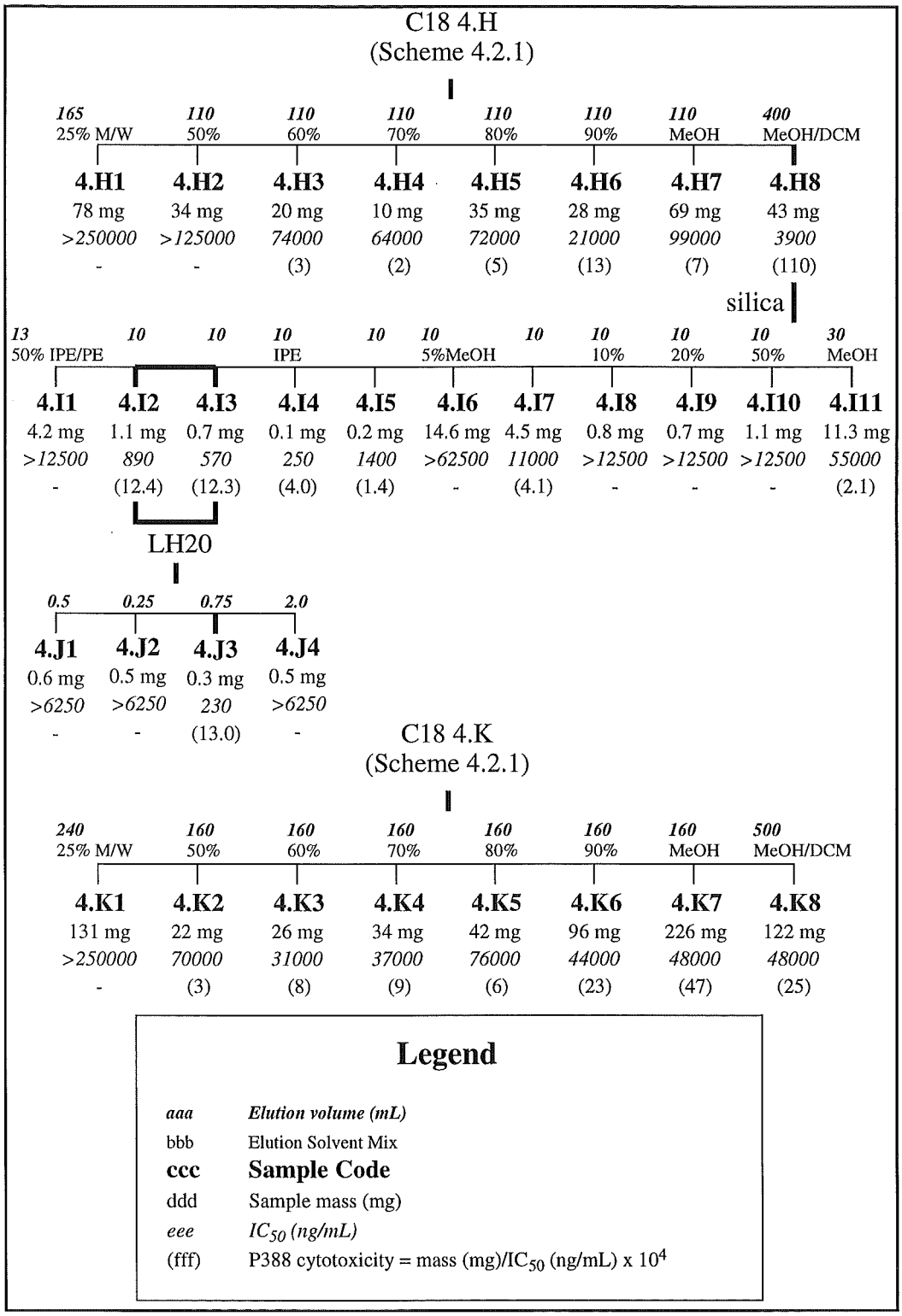

Scheme 4.2.2 *Concentration of P388 Cytotoxicity in Foveaux Strait Oysters*

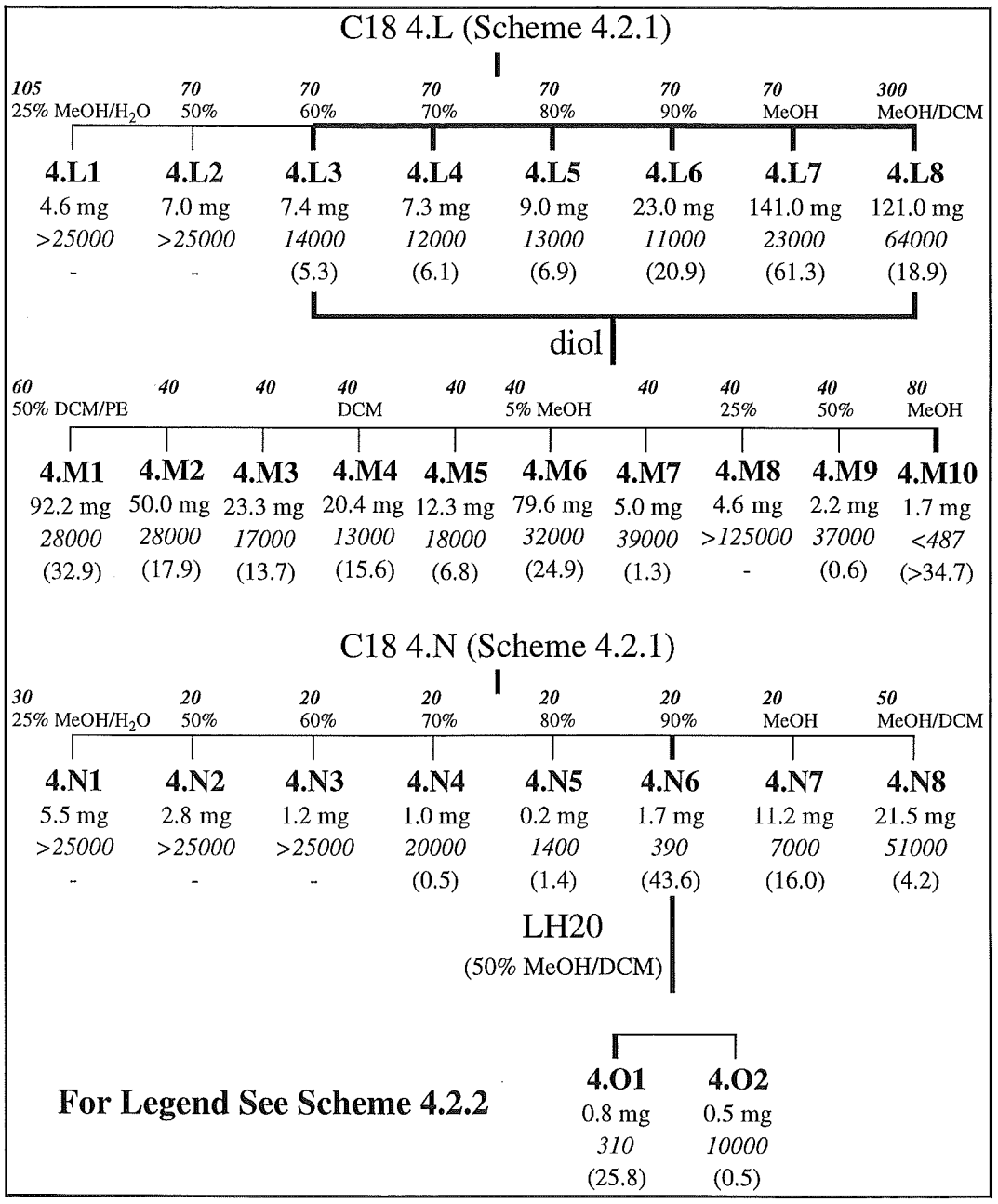

Scheme 4.2.3 *Concentration of P388 Cytotoxicity in Foveaux Strait Oysters*

Each fraction showed distinctly different chromatographic profiles. Fraction 4.J3 (Scheme 4.2.2) was extracted into water, eluted late off C18 reverse phase, eluted early off silica and late off LH-20, suggesting a small non-polar compound. Fraction 4.M10 (Scheme 4.2.3) was extracted in non polar solvents, partitioned into hexane, eluted late off

silica, streaked on reverse phase C18 and eluted very late off diol. This suggested a compound that is reasonably polar, but able to be extracted as a micelle in non-polar solvents, therefore likely to contain a non-polar backbone. Fraction 4.O1 (Scheme 4.2.3) was extracted in non polar solvents, partitioned into hexane, eluted early off an initial silica column, but late off a subsequent silica column. The bioactivity eluted with medium polarity solvents off reverse phase C18 and came off LH-20 early. This suggested a compound with possible acid or basic functional groups, of moderate polarity and medium-large size. These significantly different chromatographic profiles suggested three separate compounds and **NOT** an artifact of the overlapping of the same compound into the three fractions.

The ^{1}H NMR spectra of each cytotoxic fraction did not yield further evidence of structural type. This was a consequence resulting from the low mass of each fraction and complexity of the spectra.

The three concentrated active samples were analysed in the mouse bioassay and in the neuroblastoma assay (N2A). None of the three samples gave rise to mouse deaths at the assayed concentrations. This suggested either the levels were too low and/or the cytotoxicity was not caused by the same compound causing NSP toxicity in mice. Although all three samples exhibited mild cytotoxicity towards the N2A cell line, no evidence of any BTX-like effect was observed.

The results illustrated the necessity for the extraction of more oysters and closer initial monitoring by the mouse bioassay.

This second extraction of frozen oysters was achieved with methanol and 80% methanol/water. The extracts were combined and desalted on a large C18 reverse phase column. The oysters were then re-extracted three times with dichloromethane and when combined with the desalted methanol extract, afforded a total lipid extract.

An aliquot of this lipid extract was partitioned on diol phase, yielding sixteen fractions, designated 4.P1 - 4.P16. The P388/mouse bioassay results (Fig 4.2.1) showed clearly that the cytotoxicity and mouse toxicity were **NOT** caused by the same compound(s).

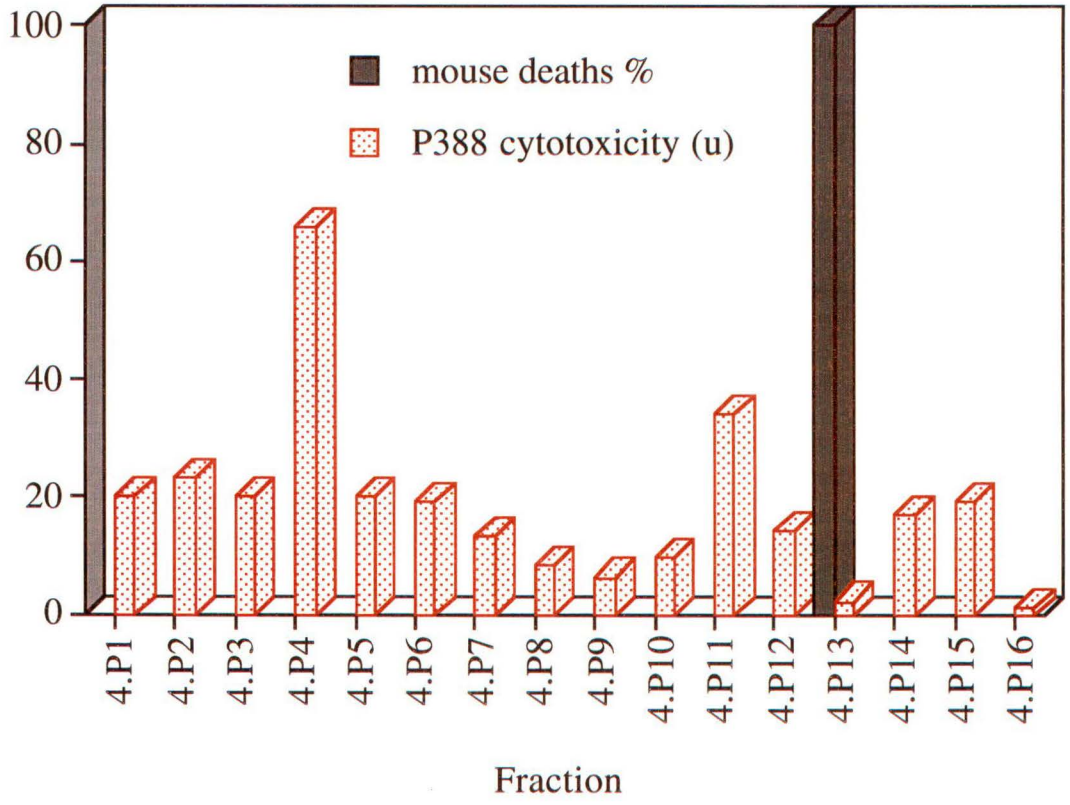

Fig 4.2.1 *Graph Showing P388 Cytotoxicity and Mouse Deaths of Fractions off a Diol Phase Column*

P388 cytotoxicity (u) = mass (mg)/IC_{50} (ng/mL) x 10^4

The emphasis of work shifted from that of P388 cytotoxicity directed isolation to mouse toxicity directed isolation.

4.2.1 Isolation of Gymnodimine

At this time it was revealed that Professor Yasumoto's research group, at Tohoku University in Japan, had performed a mouse toxicity directed isolation using an "in house" mouse bioassay. They had discovered the toxic component and tentatively named it "gymnodimine". The structure had not been solved, yet it was revealed that the toxin was a nitrogen containing macrocycle.[79]

Consequently, the use of Dragendorff's reagent[85] for the staining of TLC analyses was adopted. Dragendorff's reagent is a TLC developing spray that is selective for nitrogen containing compounds. A positive response is a dark orange colour on a light orange background.

When a TLC of fractions 4.P1 - 4.P16 was re-run and sprayed with Dragendorff's reagent, two orange spots could be detected. Fractions 4.P9 - 4.P12 had an orange spot at R_f = 0.32 and fractions 4.P13 - 4.P14 had an orange spot at R_f = 0.27. The mouse toxicity in fraction 4.P13 and mouse neurotoxic symptoms in 4.P14 appeared to correspond with the orange spot at R_f = 0.27 (Fig 4.2.2).

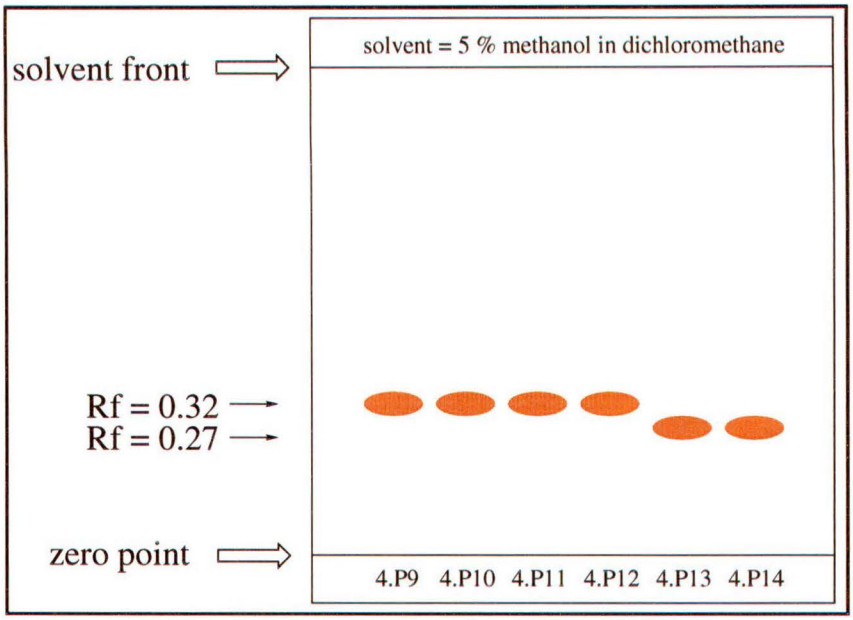

Fig 4.2.2 *Stylised Picture of TLC Chromatograph of Fractions 4.P9 - 4.P14*

The nitrogen atom in the molecule allowed the use of weak cation exchange chromatography, such as CBA (*C*ar*B*oxylic *A*cid) bonded silica phase, for quick purification. Fraction 4.P13 was chromatographed on a CBA column and the fractions analysed by TLC, using Dragendorff's reagent. The fraction that eluted at 0.5% NH_3 in methanol contained the orange spot. LREIMS (*L*ow *R*esolution *E*lectron *I*mpact *M*ass *S*pectrometry) of this fraction gave a molecular ion at *m/z* 507.3, which is the correct mass for gymnodimine.[79]

At this point further quantities of gymnodimine were required for structural elucidation and other work, including hapten design and syntheses (see Section 5.3). The low levels of gymnodimine in the oysters (*ca.* 1 mg per kg of shellfish tissue) forced the development of a rapid, efficient and cost effective extraction/isolation procedure for gymnodimine. This work is detailed in Section 5.5.

4.2.2 "Slow Acting" NSP Toxicity

While searching extracts for gymnodimine, certain side fractions exhibited death times of up to 4.5 hours in the mouse bioassay. The long death times and symptoms of gasping, prostration and hind leg paralysis were not expected as for those caused by gymnodimine.

A fraction demonstrating these long death times was passed through a diol phase column, fractions 4.Q1 - 4.Q4 collected (Scheme 4.2.4) and aliquots sent for mouse bioassay. 4.Q1 - 4.Q3 all had short "gymnodimine" death times, whereas 4.Q4 had a death time of around four hours.

4.Q4 was further chromatographed on a C18 reverse phase column to give fractions 4.R1 - 4.R8 (Scheme 4.2.4) of which aliquots were sent for both mouse bioassay and N2A assay.

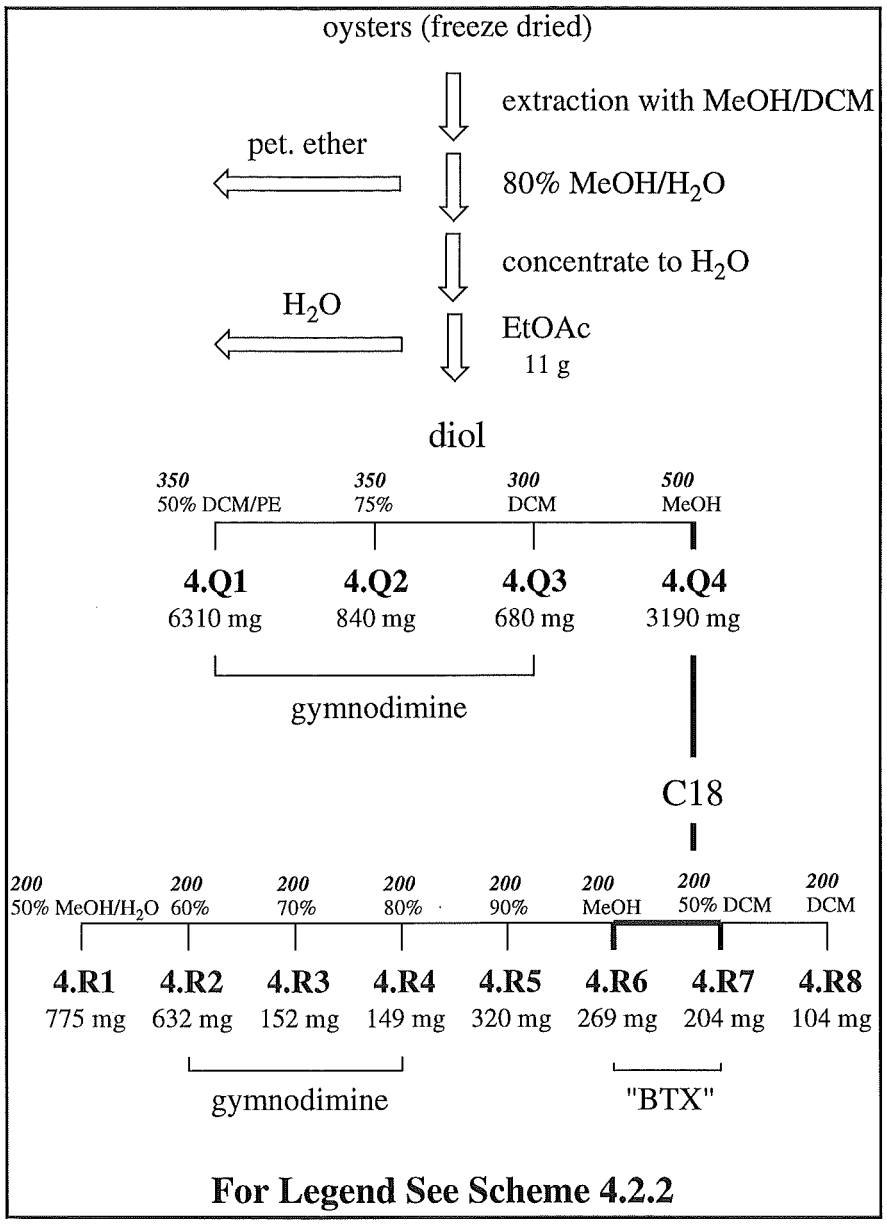

Scheme 4.2.4 *Isolation Scheme for "Slow Acting" NSP Toxicity*

The results are summarised in Table 4.2.1. These demonstrate that the longer death times seen in 4.R6 and 4.R7 also correspond with BTX like activity.

Table 4.2.1 *Table of Mouse Deaths and "BTX" Activity of Fractions off C18 Reverse Phase Column*

Fraction	Mouse Deaths (minutes)	ng "BTX" in 1 mg
4.R1	-	<150
4.R2	58	<150
4.R3	9	<150
4.R4	17	200
4.R5	*	<150
4.R6	105	310
4.R7	134	130
4.R8	†	<150

* Sample lost in transit

† death time 6 - 24 hours

Once the dilution of gymnodimine was below the "critical threshold", extremely low (0.031%) levels of BTX-like compound(s) were revealed. These levels were not picked up earlier due to a "masking effect" of mouse toxicity caused by gymnodimine.

The low levels of "BTX" were well below the regulatory limit of 20 µg/100 g shellfish, and supported the subsequent ELISA data of Garthwaite *et al*,[74] demonstrating low levels of BTX in these shellfish.

The low levels of BTX-like material did not warrant further investigation.

4.3 Conclusions

Three samples of concentrated cytotoxicity (against P388) were isolated from oysters harvested from Foveaux Strait during the early 1994 outbreak of NSP toxicity. The identification of the cytotoxic compounds in these samples was not able to be achieved due to the low mass amounts involved. These samples exhibited no measurable toxicity in the mouse bioassay and hence not considered a public health issue.

The toxin responsible for NSP toxicity in mice was isolated as part of this research, however the structure was published independently by Professor Yasumoto's research group, in Japan. The toxin was named gymnodimine.[79]

Low levels of "brevetoxin (BTX)-like" compounds was discovered from these shellfish. The levels were well below regulatory limits.

Chapter Five

Gymnodimine

5.1 Introduction

Gymnodimine (**40**) was isolated from Foveaux Strait oysters, *Tiostrea chilensis* and identified as the biotoxin responsible for the acute NSP symptoms in mice. The gross structure of gymnodimine was published by Seki *et al*,[67] however structure elucidation studies were also carried out as part of this research and are described in Section 5.2.

The absolute stereochemistry of gymnodimine was elucidated by chemical modification and X-ray crystal structure analysis. In addition, examination of differences between solid state and solution state conformations of gymnodimine were carried out. This work is described in Section 5.3.

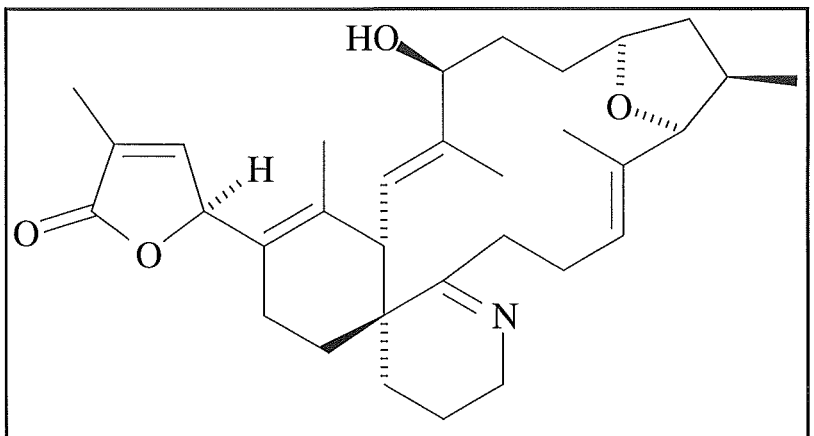

gymnodimine (**40**)

Rodent feeding trials of gymnodimine revealed that it was not toxic orally[74] and hence, not considered a public health problem. The potent toxicity observed by injection of gymnodimine into mice presents a

problem for monitoring of other lipid soluble "human toxic" toxins, presently monitored by the mouse bioassay, eg. brevetoxins.

In the routine monitoring of gymnodimine in shellfish samples by the mouse bioassay, two parallel extractions are undertaken; the New Zealand acetone extraction,[75] and the APHA ether extraction.[75] Shellfish showing positive results in the acetone extraction method are assayed using the ether extraction method. Positive results in the ether method suggest toxin(s) other than gymnodimine present in the shellfish. As a result, the APHA ether extraction method is currently used to regulate against gymnodimine. Although this method is currently the chosen procedure for regulation against gymnodimine it has two problems associated with it. The first is that occasional "false positives" occur when high levels of gymnodimine are present in the shellfish. This leads to unnecessary closure of commercial shellfish beds. The second problem is that the APHA method does not screen for toxins of low lipid solubility, such as the brevetoxin conjugates, eg. BTX-B1 (**41**).

Furthermore, acceptance of the mouse bioassay as a method of shellfish testing, is diminishing worldwide, for ethical reasons. Tolerance for the assay has ebbed to the point where some countries will soon no longer accept shellfish imports that have been tested on live animals.[86] As a result, alternative methods of toxicity testing are being developed.

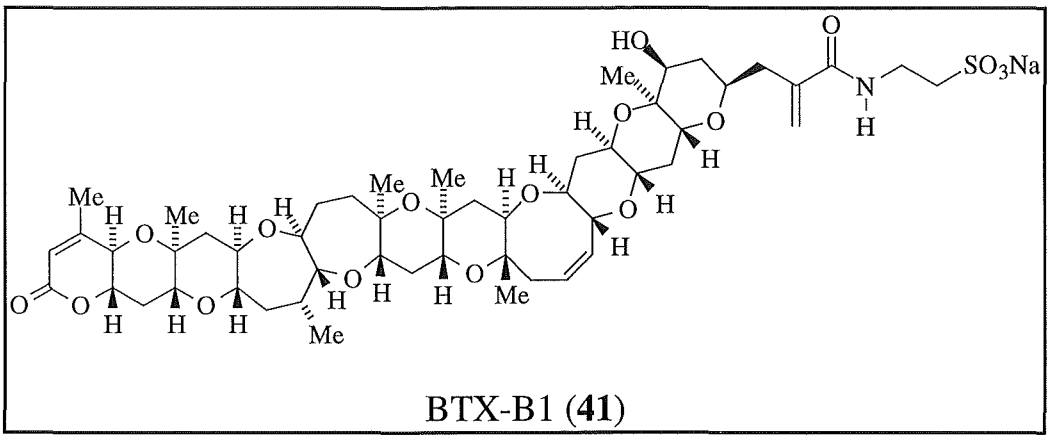

BTX-B1 (**41**)

As part of the development of new toxin specific assays, research into two new assays for specific detection of gymnodimine in shellfish was undertaken.

The synthetic modification of gymnodimine haptens, suitable for linkage to proteins, is the initial step for the development of a gymnodimine-specific ELISA. The further development of the ELISA for gymnodimine is a research objective of AgResearch at Ruakura, Hamilton, New Zealand. The design and synthesis of gymnodimine haptens suitable for an ELISA is described in Section 5.4.

A chromatography/HPLC based assay for specific detection of gymnodimine in shellfish was another assay developed as part of this research and is described in Section 5.6.

All the research described above required milligram quantities of pure gymnodimine. The low levels of the toxin in the shellfish required that an efficient large scale extraction and isolation procedure be developed to achieve sufficient quantities of the toxin. Such a method for the

large scale isolation of gymnodimine has been developed and is described in Section 5.5.

5.2 Structure Elucidation of Gymnodimine

5.2.1 Partial Structure Elucidation of Gymnodimine

LREIMS on a pure sample of gymnodimine (**40**) revealed a molecular ion *m/z* 507.3. Subsequent accurate mass measurement, under high resolution conditions, afforded *m/z* 507.3343, corresponding to $C_{32}H_{45}NO_4$.

Numerous NMR techniques were applied on the pure toxin to elucidate the connectivity and hence the structure. The methods employed were ^1H and ^{13}C NMR, along with 2D COSY, HMQC and HMBC experiments.

The ^1H NMR spectrum of gymnodimine (Fig 5.2.1), revealed four resonances in the region δ 5 - 7, each corresponding to 1 proton. In addition, signals in the region δ 3 - 4.2 accounted for a further six protons. The majority of the signals, however, lay in the region δ 1 - 2.5, suggesting a predominantly aliphatic compound. Four intense singlets in the region δ 1.5 - 2 were suggestive of vinyl methyl groups and an intense doublet at δ 1.07 indicated an extra aliphatic methyl group, attached to a methine.

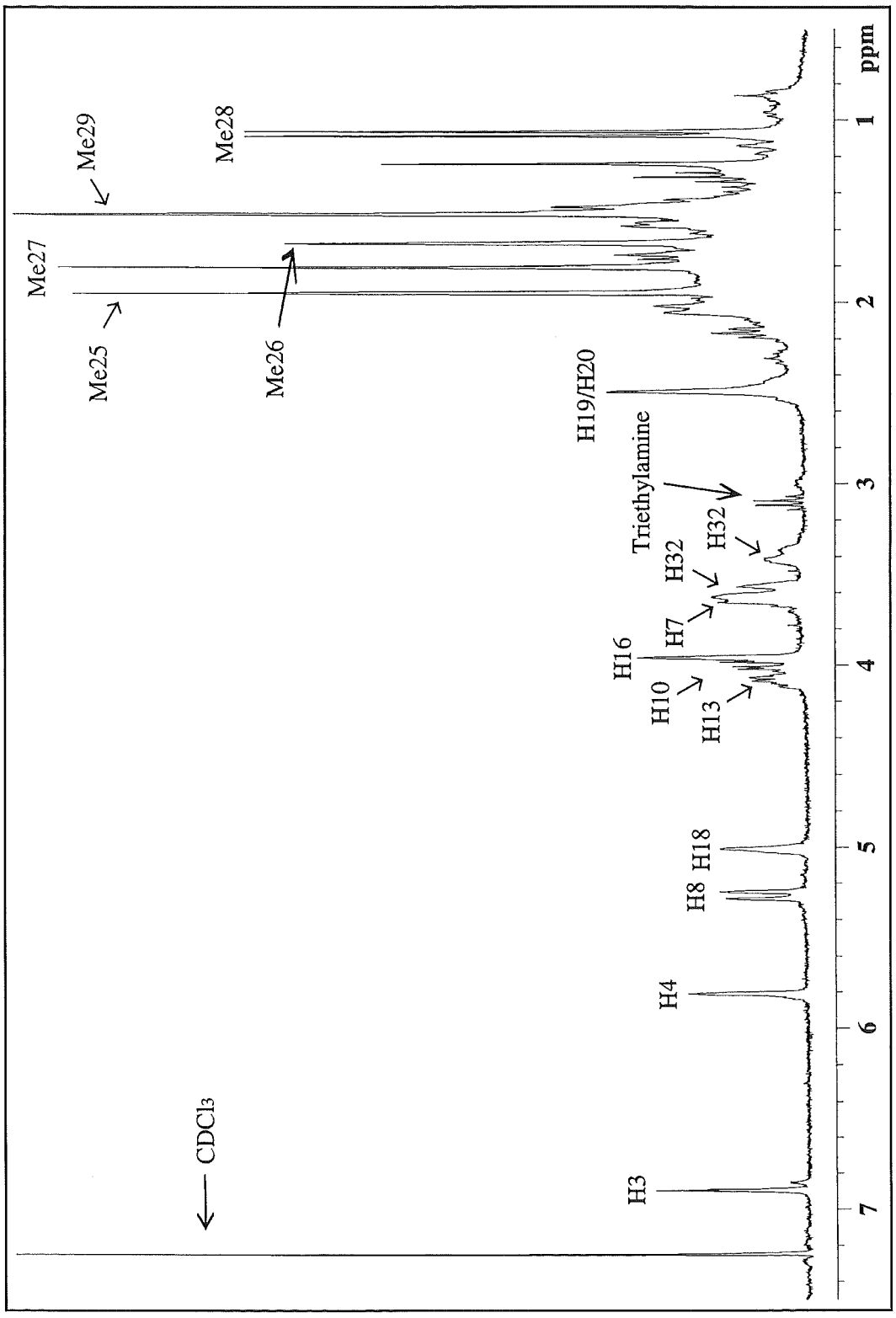

Fig 5.2.1 *^1H NMR Spectrum of Gymnodimine*

($CDCl_3$/triethylamine)

The ^{13}C NMR spectrum revealed clusters of peaks in the regions δ 10 - 22 , δ 29 - 38 and δ 75 - 90. The chemical shifts of these clusters are indicative of methyl, methylene and ether-type carbon atoms respectively. Most signals in the region δ 100 - 180 were not visible above the noise, due to the low amount of material. Carbon resonances in this region were detected in the HMQC and HMBC spectra.

Based on the 1D NMR data and 2D NMR techniques, three separate fragments could be postulated.

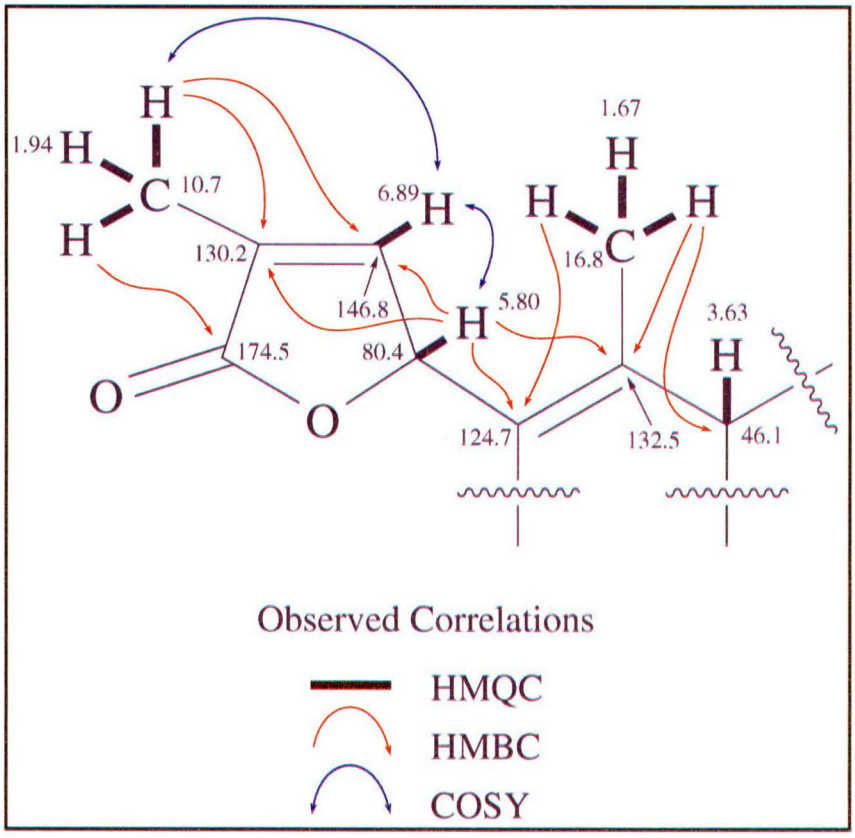

Fig 5.2.2 *Proposed Fragment 1 of Gymnodimine Obtained By NMR Experiments*

Fragment 1 (Fig 5.2.2) was proposed in the following manner:

A COSY experiment revealed vicinal coupling from the proton at δ 6.89 to a resonance at δ 5.80 and long range allylic coupling to δ 1.94, one of the vinyl methyls. An HMQC experiment showed $^{1}J_{CH}$ correlations of δ 6.89/146.8, 5.80/80.4 and 1.94/10.7, allowing assignment of these carbon chemical shifts. An HMBC experiment revealed $^{2}J_{CH}$ and $^{3}J_{CH}$ correlations from the vinyl methyl at δ 1.94 to carbon atoms at δ 130.2, 174.5 and 146.8. As the carbon chemical shift at δ 174.5 is indicative of an ester functionality, the vinyl methyl was placed on the quaternary carbon at δ 130.2.

The proton/carbon chemical shifts at δ 5.80/80.4 are indicative of a methine ester carbon. HMBC correlations from this proton revealed resonances at δ 146.8, 132.5, 124.7 and 130.2. The resonances at δ 124.7 and 132.5 were assigned as quaternary alkene carbon atoms (due to the absence of any $^{1}J_{CH}$ correlations in the HMQC spectrum). One of these carbon atoms was evidently adjacent to the carbon at δ 80.4. Due to the presence of other unrelated oxygenated carbon atoms and the mass requirement of 4 oxygen atoms in the molecule, it was only possible to accomodate one ester functional group in the molecule. The carbon resonances at δ 174.5 and 80.4 were thus linked through a cyclic α,β-unsaturated γ-lactone. The absence of an HMBC correlation from δ 5.80 to δ 174.5 was attributed to an unfavourable coupling optimisation for the experiment (J_{NXH} = 8.3 Hz was used).

The HMQC spectrum revealed the $^{1}J_{CH}$ correlation of δ 1.67/16.8. These chemical shifts are indicative of a second vinyl methyl. The HMBC spectrum revealed three correlations from this methyl to carbon atoms at δ 132.5, 124.7 and 46.1. These data established that the

methyl, and the carbon at δ 46.1, were part of a tetra-substituted double bond. The attachment of the methyl group was assigned to δ 132.5 based on chemical shift arguments. This assignment could not be made unequivocally, due to the absence of an HMBC correlation from δ 6.89 to either of these olefinic carbon atoms. Again, the absence of a correlation was attributed to unfavourable coupling optimisation in the HMBC experiment. The resonance at δ 46.1 was shown by the HMQC spectrum to be a methine carbon, with the attached proton at δ 3.63. No HMBC correlations were observed from this methine proton, preventing further extension of the fragment.

Collation of the above data led to the proposal of Fragment 1, as shown in Fig 5.2.2.

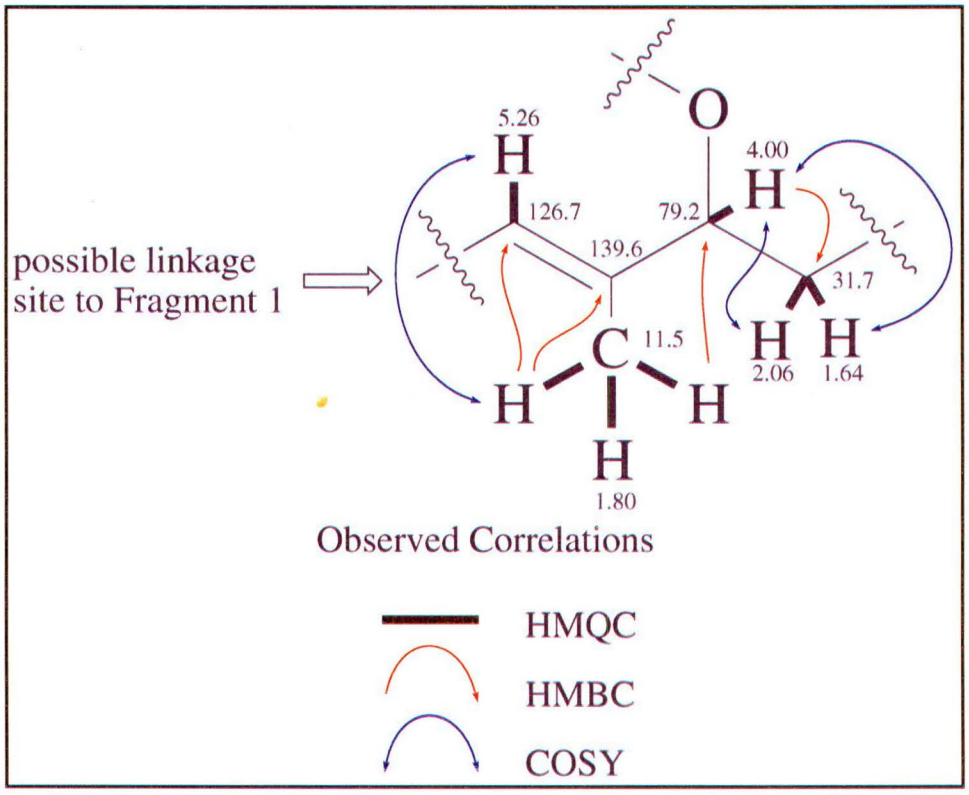

Fig 5.2.3 *Proposed Fragment 2 of Gymnodimine Obtained By NMR Experiments*

Fragment 2 (Fig 5.2.3) was proposed as follows:
The olefinic doublet positioned at δ 5.26 was coupled to a carbon at δ 126.7, as shown by the HMQC spectrum. A long range COSY correlation from this proton was observed to a three proton resonance at δ 1.80, which had an HMQC correlation to δ 11.5. This identified the third vinyl methyl. The HMBC spectrum revealed $^{2}J_{CH}$ & $^{3}J_{CH}$ correlations from this methyl group to δ 139.6, 126.7 and 79.2. From the chemical shifts of the three carbon atoms, it was clear that the methyl was attached to the carbon at δ 139.6.

The carbon resonance at δ 79.2 was shown to have a corresponding proton at δ 4.00. The chemical shift of this proton suggested an oxygenated carbon. The COSY spectrum showed a correlation from δ 4.00 to two protons at δ 2.06/1.64. The HMQC spectrum revealed that these two protons were probably bonded to the same carbon at δ 31.7. These data were confirmed by an HMBC correlation from δ 4.00 to the carbon at δ 31.7. No other $^{2}J_{CH}$ or $^{3}J_{CH}$ correlations were observed from δ 4.00 in the HMBC spectrum.

The doublet at δ 5.26 showed a strong COSY correlation to a proton at δ 3.63. There is a methine proton at δ 3.63 at the terminus of fragment 1 (Fig 5.2.2). This suggested a link between the first fragment and the second fragment. This was discounted by the absence of any HMBC correlations to/from the δ 5.26/126.7 and δ 3.63/46.1 positions. It was possible that the coupling observed from δ 5.26 was to a proton of identical resonance on another part of the molecule. This was supported by the integral. The peak at δ 3.63 is broad and integrates for three protons. Hence fragment 2 was treated

independently from fragment 1 until further structural information was obtained.

Collation of the above data led to the proposal of fragment 2, as shown in Fig 5.2.3.

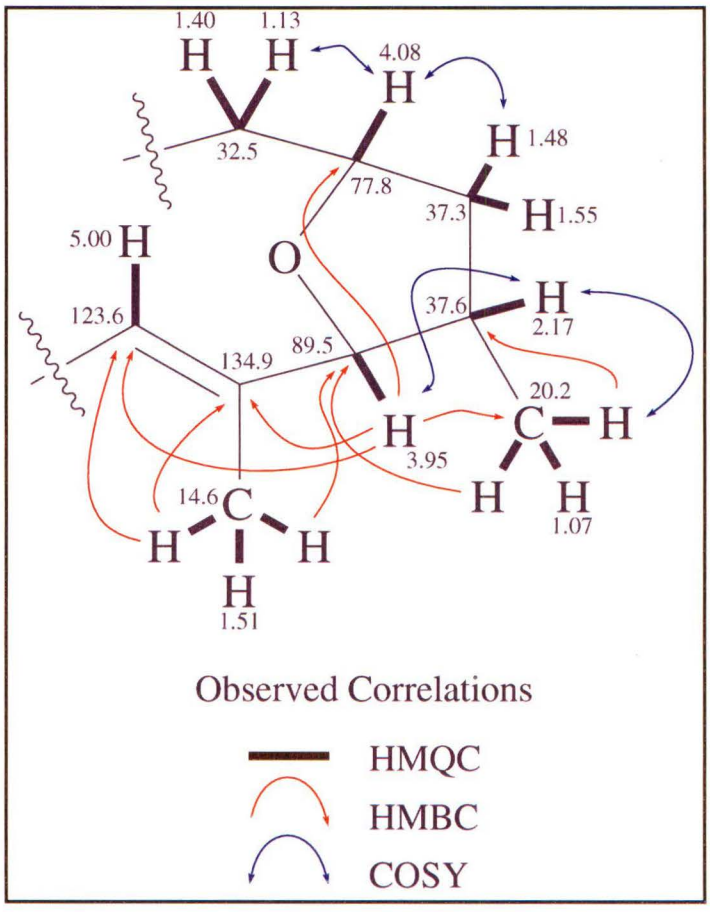

Fig 5.2.4 *Proposed Fragment 3 of Gymnodimine Obtained By NMR Experiments*

Fragment 3 (Fig 5.2.4) was proposed in the following way:
The proton resonances at δ 4.08 and 3.95 are indicative of methine protons attached to ether type carbon atoms. Their respective carbon atoms were revealed by the HMQC spectrum as δ 77.8 and δ 89.5.

These oxygenated methines were shown to be attached *via* an ether linkage by the HMBC correlation from δ 3.95 to δ 77.8.

The doublet methyl at δ 1.07 was shown to have a carbon resonance at δ 20.2 by an HMQC experiment. HMBC correlations were observed from these methyl protons to carbon atoms at δ 89.5 and δ 37.6. The proton resonance on the carbon at δ 37.6 was established by the HMQC spectrum as δ 2.17. Attachment of the methyl on this carbon was confirmed by a COSY correlation between δ 1.07 and δ 2.17. In addition, a COSY correlation between δ 2.17 and δ 3.95 gave the connectivity between these two methines.

The lack of a third HMBC correlation from the methyl δ 1.07, could best be explained by there being two virtually identical carbon resonances within three bonds of the methyl protons. A close inspection of the ^{13}C NMR spectrum around this carbon chemical shift region, revealed resonances at δ 37.6 and δ 37.3. Analysis of the HMQC spectrum revealed the resonance at δ 37.3 had two protons attached at δ 1.55 and δ 1.48.

The data above was best explained by a five membered ether ring. Further data in support of this was a COSY correlation between δ 4.08 and δ 1.48.

Vicinal COSY coupling between δ 4.08 and δ 1.13 suggested linkage of a methine group off the five membered ring at this position. However, the HMQC spectrum showed $^{1}J_{CH}$ correlations from δ 1.13 and

another proton at δ 1.40, to a single carbon atom at δ 32.5. This established a methylene attachment to the five membered ether ring.

The substitution at the δ 3.95/89.5 position of the five membered ring required further analysis. HMBC correlations from δ 3.95 were observed to carbon atoms at δ 134.9, 123.6, 37.6 and 20.2. The carbon chemical shift at δ 123.6 was characteristic of an olefin and its proton resonance established as δ 5.00 by the HMQC spectrum. From chemical shift requirements, the carbon at δ 134.9 was likely to be the linkage point of the fourth vinyl methyl. This was confirmed by HMBC correlations from the fourth vinyl methyl proton at δ 1.51 to carbon atoms at δ 134.9, 123.6 and 89.5. The key $^{3}J_{CH}$ correlation of δ 1.51/89.5 indicated that the double bond was directly attached to the ether ring.

No further correlations, which would expand Fragment 3, could be obtained from the available data. Collation of the above data led to the proposal of Fragment 3 (Fig 5.2.4).

While this work was in progress, the gross structure of gymnodimine was published by Seki *et al.*[67] The partial fragments described above were compared with the published structure of gymnodimine. The fragments showed very close correlation to the published structure (Fig 5.2.5).

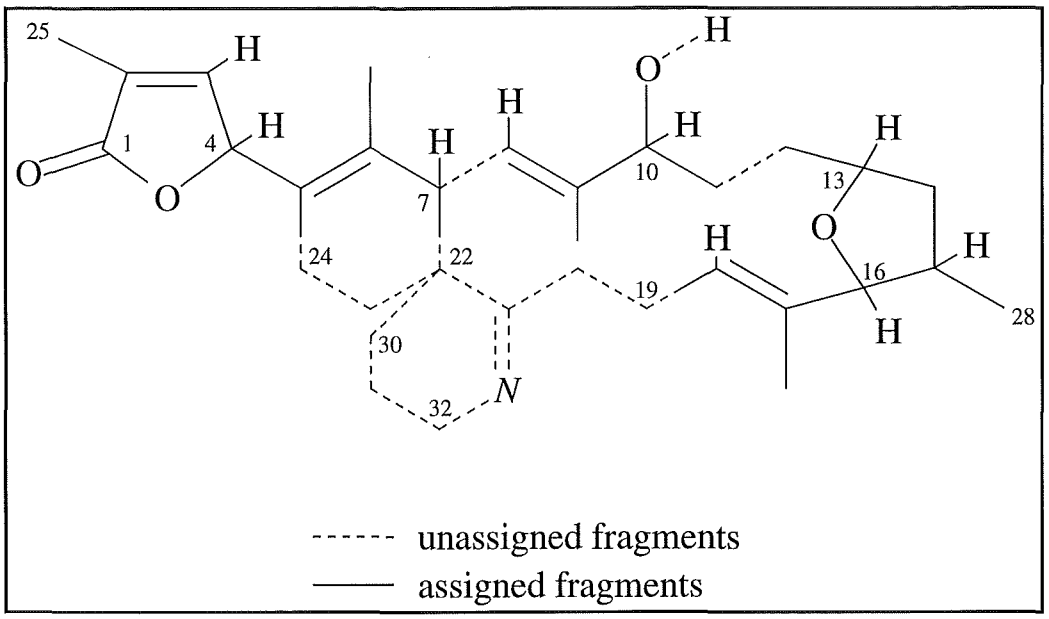

Fig 5.2.5 *Diagram Showing Partial Structure Assignment of Gymnodimine*

The parts of the molecule not assigned here were predominantly methylene groups. From the NMR data obtained, it was not feasible to assign these signals on the small amount of material available. This was largely due to the complex coupling, broadness of peaks and the close chemical shifts of methylene protons. Hence, weak correlations and extensive overlap of methylene signals were observed. To resolve this a larger sample was required.

5.2.2 Complete Structural Assignment of Gymnodimine

Various significant differences were identified between the observed and published NMR data, presumably as a direct result of the different solvents used in acquisition of NMR spectra. The spectra in Section

5.2.1 were run in $CDCl_3$, with a trace amount of triethylamine (TEA), whereas published data was obtained from NMR spectra run in d5-pyridine. On procurement of more toxin, the complete structural assignment was achieved by the combination of a direct comparison with literature NMR data and the use of the 1D and 2D NMR techniques, as outlined in Section 5.2.1. In addition, 2D TOCSY experiments were used to detect proton/proton couplings throughout entire spin systems.

Furthermore, the addition of trifluoroacetic acid (TFA) to the sample, produced significant salient changes in the NMR spectra of the toxin (Fig 5.2.6).

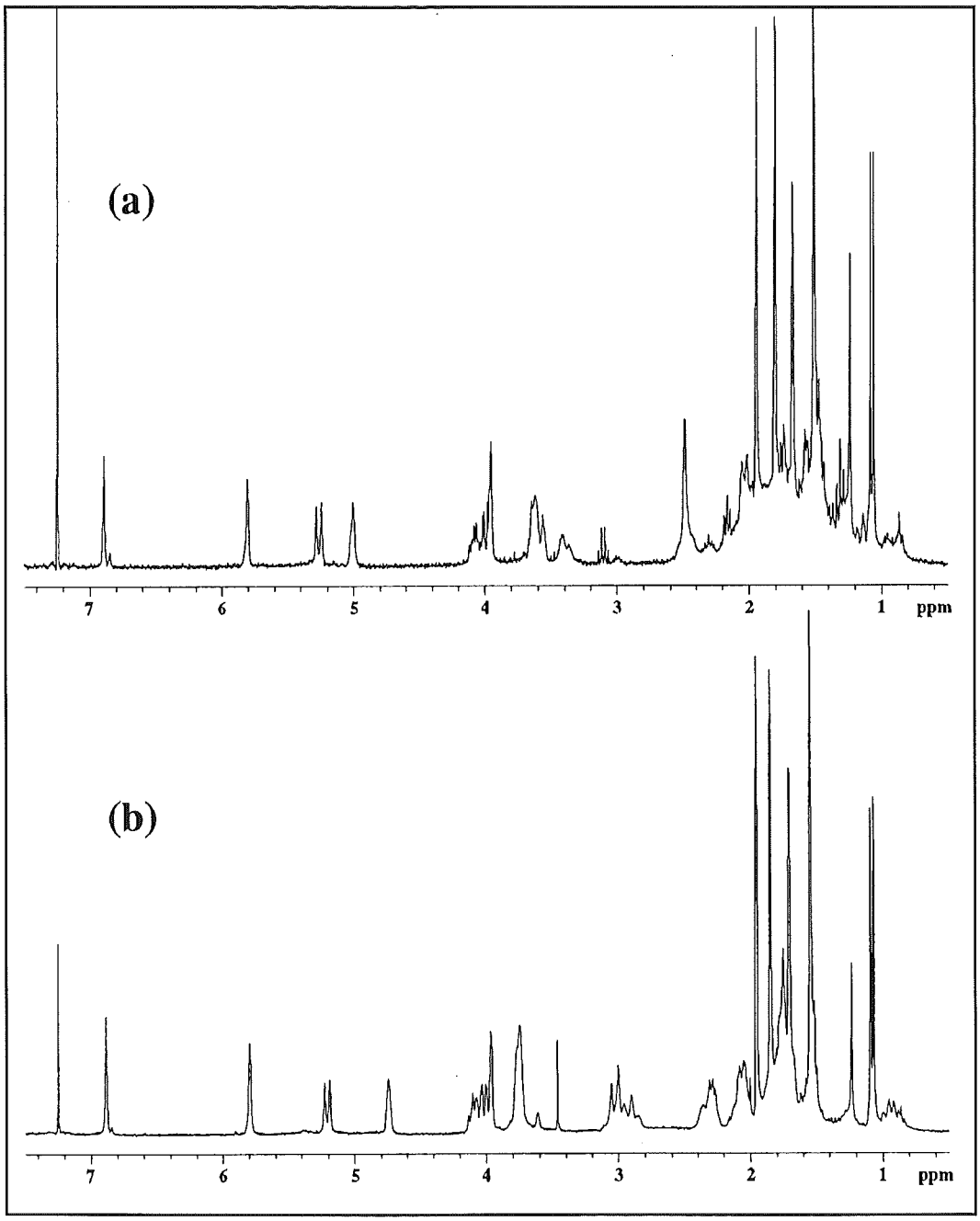

Fig 5.2.6 *Proton NMR Spectra for* ***(a)*** *Free-Base and* ***(b)*** *Acidified Gymnodimine*

It was postulated that a pH dependant imine/enamine tautomerism may be occurring in the molecule. The possibility of an imine/enamine tautomerism had also been suggested by Seki *et al.*[67]

The complete NMR assignment of both forms of gymnodimine was necessary for future stereochemical/conformational analysis of the toxin. This would be achieved by a combination of NOE and molecular modelling techniques.

On application of the NMR techniques, described above, full assignment of the free base form and near complete assignment of the salt form of gymnodimine was achieved (Table 5.2.1).

The significant differences between the chemical shift data for the published and observed data, of the free-base form of gymnodimine, are for atoms in proximity to the hydroxyl and imine functional groups (Fig 5.2.7). These data suggest pH dependent conformational changes in the molecule, and so providing a rationale for conformational modelling of gymnodimine.

Table 5.2.1 *^{13}C and ^{1}H NMR Assignments for Gymnodimine As Published (Pb),‡ Free Base (Fb)¥ and Salt Form (Sf)∞*

#	Pb ^{13}C	Pb ^{1}H	Fb ^{13}C	Fb ^{1}H	Sf ^{13}C	Sf ^{1}H
1	174.9		174.5		170.9	
2	129.8		130.2		130.9	
3	148.4	7.09	146.8	6.89	146.2	6.89
4	80.9	5.90	80.4	5.80	79.8	5.80
5	124.8		124.7		125.6	
6	133.7		132.5		131.4	
7	46.2	3.56	46.1	3.63	46.0	3.78
8	126.1	5.32	126.7	5.26	123.7	5.22
9	141.1		139.6		142.6	
10	79.4	4.33	79.2	4.00	78.2	4.03
11	32.9	2.53	31.7	2.06		2.05
		2.00		1.64		
12	35.0	1.42	32.5	1.40		
				1.13		
13	78.0	4.12	77.8	4.08	77.7	4.09
14	38.9	1.76	37.3	1.55	37.3	1.54
		1.46		1.48		
15	37.7	2.15	37.6	2.17	37.6	2.29
16	89.4	4.08	89.5	3.95	89.6	3.97
17	133.9		134.9		142.6	
18	125.9	5.42	123.6	5.00	116.7	4.75
19	22.4	2.73	21.8	2.48		3.05
		2.04		2.05		3.01
20	31.4	2.55	31.0	2.49		3.05
		2.46		2.49		2.36
21	171.4		174.0			
22	41.3		41.6			
23	33.6	1.67	33.6	1.75		
		1.32		1.51		
24	19.6	2.01	19.2	2.06		
		1.55		1.53		
25	10.6	1.95	10.7	1.94	10.7	1.96
26	16.8	1.65	16.8	1.67	16.4	1.71
27	10.9	2.05	11.2	1.80	11.5	1.86
28	20.2	1.01	20.2	1.07	19.9	1.09
29	14.5	1.53	14.6	1.51	14.5	1.54
30	26.3	1.79	26.2	1.94		
		1.34		1.47		
31	20.9	1.47	20.4	1.52		1.85
32	50.1	3.66	49.6	3.55	46.0	3.78
		3.39		3.40		3.78

‡ Spectra run in d5-pyridine on 500 MHz machine

¥ Spectra run in $CDCl_3$ with trace of triethylamine at 75/300 MHz ($^{13}C/^{1}H$)

∞ Spectra run in $CDCl_3$ with trace of trifluoroacetic acid at 75/300 MHz ($^{13}C/^{1}H$)

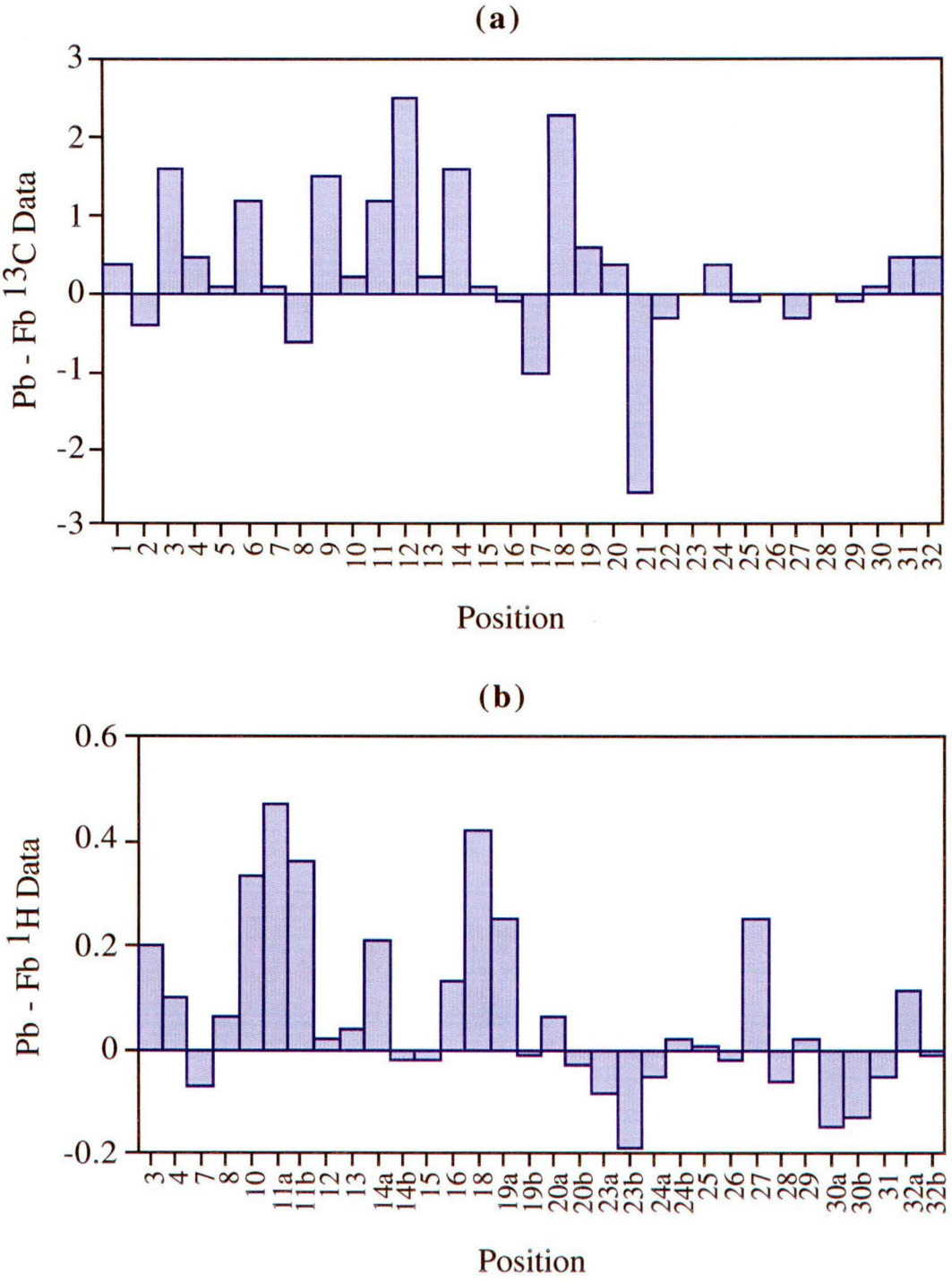

Fig 5.2.7 *(a) ^{13}C and (b) ^{1}H NMR Chemical Shift Differences Between Published (Pb) and Free-Base (Fb) Data for Gymnodimine*

The suggested enamine form of gymnodimine (Fig 5.2.8) would be characterised by an extra olefinic hydrogen atom. The lack of extra

olefinic resonances in the proton NMR spectrum of acidified gymnodimine (Fig 5.2.6(b)), gives strong evidence that the imine/enamine tautomerism is not a predominant process in gymnodimine. The changes observed in the NMR spectra, as a result of decreased pH, is evidently caused by the formation of an iminium ion.

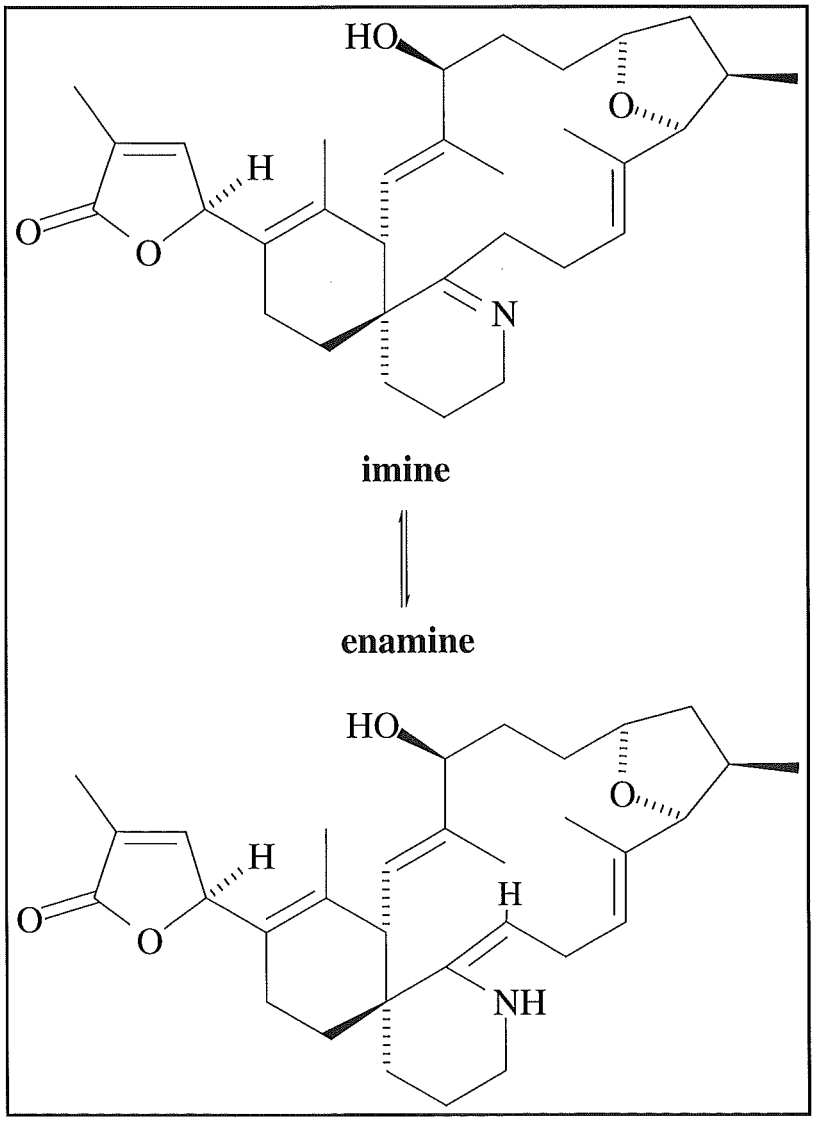

Fig 5.2.8 *Postulated pH Dependant Imine/Enamine Tautomerism of Gymnodimine (Seki et al)*

The differences between the NMR spectral data of the free-base and salt forms of gymnodimine are shown clearly in Fig 5.2.9.

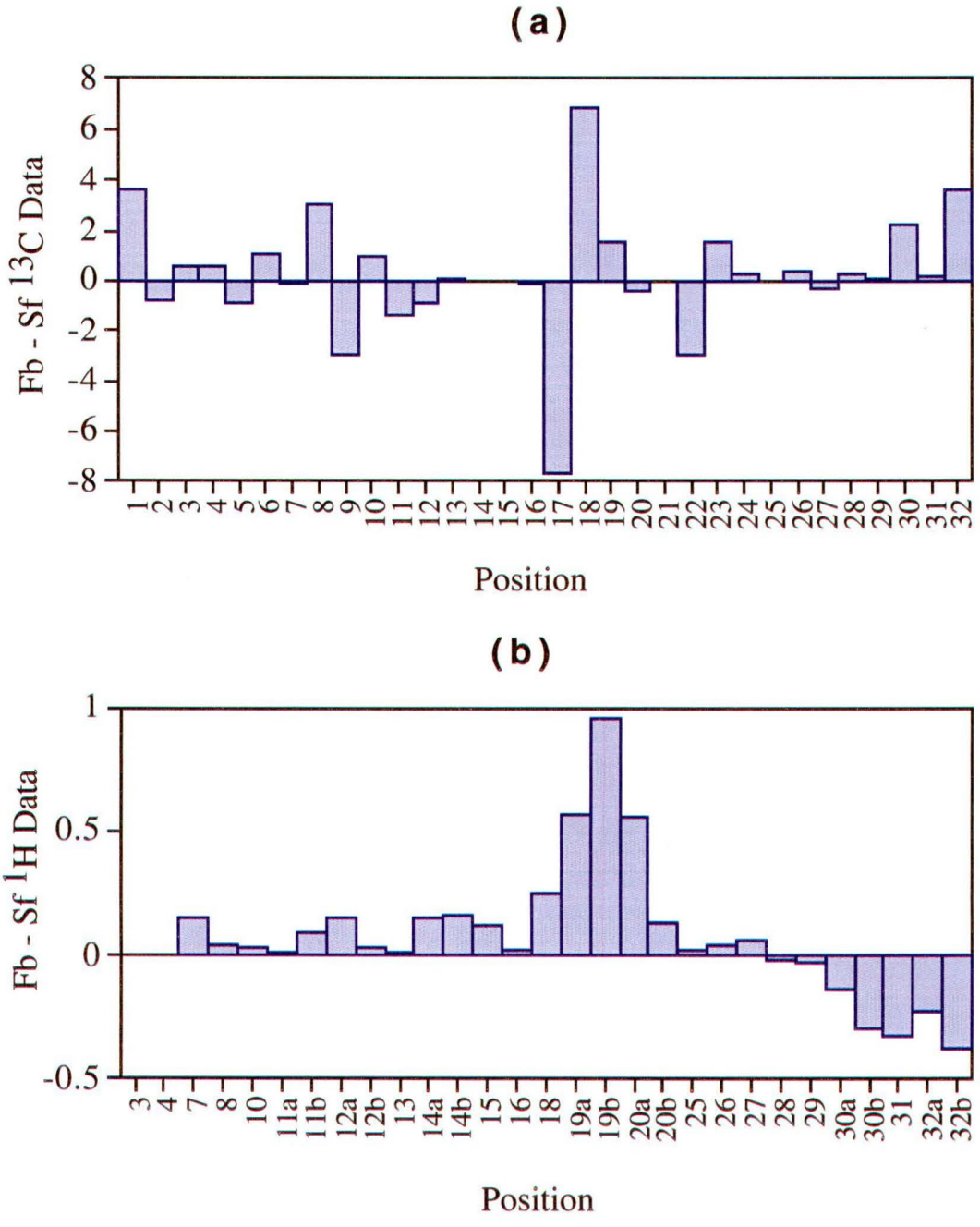

Fig 5.2.9 *^{13}C (a) and ^{1}H (b) NMR Chemical Shift Differences Between Free-Base (Fb) and Salt-Form (Sf) Data for Gymnodimine*

5.3 Absolute Stereochemistry of Gymnodimine

5.3.1 Possible Methods

The proposed strategy for the elucidation of the absolute stereochemistry of gymnodimine (**40**) consisted of two possible methods.

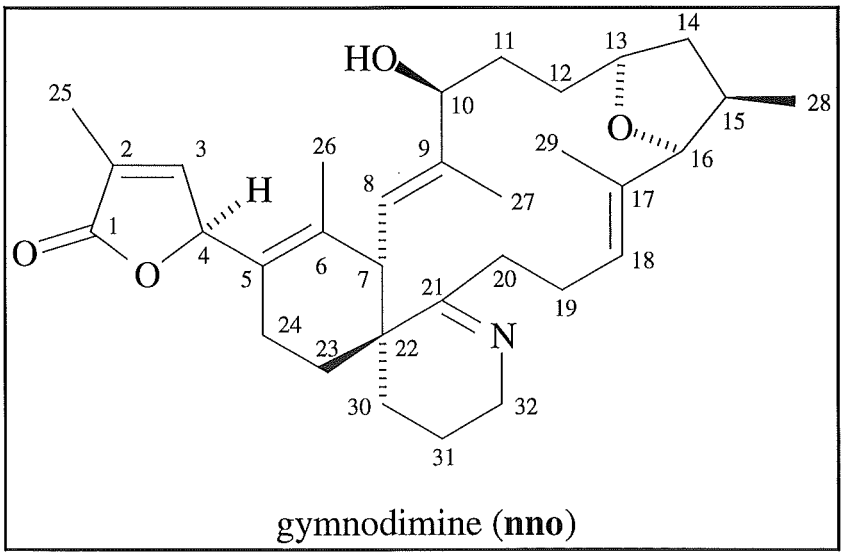

gymnodimine (**nno**)

First Approach

The first approach involved a three step procedure: initially NOE and NOESY experiments would give data on approximate proton-proton distances. By using the approximate distance information, in conjunction with a molecular dynamics program, such as the ConGen procedure,[87] relative stereochemical data could be obtained. The absolute stereochemistry could then be elucidated by attachment of

anisotropic shift reagents, such as the (*R*) and (*S*) enantiomers of MTPA (**49**)(**50**) or similar analogues, to the hydroxyl group in gymnodimine.

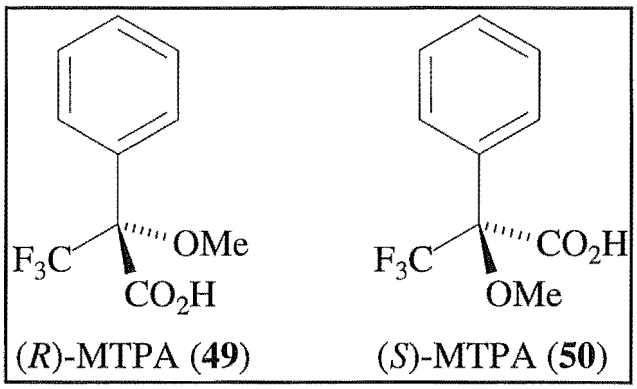

Two inherent problems were associated with this method of stereochemical analysis. These were: measurement of proton-proton distance approximations by NOE and NOESY experiments is vital to the success of this method. Slow conformational changes in the molecule caused broadening of the proton NMR signals, especially for methylene protons, making some distance assignments impractical. Furthermore, the stereogenic carbons C4 and C22 are remote from others in the molecule. The remoteness of these centres would be likely to cause difficulties in obtaining distance information, by NOE arguments. These considerations are a contributing factor to the unlikely success of this approach.

The second major problem involved the attachment of a anisotropic shift reagent to the hydroxyl group. Exploratory work revealed that the hydroxyl group was not amenable to acylation reactions, presumably as a result of steric hindrance. In addition, while attempting to acylate the hydroxyl group it was observed that the

gymnodimine itself was degrading. This degradation of the molecule was attributed to the instability of the imine.

The use of such empirical methods, using the like of MTPA, can also occasionally give erroneous results. One such example is sipholenol A (**51**).[88] Unreliable results were obtained by this method. This arose as a consequence of steric hindrance around the secondary alcohol, leading to significant conformational changes associated with the MTPA ester. As a consequence, the predictive power of the Mosher method was lost.

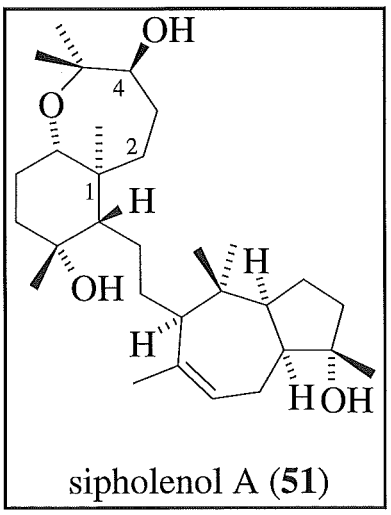

sipholenol A (**51**)

Further research concluded that care must be taken in applying Mosher's method to secondary alcohols with the OH group located in a crowded environment.[89]

Second Approach

The second strategy was to elucidate the stereochemistry by single X-ray crystallography. For X-ray analysis to be successful a single

crystal must be grown. The growth of crystals suitable for X-ray analysis is often the limiting step in this approach. With gymnodimine, suitable crystals were not available as it was a non-crystalline compound. Furthermore, with no heavy atom in the molecule only the relative *not* the absolute configuration could be obtained.

The enhancement of the crystallinity of a compound can often be accomplished by the attachment of a highly crystalline auxiliary. Specifically, the crystalline auxiliaries should contain either a stereogenic carbon atom of known chirality, or a heavy atom. The incorporation of a known stereogenic carbon atom will give conclusive proof of absolute stereochemistry, whereas the anomalous scattering of X-rays, on the heavy atom, serves as another method of absolute stereochemical elucidation.

Crystal quality is usually the major complication for elucidation of a structure by X-ray crystallography. Poor crystal traits invariably lead to erroneous refinement models and consequently, ambiguous structural elucidation. Nevertheless, clarification of the stereochemistry is unambiguous when the refinement of the structure is acceptable.

The second strategy, using X-ray analysis, was chosen due to a higher probability of success.

5.3.2 Strategy

Preliminary work revealed the instability of gymnodimine to acid chlorides, presumably due to the high reactivity of the imine. Conversion of the imine to the more stable amine was seen as a way to circumvent this problem. However, formation of the amine by reduction adds a new stereogenic centre at C21. This creates an additional complication but it does generate a position where selective addition of a chiral auxiliary can occur.

Two critical factors must be addressed before reducing the imine to the amine. Firstly, the reduction needs to be stereoselective with respect to the formation of the new stereogenic centre. Secondly, the reduction must effect only the imine group and not lead to the reduction of the other labile groups present in the molecule.

The selection of $NaCNBH_3$ fulfilled both these criteria. The cyano group increases selectivity for the imine as well as aiding in providing a highly stereoselective reduction.

5.3.3 Reduction of Gymnodimine

Reduction of gymnodimine with $NaCNBH_3$ afforded the amine, hereafter referred to as gymnodamine (**52**).

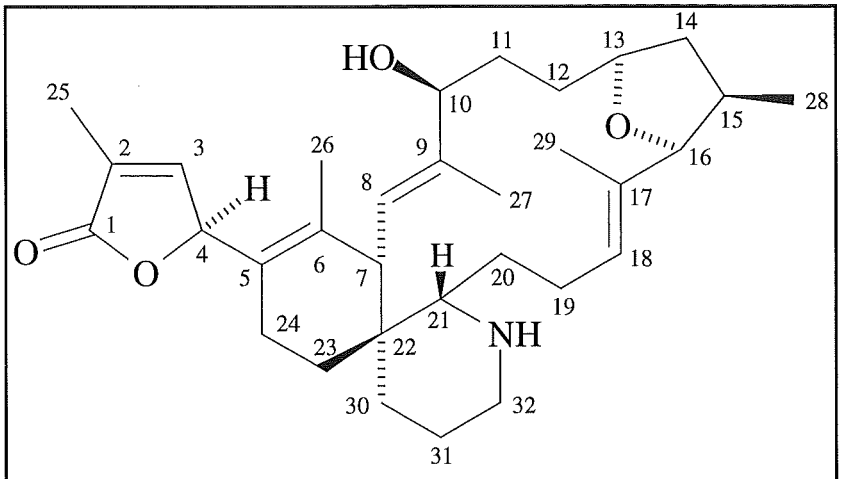

gymnodamine (**52**)

5.3.4 Spectroscopic Assignment of Gymnodamine

LREIMS on gymnodamine revealed a molecular ion *m/z* 509.3, two mass units higher than gymnodimine. Subsequent measurement of the molecular ion, under high resolution conditions, afforded *m/z* 509.3495, which corresponded to $C_{32}H_{47}NO_4$.

NMR experiments employed to assign the structure of gymnodamine included ^{1}H, ^{13}C COSY, TOCSY, HMQC, and HMBC. The low amount of material available resulted in poor data quality for the ^{13}C based experiments, hence not allowing full NMR assignment of the structure.

The ^{1}H NMR spectrum of gymnodamine (Fig 5.3.1) showed little difference to that of free-base gymnodimine (Fig 5.2.e(a)). Prominent chemical shift changes (Fig 5.3.1) were exhibited by H18 (δ 0.45,

downfield), H32 (δ 0.75/0.80, upfield) and H7 (δ 0.71, upfield). Furthermore, coalescence of Me26 and Me29 to δ 1.60 was observed. The new proton resonance exhibited by H21 was inferred by chemical shift arguments, at δ 3.65. However, conclusive proof of this assignment was obtained by a TOCSY correlation from δ 5.45 (H18) to δ 3.65.

Experimental data for gymnodamine are contained in Section 6.5.3.

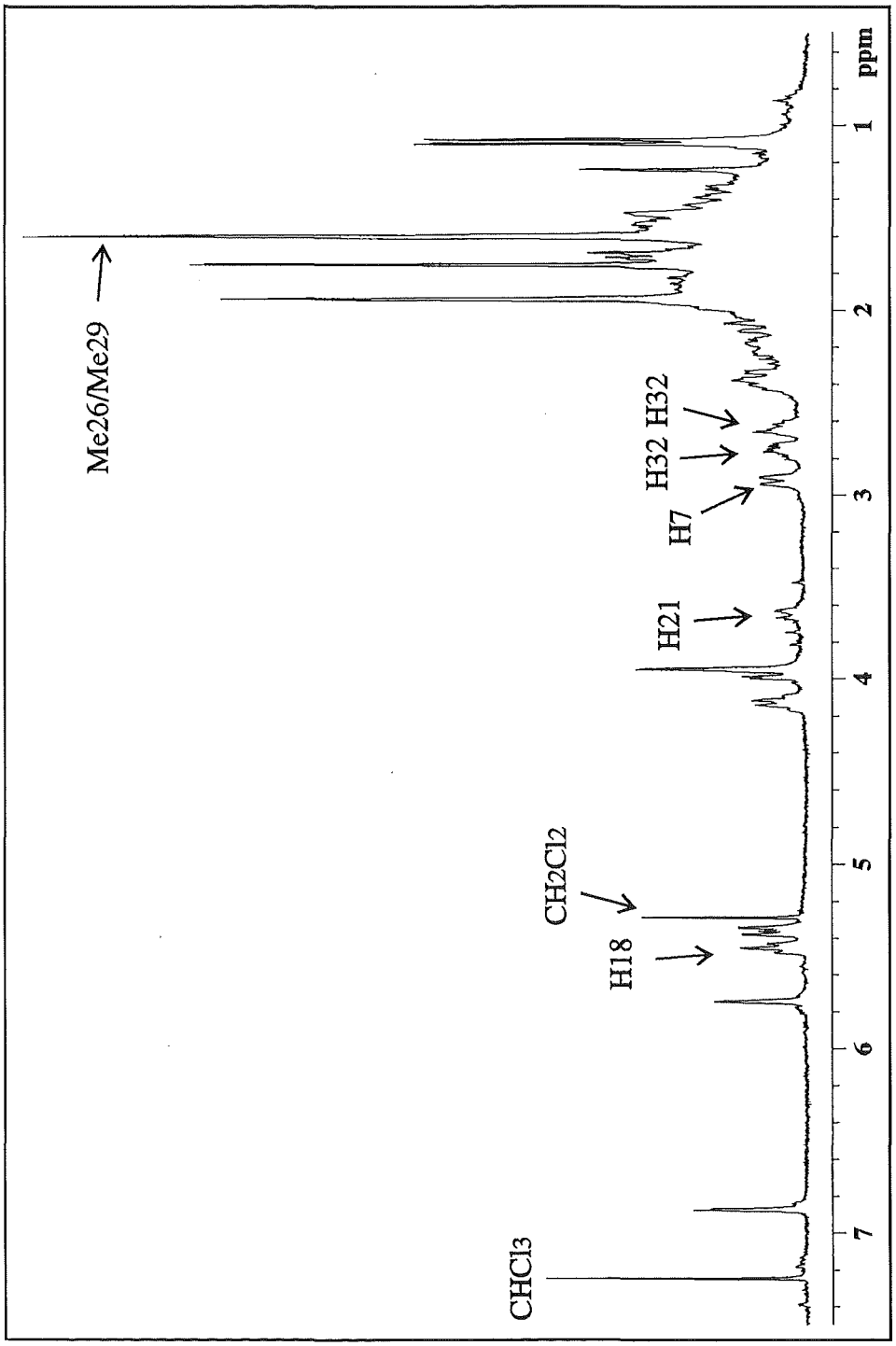

Fig 5.3.1 *^1H NMR Spectrum of Gymnodamine*

($CDCl_3$)

5.3.5 Formation of Crystalline Derivatives of Gymnodamine

The potential of each of three auxiliaries, to form a crystalline product, was explored. The three compounds examined were *p*-bromobenzoyl chloride (PBBC, **53**), *p*-bromobenzene sulfonyl chloride (BsCl, **54**) and (*1S*)-(+)-camphorsulfonyl chloride (CSCl, **55**)

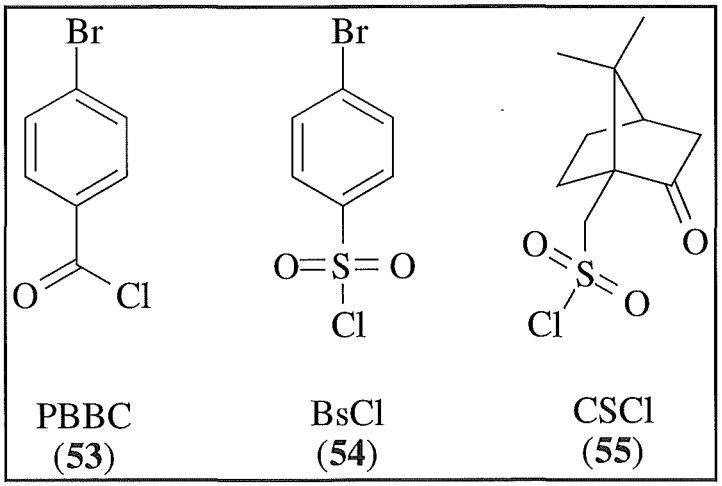

Reaction of PBBC (**53**) with gymnodamine was achieved under anhydrous conditions. The reaction mixture was purified on diol HPLC, with one product only obtained. LRFABMS gave two molecular ions, *m/z* 692.3/694.3 (1:1 intensity), showing the characteristic bromine pattern. This isotope pattern confirmed the attachment of just one *p*-bromobenzoyl group.

The proton NMR spectrum of the product showed two doublets, at δ 7.52/7.19, arising from the aromatic protons. This too served to confirm the attachment of the *p*-bromobenzoyl group. The H10 proton resonance was still at δ 3.94, giving evidence for the absence of an

ester at this position and consequently, attachment of the auxiliary as the amide (**56**).

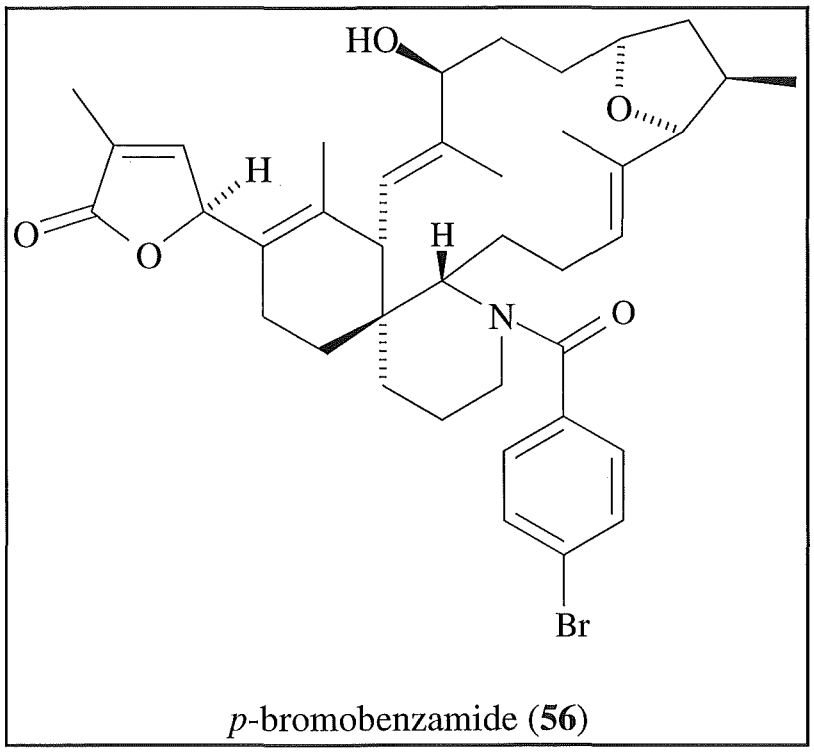

p-bromobenzamide (**56**)

The reaction between BsCl (**54**) and gymnodamine was carried out under anhydrous conditions. The organic soluble material from this reaction was analysed by proton NMR spectroscopy. The spectrum showed a proton resonance at δ 4.90, indicative of an ester functional group and suggestive of attachment of this crystalline auxiliary at both amine and hydroxyl groups. Subsequent purification on amino and diol cartridges afforded one product. A proton NMR spectrum of this product revealed the absence of the signal at δ 4.90, that had been seen in the reaction mix. Aromatic signals in the NMR spectrum verified the attachment of the *p*-bromosulfonyl group. LRFABMS was attempted on this fraction, however the molecular ion was not observed.

The reaction between (*1S*)-(+)-camphorsulfonyl chloride (CSCl, **55**) and gymnodamine was carried out under anhydrous conditions. The organic soluble material was purified on an amino cartridge and then analysed by proton NMR spectroscopy. The diastereotopic protons of CSCl were shifted upfield by around 0.8 ppm, suggesting successful coupling. Further purification on a diol cartridge was unsuccessful. No product could be discerned from any fraction off this cartridge.

Evaluation of the three auxiliaries employed revealed that PBBC had been the most successful. The reaction/purification procedure was the simplest and the product formed was able to be identified conclusively. Furthermore, this material showed potential crystallinity, appearing as a white amorphous solid.

The PBBC/gymnodamine reaction was repeated on a second batch of gymnodamine (8.0 mg). The organic soluble material was purified on diol HPLC, providing the pure *p*-bromobenzamide derivative (**56**), at a yield of 4.0 mg (37%).

5.3.6 Crystal Structure of p-Bromobenzamide (56)

Recrystallisation of the amide (**56**) was successfully achieved from a 50% CH_2Cl_2/benzene solvent mix, affording irregular shaped, transparent crystals. A single crystal, suitable for X-ray structure analysis, was separated from the bulk sample.

The data were collected using a Siemens P4 diffractometer. The structure of (**56**) was solved by direct methods (SHELXS-96). Of the 4064 reflections obtained, 4007 were unique (R_{int} = 0.0221). These reflections were used in the full-matrix, least-squares refinement (SHELXL-96), after being corrected for absorption by using the psi-scan method. Three check reflections were measured every 97 reflections throughout the data collection. All hydrogens were inserted in calculated positions. Significant residual electron density was attributed to a benzene molecule, co-crystallised in the solid state. The absolute configuration was determined from the anomalous scattering of the bromine atom. Final conventional R factors were calculated for the absolute structure [$I>2\sigma(I)$] R_1 = 0.0360, wR_2 = 0.0376 and for the inverse structure, R_1 = 0.0574.

The perspective drawing of the refined crystal structure (Fig 5.3.2) shows all stereocentres precisely, from which the assignment of 4*S*, 7*S*, 10*S*, 13*R*, 15*R*, 16*R*, 21*S*, 22*R* could be made unequivocally. From this it follows that the absolute stereochemistry of gymnodimine is 4*S*, 7*S*, 10*S*, 13*R*, 15*R*, 16*R*, 22*R*.

An ORD experiment on a sample of gymnodimine revealed that it had the same sign of rotation to that published by Seki *et al.*[67] These data confirmed the absolute stereochemistry elucidated here applies also for the published toxin.

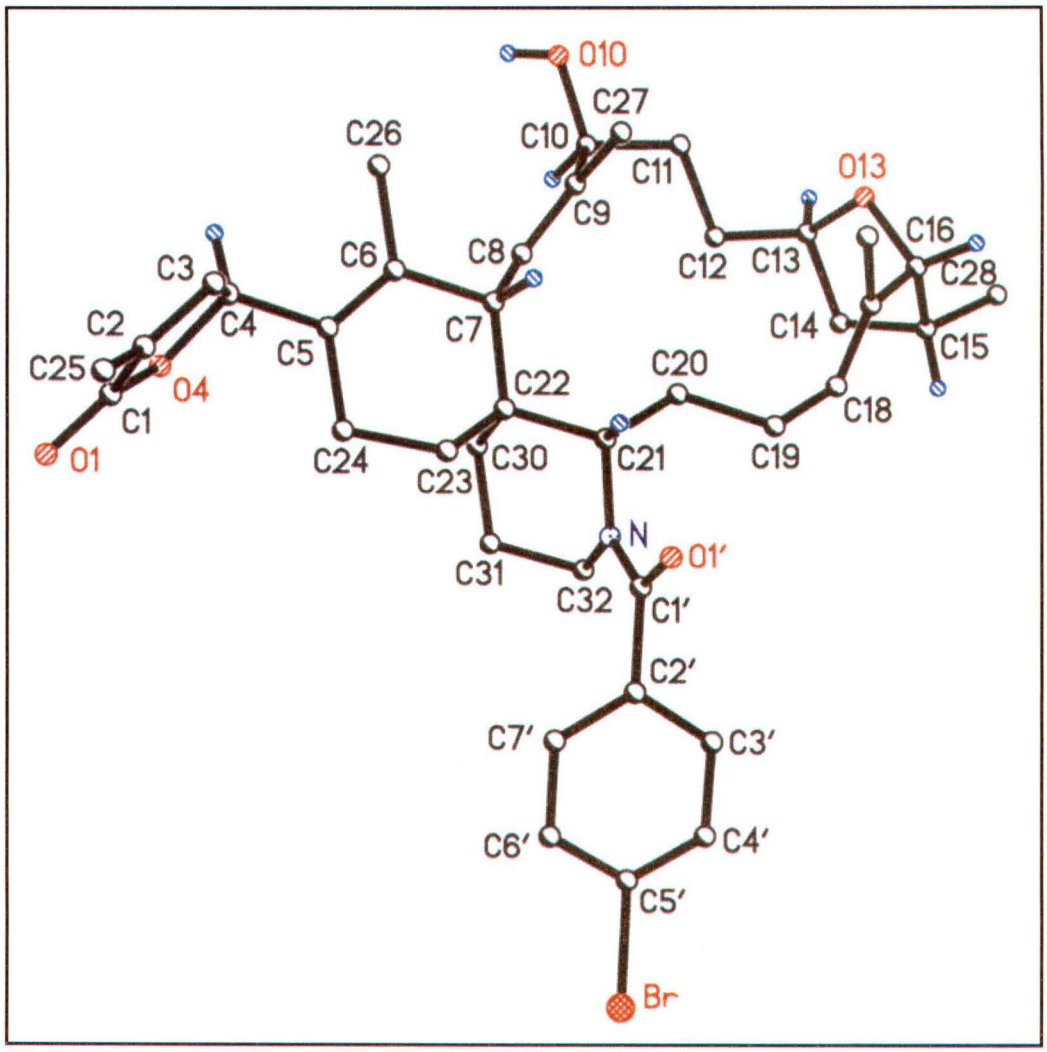

Fig 5.3.2 *Perspective Drawing of Crystal Structure of (**56**)*

The asymmetric unit cell was found to contain four independent molecules. Inter-molecular hydrogen bonding from the hydroxyl proton was observed to carbonyl oxygen atoms in the lactone and amide functional groups. Fig 5.3.3 shows the packing orientation in the crystal lattice.

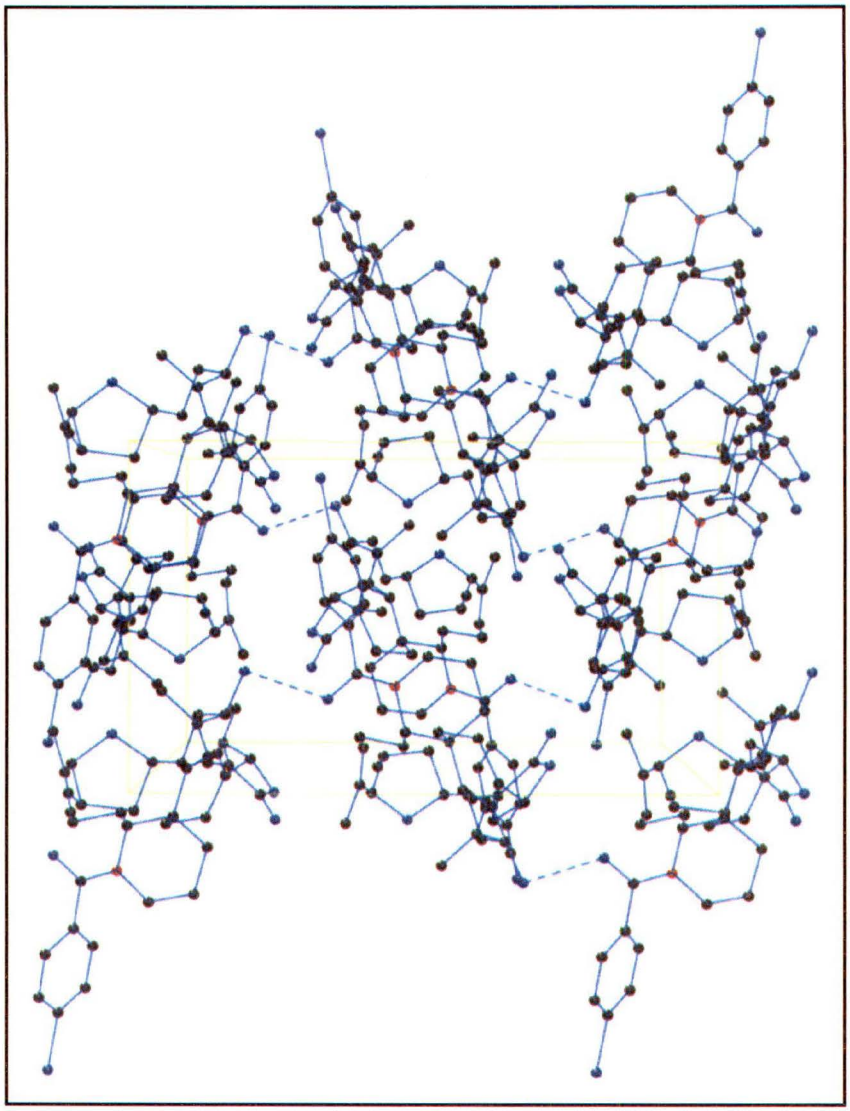

Fig 5.3.3 *Packing Diagram of Crystal Structure (**56**)*

[Hydrogen atoms omitted for clarity]

Crystallographic data are listed in Appendix 2.

5.3.7 NMR Spectral Assignment of *p*-Bromobenzamide (56)

LRFABMS gave molecular ions at *m/z* 692.3/694.3 ($[M+H]^+$, as observed for the initial sample. Subsequent HRFABMS on the 692 ion, afforded an accurate mass of 692.2971, corresponding adequately to a molecular formula of $C_{39}H_{50}O_5NBr$.

Numerous NMR techniques were utilised to give chemical shift assignments for (**56**). These NMR experiments included ^1H, ^{13}C, COSY, TOCSY, HMQC and HMBC.

The proton NMR spectrum of (**56**) (Fig 5.3.4) showed doubling of various peaks (in a ratio of approximately 3:1), attributed to two amide conformations. For ease of assignment, only signals belonging to the major amide conformation are reported. The majority of proton and carbon resonances were congruent with those observed for the amine (**52**) and so were assigned by direct comparison.

The proton and carbon resonances of the *p*-bromobenzoyl group were assigned in the following manner:

An HMQC experiment gave $^1J_{CH}$ correlations for the aromatic doublets of δ 7.52/131.8 and δ 7.19/128.0. $^2J_{CH}$ and $^3J_{CH}$ correlations were observed from δ 7.19 (H3"/H7") to δ 170.0 (C1"), 135.6 (C2") and 123.5 (C5"), in the HMBC spectrum, providing full chemical shift assignment of this moiety.

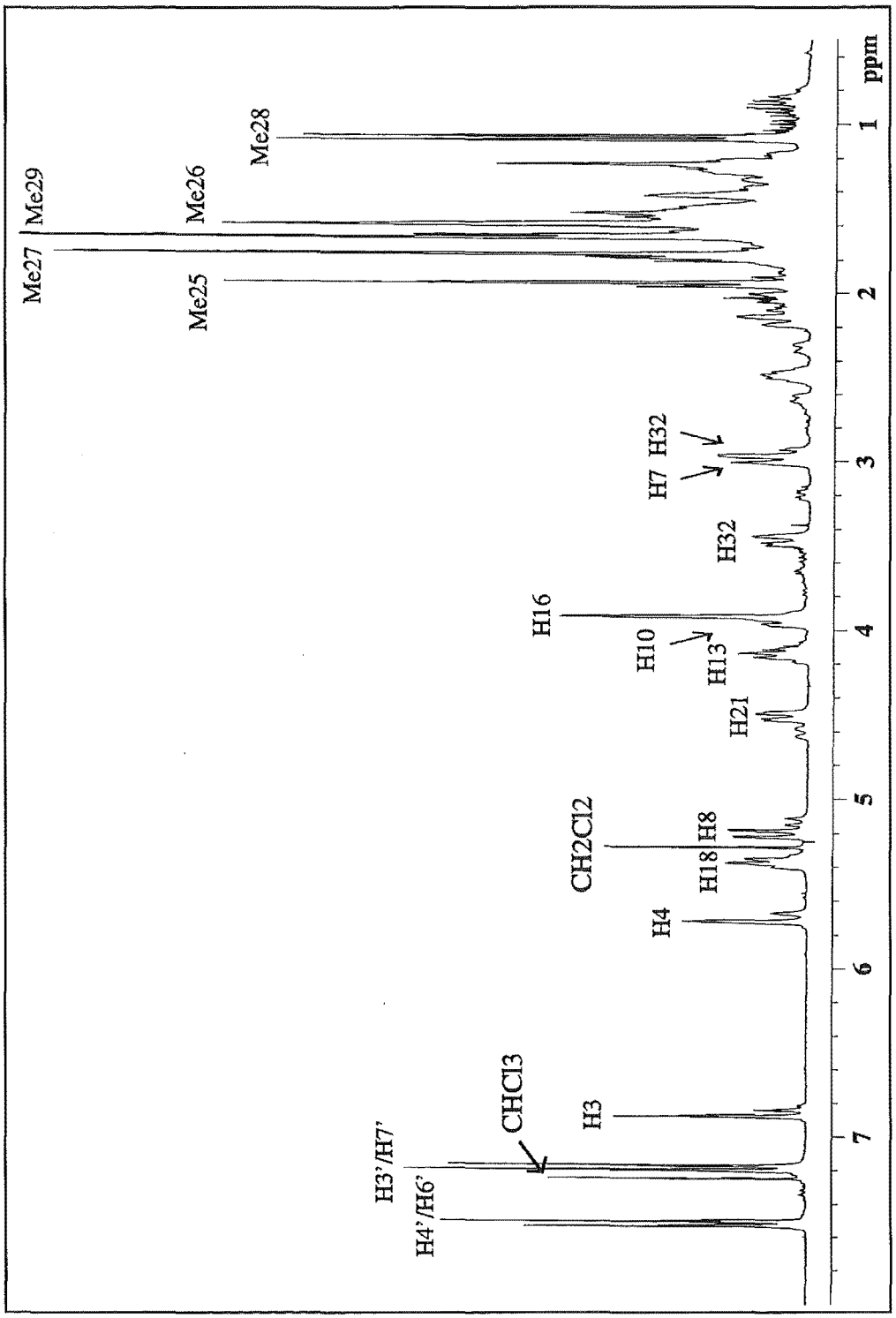

Fig 5.3.4 *^1H NMR Spectrum of p-bromobenzamide (**56**)*

($CDCl_3$)

The most notable changes in chemical shifts from the parent amine (**52**) were observed for atoms in proximity to the amide moiety. A new proton resonance at δ 4.50 (Fig 5.3.4) was assigned as H21 by chemical shift arguments. A $^1J_{CH}$ correlation was observed from this proton to a carbon atom at δ 58.5. The TOCSY spectrum showed correlations from this proton to δ 5.38 (H18), confirming this assignment as H21.

The spin system of H18-H21 was able to be assigned by a 1D TOCSY experiment, using excitation at δ 5.38 (H18) and various mixing times. The proton resonances unravelled by the 1D TOCSY, showed $^1J_{CH}$ correlations to respective carbon atoms.

The isolated resonance at δ 3.47 (Fig 5.3.4) showed geminal coupling to δ 2.97 in the COSY spectrum. These resonances were assigned as the H32 methylene protons. This was supported by the HMQC spectrum which correlated both these proton resonances to δ 42.3. Accurate chemical shift assignments could not be made for positions 23/24, as chemical shift resolution of these methylenes could not be achieved.

Collation of the NMR data gave an almost complete chemical shift assignment for the amide structure (Fig 5.3.5).

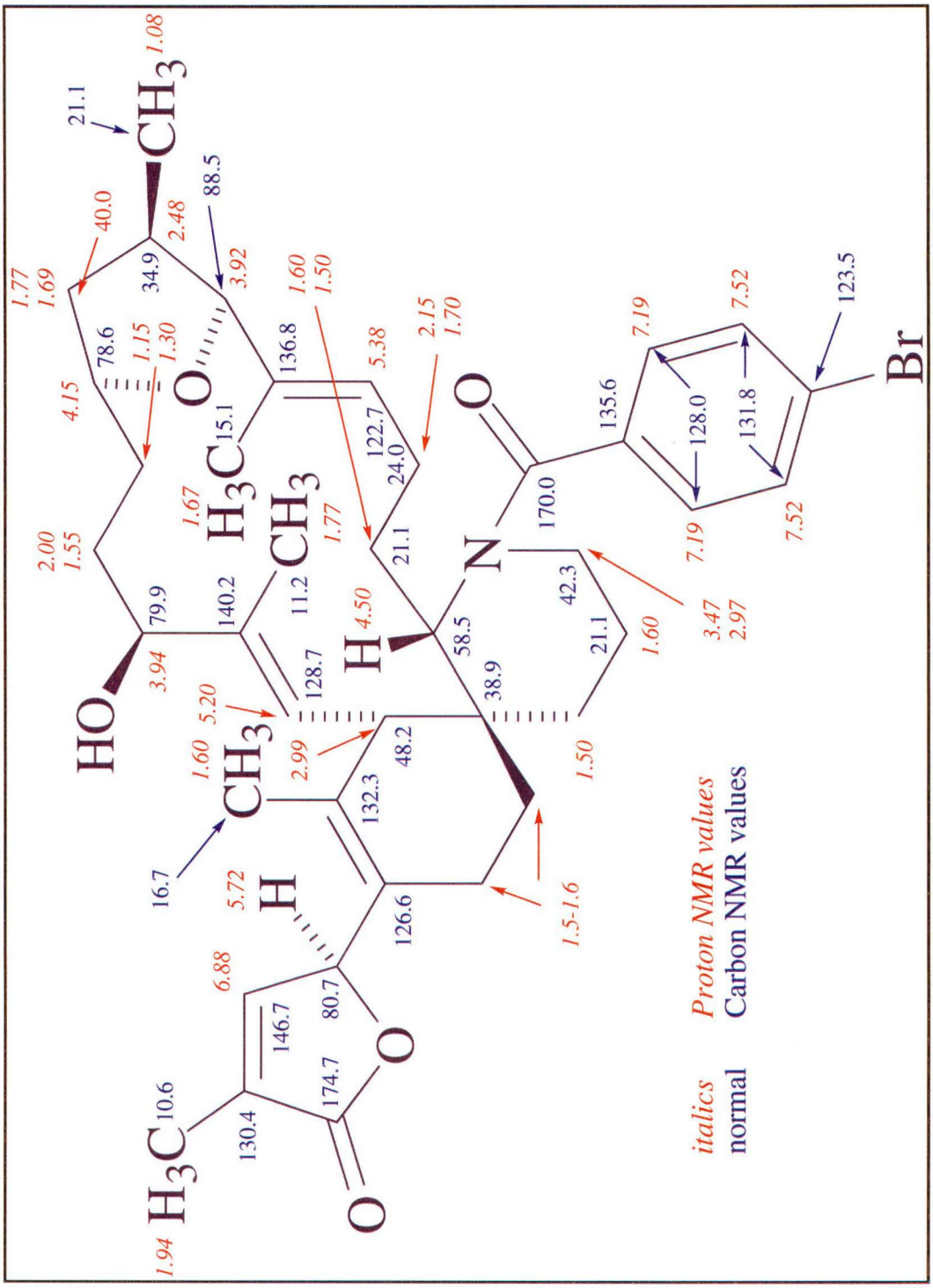

Fig 5.3.5 *NMR Spectral Assignments for Amide (56)*

5.3.8 Conformational Studies on Gymnodimine and p-bromobenzamide (56)

*p-bromobenzamide (**56**)*

An analysis of proton-proton distances for the amide (**56**) in solution was achieved by a series of NOE experiments. The results from these selected enhancements (Fig 5.3.6) were compared with the proton/proton distances measured from the crystal structure of (**56**). These data provided arguments for conformational difference between the solid and solution states. The differences were particularly highlighted by two significant enhancements observed between protons with proton-proton distances greater than 3 Å in the solid state (Fig 5.3.6).[90]

The differences between the conformations for the solid and solution states of (**56**) highlighted the necessity for modelling studies on this compound.

The cartesian coordinates from the X-ray structure of the amide (**56**) were loaded into the Chem3D[91] application and served as the basis for initial studies.

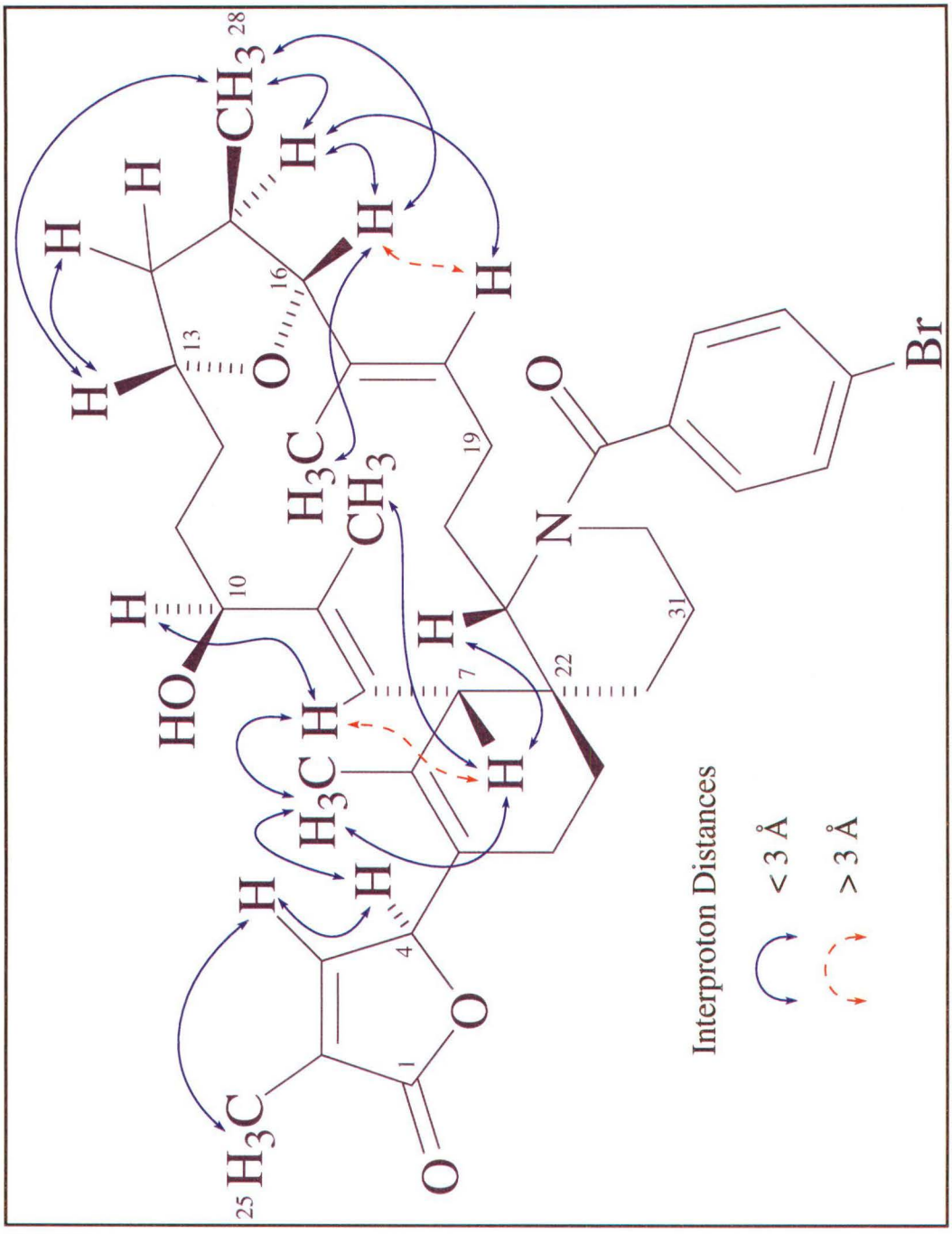

Fig 5.3.6 *Selected NOE's for Amide (56)*

Geometry minimisation of (**56**), with the program Spartan,[92] was achieved using the semi-empirical AM1 model.[93] The optimised structure produced by this minimisation is named GM-1 (Appendix Four). Analysis of the inter-proton distances of GM-1 revealed further anomalies with the NOE data. The proton-proton distances, already

over 3 Å for the crystal structure, increased even further, after minimisation. Furthermore, inter-proton distances of H8/Me26 and H13/Me28, initially at 2.835 Å and 2.870 Å respectively, increased to 3.052 Å and 3.400 Å, following minimisation. These data suggested that the energy minimum found by the modelling program was a local minimum, and that other low energy conformations of the amide were likely.

As a conformational picture of gymnodimine in solution, as opposed to the amide (**56**), was the desired result of this research, further conformational searching, or global minimisation techniques, were not employed for (**56**). The study of the conformation of gymnodimine was initiated by collection of inter-proton distance approximations in solution.

Gymnodimine

Analysis of proton-proton distances of gymnodimine, in solution, was achieved by selective NOE experiments.

The observed NOE enhancements for gymnodimine were compared with the proton-proton distances acquired from the minimised amide structure GM-1. These data revealed that six of the observed NOE's were outside the 3 Å threshold (Fig 5.3.7). In addition, three of these showed very large proton-proton distances: H15/Me29 (3.902 Å), H16/H18 (3.729 Å) and H18/Me27 (4.029 Å).

The molecular shape of the amide is significantly different to that of gymnodimine and hence does not provide an accurate model for conformational study. Consequently, a minimisation of gymnodimine was carried out using the coordinates of GM-1 as a starting point.

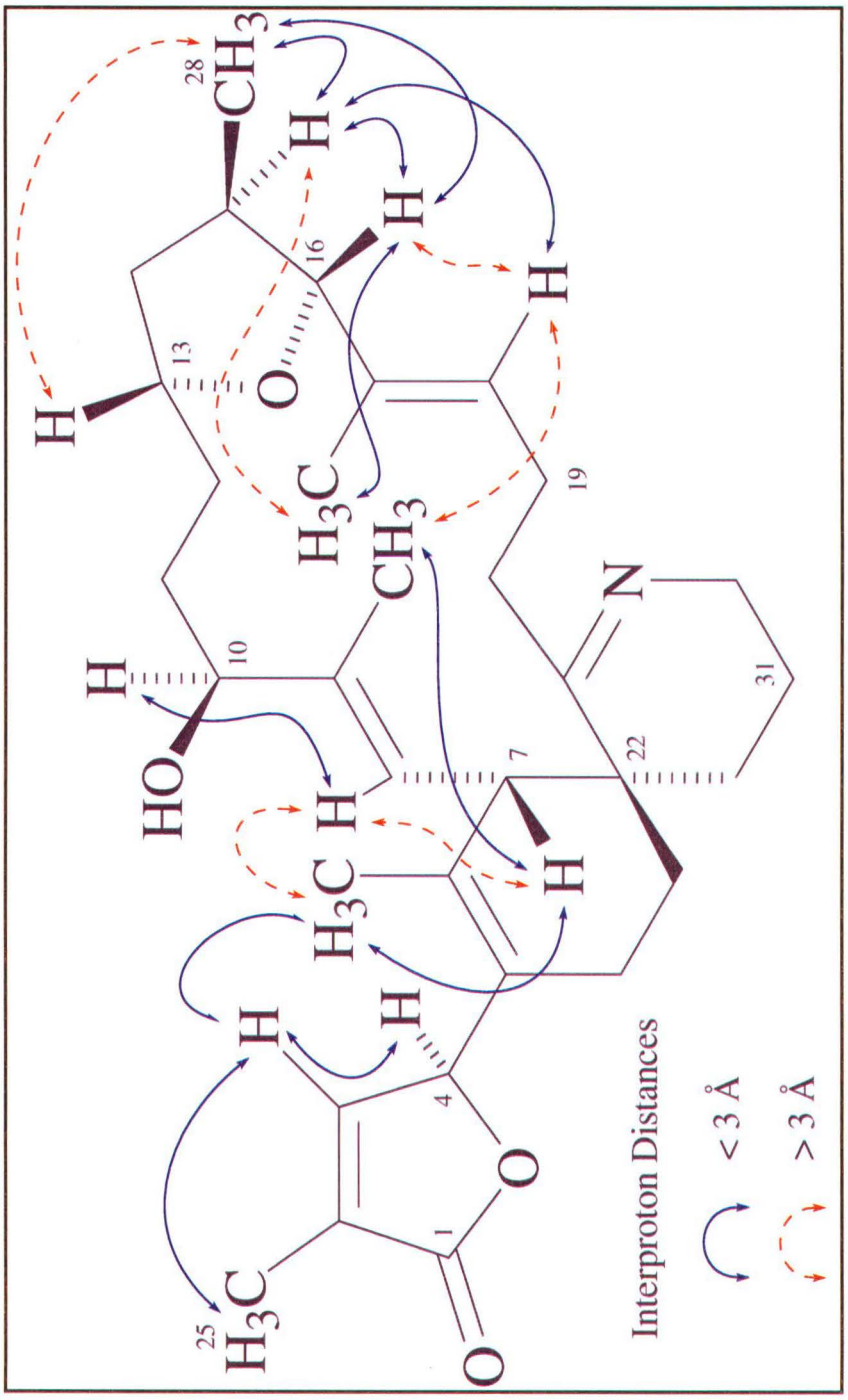

Fig 5.3.7 *Selected NOE's for Gymnodimine*

Gymnodimine was created in Spartan by modification of the GM-1 structure. This was achieved by removal of the *p*-bromobenzoyl group and re-formation of the imine bond. Geometry minimisation of this structure, again using the AM1 model, gave a new optimised structure, GM-2 (Appendix Four). The heat of formation of GM-2 was calculated as -142.7 kcal/mol.

Measurement of proton-proton distances of GM-2 revealed closing of some of the unfavourable distances. Those distances still over the 3 Å threshold included: H7/H8 (3.113 Å), H8/$H30_{eq}$ (3.040 Å), H13/Me28 (3.497 Å), H15/Me29 (3.737 Å), H16/H18 (3.744 Å) and H18/Me27 (3.897 Å).

Constrained molecular modelling was employed as the next step. Constraining of the six conflicting inter-proton distances to 2.5 Å was achieved. The distance of 2.5 Å was chosen as an arbitrary distance to attempt to "force" a conformational change of GM-2 to a global minimum. A geometry minimisation of GM-2 was employed, with these constraints, again using the AM1 model. The optimised structure produced by this minimisation is named GM-3 (Appendix Four). The heat of formation of GM-3 was calculated as 3.7 kcal/mol higher than GM-2.

To attempt to create a non-constrained minimised model the constraints applied to GM-3 were removed. After removal of the distance constraints in GM-3, another AM1 geometry minimisation was carried out. The model produced by these calculations was assigned as GM-3a

(Appendix Four). The heat of formation of GM-3a was calculated as 4.7 kcal/mol lower than GM-3 and 1 kcal/mol lower than GM-2.

Measurement of inter-proton distances of GM-3a revealed that minimisation with constraints had succeed in closing three of the conflicting distances observed in GM-2: H8/H30$_{eq}$ (1.922 Å), H15/Me29 (2.566 Å) and H18/Me27 (2.507 Å). However, the inter-proton distances of H7/H8 (3.115 Å), H13/Me28 (3.606 Å) and H16/H18 (3.471 Å) were still unfavourable.

The above data and calculations suggest that gymnodimine may contain several conformers with similar energy levels. This would then account for the broadness of many proton signals in the ^{1}H NMR spectrum, as these conformations may be interchanging on a time-scale similar to that of the NMR observations. The conformational flexibility of the molecule presents difficulties in the analysis and interpretation of NOE data, due to averaging of the proton resonances in the NMR spectrum.

Analysis of the preferred (lowest energy) conformations of gymnodimine would require much effort and time and comprises a separate topic in itself. Conformational searching on a molecule the size of gymnodimine would not guarantee a satisfactory result due to the many variables involved. Furthermore, for a molecule with the conformational flexibility of gymnodimine, the information gleaned from such a study would not in itself provide much further useful information on the conformations adopted by the molecule.

5.4 Design and Synthesis of Gymnodimine Haptens

5.4.1 Design

Three likely positions for attachment of a linker to gymnodimine (**40**) were considered possible (Fig 5.4.1).

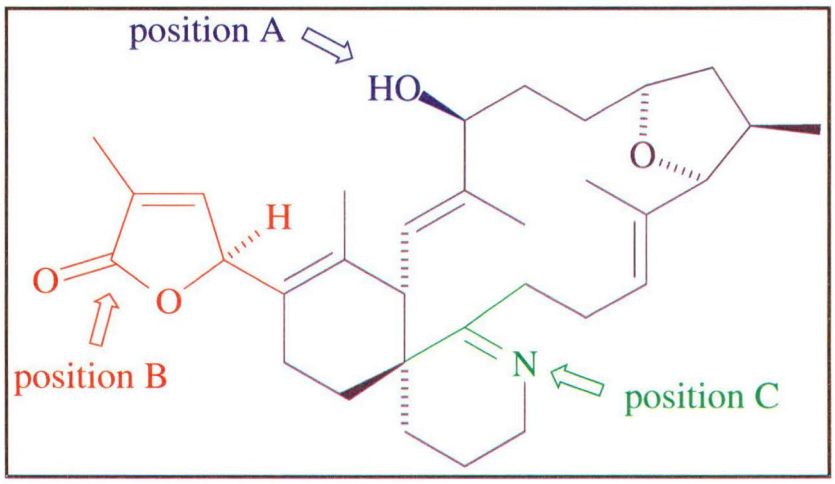

Fig 5.4.1 *Proposed Linkage Positions for Hapten Synthesis of Gymnodimine*

The hydroxyl group at position A (Fig 5.4.1) provided the most obvious linker point. However, previous attempts at derivatisation of this hydroxyl (Section 5.3.1) proved unsuccessful. The failure of the acylation was attributed to a probable steric hindrance around the hydroxyl group. Furthermore, degradation of the toxin suggested lability of the imine to standard acylation methods.

Position B required the opening of the butenolide (Fig 5.4.1). Butenolides are not normally amenable to opening under standard

conditions, although reagents such as $(CH_3)_2AlNH_2$[94] and $(CH_3)_3SiI$[95] have been reported in the literature. However, the lability of the imine, suggests that success with these reagents would be unlikely.

The imine (Fig 5.4.1) does not itself offer a direct position for attachment of a linker group. Fortunately, previous work revealed the ability to stereoselectively reduce the imine to the more stable amine (Section 5.3). The greater nucelophilicity of the amine over the hydroxyl group provides a regiospecific point of attachment at position C. Hence the amine provided a unique opportunity for linker attachment at position C and was judged the approach most likely to succeed.

Linker groups examined for attachment were succinic semialdehyde (**57**), succinic anhydride (**58**) and *p*-maleimidophenyl isocyanate (PMPI, **45**).

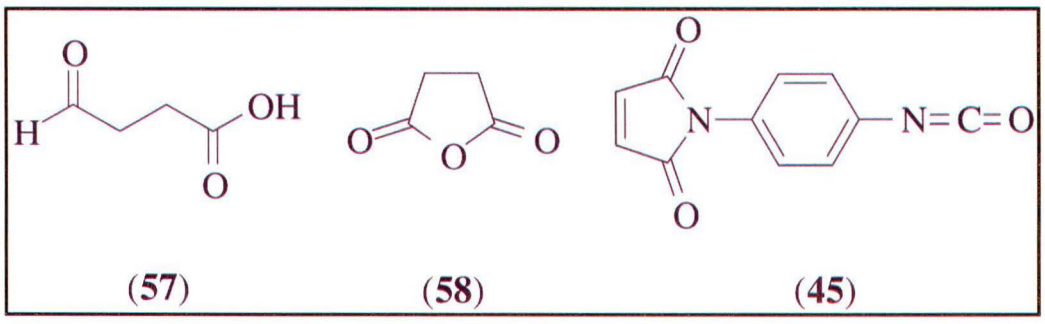

(57) (58) (45)

Both succinic semialdehyde and succinic anhydride provide linkers of identical chain lengths, although offer different linkage chemistries to the toxin. PMPI provides alternative linkage and conjugation chemistry to the first two linkers. The maleimide moiety of PMPI supplies selectivity for protein conjugation by binding to sulfhydryl (S-

H) residues in those proteins *via* Michael addition to the maleimide group.

5.4.2 Syntheses

The reaction between gymnodamine (**52**) and succinic semialdehyde (**57**), in the presence of $NaCNBH_3$ was carried out under anhydrous conditions. After work-up, the reaction mixture was chromatographed on a reverse phase C18 column. The desired gymnodamine-amine linker (**59**) was isolated (64% yield).

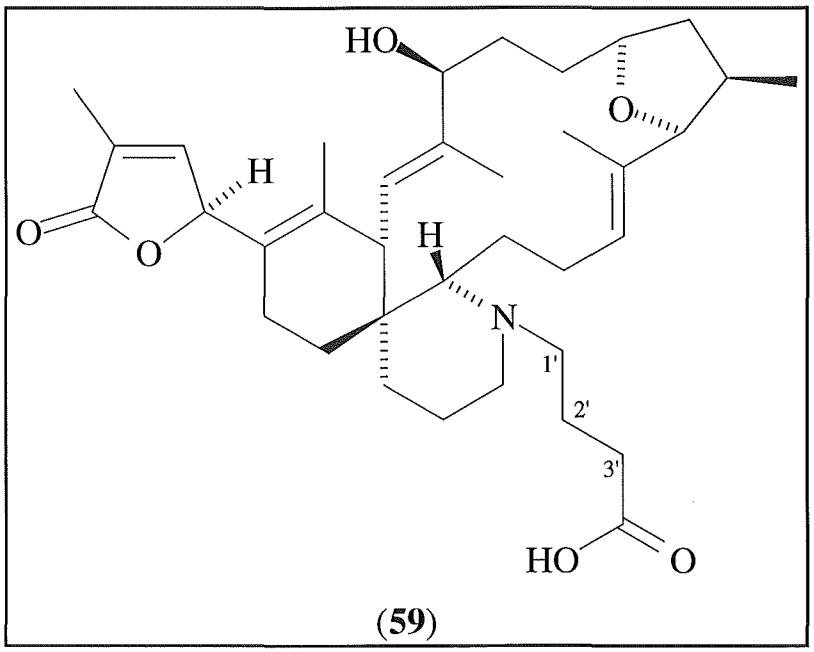

(**59**)

LRFABMS on (**59**) afforded a molecular ion *m/z*, 596.2 $[M+H]^+$. Subsequent measurement of the molecular ion, under high resolution conditions, afforded *m/z* 596.3965, corresponding to a molecular formula of $C_{36}H_{53}NO_6$.

The ^1H NMR spectrum of (**59**) contained an extra triplet at δ 2.91. A 1D TOCSY experiment, using excitation at this resonance, established that this resonance was part of the spin system H1'-H3', and confirmed the H2' and H3' resonances. These signals showed good chemical shift agreement with a model compound (**60**)(Fig 5.4.2).

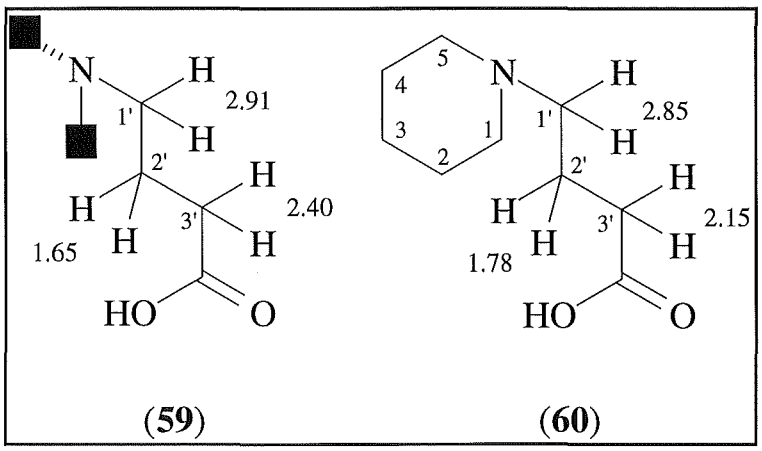

Fig 5.4.2 *Proton Chemical Shifts for H1'-H3' Spin System of Gymnodamine-Amine Linker (**59**) and Model Compound (**60**)*

Experimental data for (**59**) and (**60**) are contained in Section 6.5.4.

The reaction between gymnodamine and succinic anhydride (**58**) was performed under anhydrous conditions. After work-up, the reaction mixture was purified by reverse phase C18 HPLC. The desired gymnodamine-amide linker (**61**) was isolated (21% yield). Recovery of gymnodamine (35% of starting mass) from the HPLC column revealed that the reaction had not reached completion.

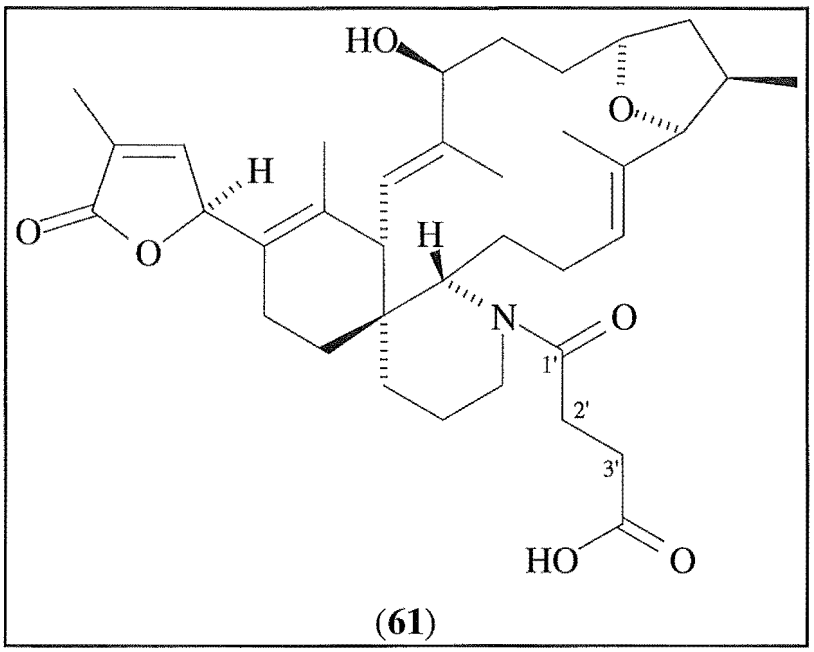

(61)

LRFABMS on (**61**) afforded a molecular ion of *m/z* 610.2 $[M+H]^+$. Subsequent measurement of the molecular ion, under high resolution conditions, afforded *m/z* 610.3741, corresponding to a molecular formula of $C_{36}H_{51}NO_7$.

The ^1H NMR spectrum of (**61**) revealed an increased broadening of the majority of signals over those observed in the spectrum of gymnodamine. This suggested conformational changes between the cis/trans amide forms. A broad peak at δ 2.58, equivalent to four protons, was at the correct chemical shift for the H2'/H3' protons. This was confirmed by synthesis of the model compound (**62**). Proton signals belonging to H2'/H3' of (**62**) were identified, in the ^1H NMR spectrum, at δ 2.64/2.52 (Fig 5.4.3). Attachment of the linker at the amine, and not the hydroxyl group, was proven by an NOE experiment on (**61**). Selective irradiation at δ 5.22 (H7), revealed an enhancement at δ 3.96 (H10). This is the typical and expected chemical shift for this proton in this series.

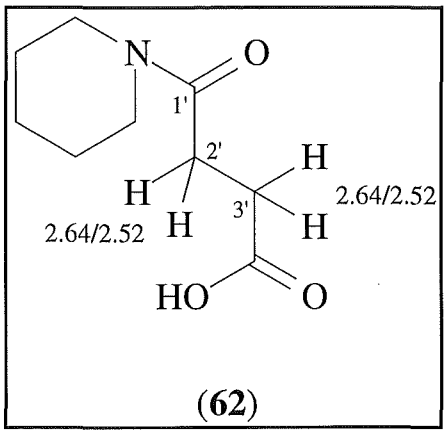

(62)

Fig 5.4.3 *^{1}H NMR Chemical Shift Positions of H2' and H3' of (**62**)*

Experimental data for (**61**) and (**62**) are contained in Section 6.5.4.

The reaction between PMPI (**45**) and gymnodamine was performed in a sealed glass NMR tube, under anhydrous conditions. Progress of the reaction was monitored by ^{1}H NMR at regular intervals. After 98 hours, disappearance of the signals, for the phenyl protons on PMPI, signalled the completion of the reaction. Upon work-up, the reaction mixture was purified by reverse phase C18 HPLC. Two maleimide linker compounds were isolated. The major product (0.5 mg, 23% yield) was the gymnodamine-urea maleimide linker (**63**), while the minor product (0.25 mg, 9% yield) was the gymnodamine-*di*-urea/carbamate maleimide linker (**64**).

LRFABMS on (**63**) produced a molecular ion *m/z*, 724.4 $[M+H]^+$. Subsequent measurement of the molecular ion, under high resolution conditions, afforded *m/z* 724.3990, which corresponded satisfactorily to a molecular formula of $C_{43}H_{53}N_3O_7$.

The ^{1}H NMR spectrum of (**63**) revealed a 2H singlet at δ 6.82. This was due to the symmetric maleimide protons. In addition, the doublets at δ 7.43 (J = 8.3) and δ 7.23 (partially obscured by $CHCl_3$ solvent peak), were assigned as the phenyl protons.

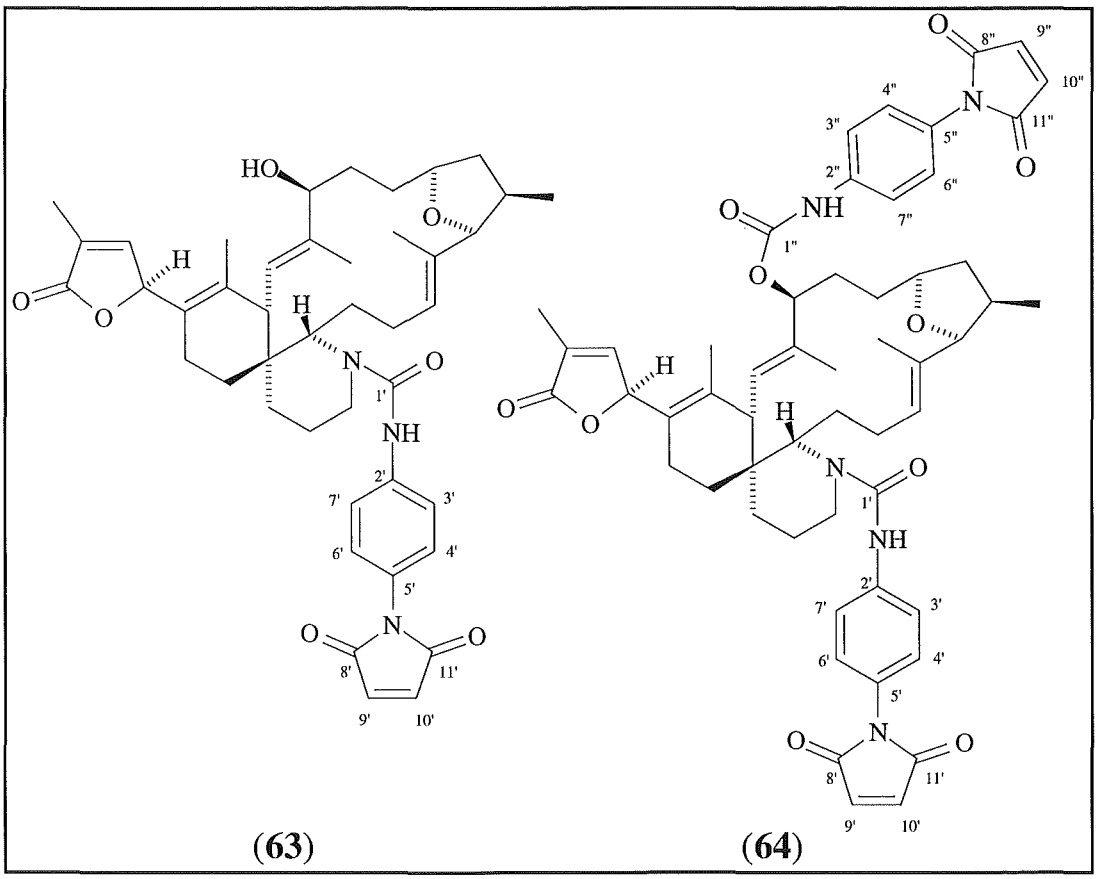

The ^{1}H NMR spectrum of (**64**) revealed doubling of the maleimide proton singlet (δ 6.82/6.83), indicative of a *di*-linked product. Furthermore, an extra proton resonance at δ 5.45 was distinctive of a downfield shift of H10, due to a carbamate moiety at this position. LRFABMS was attempted on this sample, however the expected molecular ion was not observed.

Experimental data for (**63**) and (**64**) are contained in Section 6.5.4.

5.4.3 Results

The carboxylic acid haptens (**59**) and (**61**) were selected for developmental study. The similarity of each linker provided the type of molecules necessary for further progress. The maleimide linker (**63**) was not chosen, due to the size of the linker group. The success of the maleimide linker could be hampered by recognition of the linker itself, which can lead to possible cross reactivity in the assay.

Further evidence for the unlikely success of the PMPI linker (**63**) was obtained from the minimised model of this molecule, GM-4 (Appendix 4). AM1 minimisation could not be carried out as the limit for AM1 semi-empirical minimisation is 100 atoms.[92] The Sybyl force field was used. The model GM-4 (Appendix 4) clearly shows the maleimide linker folded back and close in space to the butenolide. This linker would deliver the toxin close in space to the conjugated protein and consequently reduce the chance of recognition of the toxin.

In addition, modelling studies were carried out on the haptens (**59**) and (**61**), using an AM1 force field and Spartan application.[92] The models produced were: gymnodamine-amine linker, GM-5 (Appendix 4) and gymnodamine-amide linker, GM-6 (Appendix 4).

The models GM-5 and GM-6 (Appendix 4) show complementary conformations, with the carboxylic acid linker arms well removed from the body of the toxin.

Haptens (**59**) and (**61**) were sent to AgResearch for ELISA development. The subsequent results discussed in this section are those obtained by AgResearch.

A gymnodimine antisera was raised against a sample of gymnodamine (supplied by Professor Yasumoto, Japan) conjugated to a glycoprotein *via* a Schiffs base. The antisera was raised by inoculation of the conjugate into sheep.

Gymnodimine haptens (**59**) and (**61**) were conjugated separately to ovalbumin (OVA) to achieve two separate protein conjugates. These were tested as plate coaters for the selectivity of the gymnodimine antisera.

The results (Fig 5.4.4) revealed selective binding to both conjugates. The binding was equivalent for each conjugate. These data reveal that neither the linkage sites or the proteins are recognised by the antibody. This is because a different protein was used to elicit the immune response from the one used as the plate coater. In addition, the amine and amide linkage chemistry of the haptens is significantly different to expect varying binding potentials if these were recognised.

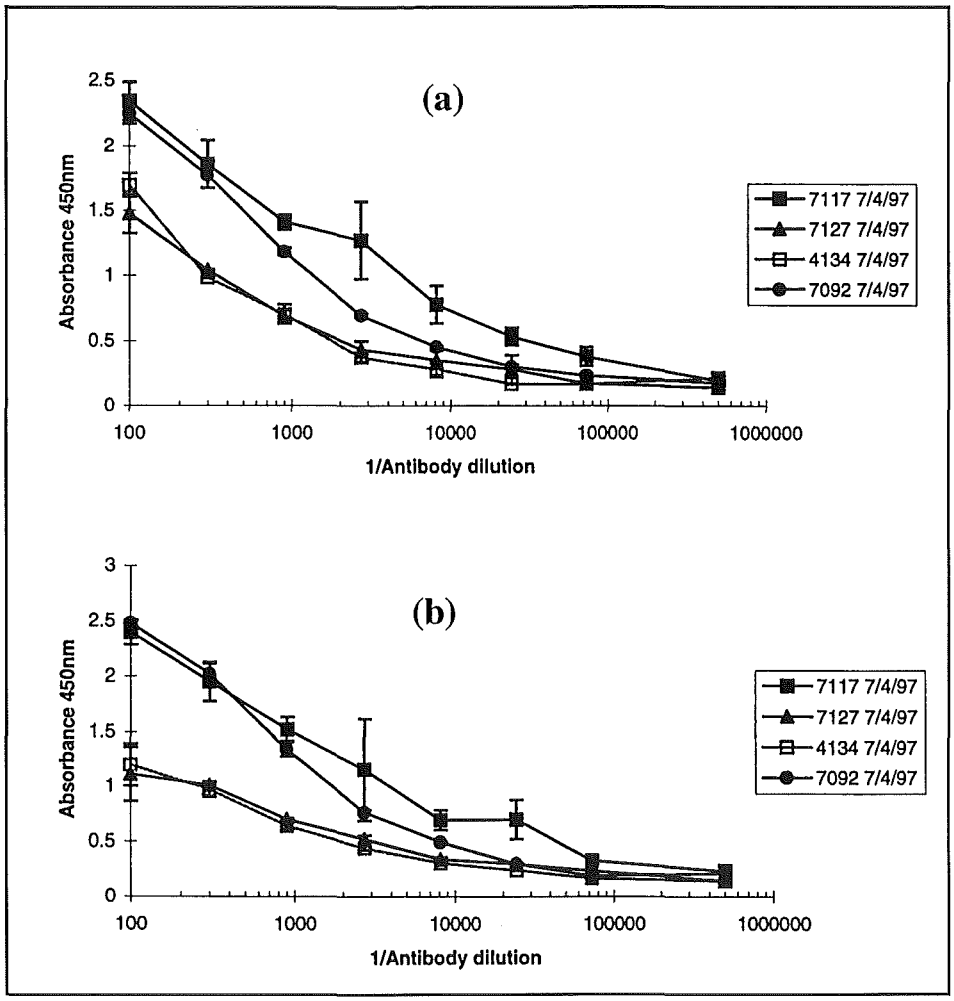

Fig 5.4.4 *ELISA Results for (a) (**59**)-OVA Conjugate and (b) (**61**)-OVA Conjugate*

The indirect ELISA (Appendix 1) was used to assay authentic samples of gymnodimine and gymnodamine (prepared at Canterbury). Competition for the gymnodimine antisera was not observed for either toxin. These data suggest the antisera raised originally was not suitable for an ELISA. Consequently, at the time of writing, re-immunisation has been initiated at AgResearch, using the OVA conjugates prepared from (**59**) and (**61**).

5.5 Development of a Large Scale Isolation Scheme for Gymnodimine

5.5.1 Introduction

Gymnodimine (**40**) is a contaminant of shellfish due to accumulation of the toxin after filter feeding on the dinoflagellate, *Gymnodinium* cf. *mikimotoi*. Being a contaminant, the level of gymnodimine in shellfish is very low.

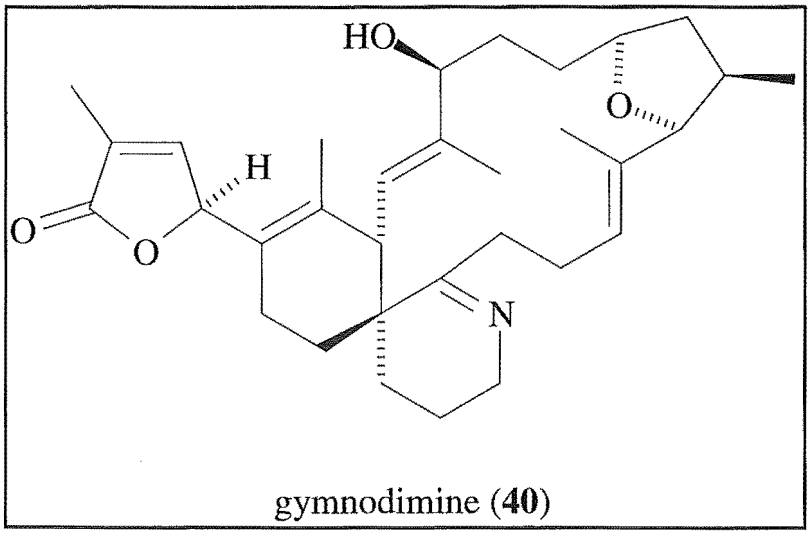

gymnodimine (**40**)

The shellfish extracted during the preliminary investigation, yielded less than 1 mg of purified gymnodimine per kg of shellfish tissue, or alternatively, a yield less than 1 x 10^{-4}% (wet weight). These low yields require the extraction of large quantities of shellfish to obtain even modest supplies of gymnodimine.

These problems are compounded further when the high lipid content of oysters and the lipid solubility of gymnodimine are addressed.

Purification of gymnodimine in the presence of the high amount of lipids is a complex exercise, especially when large scale work is being contemplated.

5.5.2 Development of Protocol

The preliminary work revolved around following a more "classical" approach to toxin isolation, as shown in Scheme 5.5.1. The oysters were freeze dried, to make handling of large quantities easier, then extracted with dichloromethane and aqueous methanol. An aqueous methanol *vs* hexane solvent partition removed abundant, non polar material, including triglycerides and steroids. Concentration of the aqueous methanol phase to water, followed by solvent partition against ethyl acetate, yielded the organic extract, 5.A(EtOAc).

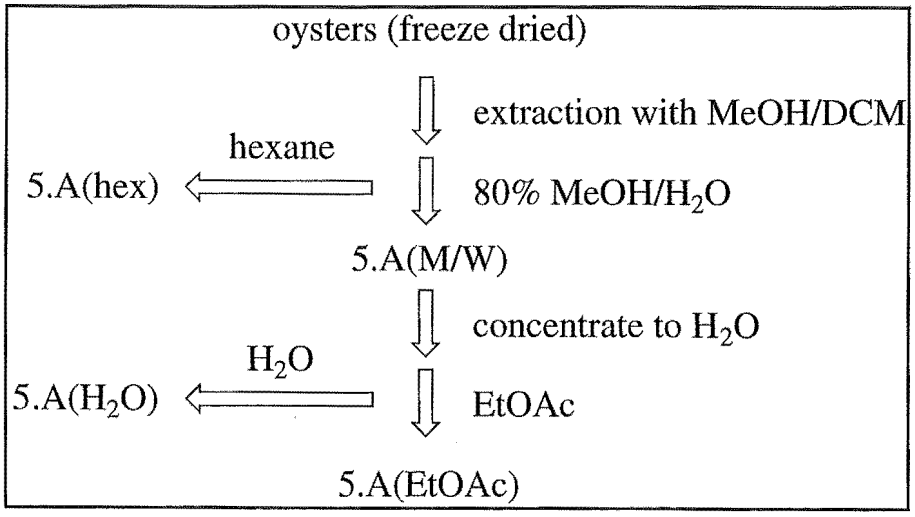

Scheme 5.5.1 *Preliminary Extraction/Solvent Partition Scheme of Foveaux Strait Oysters*

Mouse bioassays of the partitions gave some surprising results. Gymnodimine is a lipid soluble toxin, however fraction 5.A(H_2O)(Scheme 5.5.1) showed death times of 7.5 minutes, with typical gymnodimine symptoms, at approximately 80 MU/g of sample. Fraction 5.A(EtOAc)(Scheme 5.5.1) showed varying death times of 7 minutes, 4.5 hours, and 6 - 22 hours for three different mice. The short death times were characteristic of gymnodimine, whereas the long death times were subsequently found to be caused by low levels of BTX-like material.

These results suggested that gymnodimine was reasonably water soluble. The pH of fraction 5.A(H_2O)(Scheme 5.5.1) was checked and found to be 4.5. It is likely that formation of an iminium ion occurs at this acidic pH, hence making gymnodimine (more) water soluble.

Fraction 5.A(H_2O)(Scheme 5.5.1) was adjusted to pH 8.5 with $NaHCO_3$ and again partitioned with ethyl acetate. This ethyl acetate partition was analysed by TLC. On spraying with Dragendorff's reagent,[85] an orange spot was clearly visible at the same R_f as the reference material. Gymnodimine was subsequently purified from this fraction (Section 6.5.5).

The water solubility of gymnodimine in acidic conditions was advantageous for its purification, yet some material still appeared in the ethyl acetate phase. The use of dichloromethane, instead of ethyl acetate, was a likely alternative that needed to be examined.

Extraction of a new batch of frozen oysters with methanol (at an effective concentration of 80% methanol/water) was used, followed by a dichloromethane *vs* acidic water solvent partition. The aqueous layer was made alkaline with $NaHCO_3$ and partitioned against ethyl acetate, as shown in Scheme 5.5.2.

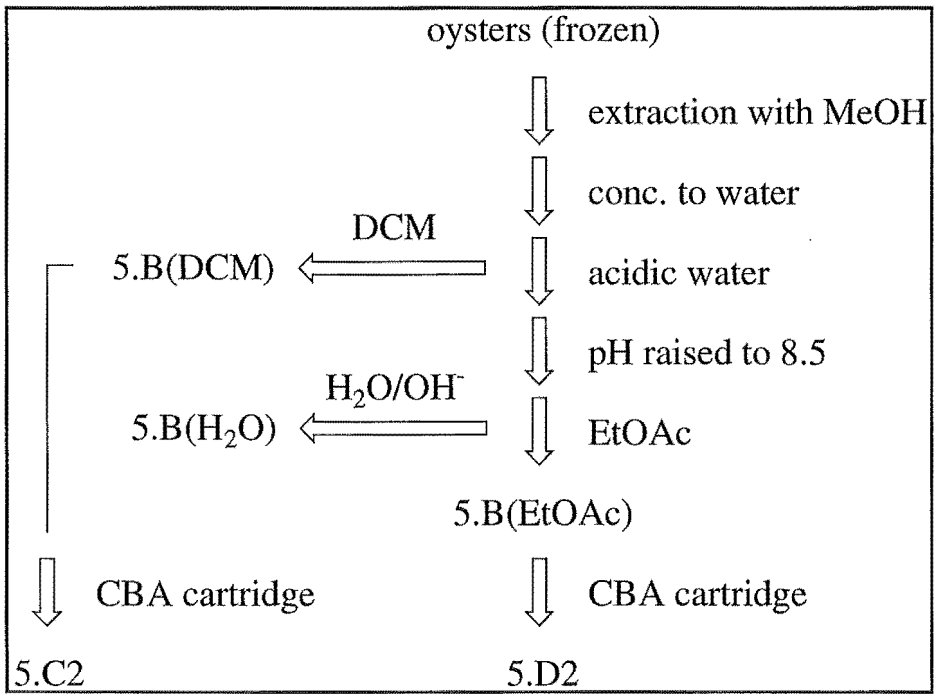

Scheme 5.5.2 *Second Extraction/Solvent Partition Scheme of Foveaux Strait Oysters*

Analysis of fraction 5.B(EtOAc) by TLC showed the absence of an orange spot of gymnodimine when sprayed with Dragendorff's reagent.

Sub-samples of 5.B(EtOAc) and 5.B(DCM) were run through CBA cartridges and the 2% ammonia/methanol eluents analysed by TLC (Scheme 5.5.2). On spraying with Dragendorff's reagent, fraction 5.C2 showed a distinct orange spot, however fraction 5.D2 did not.

This work suggested that the entire detectable amount of gymnodimine had partitioned in the dichloromethane phase and was in fraction 5.B(DCM). This was unexpected, as dichloromethane is a less polar solvent than ethyl acetate. However, the superior solvating properties of dichloromethane over ethyl acetate are exhibited.

This led to a search for a suitable alternative to ethyl acetate and dichloromethane.

The low solubility of gymnodimine in ether was demonstrated by the APHA ether extraction[96] procedure. With this knowledge, fraction 5.B(DCM) was dried and partitioned between ether and acidic water at pH 4.5. The acidic water phase was then made to pH 8.5 with $NaHCO_3$ and partitioned against ethyl acetate, as summarised in Scheme 5.5.3.

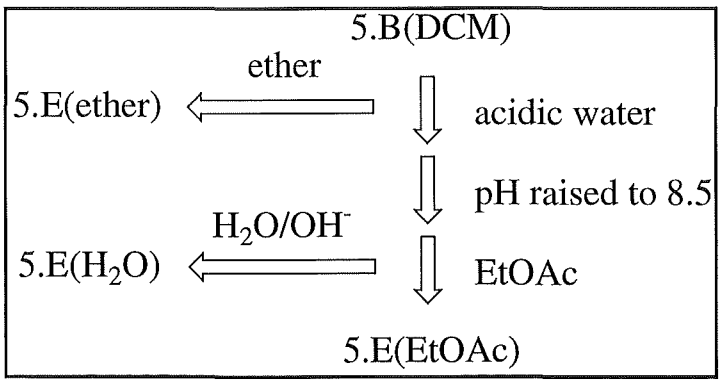

Scheme 5.5.3 *Improved Solvent Partition Scheme of Foveaux Strait Oysters*

Fractions 5.E(ether) and 5.E(EtOAc) were both analysed by TLC with Dragendorff's reagent. Fraction 5.E(ether) showed no sign of any gymnodimine, however fraction 5.E(EtOAc) showed an intense orange spot at the correct R_f. This suggested that use of the acidic water *vs*

ether solvent partition gave the necessary differentiation to concentrate gymnodimine by solvent partitioning techniques.

Fraction 5.E(EtOAc) was chromatographed further on CBA, (Scheme 5.5.4) from which gymnodimine was eluted in fraction 5.F3. Analysis of 5.F3 by TLC and ^{1}H NMR spectroscopy showed it to be of high purity. This was supported by analytical C18 reverse phase HPLC (Fig 5.5.1) on this fraction which revealed gymnodimine as the major component.

Fraction 5.F3 was subsequently chromatographed by C18 reverse phase HPLC (Scheme 5.5.4) to afford pure gymnodimine.

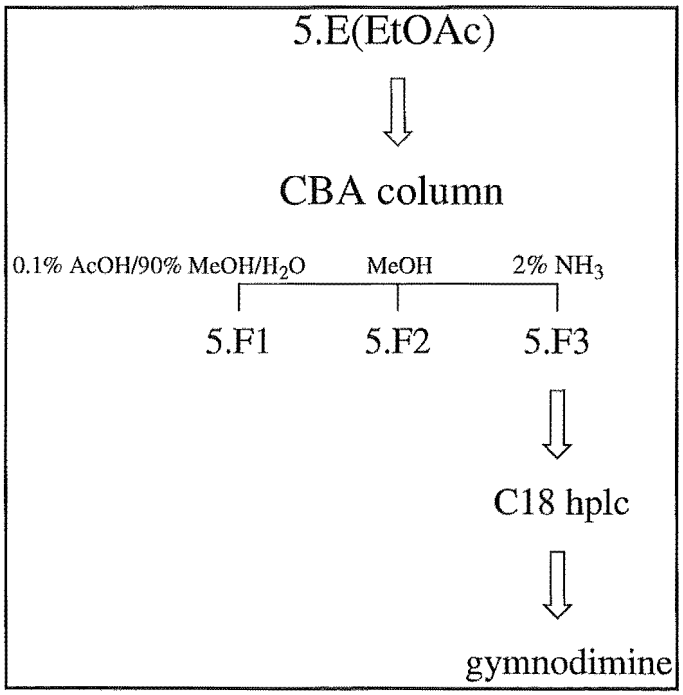

Scheme 5.5.4 *Purification of Gymnodimine*

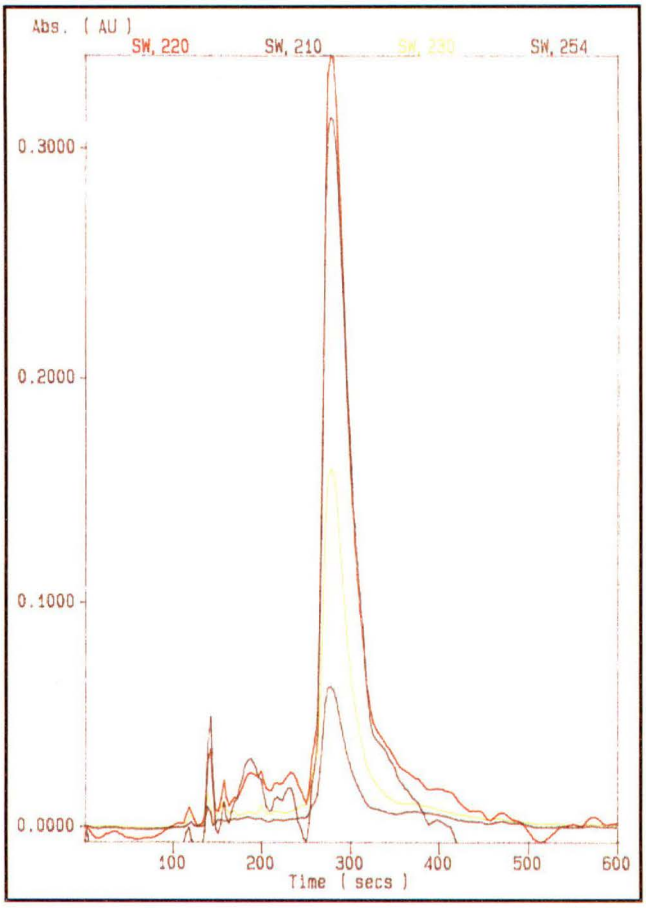

Fig 5.5.1 *HPLC Chromatogram of Fraction 5.F3 (Scheme 5.5.4)*

This new method enabled gymnodimine to be extracted and purified from 5 kg of oysters in just 1 week. The yield was 1 mg/kg of frozen shellfish tissue. The major advantage of this method is that by utilising the solvent partitions after extraction, the mass can be reduced substantially before any solid phase chromatography is required. The extract from 5 kg of shellfish tissue was concentrated to just 200 mg using these solvent partitions.

The protocol was subsequently modified to include the more polar extraction solvent of 60% methanol/39% water/1% acetic acid for freeze dried oysters and 80% methanol/19% water/1% acetic acid for frozen oysters. The acetic acid was added to ensure acidic extraction

conditions and the difference in extraction solvents is due to water already present in the frozen shellfish. In addition, the preliminary solvent partition of dichloromethane *vs* acidic water was changed to dichloromethane *vs* alkaline water. The situation was complicated when the solution was saturated with $NaHCO_3$ to ensure alkaline conditions. Occasionally, emulsions formed between the two immiscible solvents. The protocol was modified again to include ammonia and $NaHCO_3$. The acidic solution was made neutral with ammonia, with sufficient $NaHCO_3$ added to ensure pH 8.5, but not saturation. This solved the problem of emulsions.

The modified protocol was used on a 2 kg batch of freeze dried oysters (10 kg frozen). The extraction and solvent partitions are summarised in Scheme 5.5.5.

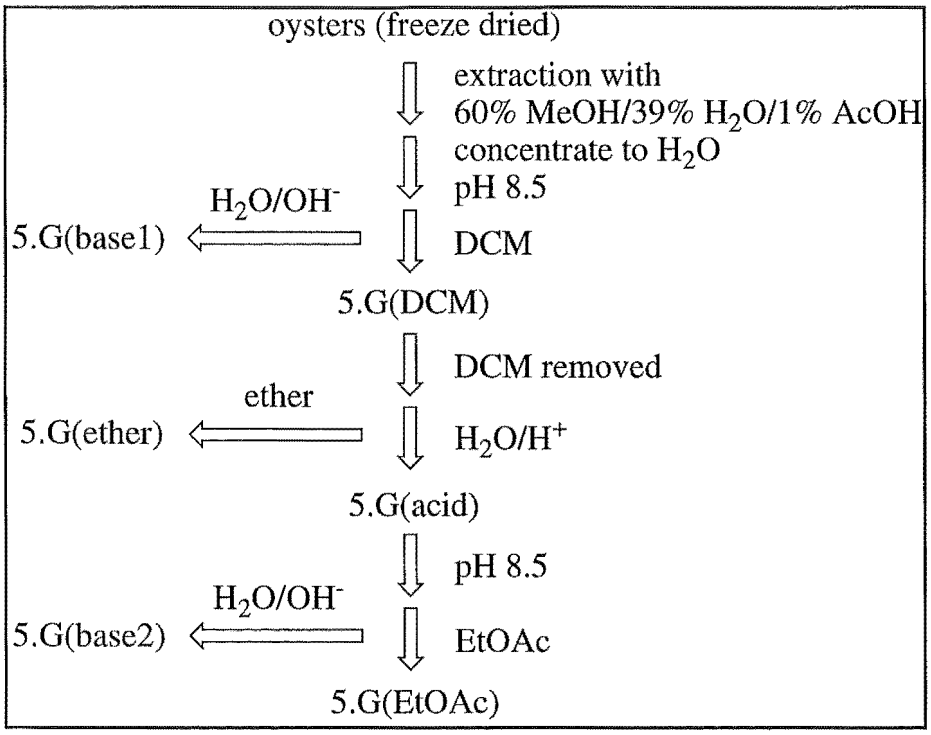

Scheme 5.5.5 *Modified Extraction/Preliminary Isolation Protocol for Gymnodimine*

The protocol was very successful as gymnodimine was observed by TLC in fraction 5.G(DCM). The major advantage from using extraction solvents of high polarity, was that the weight of the final fraction 5.G(EtOAc), was only 230 mg.

The concentrating of gymnodimine completely into fraction 5.G(EtOAc), could be shown by HPLC analysis of fractions 5.G(base1), 5.G(ether) and 5.G(base2). A gradient acetonitrile/water elution was used on an analytical C18 reverse phase HPLC column. Analysis of each fraction, by comparison with authentic gymnodimine, was made using both UV_{max} and retention time. The results established unambiguously that there was no gymnodimine in these three side fractions.

5.5.3 Final Purification of Gymnodimine

The high proportion of gymnodimine in fraction 5.G(EtOAc)(Scheme 5.5.5) provided the opportunity to use alternative methods of chromatography to CBA for the final purification stages. Preliminary results demonstrated that gymnodimine showed different characteristics on the diol phase, depending on whether it was in the free base or salt forms.

Fraction 5.G(EtOAc)(230 mg)(Scheme 5.5.5) was chromatographed on diol phase with gymnodimine eluting in one fraction at 80% dichloromethane/petroleum ether, at a weight of 48 mg. TLC analysis of this fraction revealed that gymnodimine was the most polar

compound in the mixture. The fraction was acidified with acetic acid and the protonation of gymnodimine checked by ^1H NMR spectroscopy. The ^1H NMR spectrum showed full protonation, with a shift of δ 5.0 to δ 4.7 ppm (Fig 5.2.6).

The sample was then re-run through diol phase. This, however, was unsuccessful in removing impurities and was consequently eliminated.

LH-20 gel permeation chromatography had already been attempted on an earlier sample as an alternative mild method. This again proved unsuccessful, with gymnodimine "streaking" on the column and appearing in nearly every fraction collected.

Attempts at using different HPLC phases were also variable in success. Cyano phase HPLC was unsuccessful using normal phase solvents of isopropanol/hexane, but did give good separation with reverse phase solvents such as methanol and water. However, the separation was associated with loss of material. The UV_{max} for gymnodimine is at just 215 nm, precluding the use of dichloromethane on diol phase HPLC. Diol phase HPLC was still attempted but using isopropanol/hexane mixtures. However, separation was unsuccessful.

C18 reverse phase HPLC was used using trifluoroacetic acid (TFA) and triethylamine (TEA) as polar modifiers in the water. Both modifiers were successful with 100% purity achieved. However, the suitability of this method was questioned as some loss of material occurred.

These results all demonstrated that no matter what phase was used for HPLC it was accompanied by some loss of material. Hence, preparative HPLC should only be used when absolutely necessary.

Repeating the protocol in Scheme 5.5.5 on a further 5 kg of frozen oysters yielded an extract of 298 mg (ethyl acetate phase). By chromatographing this fraction on diol phase, collecting smaller fractions and lowering elution strength, it was possible to concentrate all the gymnodimine with just one contaminant.

The contaminant was established to be a fatty acid by ^{1}H NMR spectroscopy. This was successfully removed by passing the mixture through an amino phase column. This method resulted in the highest yield of pure gymnodimine (8.4 mg, 1.68×10^{-4} yield, wet weight) when compared to previous methods.

5.6 Development of a Chromatography Based Assay for Gymnodimine

5.6.1 Introduction

The extremely efficient methodology that the large scale isolation of gymnodimine (**40**)(Section 5.5) was based on was modified to develop an assay specific to this toxin. The methods used in developing the assay were TLC, HPLC, and NMR spectroscopy. Incorporation of these techniques provided specific methods of detection.

The assay requires several chromatographic steps of extractions and solvent partitions to achieve a partially purified extract suitable for analysis. Oysters known to contain gymnodimine were used in the assay set-up.

5.6.2 Methodology

The extraction/isolation methodology used for the assay is virtually equivalent to that used for the large scale extraction. The procedure has been modified to accommodate analyses for both shellfish and algae. The procedure is detailed in Section 6.5.6. The algae analysed were *Gymnodinium* cf *mikimotoi*, cultured by Dr Lincoln Mackenzie at the Cawthron Institute in Nelson.

5.6.3 Results

Thin Layer Chromatography Analysis

As a consequence of the nitrogen atom present in gymnodimine a characteristic orange colour is formed when it is sprayed with Dragendorff's reagent. In addition, comparisons of compound retention (R_f), are particularly useful and can be achieved by eluting against an authentic sample of gymnodimine. These particular features provide a very powerful tool for qualitative analysis.

Resolution and colour clarity were the major criteria for the selection of the chromatographic phase for analysis. Of the many phases examined, silica gave the best results. The best solvent conditions were achieved by elution with 7.5% methanol/CH_2Cl_2 (1% AcOH). Variations in pH of elution solvent created marked differences in R_f values. Inclusion of acetic acid in the developing solvent ensured uniform pH elution conditions.

TLC proved successful in identifying gymnodimine in both the shellfish and algae (Fig 5.6.1).

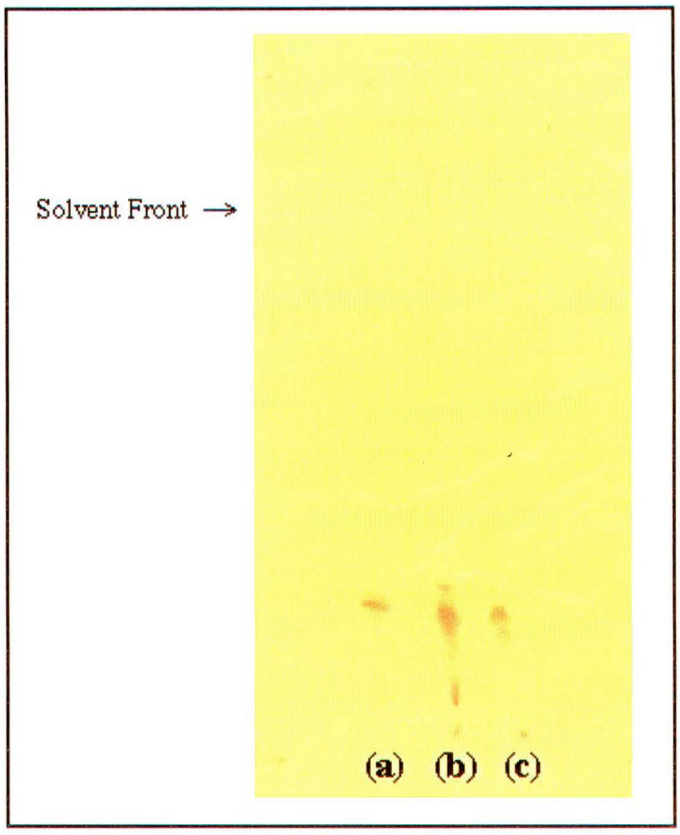

Fig 5.6.1 *Silica TLC Chromatograph of (**a**) Authentic Gymnodimine, (**b**) Shellfish Test Sample and (**c**) Algae Test Sample*

[Elution solvent = 7.5% methanol/CH_2Cl_2 (1% AcOH)]

[Dragendorff Spray]

High Performance Liquid Chromatography Analysis

HPLC provided a highly specific analytical tool once the correct conditions had been achieved. Accurate analysis could be accomplished by comparisons of retention times, UV chromophore and peak shape with an authentic sample of gymnodimine.

The conditions were optimised by use of a reverse phase C18 column with a gradient elution of acetonitrile and water. Trifluoroacetic acid (TFA) was added to the water as an acidic polar modifier. The

gradient scheme (Fig 5.6.2) minimised problems of peak broadening and co-eluting peaks, which were the problems observed with isocratic elution schemes.

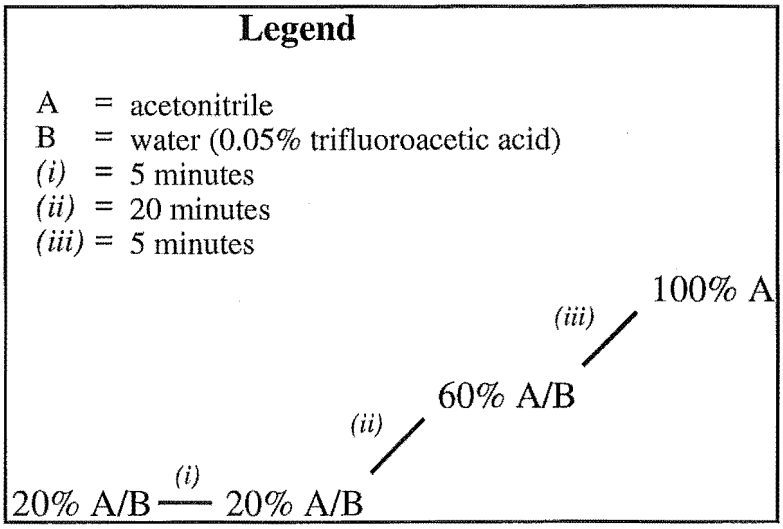

Fig 5.6.2 *Gradient Elution Scheme Used for HPLC Analysis*

Results obtained on test samples analysed by the gradient HPLC are shown in Fig 5.6.3.

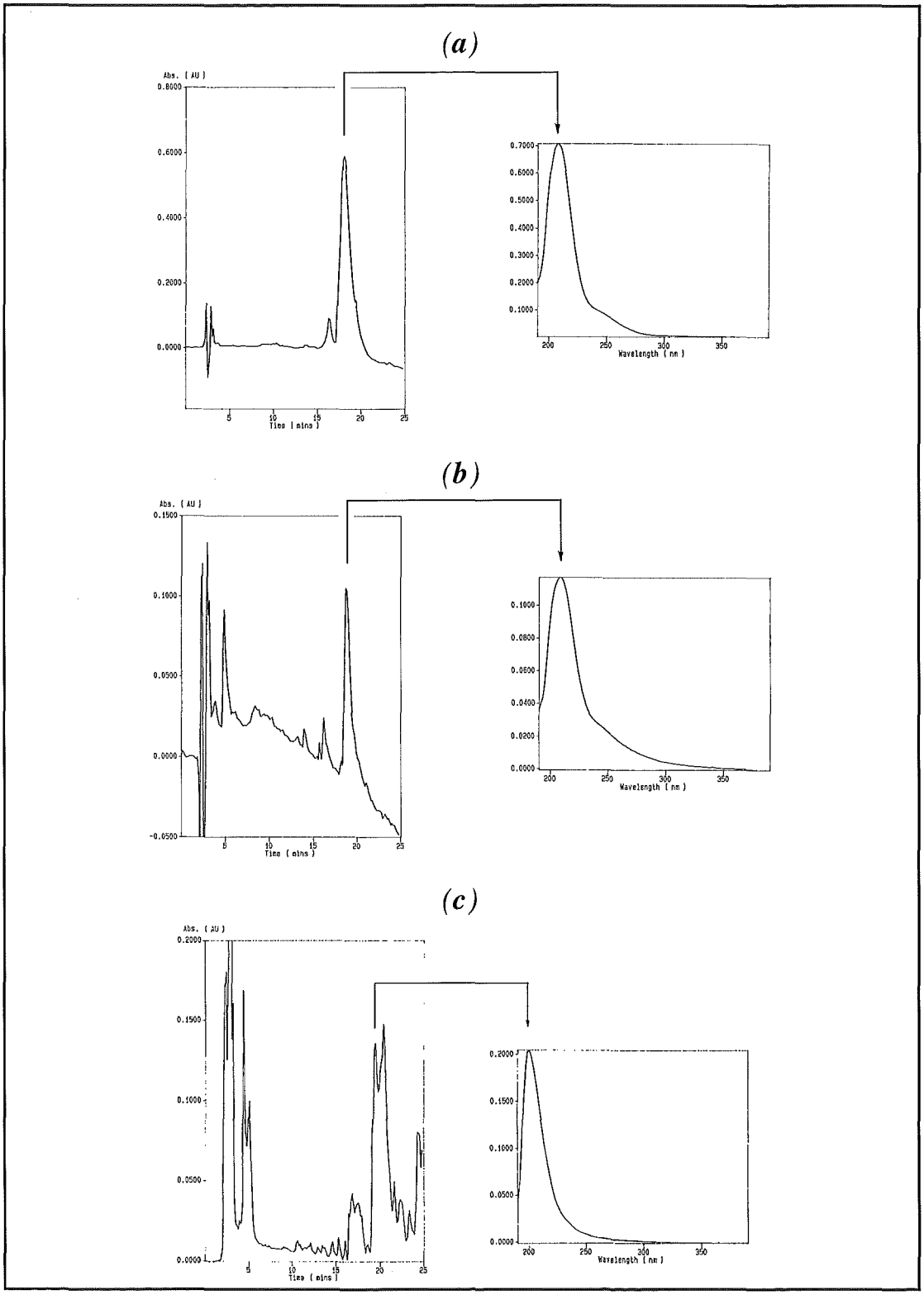

Fig 5.6.3 *HPLC Chromatograph of (**a**) Authentic Gymnodimine, (**b**) Shellfish Test Sample and (**c**) Algae Test Sample*

Proton NMR Analysis

The signals exhibited by the lactone protons in the ^1H NMR spectrum of gymnodimine, are well isolated and characteristic to the compound. Proton NMR provided a complementary analytical method to TLC and HPLC.

Comparisons of the test samples with that of authentic gymnodimine, were made using ^1H NMR spectroscopy. The spectra (in $CDCl_3$) revealed the characteristic lactone peaks for the samples tested (Fig 5.6.4). The slight difference in chemical shifts for the shellfish test sample (Fig 5.6.4(b)) are due to 10% CD_3OD added to aid in solubility.

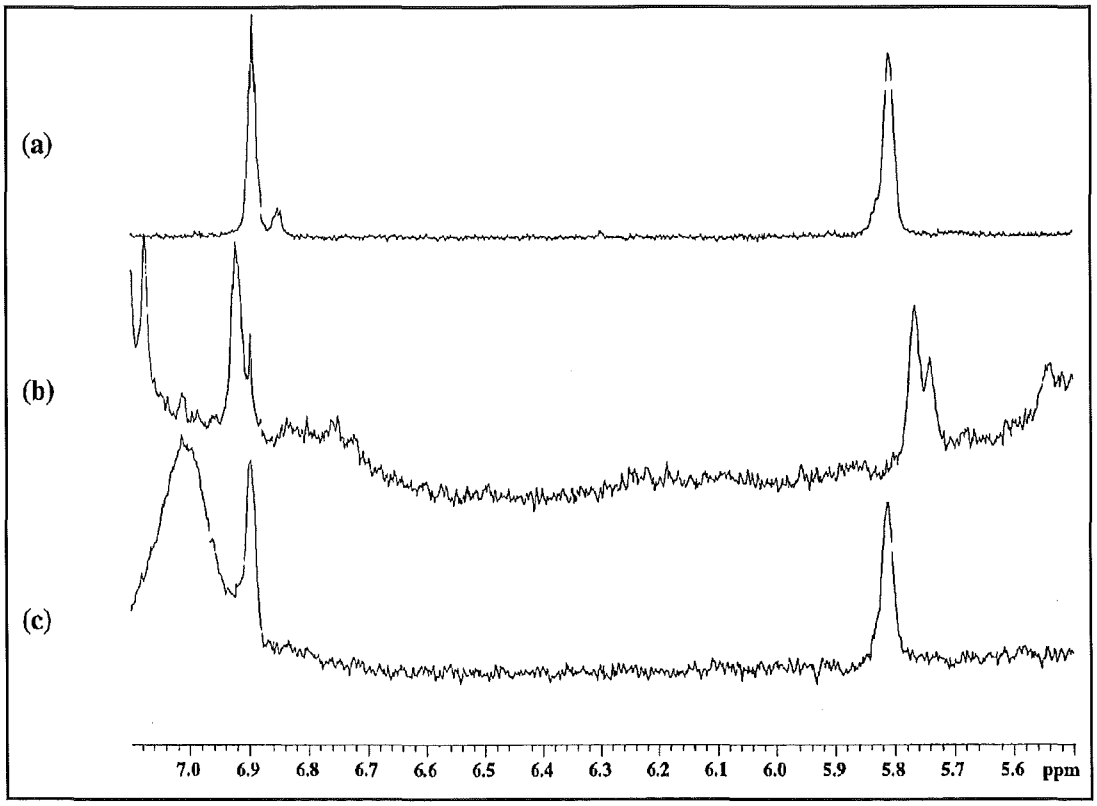

Fig 5.6.4 *Proton NMR Spectra of (**a**) Gymnodimine, (**b**) Shellfish Test Sample and (**c**) Algae Test Sample, Showing Lactone Resonances*

5.7 Conclusions

5.7.2 Structure Elucidation of Gymnodimine

Structural elucidation of gymnodimine (**40**) was first achieved by Professor Yasumoto's research group.[67] However, parallel elucidation was carried out as part of this research. The NMR data contained in Section 5.2 established that the postulated pH dependent imine/enamine tautomerism[67] was not a contributing process. The salient changes observed in the NMR spectra, on addition of acid, were attributed to formation of an iminium ion.

5.7.3 Absolute Stereochemistry of Gymnodimine

The absolute stereochemistry of gymnodimine was solved by X-ray crystallography on the crystalline *p*-bromobenzamide derivative (**56**). The measurement of observed NOE's for (**56**) and gymnodimine provided information on conformational differences between the solid and solution phase structure of gymnodimine. Constrained molecular modelling suggested the presence of many low energy conformers of gymnodimine.

5.7.4 Design and Syntheses of Gymnodimine Haptens

The design and syntheses of three haptens for the development of an ELISA for gymnodimine were carried out. The haptens (**59**) and (**61**) were tested for selective binding against a gymnodimine antisera. Both haptens revealed binding in ELISA, however gymnodimine and gymnodamine (**52**) exhibited no competition.

5.7.5 Development of a Large Scale Isolation Scheme for Gymnodimine

An efficient extraction/isolation scheme was devised for gymnodimine from oysters. This scheme overcomes many of the problems encountered with large scale isolation procedures, particularly handling difficulties using bulky extracts and large column sizes and expending much valuable time.

Furthermore, the use of the mouse bioassay is not needed during the isolation process as gymnodimine can be tracked by the use of TLC (with Dragendorff development), HPLC, or ^{1}H NMR spectroscopy.

The low levels of toxin in the isolation means contaminants are usually needed to be removed by HPLC. In doing so some material is invariably lost. The use of HPLC was avoided in most cases by efficient use of diol and amino phase columns, resulting in increased yield of toxin.

5.7.6 Development of a Chromatography Based Assay for Gymnodimine

A chromatography/HPLC based technique has been developed for the specific detection of gymnodimine in shellfish and algae. The advantages of the assay are that it takes just a few hours from shellfish/algae to a result and gives a definitive answer.

The assay is only intended as a "back-up" assay to the mouse bioassay and requires further development to reach a quantitative level. In addition, any future gymnodimine analogues discovered need to be incorporated into the assay.

Chapter Six

Experimental

6.1 General Methods

6.1.1 Nuclear Magnetic Resonance

Proton detected NMR spectra were recorded on a Varian Unity 300 spectrometer at 23°C, operating at 300 MHz. Carbon detected NMR spectra were recorded on a Varian XL300 spectrometer at 23°C, operating at 75 MHz. Other NMR experiments described in this thesis *viz.* 1D-TOCSY, 2D-TOCSY, COSY, NOE, NOESY and the reverse-detected HMQC and HMBC experiments were all recorded on the Unity spectrometer, at 300 MHz. This instrument was fitted with a Nalorac Z.spec MID300 3 mm Indirect Detection Probe. Chemical shifts in this thesis were described in parts per million (ppm), on the δ scale, and were referenced to the appropriate solvent peaks: $CDCl_3$ referenced to $\mathbf{CH}Cl_3$ at δ_H 7.25 ppm (^1H) and $CHCl_3$ at δ_C 77.0 ppm (^{13}C); CD_3OD referenced to $\mathbf{CH}D_2OD$ at δ_H 3.30 ppm (^1H) and CD_3OD at δ_C 49.3 ppm (^{13}C); D_2O referenced to **HOD** at δ_H 4.70 ppm (^1H). ^1H NMR spectra were recorded using an acquisition time (AT) of 2 s, except for those run in CD_3OD, which ran suppression of the HOD solvent peak, under the following conditions; relaxation delay (D1) =1 s, decoupler power = 4, steady state = 4, decoupler mode = 'ynn'. ^{13}C NMR spectra were recorded using an acquisition time of 0.5 s. All difference NOE experiments were recorded on undegassed solutions, with AT = 1 s and an irradiation time of 2 s. The decoupler was offset 10,000 Hz for the control experiment. Percentage enhancements reported in this thesis represent the observed increase in the intensity of a specific resonance relative to the corresponding signal in the control spectrum. NOESY

experiments were run using an AT = 0.46 s, D1 = 0.60 s and a mixing time of 0.30 s. COSY experiments were recorded using an acquisition time of 0.24 s and a relaxation delay of 1 s. 2D-TOCSY spectra were recorded using an acquisition time of 0.50 s, a relaxation delay of 0.60 s and a mixing time of 80 ms. 1D-TOCSY spectra were recorded using an acquisition time of 2 s, a relaxation delay of 1 s and mixing times as indicated in the discussion. HMQC experiments were recorded with an acquisition time of 0.2 s, a relaxation delay of 0.4 s and $J_{X\text{-}H}$=130 Hz. HMBC experiments were recorded with an acquisition time of 0.21 s, a relaxation delay of 0.3 s, J = 140 Hz and J_{NXH} = 8.3 Hz.

6.1.2 Mass Spectrometry

Mass Spectrometry at Canterbury University was performed on a Kratos MS80 Mass Spectrometer operated at 4 kV. FAB was performed with an Ion Tech ZN11FN ion gun using Xe as the reagent gas, operating at 8 kV and 2 mA with either NOBA (*m*-nitrobenzyl alcohol), m-b (magic bullet, 50% thioerythritol/thiothreitol), or glycerol as matrix.

Some samples were analysed at other institutions hence the place where the samples were run are stated as follows: (Canterbury) Bruce Clark, (Chemistry Department, University of Canterbury, Christchurch, New Zealand); (NIH) sent to Lewis Pannell (NIDDK, NIH, U.S.A.); (ESR) sent to Dr Porter (Institute of Environmental and Scientific Research, Gracefield Research Centre, Lower Hutt, New Zealand).

6.1.3 High Performance Liquid Chromatography

Analytical HPLC was performed on a Philips PU4100 Liquid Chromatograph equipped with a Philips PU4120 Diode Array Detector interfaced to a PC General 486 computer running Philips PU6003 Diode Array Detector System Software (V3.0) and a Hewlett Packard 7475A Plotter. H_2O was purified using a MilliQ deionising system. MeOH (J.T. Baker, HPLC reagent grade) and acetonitrile (BDH, HiPerSolv) solvents were used undistilled. All other solvents were of technical grade and were purified and re-distilled before use. Hexane was prepared from petroleum ether (10 L, b.pt. 60-70°C), nitrated with a mixture of *c*. HNO_3 (1 L) and *c*. H_2SO_4 (1 L) for two days. After this time, the nitrating mixture was removed and the organic layer washed with H_2O (20 L), and dried over $CaCl_2$ overnight. The resulting solution was filtered through activated alumina (Laporate, 100 mesh) and distilled. All solvents (with the exception of MilliQ water) were filtered through a Millipore filter apparatus, equipped with a Rainin Nylon-66 filter (0.45 μm) prior to use. All samples were filtered through a syringe filter (Alltech, 0.45 μm) prior to injection.

The analytical reverse phase C18 column used was a Microsorb-MV, 86200-C5, 5 μm, 100 Å, 250 x 4.6 mm, Rainin Instrument Company Inc, USA. The analytical reverse phase C8 column used was an Econosphere, 5 μm, 250 x 4.6 mm, Alltech/Applied Science, USA. The analytical diol column used was a LiChrospher® 5 μm, 100 Å, 250 x 4.6 mm, E. Merck, Darmstadt, Federal Republic of Germany.

Medium pressure column chromatography was performed on a Lobar chromatography setup, with a variable speed electric pump, to achieve a typical flow rate of 10 mL/min. The C18 lobar column used was a Lichroprep® RP-18, 40-63 μm, 310 x 25 mm, E. Merck, Darmstadt, Federal Republic of Germany.

6.1.4 Column Chromatography

All column chromatography was performed with glass columns of stated dimensions. "Flash" columns were run under N_2 gas (oxygen free) pressure (0.5 kPa). Solvents used were all commercial grade, distilled once in glass distillation apparatus, except methanol (MeOH), which was distilled twice.

Octadecyl (C18) reverse-phase packing used for preparative and flash column chromatography was prepared from silica gel (Davisil, 35-70 μm) using a solution of octadecyltrichlorosilane (2 % *v/v*, EGA-Chemie) in carbon tetrachloride.[97] The silica gel was stirred gently with a teflon-coated magnetic follower overnight before washing with carbon tetrachloride (x 2). Unreacted chloride groups were removed by washing with dry MeOH. A carbon tetrachloride solution of trimethylchlorosilane (2 % *v/v*, Aldrich) was used to end-cap any unreacted hydroxyl groups. The reverse-phase material was finally washed with dichloromethane (CH_2Cl_2) (x 2) and MeOH (x 2) to remove the reagents. The C18 reverse-phase material was extensively washed with MeOH immediately before use. Small scale preparative

C18 reverse-phase column chromatography was performed using Alltech disposable cartridges (200 mg).

Bakerbond diol (Bb)(40 μm APD) or Merck diol (Mk)(40 μm APD) packing material was used for diol column chromatography. Small scale preparative diol column chromatography was performed using Alltech disposable cartridges (200 mg).

Bakerbond CBA (40 μm APD) packing material was used for carboxylic acid (CBA) column chromatography. Small scale preparative CBA column chromatography was performed using 500 mg CBA BondElut cartridges.

Amino column chromatography was performed using Bakerbond amino (40 μm APD) packing material. On a smaller scale amino BondElut disposable cartridges (200 mg) were used.

Alumina column chromatography was performed using activated alumina (Type H, 100-200 Mesh, Laporte).

Pre-swollen Sephadex LH-20 (Pharmacia Biotech AB) was used for gel permeation chromatography.

Celite filtration and coating was performed using diatomaceous earth (Celite Corporation).

6.1.5 Thin Layer Chromatography

The silica analytical TLC described in this thesis was performed using Merck silica gel 60 F_{254} aluminium-backed sheets, 0.2 mm in thickness. DIOL analytical TLC was performed using Merck F_{254} glass-backed plates of 0.2 mm thickness. Whatman MKC ^{18}F TLC plates of 0.2 mm thickness were used for analytical C18 TLC. Amino analytical TLC was performed on Merck F_{254} glass-backed plates of 0.2 mm thickness. All TLC plates were visualised initially, under short-wave (λ 254 nm) light and subsequently, with phosphomolybdic acid in ethanol spray (10 % phosphomolybdic acid in ethanol *w/v*). TLC plates containing gymnodimine and derivatives were visualised with Dragendorff's reagent.[85] C18 reverse phase TLC plates containing yessotoxin were visualised with *c.* H_2SO_4 in ethanol (1:1). Other TLC plates were visualised with ninhydrin in acetone (10% *w/v*)

6.1.6 Dry Solvents

Dichloromethane was dried initially over calcium chloride then distilled from calcium hydride. Dry 1,4-dioxane was achieved by distillation over calcium hydride. Dry pyridine was attained by reflux over potassium hydroxide pellets, followed by distillation with careful exclusion of moisture. Dry methanol was distilled from magnesium metal and iodine. All dry solvents were distilled immediately prior to use.

6.2 Work Described In Chapter Two

6.2.1 Collection

New Zealand green-lipped mussels (*Perna canaliculus*) were harvested commercially from the Coromandel area on 8 January 1993.

6.2.2 Total Lipid Extract

Mussel viscera (6 kg) were prepared for analysis by Environmental Science and Research (ESR), in Lower Hutt, New Zealand, by the following method:

(1) 100 g of shucked and drained shellfish were blended with redistilled acetone (300 mL) (20 seconds), and filtered through Whatman 541 filter paper.

(2) The residue was further extracted with acetone (200 mL), filtered and the acetone extracts combined in a r.b. flask (1000 mL).

(3) The acetone was removed by rotary evaporation.

(4) The resultant aqueous/lipid mixture was acidified with HCl (1 M) to pH 2.5 (using narrow band pH paper) and poured into a separatory funnel (500 mL) and the residue in the RB flask washed in with three portions using redistilled DCM (3 x 100 mL).

(5) The separatory funnel was gently shaken and the lower DCM layer run off through muffled anhydrous Na_2SO_4 (10 g), prewetted with DCM in a glass funnel, into a RB flask (250 mL).

(6) The aqueous layer was further extracted with DCM (80 mL) and the DCM extracts combined. The Na_2SO_4 was washed with DCM (20 mL) making a total of 200 mL of DCM extract.

The total extract from 6 kg shellfish (described in step (6)) was sent as a DCM solution (180 mL) to Canterbury University. The extract was coded ES1-127.

An aliquot (500 μL) of ES1-127 was dried thoroughly, *in vacuo*, until a constant weight (264 mg) was achieved. P388 assay (100 mg/mL, 75% MeOH/DCM) gave an IC_{50} value of 56.2 μg/mL.

A second aliquot (10 mL) of ES1-127 was dried thoroughly, *in vacuo* and partitioned between 80% MeOH/H_2O (3 x 500 mL) and PE (3 x 500 mL). Solvents were removed, *in vacuo*, to afford the aqueous methanol phase (1.13 g) and the PE phase (4.12 g). P388 assays gave an IC_{50} value of 14.1 μg/mL (100 mg/mL assay concentration, 75% MeOH/DCM) for the aq. MeOH phase, and an IC_{50} value of >1,250,000 μg/mL (100 mg/mL assay concentration, 75% MeOH/DCM) for the PE phase.

Aliquots (5%) of each phase were sent for mouse bioassays (ESR). Results were: aq. MeOH phase, 1/2 mouse deaths in 137 min (32 mg/mouse, i.p.); PE phase, 0/2 mouse deaths (53 mg/mouse, i.p.).

The remaining aq. MeOH extract (1.07 g) was dissolved in DCM (10 mL) and celite (1.1 g) added. The solvent was removed, *in vacuo* and the resulting solid loaded onto the head of a column (30 mm i.d.),

packed with C18 phase material (100 g), equilibrated to 50% MeOH/H_2O. A step gradient elution was run, under "flash" conditions, starting at 50% MeOH/H_2O, through MeOH, finishing with 50% DCM/MeOH. Fractions 2.A1 - 2.A10 (200 mL fractions) were collected, with a resulting mass recovery of 99%. Fraction weights and corresponding P388 IC_{50} values were recorded as follows (**x** mg, *y* ng/mL); 2.A1 (**17.0**, *>125,000*), 2.A2 (**6.8**, *>125,000*), 2.A3 (**8.0**, *<975*), 2.A4 (**16.5**, *<975*), 2.A5 (**30.0**, *1,584*), 2.A6 (**20.5**, *31,622*), 2.A7 (**50.0**, *39,810*), 2.A8 (**85.5**, *39,810*), 2.A9 (**37.0**, *44,668*) and 2.A10 (**789.0**, *89,125*).

An aliquot of 2.A4 (4.5 mg; equivalent to 10 g of crude extract) was sent for mouse bioassays (ESR). Results were: 3/3 mouse deaths, all 3 in 20 minutes.

Fractions 2.A3 and 2.A4 were combined (20 mg), solvents removed, *in vacuo* and sample re-dissolved in DCM (1 mL). The solution was pipetted onto the head of a column (20 mm i.d.), containing LH-20 (10 g), pre-swelled in DCM (2 hr). Fractions collected were: 2.B1 - 2.B5 (DCM; 4, 6, 5, 5, 10 mL fractions), 2.B6 - 2.B7 (50% MeOH/DCM; 10, 10 mL fractions) and 2.B8 (MeOH; 30 mL). There was a 91% mass recovery. Fraction weights and corresponding P388 IC_{50} values were recorded as follows (**x** mg, *y* ng/mL); 2.B1 (**0.2**, *4,626*), 2.B2 (**1.0**, *>12,500*), 2.B3 (**1.3**, *>12,500*), 2.B4 (**1.1**, *>12,500*), 2.B5 (**0.4**, *>12,500*), 2.B6 (**0.2**, *>12,500*), 2.B7 (**7.0**, *665*) and 2.B1 (**7.0**, *1,600*).

Fractions 2.B7 and 2.B8 were combined (14.0 mg), solvents evaporated, *in vacuo* and sample dissolved in 10% MeOH/DCM (1 mL). The

solution was pipetted onto a column (10 mm i.d.), packed with LH-20 (5 g), pre-swelled in 10% MeOH/DCM (2 hr). Nine fractions were collected; 1 - 5 (10% MeOH/DCM; 23, 3, 5, 7, 7 mL fractions), 6 - 8 (50% MeOH/DCM; 10, 10, 4 mL fractions) and 9 (MeOH; 20 mL). There was 91% mass recovery. Fraction weights and corresponding P388 IC_{50} values were recorded as follows (**x** mg, *y* ng/mL); 1 (**1.1**, *>12,500*), 2 (**0.5**, *>12,500*), 3 (**1.3**, *>12,500*), 4 (**1.7**, *>1,614*), 5 (**1.0**, *3,453*), 6 (**0.5**, *4,626*), 7 (**0.8**, *6,197*), 8 (**1.9**, *1,170*) and 9 (**3.9**, *1,436*).

Alternative Extraction Method

Preliminary Work

Frozen mussel viscera (102 g) were lyophilised (2 days). The dried material (28.65 g) was crushed to afford a coarse powder and extracted with H_2O (2 x 100 mL), MeOH (2 x 100 mL), EtOAc (2 x 100 mL) and DCM (2 x 100 mL), to afford 4 separate extracts. Extract weights and corresponding P388 IC_{50} values were recorded as follows (**x** g, *y* μg/mL); H_2O extract (**8.40**, *>1,250*), MeOH extract (**2.09**, *>1,250*), EtOAc extract (**0.90**, *316*) and DCM extract (**0.12**, *224*). Aliquots of each extract was sent for mouse bioassay (ESR). The results were: H_2O extract, 2/2 mouse deaths, 10 min (1 g/mouse), MeOH extract, 1/2 mouse deaths, 27 min (250 mg/mouse), EtOAc extract, 0/2 mouse deaths (100 mg/mouse) and DCM extract 0/2 mouse deaths (55 mg/mouse).

Method

Frozen mussel viscera (1.9 kg) were lyophilised (4 days). The dried shellfish (430 g) were crushed to afford a coarse powder and placed in a beaker (5 L). H_2O (2.5 L) was added and the mixture stirred (5 min). The resulting pulp was divided equally into two beakers (5 L), H_2O (2.5 L/beaker) was added and mixtures stirred (10 min). Each mixture was left to settle (3 hr). The supernatant was siphoned off and filtered through cotton wool. The mussel "paste" was then stirred with H_2O (2.5 L/beaker) and left to settle overnight. The supernatant was siphoned off, filtered through cotton wool and combined with the first H_2O extract (9 L, total). The mussel "paste" was then combined and MeOH (2.5 L) added, to achieve an effective concentration of 40% MeOH/H_2O. The mixture was subsequently blended (5 min) and filtered through a bed of celite, to afford the 40% MeOH/H_2O extract (3.5 L). The macerated mussel residue was then blended with 70% MeOH/H_2O (4 L, 5 min) and filtered, to afford the 70% MeOH/H_2O extract (4.0 L).

Small aliquots (0.1% volume) of each were dried, *in vacuo*, for estimation of extract weights and submitted for P388 assays. Estimated extract weights and corresponding P388 IC_{50} values were recorded as follows (**x** g, *y* μg/mL); H_2O extract (**131.0**, *391*), 40% MeOH/H_2O extract (**10.5**, *146*) and 70% MeOH/H_2O extract (**6.8**, *558*).

Scheme 2.2.1

(Elution solvents and volumes not referred to in text are recorded in scheme)

All three extracts were combined and concentrated, *in vacuo*, to a H_2O extract (3.5 L). The aqueous solution was partitioned against PE (3.5 L) and the H_2O layer then removed of residual PE, *in vacuo*. The aqueous extract (3.25 L) was subsequently poured onto the head of a column (170 mm i.d.), containing C18 phase material (1 kg) that had been equilibrated to H_2O. Column elution was achieved under vacuum. Once the aqueous extract had been absorbed the column was eluted with H_2O (3 L) followed by 80% MeOH/H_2O (4 L) and MeOH (4 L).

The aq. methanol elutions were combined, dried *in vacuo* and re-dissolved in 30% MeOH/H_2O (20 mL). The solution was pipetted onto the head of a column (40 mm i.d.), containing C18 phase material equilibrated to 30% MeOH/H_2O. Step gradient elution of the column was achieved under "flash" conditions to afford fractions 2.C1 - 2.C6.

Fractions 2.C2 - 2.C4 were combined (650 mg), coated onto celite (1.3 g) and dried, *in vacuo*. The dried residue was subsequently packed onto the head of a column (15 mm i.d.), containing diol phase material (12 g) and equilibrated to DCM. Step gradient elution afforded fractions 2.D1 - 2.D10, with 75% mass recovery.

Fraction 2.D8 (60 mg, IC_{50} <975 ng/mL) was dissolved in MeOH (1 mL) and pipetted onto the head of a column (20 mm i.d.), containing LH-20 (50 g), pre-swelled in MeOH (1 hr). The column was run with a

flow rate of 2.5 mL/min. Fractions 2.E1 - 2.E10 were collected, with a 100% mass recovery.

Fraction 2.D9 (127 mg, IC_{50} <975 ng/mL) was dissolved in MeOH (2 mL) and pipetted onto the head of a column (40 mm i.d.), packed with LH-20 (110 g), pre-swelled in MeOH (2 hr). The column was eluted at 2.5 mL/min, from which fractions 2.F1 - 2.F10 were collected, with a 100% mass recovery.

An aliquot of fraction 2.D1 (5 mg) was dissolved in DCM (200 μL) and pipetted onto the head of a column (5 mm i.d.), containing amino phase material (500 mg), equilibrated to DCM. Elution was carried out with DCM (3 mL), MeOH (3 mL) and 1% TFA/MeOH (3 mL). Fraction weights and corresponding P388 IC_{50} values were recorded as follows (**x** mg, *y* ng/mL); DCM fraction (**1.7**, *429*), MeOH fraction (**0.8**, *4,791*) and 1% TFA/MeOH fraction (**2.7**, *>12,500*).

The remainder of fraction 2.D1 (91 mg) was dissolved in 5% MeOH/DCM (1 mL) and pipetted onto the head of a column (10 mm i.d.), containing amino phase material (2.7 g), equilibrated to 5% MeOH/DCM. Elution was carried out with 5% MeOH/DCM (15 mL), MeOH (15 mL) and 1% TFA/MeOH (15 mL). Fraction weights and corresponding P388 IC_{50} values were recorded as follows (**x** mg, *y* ng/mL); 5% MeOH/DCM fraction (**17.8**, *22,261*), MeOH fraction (**4.7**, *>25,000*) and 1% TFA/MeOH fraction (**83.0**, *>25,000*).

6.2.3 Isolation of Cytotoxic Compound

Frozen mussel viscera (6.5 kg) were lyophilised. The dried shellfish (1.3 kg) were crushed to a coarse powder, split into portions (100 g) and extracted separately using the following protocol:

(1) Crushed dried mussels were divided into equal portions (100 g).

(2) The powder was stirred with H_2O (250 mL, 60 min) and centrifuged (5 min). The supernatant was removed and kept. The solid residue was re-stirred with H_2O (250 mL, 30 min), centrifuged again and the supernatant removed. The process was repeated two more times. Extractions were combined as the total H_2O extract.

(3) The centrifuge pellet was stirred with 70% MeOH/H_2O (250 mL, 60 min) and filtered. The filter cake was then stirred with 70% MeOH/H_2O (250 mL, 30 min) and filtered again. Both extractions were combined as the total aq. MeOH extract.

(4) The total H_2O and aq. MeOH extracts were combined and shaken gently with PE (250 mL) in a separating funnel (2 L). This was left to separate overnight then the lower aq. methanol layer was run off. This layer was re-extract twice more with PE (2 x 250 mL) in an identical fashion as above.

(5) All aq. methanol extracts were combined as total aq. methanol extract.

Scheme 2.2.2

(Elution solvents and volumes not referred to in text are recorded in scheme)

The total aq. MeOH extract, described in (5) (20 L), was concentrated, *in vacuo*, to H_2O (2.5 L). The resulting solution was poured through a funnel onto the head of a column (170 mm i.d.), packed with C18 phase material (1 kg), equilibrated to H_2O. Step gradient elution, under vacuum, afforded fractions 2.H1 - 2.H7.

Fraction 2.H5 (1.2 g, IC_{50} <975 ng/mL) was coated onto celite (2.4 g) and the solvents removed, *in vacuo*. The resulting residue was dry packed onto the head of a column (25 mm i.d.), filled with diol phase material (55 g), equilibrated to DCM. A step gradient elution was run, affording fractions 2.I1 - 2.I11, with an 87% mass recovery.

Fractions 2.I5 - 2.I7 were combined (150 mg) and solvents evaporated, *in vacuo*. The resulting residue was dissolved in MeOH (3 mL), filtered through an HPLC filter (0.45 μ) and concentrated to 1 mL, under N_2 flow. The solution was then pipetted onto the head of a column (25 mm i.d.), filled with LH-20 phase material (75 g), pre-swelled in MeOH (1 hr). Elution at 2 drops/sec, afforded fractions 2.J1 - 2.J7, with a mass recovery of 98%.

Fraction 2.I9 (248 mg, IC_{50} 262 ng/mL) was dissolved in MeOH (3 mL), filtered through an HPLC filter (0.45 μ) and concentrated to 1 mL, under N_2 flow. The solution was then pipetted onto the head of a column (25 mm i.d.), filled with LH-20 phase material (75 g), pre-

swelled in MeOH (1 hr). Elution with MeOH, at 2 drops/sec, afforded fractions 2.K1 - 2.K7, with a mass recovery of 70%.

Fractions 2.K6 and 2.K7 were combined (9.4 mg, IC_{50} <<19.5 ng/mL), the solvents removed, under N_2 flow and the solid residue dissolved in 50% MeOH/DCM (1 mL). The resulting solution was then pipetted onto the head of a column (10 mm i.d.), filled with LH-20 phase material (10 g), pre-swelled in 50% MeOH/DCM (2 hr). Elution with 50% MeOH/DCM, at 1 drop/sec, afforded fractions 2.L1 - 2.L7, with a 100% mass recovery.

6.3 Work Described In Chapter Three

6.3.2 Spectroscopic Assignment of YTX

YTX: Negative ion LRFABMS (NOBA) (Canterbury); $[M-Na]^-$ 1163.5. Positive ion HRFABMS (m-b, CsI) (NIH); $[M-2Na+3Cs]^+$ 1539.1680, $C_{55}H_{80}O_{21}S_2Cs_3$ requires 1539.1787.

6.3.3 Stereochemical Assignment of YTX

Desulfation of YTX

A YTX containing sample of unknown purity was used for the reaction. The YTX containing sample (30 mg) was dissolved in 50% 1,4-dioxane/pyridine (3 mL) and transferred into a pear-shaped flask (4 mL). The solution was refluxed at 120 °C (3 hr). The solvents were removed, *in vacuo* and the residue dried thoroughly, under high vacuum (5 hr).

The reaction mixture was dissolved in 70% MeOH/H_2O(1% AcOH) (1 mL) and pipetted onto the head of a column (5 mm i.d.), containing C18 sorbent (3 g), equilibrated to the same solvent. Step gradient elution was achieved with 70% MeOH/H_2O(1% AcOH) through to MeOH (15 mL/fraction). Five fractions were taken.

The fraction eluting at 90% MeOH/H_2O(1% AcOH) was dried *in vacuo*. This sample (2.4 mg) was dissolved in MeOH (500 μL) and pipetted

onto a cartridge containing amino phase material (200 mg), equilibrated to MeOH. The cartridge was eluted twice with MeOH (2, 3 mL) and once 1% TFA/MeOH (4 mL) and 5% TFA/MeOH (5 mL). The first fraction eluted off the cartridge was D-YTX (**44**) (0.8 mg).

D-YTX (**44**): LRFABMS (NOBA) (Canterbury); $[M\text{-}H_2O+H]^+$ 965.5. HRFABMS (NOBA) (Canterbury); $[M\text{-}H_2O+H]^+$ 965.5619, $C_{55}H_{81}O_{14}$ requires 965.5626.

6.3.4 Design and Synthesis of YTX Haptens

Synthesis

PMPI Attachment

PMPI + D-YTX (**44**): D-YTX (0.8 mg) was transferred to a glass NMR tube (CH_2Cl_2, 150 µL). The end of the tube was sealed with a supa-seal and the solvent removed under high vacuum. The sample was then further dried under the high vacuum (4 hr). PMPI (1.7 mg) was dissolved in $CDCl_3$ (283 µL) from a newly opened ampoule. An aliquot of this solution (150 µL) was removed, by syringe, and injected through the supa-seal, into the NMR tube. The top of the tube was sealed further with parafilm. The reaction was left (23 °C, 167 hr).

The reaction solution was transferred from the NMR tube into a vial (7 mL) and residue washed in with DCM (2 x 100 µL). H_2O (100 µL) and ACN (1 mL) were added to the solution and all solvents removed, under

N_2 flow. The residue was then dissolved in DCM (1 mL). This solution was filtered through an HPLC filter (0.45 μm) and the filter washed with a further three times with DCM (3 x 1 mL). The solid residue was further dried under high vacuum. The HPLC filter was washed with EtOAc (2 mL) and ACN (2 mL) into a new vial (7 mL).

The DCM soluble material was transferred into a new vial (2 mL) in DCM and the solvent removed, under N_2 flow. The solid residue was dissolved in ACN (30 μL) and an aliquot (15 μL) injected onto a reverse phase C8 HPLC column. The column had been equilibrated to 40% ACN/H_2O. Eleven fractions were collected during gradient elution from 40% ACN/H_2O to 60% ACN/H_2O over 20 minutes, running at 1 mL/min. Chromatography was repeated on the other half of the sample. All corresponding fractions were combined. Fraction retention times and weights were recorded as follows (**x min**, *y mg*): 1 (**0-3**, *0.1*), 2 (**3-4**, *0.6*), 3 (**4-5.5**, *0.1*), 4 (**5.5-7.5**, *0.1*), 5 (**7.5-11**, *0.1*), 6 (**11-13**, *0.3*), 7 (**13-15**, *0.4*), 8 (**15-16.5**, *0.4*), 9 (**16.5-17.5**, *0.2*), 10 (**17.5-18.5**, *0.1*), 11 (**18.5-20**, *1.0*).

Aminolysis

YTX + Ammonia: Fraction 3.F4 (0.5 mg) was transferred, in MeOH (1 mL), into a vial (7 mL) and the solvent removed under N_2 flow. 50% MeOH/NH_3 (28% ammonia) (1 mL) was added to the vial the vial was sealed with a lid and the reaction stirred (1 hr). Solvents were removed under N_2 flow and residue dried thoroughly under high vacuum (2 hr).

Reverse phase C18 TLC plates were developed using 80% MeOH/H_2O.

YTX + Glycine: The fraction from the previous reaction was transferred, in MeOH (1 mL), to a pear shaped flask (5 mL). The solvent was removed under N_2 flow. Glycine (5.6 mg) was dissolved in 50% MeOH/H_2O (5.6 mL) and an aliquot (300 μL) added to the flask. A reflux condenser was attached and the flask was stirred (60 °C, 64 hr). Solvents were removed, under N_2 flow and the solid residue dried thoroughly under high vacuum (3 hr).

Ozonolysis

Initial Ozonolysis: Fraction 2.L6 (Scheme 2.2.2)(100 μg) was transferred, in MeOH (2 mL), into a vial (7 mL). A dry ice/acetone bath (-78 °C) was set-up and the vial immersed into it. Ozone was bubbled through (12 min). Ozone conditions: internal pressure = 8 psi, outlet = 0.7 psi, power = 100 W. The vial was removed from the bath and N_2 gas was bubbled through (2 min). Me_2S (200 μL) was added and the vial agitated. Solvents were removed, under N_2 flow and the residue dried thoroughly, under high vacuum.

Second Ozonolysis: Fraction 2.L6 (Scheme 2.2.2)(1 mg) was transferred, in MeOH (2 mL), into a vial (7 mL). A dry ice/acetone bath (-78 °C) was set-up and the vial immersed into it. Ozone was bubbled through (12 min). Ozone conditions: internal pressure = 8 psi, outlet = 0.7 psi, power = 100 W. The vial was removed from the bath and N_2 gas was bubbled through (2 min). Me_2S (200 μL) was added and the vial agitated. Solvents were removed, under N_2 flow and the residue dried thoroughly, under high vacuum.

LRFABMS (NIH): Negative ion (NOBA) *m/z* 1129, 1127, 1047.4, 945, 815. (m-b) *m/z* 1129, 1127, 1047, 945, 815. Positive ion (m-b) *m/z* 1505, 1503, 1423.

Third Ozonolysis: Fraction 3.F3 (Scheme 3.5.1)(1 mg) was transferred, in MeOH (2 mL), into a vial (7 mL). A dry ice/acetone bath (-78 °C) was set-up and the vial immersed into it. Ozone was bubbled through (12 min). Ozone conditions: internal pressure = 8 psi, outlet = 0.7 psi, power = 100 W. The vial was removed from the bath and N_2 gas was bubbled through (2 min). Me_2S (200 μL) was added and the vial agitated. Solvents were removed, under N_2 flow and the residue dried thoroughly, under high vacuum.

6.3.5 Development of a Large Scale Isolation Method for YTX

Extraction Methodology

Mussel viscera (25 kg) were freeze dried in an industrial scale freeze drier, situated at Industrial Research Limited (IRL), at Gracefield Research Centre, Wellington. The dried mussel tissue (5 kg) was divided into five equal portions. The following extraction methodology was carried out:

(1) Freeze dried, powdered mussels (1 kg) were blended with 70% MeOH/H_2O (3 L) and filtered through a bed of celite. This

process was repeated with 70% MeOH/H_2O (2 L) and all extracts combined.

(2) Partially extracted mussels (500 g) were blended with MeOH (250 mL) and filtered through a bed of celite. This process was repeated once more. P388 IC_{50} value = 45,027 ng/mL.

(3) Partially extracted mussels (500 g) were placed in a r.b. flask (3 L). MeOH (500 mL) was added and the mixture refluxed (30 min). The mixture was left to cool (60 °C) and filtered through a bed of celite. The celite was then washed with MeOH (100 mL). P388 IC_{50} value 23,851 ng/mL.

The remainder of the partially extracted mussels was divided into four portions. Each portion was placed in a r.b. flask (10 L) and MeOH (4 L) added. The mixture was refluxed (30 min). After cooling (60 °C) the mixture was filtered through a bed of celite. The filtrate was further cooled (4 °C) and the supernatant poured off. All four extractions were combined. P388 IC_{50} value 16,346 ng/mL.

Preliminary Isolation

The aq. MeOH extract from (1) was washed twice with PE (2 x 1 L). The aq. MeOH partitions were combined and concentrated to H_2O, *in vacuo*. The resulting aqueous extract was divided into three equal portions and each diluted with water to achieve a volume of 2.5 L. Each portion was then partitioned three times against EtOAc (3 x 1 L). All partitions were dried *in vacuo*. P388 IC_{50} values were: PE phase, IC_{50} value 22,649 ng/mL, H_2O phase IC_{50} value 189,026 ng/mL, EtOAc phase IC_{50} value 14,552 ng/mL.

The EtOAc phase material (40 g) was dissolved in 50% MeOH/DCM (100 mL) and celite (80 g) added. The solvents were removed *in vacuo*. The resulting solid residue was applied to the head of a column (100 mm i.d.), containing C18 material (1 kg), equilibrated to 50% MeOH/H_2O. Step gradient elution of 50% MeOH/H_2O to MeOH (2 L/fraction), followed by a 50% MeOH/DCM strip (3 L), afforded seven fractions. A 91% mass recovery and 80% recovery of cytotoxicity was achieved.

The extract obtained by refluxing the mussels in MeOH (3) was concentrated to H_2O, *in vacuo*. The resulting aqueous solution (1 L) was made to 75% MeOH/H_2O (4 L) by the addition of methanol (3 L). This solution was partitioned three times against PE (3 x 1 L). P388 IC_{50} values were: aq. MeOH phase IC_{50} value 14,981 ng/mL, PE phase IC_{50} value 71,721 ng/mL.

The aq. MeOH phase was concentrated to approximately 50% MeOH/H_2O (2.5 L) and poured onto the head of a column (80 mm i.d.), containing C18 material (250 g), equilibrated to 50% MeOH/H_2O. Step gradient elution through to MeOH (1 L/fraction), followed by 50% DCM/MeOH (1 L), afforded 6 fractions.

An aliquot of the PE phase (1 g) was dried thoroughly under high vacuum. The residue was dissolved in 75% DCM/PE (2 mL) and pipetted onto the head of a column (15 mm i.d.), containing silica gel (10 g), equilibrated to 75% DCM/PE. Elution with 75% DCM/PE (30 mL), DCM (10 mL), followed by a step gradient from 10% MeOH/DCM to MeOH (20 mL/fraction), afforded 6 fractions. Fraction weights and corresponding P388 IC_{50} values were recorded as follows (**x** mg, *y*

ng/mL); 75% DCM/PE fraction (**218.0**, *11,925*), DCM fraction (**4.0**, *25,390*), 10% MeOH fraction (**2.6**, *20,716*), 20% MeOH fraction (**281.0**, *31,118*), 50% MeOH fraction (**46.0**, *45,407*) and MeOH fraction (**33.0**, *>62,500*).

An aliquot (25 mL) of the crude extract obtained by reflux extraction was concentrated to H_2O (5 mL) and more H_2O (5 mL) added. The resulting aqueous solution was partitioned against n-butanol (10 mL) and the phases were left to separate. Fraction weights and corresponding P388 IC_{50} values were recorded as follows (**x** mg, *y* ng/mL); n-butanol phase (**12.0**, *1,803*) and H_2O phase (**38.4**, *>62,500*).

The n-butanol phase (12.0 mg) was dissolved in 50% MeOH/DCM (500 µL) and pipetted onto a column (5 mm i.d.), filled with alumina (600 mg), equilibrated to 50% MeOH/DCM. The column was washed with 50% MeOH/DCM (2.5 mL) and 2% NH_3/50%MeOH/H_2O (4 mL). Fraction weights and corresponding P388 IC_{50} values were recorded as follows (**x** mg, *y* ng/mL); 50% MeOH/DCM fraction (**2.8**, *37,048*) and H_2O phase (**8.0**, *10,017*).

Scheme 3.5.1

(Elution solvents and volumes not referred to in text are recorded in scheme)

Lyophilised mussel viscera (2 kg) were crushed to afford a coarse powder and placed inside a cheese cloth. The ends of the cheese cloth were tied with string. The cheese cloth/mussels was placed in a large steel vessel (20 L) and H_2O added (10 L). The water was heated (100 °C) with an open flame and left to cool (60 °C). The cheese cloth was

removed and hand squeezed to remove excess H_2O. The remaining water in the steel vessel was decanted into a flask (10 L). The resulting aqueous extract (7.5 L) was covered with a layer (2 cm) of n-butanol to prevent microbial growth.

The mussels were removed from the cheese cloth and transferred into a r.b. flask (10 L). MeOH (6 L) was added and the mixture refluxed (30 min). The mixture was left to cool (60 °C) and filtered through a bed of celite to afford the first MeOH extract.

The solid residue was transferred back to the same r.b. flask and MeOH (4 L) added. The mixture was refluxed (30 min), left to cool (60 °C) and was then filtered through the same bed of celite as above, to afford the second MeOH extract.

The aqueous extract was divided into three equal volumes and each partitioned twice against n-butanol (2 x 2.5 L). Combination of all the n-butanol phases, followed by removal of solvent, *in vacuo*, afforded the first n-butanol partition.

The first MeOH extract was concentrated, *in vacuo*, to H_2O and further H_2O added (1 L). The resulting aqueous solution was partitioned three times with n-butanol (2, 1, 1 L). All the n-butanol phases were combined and the solvent removed, *in vacuo*, to afford the second n-butanol partition.

The second MeOH extract was concentrated, *in vacuo* (2.5 L) and water added (500 mL). The resulting solution was partitioned twice against PE (2 x 1 L).

The aq. MeOH phase was subsequently concentrated, *in vacuo*, to H_2O (1 L) and further H_2O added (2 L). The resulting aqueous solution was partitioned twice against n-butanol (2, 1.5 L). The n-butanol phase was added to the second butanol partition and solvent removed, *in vacuo*.

The first n-butanol partition (58 g) was dissolved in 50% DCM/MeOH (200 mL) and pipetted onto the head of a column (80 mm i.d.), containing alumina (25 cm), dry packed. The column was washed with 50% DCM/MeOH (2 L) and 2.5% NH_3 in 50% MeOH/H_2O (2 L). The aq. MeOH fraction was dried, *in vacuo* to afford the first alumina fraction.

The second n-butanol partition (44 g) was dissolved in 50% DCM/MeOH (200 mL) and pipetted onto the head of a column (80 mm i.d.), containing alumina (23 cm), dry packed. The column was washed with 50% DCM/MeOH (2 L) and 2.5% NH_3 in 50% MeOH/H_2O (2 L). The aq. MeOH fraction was dried, *in vacuo* to afford the second alumina fraction.

The first alumina fraction (6 g) was dissolved in MeOH (10 mL) and pipetted onto the head of a column (25 mm i.d.) containing LH-20 (1.7 m), pre-swelled in MeOH (15 hr). Elution afforded fractions 3.A1 to 3.A5.

The second alumina fraction (11 g) was dissolved in MeOH (20 mL) and divided into two equal portions. Each was treated separately. The first was pipetted onto the head of a column (25 mm i.d.) containing LH-20 (1.7 m), pre-swelled in MeOH (15 hr). Elution afforded fractions 3.B1 to 3.B5. The second was pipetted onto the head of a column (25 mm i.d.) containing LH-20 (1.7 m), pre-swelled in MeOH (15 hr). Elution afforded fractions 3.C1 to 3.C5.

Fractions 3.A5, 3.B5 and 3.C5 were combined and solvent removed, *in vacuo*. The resulting residue (358 mg) was dissolved in MeOH (1 mL) and pipetted onto the head of a column (10 mm i.d.), containing LH-20 (75 g), pre-swelled in MeOH (15 hr). Elution afforded fractions 3.D1 to 3.D11.

Fractions 3.D6 to 3.D8 were combined and solvent removed *in vacuo*. The resulting residue (130 mg) was dissolved in 60% MeOH/H_2O (2 mL) and injected onto a C18 lobar column, equilibrated to 60% MeOH/H_2O and running at 5 mL/min. Elution was run at 60% MeOH/H_2O for 39 minutes (195 mL), affording fractions 3.E1 to 3.E5. The column was finally washed with MeOH (250 mL) to afford fraction 3.E6.

Fraction 3.E6 was dried, *in vacuo* and the resulting residue (5.0 mg) dissolved in 10% MeOH/DCM (500 μL). An aliquot (100 μL) was pipetted onto the head of a cartridge containing diol phase material (100 mg), equilibrated to 10% MeOH/DCM. Step gradient elution from 10% MeOH/DCM to 50% MeOH/DCM achieved fractions 3.F1 to 3.F4. The remaining solution (400 μL) was purified, as above, on 4 separate

identical diol cartridges. Combination of all relevant fractions afforded YTX in fraction 3.F3 (1.6 mg, 1.6×10^{-5}% yield, w/w).

6.4 Work Described In Chapter Four

6.4.1 Collection

Commercial oysters (*Tiostrea chilensis*) were harvested around Foveaux Strait area. Analysis by mouse bioassay showed; >306 MU/100 g oyster flesh, in the acetone extract and 23 MU/100 g oyster flesh, in the ether extract.

6.4.2 Investigation of Toxicity

Scheme 4.2.1

(Elution solvents and volumes not referred to in text are recorded in scheme)

Frozen oysters (600 g) were lyophilised (2 days). The dried oysters were crushed to form a coarse powder (129 g). The powder was washed with a succession of solvents (2 x 750 mL, 30 min each) and filtered, keeping each extract separate.

Fractions 4.A1 and 4.A2 were combined (43.9 g) and concentrated, *in vacuo*, to H_2O (30 - 40 mL). The solution was then pipetted onto the head of a column (100 mm i.d.), containing C18 phase material (100 g), equilibrated to H_2O. Elution was achieved, under vacuum, to afford fractions 4.B1 - 4.B7, with a mass recovery of 46%.

Fractions 4.A4 and 4.A6 were combined (14.5 g) and the solvents removed, *in vacuo*. The solid residue was then partitioned between 80% MeOH/H_2O (3 x 500 mL) and PE (3 x 500 mL) to afford fractions 4.C1 and 4.C2.

Fractions 4.B4 - 4.B7 were combined (787 mg) and the solvents removed, *in vacuo*. The solid residue was then partitioned between 80% MeOH/H_2O (3 x 200 mL) and PE (3 x 200 mL) to afford fractions 4.D1 and 4.D2.

Fraction 4.C1 (6.5 g, IC_{50} 491 µg/mL) was dried, *in vacuo* and dissolved in 50% MeOH/H_2O (15 mL). This solution was subsequently pipetted onto the head of a column (40 mm i.d.), packed with C18 phase material (100 g), equilibrated to 50% MeOH/H_2O. Step gradient elution was achieved under "flash" conditions to afford fractions 4.E1 - 4.E8, with a 85% mass recovery.

Fraction 4.C2 (6.3 g, IC_{50} 229 µg/mL) was dried, *in vacuo* and dissolved in PE (15 mL). The resulting solution was pipetted onto the head of a column (40 mm i.d.), containing silica (100g), equilibrated to PE. Step gradient elution afforded fractions 4.F1 - 4.F9, with a 93% mass recovery.

Fraction 4.F3 (198 mg, IC_{50} 56 µg/mL) was dried, *in vacuo* and dissolved in PE (5 mL). This solution was pipetted onto the head of a column (20 mm i.d.), filled with silica (25 g), equilibrated to PE. Step gradient elution afforded fractions 4.G1 - 4.G8, with a 100% mass recovery.

Scheme 4.2.2

(Elution solvents and volumes not referred to in text are recorded in scheme)

Fraction 4.D1 (530 mg, IC_{50} 39 μg/mL, Scheme 4.2.1) was coated onto celite (1 g) and dried, *in vacuo*. The solid residue was dry packed onto the head of a column (25 mm i.d.), filled with C18 phase material (55g), equilibrated to 25% MeOH/H_2O. Step gradient elution was achieved under "flash" conditions to afford fractions 4.H1 - 4.H8, with a mass recovery of 60%.

Fraction 4.H8 (43 mg, IC_{50} 3.9 μg/mL) was coated onto celite (80 mg) and the solvents removed, *in vacuo*. The resulting residue was dry packed onto the head of a column (10 mm i.d.), containing silica (5 g), equilibrated to 50% IPE/PE. Step gradient elution yielded fractions 4.I1 - 4.I11, with a 92% mass recovery.

Fractions 4.E2 - 4.E6 (Scheme 4.2.1) were combined (817 mg), coated onto celite (1.6 g) and solvents removed, *in vacuo*. The solid was subsequently dry packed onto the head of a column (40 mm i.d.), containing C18 phase material (80 g), equilibrated to 25% MeOH/H_2O. Step gradient elution was achieved under "flash" conditions to afford fractions 4.K1 - 4.K8.

Scheme 4.2.3

(Elution solvents and volumes not referred to in text are recorded in scheme)

Fractions 4.F7 and 4.F8 (Scheme 4.2.1) were combined (344 mg), coated onto celite (680 mg) and the solvents removed, *in vacuo*. The resulting

solid residue was dry packed onto the head of a column (25 mm i.d.), containing C18 phase material (35 g), equilibrated to 25% MeOH/H_2O. Step gradient elution was achieved under "flash" conditions to afford fractions 4.L1 - 4.L8.

Fractions 4.L3 - 4.L8 were combined (308 mg), coated onto celite (600 mg) and the solvents removed, *in vacuo*. The dry residue was packed onto the head of a column (20 mm i.d.), containing diol phase material (12 g), equilibrated to 50% DCM/PE. Step gradient elution afforded fractions 4.M1 - 4.M10.

Fractions 4.G7 and 4.G8 were combined (61 mg), coated onto celite (120 mg) and the solvents removed, *in vacuo*. The resulting solid residue was dry packed onto the head of a column (20 mm i.d.), containing C18 phase material (10 g), equilibrated to 25% MeOH/H_2O. Step gradient elution was achieved under "flash" conditions to afford fractions 4.N1 - 4.N8.

Fraction 4.N6 (1.7 mg) was dried, *in vacuo* and dissolved in 50% MeOH/DCM (100 µL). This solution was pipetted onto the head of a column (5 mm i.d.), containing LH-20 (2 g), pre-swelled in 50% MeOH/DCM (1 hr). Elution with 50% MeOH/DCM afforded fractions 4.O1 and 4.O2 (Scheme 4.2.3).

Mouse Bioassay Results

Fraction 4.J3: 20 µg/mouse, 0/1 mice died, MLD >1.0 mg/kg.
Fraction 4.N10: 28 µg/mouse, 0/2 mice died, MLD >1.4 mg/kg.

Fraction 4.O1: 28 μg/mouse, 0/2 mice died, MLD >1.4 mg/kg.

Second Extraction

Frozen oysters (1 kg) were thawed in MeOH (4 L), blended (5 min) and filtered through a bed of celite. The extraction was repeated with 80% MeOH/H_2O (2 L) and the filtrates combined to afford the aqueous MeOH extract. The macerated oysters were subsequently extracted with DCM (2 x 2 L) and, after filtration, afforded the DCM extract. The aq. MeOH extract was concentrated, *in vacuo*, to water (1 L). This solution was poured through a funnel onto the head of a column (100 mm i.d.), containing C18 phase material (100 g), equilibrated to H_2O. The solvent was eluted through and the column washed with H_2O (300 mL). This fraction was discarded. The column was subsequently eluted with MeOH (500 mL) and DCM (500 mL). These washings were combined with the DCM extract to afford the total organic extract.

A subsample (2 g) of the total organic extract was dissolved in PE (5 mL), to which DCM (5 drops) was added to aid in solubility. This solution was pipetted onto the head of a column (25 mm), containing diol phase material (40 g), equilibrated to PE. Subsequent step gradient elution afforded fractions 4.P1 - 4.P16 (Fig 4.2.1).

Isolation of Gymnodimine

Fraction 4.P13 (Fig 4.2.1) was dried, *in vacuo* and dissolved in MeOH (250 μL). This solution was pipetted onto the head of a column (5 mm i.d.), containing carboxylic acid phase material (3.5 cm long),

equilibrated to MeOH. Elution was achieved with MeOH (3 mL), 0.5% NH_3/MeOH (8 mL) and 2% NH_3/MeOH (4 mL).

"Slow Acting" NSP Toxicity

Scheme 4.2.4

(Elution solvents and volumes not referred to in text are recorded in scheme)

The EtOAc partition (11 g) was dried, *in vacuo* and dissolved in 50% DCM/PE (10 mL). This solution was pipetted onto the head of a column (25 mm i.d.), containing diol (75 g), equilibrated to 50% DCM/PE. Step gradient elution afforded fractions 4.Q1 - 4.Q4.

Fraction 4.Q4 (3.19 g) was dried, *in vacuo*, coated onto celite (6 g) and wetted with 50% MeOH/H_2O (10 mL). This material was then added as a slurry onto the head of a column (25 mm i.d.), containing C18 phase material (100 g), equilibrated to 50% MeOH/H_2O. Step gradient elution afforded fractions 4.R1 - 4.R8.

6.5 Work Described In Chapter Five

6.5.2 Structure Elucidation of Gymnodimine

Gymnodimine (**40**): $[\alpha]^{25}_{D}$ = -4.7° (*c* 7.5x10^{-3}, MeOH). LREIMS (Canterbury) *m/z* 507.3. HREIMS (ESR) *m/z* 507.3343. $C_{32}H_{45}NO_4$ requires 507.3348. Mouse lethality, MLD = 625-835 μg/kg (i.p.).

6.5.3 Absolute Stereochemistry of Gymnodimine

Strategy

Preparation of PBBC: *p*-bromobenzoic acid (2 mg) was refluxed with redistilled $SOCl_2$ (100 μL) (1 hr). The $SOCl_2$ was evaporated under N_2 flow and the solid residue dried under high vacuum (15 min).

PBBC + gymnodimine: The solid residue above was dissolved in dry DCM (1 mL) and an aliquot (500 μL) transferred to a reacti-vial (3 mL), containing a magnetic flea. Pyridine (2 μL) was added, followed by gymnodimine (500 μg) in dry DCM (1 mL). The reacti-vial was sealed and the reaction stirred, under anhydrous conditions (1 hr). The solvents were removed, under high vacuum and the solid re-dissolved in 50% MeOH/DCM (2 mL).

Reduction of Gymnodimine

Gymnodimine (6.0 mg) was transferred into a r.b. flask (5 mL), in MeOH (2 mL). The solvent was removed under N_2 flow. $NaCNBH_3$ (4.0 mg) was dissolved in MeOH (3.2 mL) and an aliquot (1.2 mL) added to the r.b. flask. Acetic acid (5 μL) was added and the solution stirred (2 hr). The flask contents were transferred into a vial (7 mL) and residues washed in with 50% MeOH/DCM (2 x 1 mL). Solvents were removed, under N_2 flow and the residue dried under high vacuum (30 min). The solid material was dissolved in dry DCM (1 mL) then filtered through an HPLC filter (0.45 μm) into a new vial (7 mL). The filter was subsequently washed with dry DCM (3 x 1 mL) into the same vial. The filter was finally washed with MeOH (5 mL) into a second new vial (7 mL). Solvents were removed, under N_2 flow and the sample dried thoroughly under high vacuum (3 hr).

The DCM soluble material (4.5 mg) was pure gymnodamine. The MeOH soluble material was dissolved in 20% MeOH/H_2O(1% AcOH) (100 μL) and pipetted onto the head of a cartridge containing C18 phase material (100 mg), equilibrated to the same solvent. The cartridge was washed with 20% MeOH/H_2O(1% AcOH) (1.5 mL) and the eluent discarded. The cartridge was subsequently washed with MeOH (1.5 mL). The solvents were removed, under N_2 flow and the residue dried under high vacuum (3 hr). The combined weights of this material (1.1 mg) and DCM soluble material (4.5 mg), gave a yield of 93% for the reduction.

Gymnodamine (**52**): LREIMS (Canterbury), *m/z* 509; HREIMS; (Canterbury), *m/z* 509.3495. $C_{32}H_{47}NO_4$ requires 509.3505. Mouse lethality, MLD = > 4,040 μg/kg (i.p.). NMR data:

δ_C ($CDCl_3$) 174.9 (C1), 146.7 (C3), 138.2 (C9), 135.2 (C17), 132.8 (C5), 130.3 (C8), 130.0 (C2), 125.9 (C6), 124.8 (C18), 88.8 (C16), 81.2 (C4), 79.8 (C10), 78.5 (C13), 47.5 (C7), 41.0 (C32), 39.3 (C14), 35.7 (C15), 34.0 (C12), 20.7 (Me28), 16.7 (Me26), 14.9 (Me29), 11.0 (Me27), 10.0 (Me25).

δ_H ($CDCl_3$) 6.85 (1H, brs, H3), 5.75 (1H, brs, H4), 5.45 (1H, t *J* = 6.8, 6.9, H18), 5.35 (1H, d *J* = 11.2, H8), 4.17 (1H, brq *J* unresovled, H13), 4.00 (1H, obs., H10), 3.97 (1H, brs, H16), 3.65 (1H, d *J* = 10.3, H21), 2.92 (1H, d *J* = 11.3, H7), 2.76 (1H, m, H32), 2.66 (1H, m, H32), 1.94 (3H, s, Me25), 1.75 (3H, s, Me27), 1.60 (6H, s, Me26, Me29), 1.09 (3H, d *J* = 7.4, Me28).

Formation of Crystalline Derivatives of Gymnodamine

PBBC + Gymnodamine: gymnodamine (1.0 mg) was transferred to a reacti-vial (2 mL), in MeOH (1 mL). The solvent was removed, under N_2 flow. A lid and septum were placed on the reacti-vial and the sample dried thoroughly, under high vacuum (5 hr). PBBC (9.2 mg) was dissolved in dry DCM (1 mL). DMAP (7.2 mg) was dissolved in dry DCM (1.44 mL). Hunig's base (37.5 μL) was diluted with dry DCM (5 mL). Aliquots of DMAP solution (10 μL), PBBC solution (100 μL) and Hunig's base solution (100 μL) were combined and dry DCM added (90 μL). The resulting solution was then injected through the septum of the reacti-vial containing gymnodamine, in an ice bath. The reaction was stirred, under anhydrous conditions, at 0°C (15 min). The reaction

mixture was then diluted with DCM (2 mL) and washed with aqueous citric acid (10% v/w, 2 mL) and H_2O (2 x 2 mL). The organic phase was dried over Na_2SO_4 (1 g) and washed with DCM (2 x 1 mL), to afford the reaction product (1.2 mg).

The reaction product (1.2 mg) was dissolved in DCM (100 µL) and pipetted onto the head of a cartridge containing diol phase material (200 mg), equilibrated to DCM. Elution with DCM (2 mL) and 10% MeOH/DCM (3 mL), afforded 2 fractions. The 10% MeOH/DCM fraction (0.9 mg) was dissolved in DCM (75 µL). Aliquots (15 µL) were injected into an analytical diol HPLC column (5 separate runs), equilibrated to 1.5% MeOH/DCM and running at 1 mL/min. The peak eluting at Rt = 200 s was the amide (**56**) (0.7 mg, 51% yield).

p-bromobenzamide (**56**): LRFABMS (NOBA) (Canterbury); $[M+H]^+$ 692.3/694.3. melting point 251-253 °C.

BsCl + Gymnodamine: gymnodamine (1 mg) was transferred into a reacti-vial (1 mL) in MeOH (500 µL) and solvent removed under N_2 flow. The reacti-vial was sealed and dried thoroughly under high vacuum (5 hr). BsCl (32 mg) was dissolved in dry pyridine (2.13 mL) and an aliquot (100 µL) injected into the reacti-vial. Hunig's base (5 µL) was added and the reaction stirred (24 hr), under anhydrous conditions. Pyridine was removed, under N_2 flow and the residue dried thoroughly under high vacuum. The material was transferred into a new vial (7 mL) with MeOH (2 mL), DCM (2 mL) and H_2O (1 mL). All solvents were removed under N_2 flow and the residue dried thoroughly under high vacuum. The solid material was dissolved in dry DCM (1 mL) and

filtered through an HPLC filter (0.45 μm) into a new vial (7 mL). The filter was then washed with dry DCM (3 x 1 mL) into the same vial. The filter was finally washed with MeOH (5 mL) into a second new vial (7 mL). Solvents were removed under N_2 flow and the sample dried thoroughly under high vacuum (3 hr).

The DCM soluble material (3.8 mg) was dissolved in MeOH (100 μL) and pipetted onto the head of a cartridge containing amino phase material (200 mg), prepared by washing with 2% NH_3/MeOH (6 mL) and equilibrated to MeOH (10 mL). The cartridge was washed with MeOH (1 mL) to afford the reaction product (0.9 mg).

The reaction product (0.9 mg) was dissolved in 50% DCM/PE (200 μL) and pipetted onto the head of a cartridge containing diol phase material (100 mg), equilibrated to the same solvent mixture. The cartridge was subsequently washed with 50% DCM/PE (400, 200 μL), 80% DCM/PE (2 x 200 μL), DCM (2 x 400 μL) and MeOH (1 mL). Seven fractions were collected. The first fraction eluting at 80% DCM/PE (0.5 mg) was the reaction product.

CSCl + Gymnodamine: gymnodamine (500 μg) was transferred into a reacti-vial (1 mL) in MeOH (500 μL) and solvent removed under N_2 flow. The reacti-vial was sealed with a septum and dried thoroughly under high vacuum (5 hr). CSCl (11.4 mg) was dissolved in dry pyridine (1.52 mL) and an aliquot (100 μL) injected into the reacti-vial. Hunig's base (5 μL) was injected and the reaction stirred (24 hr). Solvents were removed under N_2 flow and sample dried under high vacuum (3 hr). The residue was transferred into a new vial (7 mL) with

MeOH (2 mL), DCM (2 mL) and H_2O (1 mL). All solvents were removed under N_2 flow and the sample dried thoroughly under high vacuum. The solid material was dissolved in dry DCM (1 mL) and filtered through an HPLC filter (0.45 μm) into a new vial (7 mL). The filter was then washed with dry DCM (3 x 1 mL) into the same vial. The filter was finally washed with MeOH (5 mL) into a second new vial (7 mL). Solvents were removed under N_2 flow and the sample dried thoroughly under high vacuum (3 hr).

The DCM soluble material (1.8 mg) was dissolved in MeOH (100 μL) and pipetted onto the head of a cartridge containing amino phase material (200 mg), prepared by washing with 2% NH_3/MeOH (6 mL) and equilibrated to MeOH (10 mL). The cartridge was washed with MeOH (1 mL) to afford the reaction product (0.4 mg).

The reaction product (0.4 mg) was dissolved in 50% DCM/PE (200 μL) and pipetted onto the head of a cartridge containing diol phase material (100 mg), equilibrated to the same solvent mixture. The cartridge was subsequently washed with 50% DCM/PE (400, 200 μL), 80% DCM/PE (2 x 200 μL), DCM (2 x 400 μL) and MeOH (1 mL). Seven fractions were collected.

Second Reduction of Gymnodamine: gymnodimine (8.0 mg) was transferred into a r.b. flask (5 mL) in MeOH (2 mL) and solvent removed under N_2 flow. $NaCNBH_3$ (6.8 mg) was dissolved in MeOH (3.4 mL) and an aliquot (1 mL) added to the r.b. flask. AcOH (5 μL) was added and the reaction stirred (4.5 hr). All solvents were removed under N_2 flow and residue dried thoroughly under high vacuum (2 hr).

The sample was dissolved in dry DCM (1 mL) and filtered through an HPLC filter (0.45 μm). The r.b. flask was subsequently washed with dry DCM (4 x 1 mL) and passed through the filter. The DCM soluble material was pure gymnodamine (8.0 mg, 100% yield).

PBBC + Gymnodamine: gymnodamine (8.0 mg), was transferred into a reacti-vial (4 mL) in MeOH (2 mL). Solvent was removed under N_2 flow, the reacti-vial was sealed and the sample dried thoroughly under high vacuum (3 hr). PBBC (23.0 mg), freshly recrystallised from PE, was dissolved in dry DCM (2.61 mL). DMAP (3.6 mg) was dissolved in dry DCM (7.35 mL). Aliquots of PBBC and DMAP solutions (500 μL) were injected into the reacti-vial, in an ice bath (0 °C). Hunig's base (3.47 μL) was injected and the solution stirred at 0 °C (30 min). H_2O (100 μL) was added, solvents removed under N_2 flow and residue dried thoroughly, under high vacuum. The reaction material was dissolved in DCM (2 mL) and washed with aqueous citric acid (10% v/w, 2 mL) and H_2O (2 x 1 mL). The DCM phase was dried over Na_2SO_4 (2 g).

The DCM soluble material was re-dissolved in DCM (150 μL) and chromatographed in ten replicate runs (15 μL each) through an analytical diol HPLC column, equilibrated to DCM (1 mL/min). After each run the column was washed with 5% MeOH/DCM (5 mL) and re-equilibrated to DCM (10 mL). Six fractions were collected. The peak eluting at Rt = 350 s, was pure *p*-bromobenzamide (**56**) (4 mg, 37% yield).

*Crystal Structure of p-Bromobenzamide (**56**)*

Recrystallisation of (**56**): Material transferred into a Craigie tube (5 mm i.d.) in DCM (500 μL) and solvent removed under high vacuum (1 hr). The sample was dissolved in DCM (100 μL) and benzene (100 μL) added. The tube was partially sealed with a glass rod and kept at 0 °C (10 days). The resulting crystalline solid was removed, covered with H_2O and two crystals separated from the bulk material with a needle.

*NMR Assignment of p-Bromobenzamide (**56**)*

p-bromobenzamide (**56**): LRFABMS (NOBA) (Canterbury); $[M+H]^+$ 692.1/694.1; HRFABMS (NOBA) (Canterbury); $[M+H]^+$ 692.2971, $C_{39}H_{51}NO_5Br$ requires 692.2951.

6.5.4 Hapten Design and Synthesis of Gymnodimine

Synthesis

Gymnodamine + Succinic Semialdehyde: gymnodamine (2.0 mg) was transferred into a vial (7 mL) in MeOH (500 μL). Solvent was removed under N_2 flow and the sample dried thoroughly under high vacuum (5 hr). Succinic semialdehyde (2.0 mg) was dried thoroughly under high vacuum and dry MeOH (100 μL) added. $NaCNBH_3$ (6.3 mg) was dissolved in dry MeOH (2.1 mL). The succinic semialdehyde solution was added to the reaction vial followed by an aliquot (100 μL) of the

$NaCNBH_3$ solution, AcOH (1 μL) and dry MeOH (1.8 mL). Finally, a magnetic flea and five molecular sieves (type 4A) were added to the vial. The vial was sealed with a lid and parafilm and the reaction stirred (3 days). The vial contents were filtered through celite (1 g) and washed with MeOH (5 mL). The eluent was subsequently passed through an HPLC filter (0.45 μm) and the filter washed with MeOH (2 mL). The solvent was removed under N_2 flow and the residue dried under high vacuum.

The residue was dissolved in 20% MeOH/H_2O(1% AcOH) (100 μL) and pipetted onto the head of a column (5 mm i.d.), containing C18 material (4 cm), equilibrated to 20% MeOH/H_2O(1% AcOH). The column was washed with a succession of solvents from 20%-70% MeOH/H_2O(1% AcOH), with five fractions collected (1.5 mL/fraction). The fraction eluting at 70% MeOH/H_2O(1% AcOH) was the gymnodamine-amine linker (**59**)(1.5 mg, 64% yield).

Gymnodamine-amine linker (**59**): HRFABMS (NOBA) (Canterbury); $[M+H]^+$ 596.3965, $C_{36}H_{54}NO_6$ requires 596.3951. NMR data:
δ_H (CD_3OD) 7.12 (1H, brs, H3), 5.85 (1H, brs, H4), 5.60 (1H, brs, H18), 5.34 (1H, d *J* = 11.2, H8), 4.16 (1H, brq *J* unresolved, H13), 4.05 (1H, brs, H16), 3.97 (1H, d *J* = 10.2, H10), 2.91 (2H, brt, 12.2, 9.7, H1'), 2.40 (2H, obs, H3'), 1.93 (3H, s, Me25), 1.70 (3H, s, Me27), 1.65 (2H, obs, H2'), 1.58 (6H, s, Me26, Me29), 1.11 (3H, d *J* = 6.9, Me28).

<u>Piperidine + Succinic Semialdehyde</u>: succinic semialdehyde (1.5 mg) was dried thoroughly, in a vial (7 mL), under high vacuum (3 hr). $NaCNBH_3$ (3.7 mg) was dissolved in dry MeOH (3.27 mL) and an

aliquot (1 mL) was added to the reaction vial. Piperidine (7.4 μL) was added, the vial was sealed with a lid and parafilm and the reaction stirred (41 hr). Solvent was removed under N_2 flow and residue dried thoroughly under high vacuum (4 hr). The reaction product was (**60**).

Compound (**60**): NMR data:

δ_H (D_2O) 3.02 (4H, t, J = 5.4, 5.8, H1/H5), 2.85 (2H, t, J = 7.4, 8.3, H1'), 2.15 (2H, t, J = 6.9, 7.3, H3'), 1.78 (2H, dt, J = 7.3, 7.8, 7.4, 7.3, H2'), 1.65 (4H, m, H2/H4), 1.50 (2H, m, H3).

Gymnodamine + Succinic Anhydride: gymnodamine (2.0 mg) was transferred into a reacti-vial (1 mL), in MeOH (500 μL). The solvent was removed under N_2 flow, the reacti-vial was sealed and the residue dried thoroughly under high vacuum (3 hr). DMAP (4.8 mg) was dissolved in dry pyridine (8.42 mL) and succinic anhydride (7.2 mg) was also dissolved in dry pyridine (1.53 mL). Aliquots (83 μL) of each solution were injected into the reacti-vial and the reaction stirred (17 hr). Pyridine was removed under N_2 flow. The solid residue was subsequently washed into a vial (2 mL) three times with MeOH (3 x 500 μL). Solvent was removed under N_2 flow and the residue dried thoroughly under high vacuum (3 hr).

This sample was dissolved in MeOH (60 μL). Aliquots (15 μL) were chromatographed, in four replicate runs, on an analytical reverse phase C18 HPLC column, equilibrated to 60% MeOH/H_2O(0.05% TFA) (1 mL/min). The fraction eluting at Rt = 5.0 min was gymnodamine, while the fraction eluting at Rt = 10.2 min was the gymnodamine-amide linker (**61**).

gymnodamine-amide linker (**61**): HRFABMS (NOBA) (Canterbury); $[M+H]^+$ 610.3741, $C_{36}H_{52}NO_7$ requires 610.3744. NMR data:
δ_H (CD_3OD) 7.12 (1H, brs, H3), 5.85 (1H, brs, H4), 5.45 (1H, brm, H18), 5.21 (1H, d J = 10.8, H8), 4.42 (1H, brd J = 10.8, H21), 4.15 (1H, brm, H13), 3.91 (1H, brs, H16), 3.80 (1H, brd J = 14.6, H10), 3.03 (2H, brt J unresolved), 2.97 (1H, brd J = 10.3, H7), 2.58 (4H, brm, H2'/H3'), 1.89 (3H, s, Me25), 1.76 (3H, s, Me27), 1.66 (6H, s, Me26/Me29), 1.07 (3H, d J = 6.8, Me28).

Piperidine + Succinic Anhydride: DMAP (4.8 mg) was dissolved in dry pyridine (8.42 mL) and succinic anhydride (7.2 mg) was dissolved in dry pyridine (1.53 mL). Aliquots (100 µL) of each were injected into a dry reacti-vial (1 mL), followed by piperidine (0.385 µL). The reaction was stirred under anhydrous conditions (17 hr). Pyridine was removed under N_2 flow and the residue dried thoroughly under high vacuum (3 hr). The reaction product was (**62**).

Compound (**62**): NMR data:
δ_H (CD_3OD) 3.51 (4H, q, J = 5.3, 5.4, 5.4, H1/H5), 2.64 (2H, t, J = 6.8, 6.4, H2' or H3'), 2.52 (2H, t, J = 6.3, 6.1, H2' or H3'), 1.65 (4H, m, H2/H4), 1.52 (2H, m, H3).

Gymnodamine + PMPI: gymnodamine (1.5 mg) was transferred into an NMR tube in DCM (150 µL) and a supa-seal placed on the end of the tube. Solvent was removed under high vacuum (5 hr). PMPI (1.2 mg) was dissolved in 0.1% d5-pyridine/$CDCl_3$ (260 µL). An aliquot (150 µL) was removed and injected into the NMR tube. Parafilm was applied around the supa-seal to minimise moisture influx. The reaction was

monitored by ^{1}H NMR at t (hr) = 0.5, 1.5, 3.5, 7, 25 and 98. The material was transferred from the NMR tube into a vial (7 mL) and the tube washed with DCM (250 µL) and EtOAc (250 µL). The solvents were evaporated under N_2 flow. The solid residue was dissolved in DCM (500 µL) and passed through an HPLC filter (0.45 µm) into a new vial (2 mL). The filter was washed twice more with DCM (2 x 500 µL). The filter was finally washed with EtOAc (1 mL) and ACN (1 mL) into a second vial (7 mL).

The DCM soluble material was dried thoroughly under N_2 flow and dissolved in ACN (60 µL). Aliquots (15 µL) were injected in four replicate runs on an analytical reverse phase C18 column, equilibrated to 40% ACN/H_2O (1 mL/min). A gradient elution of 40% ACN/H_2O to 80% ACN/H_2O (12 min) followed by 80% ACN/H_2O (3 min) was used from which seven fractions were collected. The peak eluting at Rt = 9.0 min was the gymnodamine-urea maleimide linker (**63**), while the peak eluting at Rt = 10.3 min was considered to be the gymnodamine-*di*-urea/carbamate maleimide linker (**64**).

Gymnodamine-urea maleimide linker (**63**): HRFABMS (NOBA) (NIH); $[M+H]^+$ 724.3990, $C_{43}H_{54}N_3O_7$ requires 724.3961. NMR data:
δ_H ($CDCl_3$) 7.43 (2H, d *J* = 8.3, H3'/H7' or H4'/H6'), 7.23 (2H, obs.d *J* unresolved, H3'/H7' or H4'/H6'), 6.85 (1H, brs, H3), 6.82 (2H, s, H9'H10'), 5.72 (1H, brs, H4), 5.37 (1H, brm, H18), 5.22(1H, brd *J* = 11.2, H8), 4.14 (1H, brm, H13), 3.98 (1H, obs, H10), 3.92 (1H brs, H16), 3.65 (1H, brs, H7), 1.93 (3H, s, Me25), 1.78 (3H, s, Me27), 1.65 (3H, s, Me26), 1.60 (3H, s, Me29), 1.08 (3H, d *J* = 6.8, Me28).

Gymnodamine-*di*-linked product (**64**): LRFABMS (NOBA) (NIH); no molecular ion observed. NMR data:
δ_H ($CDCl_3$) 7.45 (4H, brm, H3'/H7'/H3"/H7" or H4'/H6'/H4"/H6"), 7.25 (4H, obs, H3'/H7'/H3"/H7" or H4'/H6'/H4"/H6"), 6.83 (2H, s, H9'/H10' or H9"/H10"), 6.82 (2H, s, H9'/H10' or H9"/H10"), 6.61 (1H, brs, H3), 5.69 (1H, brs, H4), 5.45 (1H, brm, H10), 5.40 (1H, brm, H18), 5.09 (1H, brd J = 11.0, H8), 4.18 (1H, brm, H13), 3.93 (1H, brs, H16), 1.92 (3H, s, Me25), 1.78 (3H, s, Me27), 1.66 (3H, s, Me26), 1.60 (obs, Me29), 1.08 (3H, brd J unresolved).

6.5.5 Large Scale Isolation Scheme

First Extraction

Frozen oysters (12.5 kg) were lyophilised (2 days). The dried oysters (2.5 kg) were crushed to form a coarse powder and weighed into portions (100 g).

The following protocol was applied to each portion:

(1) One portion of freeze dried oysters (100 g) was stirred with DCM (250 mL, 60 min) and filtered. This was process was repeated twice with DCM (2 x 250 mL, 30 min), on the filter cake. All three extracts were combined as the total DCM extract.

(2) The filter cake was stirred with 80% MeOH/H_2O (250 mL, 60 min) and filtered. This process was repeated twice more with 80% MeOH/H_2O (2 x 250 mL, 30 min). All three aq. MeOH extracts

were combined and residual DCM removed by under vacuum. This afforded the total aq. MeOH extract.

(3) The total DCM extract was evaporated to dryness and dissolved in PE (250 mL).

(4) The extracts from steps (2) and (3) were shaken together vigorously (5 min) in a separating funnel (2L) and left for the two phases to separate.

(5) The aq. MeOH layer was run off and poured into a second separating funnel (2L). This solution was then shaken further with PE (2 x 250 mL, 5 min).

(6) All three PE partitions were combined and PE removed by roto-vap. The PE extract was coded as OP_{hex}.

(7) The aq. MeOH layer was run off.

Scheme 5.5.1

(Elution solvents and volumes not referred to in text are recorded in scheme)

The total aq. MeOH partition (5.A(M/W)) was concentrated, *in vacuo*, to H_2O (2 L). The aqueous extract was subsequently partitioned against EtOAc five times (1000, 2 x 750, 2 x 500 mL), to afford 5.A(EtOAc) and 5.A(H_2O).

The pH of 5.A(H_2O) was checked with narrow band (4-6) pH paper. This extract was made to pH 8.5, by slow addition of $NaHCO_3$ (with stirring) and the pH checked regularly with narrow band (8-10) pH paper. The volume was made to 2.5 L with H_2O and partitioned against EtOAc (2 L). The resulting emulsion was broken by filtration through a

bed of celite. The aqueous layer was then partitioned three times against EtOAc (3 x 1 L).

Purification of Gymnodimine

The total EtOAc partition (450 mg) was coated onto celite (900 mg) and solvents removed, *in vacuo*. The dried residue was wetted with PE (1 mL) and slurried onto the head of a column (25 mm i.d.), containing diol (20 g), equilibrated to PE. Step gradient elution using PE/DCM/EtOAc/MeOH mixtures afforded twelve fractions (50 mL/fraction), with 100% mass recovery.

Fractions 4 - 6 were combined (124 mg) and dried, *in vacuo*. The dried solid was dissolved in 5% MeOH/DCM (2 mL) and pipetted onto the head of a column (10 mm i.d.), containing carboxylic acid phase material (2.5 g), prepared by washing with MeOH (40 mL) and equilibrated to 5% MeOH/DCM. Subsequent elution was achieved with 5% MeOH/DCM (20 mL), MeOH (20 mL) and 1% NH_3/MeOH (40 mL).

The 1% NH_3/MeOH fraction (5.5 mg) was dried thoroughly, *in vacuo*, dissolved in DCM (200 µL) and pipetted onto a cartridge containing cyano phase material (200 mg), equilibrated to DCM. Elution was achieved with DCM (5 mL), 25% IPA/DCM (5 mL), 50% IPA/DCM (5 mL), IPA (5 mL) and MeOH (5 mL).

The fraction eluting with DCM (3.0 mg) was dried, under N_2 flow and dissolved in MeOH (300 µL). This solution was injected on to a semi-

preparative cyano HPLC column, equilibrated to 60% MeOH/H_2O(0.05% TFA) (5 mL/min). Three fractions were collected with UV detection at 210 nm. The fractions collected had retention times of 0 - 12, 12 - 15, 15 - 24 min, respectively.

The fraction eluting at 15 - 24 min was dried, *in vacuo* and dissolved in MeOH (100 μL). This solution was injected (in five replicate HPLC runs of 20 μL each) on to an analytical cyano HPLC column, equilibrated to 70% MeOH/H_2O(0.05% TFA) (1 mL/min). The peak eluting at 17.5 min was gymnodimine (1 mg, $8x10^{-6}$ yield, wet weight)).

Second Extraction

Scheme 5.5.2

Frozen oysters (5 kg) were thawed in MeOH (4 L), blended (5 min) and filtered through a bed of celite. This process was repeated twice more with MeOH (4, 2 L). The extracts were all combined and concentrated to H_2O (2 L), *in vacuo*. The aqueous extract was then made to a volume of 3 L with H_2O. The pH was lowered to 4.5 by gradual addition of AcOH (with stirring) and monitoring with narrow band (4-6) pH paper. The acidic aqueous extract was subsequently partitioned twice against DCM (2 x 2.5 L) to afford 5.B(DCM) as the organic phase. The aqueous phase was then adjusted to pH 8.5, with gradual addition of $NaHCO_3$ (with stirring) and monitoring with narrow band (8-10) pH paper. The alkaline aqueous extract was then partitioned four times against EtOAc (4 x 1.5 L).

Aliquots (25 mg each) of 5.B(DCM) and 5.B(EtOAc) were dissolved in 0.1% AcOH / 90% MeOH / 10% H_2O (500 µL each) and pipetted onto separate carboxylic acid cartridges (1 g), prepared by washing with MeOH (5 mL) and 0.1% AcOH / 90% MeOH / 10% H_2O (10 mL). Each cartridge was washed with 0.1% AcOH / 90% MeOH / 10% H_2O (2.5 mL), MeOH (1 mL) and 2% NH_3/MeOH (5 mL).

Scheme 5.5.3

Fraction 5.B(DCM) (13 g, Scheme 5.5.2) was dried, *in vacuo* and partitioned between ether (2 x 2 L) and 0.1% AcOH/H_2O (2, 1, 1 L). The acidic aqueous phase was adjusted to pH 8.5 by gradual addition of $NaHCO_3$ (with stirring) and monitoring with narrow band (8-10) pH paper. The resulting alkaline aqueous solution was partitioned three times against EtOAc (3 x 1.5 L) to afford 5.E(EtOAc) and 5.E(H_2O).

Scheme 5.5.4

Fraction 5.E(EtOAc) (150 mg, Scheme 5.5.3) was dried, *in vacuo* and dissolved in 0.1% AcOH / 90% MeOH / 10% H_2O (3 mL). This solution was subsequently pipetted onto the head of a column (25 mm i.d.), containing carboxylic acid phase material (30 g), prepared by washing with 0.1% AcOH / % MeOH / 10% H_2O (250 mL), 2% AcOH / 88% MeOH / 10% H_2O (250 mL) and 0.1% AcOH / 90% MeOH / 10% H_2O (250 mL). Solvent elution afforded fractions 5.F1 - 5.F3.

Fraction 5.F3 (11.5 mg) was dissolved in MeOH (200 µL) and chromatographed (in ten replicate runs of 20 µL/run) on an analytical

reverse phase C18 HPLC column, equilibrated to 70% MeOH/H_2O(0.05% TFA) (1 mL/min). The peak eluting at 4.1 min was gymnodimine (5 mg, $1x10^{-4}$ yield, wet weight).

Third Extraction

Scheme 5.5.5

Frozen oysters (10 kg) were lyophilised. The dried flesh was crushed to form a coarse powder (2 kg). The powder was then divided into three equal portions and each extracted separately as follows:
The powder was extracted with 60% MeOH / 39% H_2O / 1% AcOH (3 L) and filtered through a bed of celite. The extraction process was then repeated twice more with the same solvent system (2 x 2 L). The aqueous methanol extracts were all combined and concentrated, *in vacuo*, to H_2O (1.5 L). The volume was then increased to 3 L with further H_2O, and the pH adjusted to 7 by careful addition of NH_3 (with stirring) and pH monitoring with narrow band (4-6 and 8-10) pH paper. After neutralisation, the solution was adjusted to pH 8.5 with gradual addition of $NaHCO_3$ (with stirring) and monitoring by narrow band (8-10) pH paper. Each alkaline aqueous extract was subsequently partitioned three times against DCM (2, 2, 1 L). Combination of each DCM partition gave the total DCM extract (5.G(DCM).

Extract 5.G(DCM) was dried, *in vacuo* and partitioned twice between ether (2 x 2 L) and 0.5% AcOH/H_2O (2 x 2 L). Residual ether was removed from the acidic H_2O phase, *in vacuo* and the acidic aqueous solution neutralised by careful addition of NH_3, with constant stirring and frequent monitoring with narrow band (4-6 and 8-10) pH paper. The

neutral solution was then adjusted to pH 8.5 with gradual addition of $NaHCO_3$ (with stirring) and by monitoring with narrow band (8-10) pH paper. The alkaline solution was then partitioned three times against EtOAc (3 x 1.5 L). The EtOAc phase was dried with anhydrous Na_2SO_4 to afford 5.G(EtOAc).

Final Purification of Gymnodimine

Fraction 5.G(EtOAc) (230 mg, Scheme 5.5.5) was dissolved in DCM (2 mL) and pipetted onto the head of a column (25 mm i.d.), containing diol(Mk) (25 g), equilibrated to 50% DCM/PE. Step gradient elution of 50% DCM/PE (50 mL), 65% DCM/PE (50 mL), 80% DCM/PE (100 mL), DCM (100 mL), 1%TEA/DCM (100 mL) and MeOH (100 mL) afforded six fractions, with 99% mass recovery.

The fraction eluting at 80% DCM/PE was acidified by addition of AcOH (0.5 mL). Excess AcOH was removed, *in vacuo*. This sample (48 mg) was dissolved in DCM (1 mL) and pipetted onto the head of a column (15 mm i.d.), containing diol(Bb) phase material (5 g), equilibrated to DCM. Step gradient elution of DCM (6 mL), DCM (9 mL), 50% EtOAc/DCM (12 mL), EtOAc (15 mL), 10% MeOH/EtOAc (15 mL) and MeOH (20 mL) afforded six fractions, with 100% mass recovery.

Fourth Extraction

Frozen oysters (5 kg) were thawed in 80% MeOH/19% H_2O/1% AcOH (4 L), blended and filtered through a bed of celite. This extraction process was repeated with the same solvent system (4 L). Extracts were

combined and concentrated, *in vacuo*, to H_2O (2 L). The volume was increased to 3 L by the addition of further H_2O and the pH adjusted to 7 by careful addition of NH_3, with constant stirring and frequent monitoring with narrow band (4-6 and 8-10) pH paper. The neutral solution was then adjusted to pH 8.5 with gradual addition of $NaHCO_3$ (with stirring) and monitoring by narrow band (8-10) pH paper. The alkaline solution was partitioned three times against DCM (3, 2, 2 L). The DCM phase was dried, *in vacuo* and partitioned twice between ether (2 x 250 mL) and 0.5% AcOH/H_2O (2 x 250 mL). Residual ether was removed, *in vacuo* and the resulting solution adjusted to pH 7 by careful addition of NH_3, with constant stirring and frequent monitoring with narrow band (4-6 and 8-10) pH paper. The neutral solution was then adjusted to pH 8.5 with gradual addition of $NaHCO_3$ (with stirring) and monitoring by narrow band (8-10) pH paper. The alkaline aqueous solution was partitioned three times against EtOAc (3 x 200 mL). The EtOAc phase was subsequently dried over anhydrous Na_2SO_4, to achieve the total EtOAc partition.

The total EtOAc partition (298 mg) was dried, *in vacuo*, dissolved in 50% DCM/PE (1 mL) and pipetted onto the head of a column (25 mm i.d.), containing diol(Mk) (30 g), equilibrated to 50% DCM/PE. Step gradient elution of 50% DCM/PE (4 fractions), 65% DCM/PE (3 fractions), 75% DCM/PE (3 fractions), 80% DCM/PE (5 fractions), and MeOH (1 fraction) (20 mL fraction volumes) afforded sixteen fractions, with a 97% mass recovery.

Fractions containing gymnodimine were combined (79 mg) and dried, *in vacuo*. The residue was dissolved in MeOH (1 mL) and pipetted onto

the head of a column (17 mm i.d.), containing amino phase (10 g), prepared by washing with 2% NH_3/MeOH (50 mL) and MeOH (250 mL). Elution with MeOH afforded gymnodimine (8.4 mg, $1.68x10^{-4}$ yield, wet weight).

6.5.6 Development of a Chromatography Based Assay for Gymnodimine

Methodology

Shellfish:

(1) Take shucked and frozen shellfish (75 g) and thaw in 0.1%AcOH/80% MeOH/20% H_2O (180 mL)(5 minutes). Blend (30 seconds) and filter, under vacuum, through Whatman filter paper (grade 1, 9 cm diameter) into a Buchner flask (1000 mL). Note: filtration is slow.

(2) Re-extract with the same solvent (120 mL), filter as before and combine both extracts.

(3) Transfer into a r.b. flask (1000 mL) and remove the MeOH by rotary evaporation until only water remains in the extract. Note: care should be taken as foaming or bumping may occur.

(4) Dilute the extract with distilled water to achieve a volume of 200 mL. Adjust the pH to 8 - 8.5 using $NaHCO_3$ and transfer into a separating funnel (500 mL). Wash the insoluble material in with DCM (2 x 100 mL).

(5) Shake the separating funnel (with the pressure released as required) and leave the phases to separate. Run the lower DCM layer off.

(6) Repeat step (5) with more DCM (200 mL). Combine DCM partitions and remove solvent by rotary evaporation.

(7) Dissolve the extract in diethyl ether (200 mL) and transfer into the same separating funnel as before. Wash the r.b. flask with 0.5% AcOH/H_2O (2 x 100 mL) and add to the separating funnel.

(8) Shake the separating funnel as before and let phases separate. Run off lower aqueous phase. Repeat with 0.5% AcOH/H_2O (200 mL) and combine aqueous layers.

(9) Wash the aqueous partition once more with diethyl ether (50 mL).

(10) Take aqueous partition and remove residual ether by rotary evaporation. Adjust the pH to 8 - 8.5 as in step (4).

(11) Partition 3 times with EtOAc (3 x 200 mL). Combine the EtOAc partitions.

(12) Run the EtOAc partition through a bed of Na_2SO_4 (2 g) into a r.b. flask (1000 mL).

(13) Remove EtOAc by rotary evaporation and dissolve in MeOH (3 x 2 mL) and transfer to a vial (7 mL).

(14) Remove solvent under N_2 and dissolve sample in 5% MeOH/DCM (100 µL) for TLC analysis.

Algae:

Algae were received impregnated onto filter paper at 0 °C.

(1) Take frozen algae/filter paper and blend in 0.1%AcOH/80% MeOH/20% H_2O (150 mL)(30 seconds) and filter, under vacuum, through Whatman filter paper (grade 1, 9 cm diameter) into a Buchner flask (1000 mL). Note: filtration is slow.

(2) Re-extract with the same solvent (100 mL), filter as before and combine both extracts.

(3) Transfer into a r.b. flask (500 mL) and remove the MeOH by rotary evaporation until only water remains in the extract. Note: care should be taken as foaming or bumping may occur.

(4) Dilute the extract with distilled water to achieve a volume of 50 mL. Adjust the pH to 8 - 8.5 using $NaHCO_3$ and transfer into a separating funnel (250 mL). Wash the insoluble material in with DCM (2 x 25 mL).

(5) Shake the separating funnel (with the pressure released as required) and leave the phases to separate. Run the lower DCM layer off.

(6) Repeat step (5) with more DCM (50 mL). Combine DCM partitions and remove solvent by rotary evaporation.

(7) Dissolve the extract in diethyl ether (50 mL) and transfer into the same separating funnel as before. Wash the r.b. flask with 0.5% AcOH/H_2O (2 x 25 mL) and add to the separating funnel.

(8) Shake the separating funnel as before and let phases separate. Run off lower aqueous phase. Repeat with 0.5% AcOH/H_2O (50 mL) and combine aqueous layers.

(9) Wash the aqueous partition once more with diethyl ether (50 mL).

(10) Take aqueous partition and remove residual ether by rotary evaporation. Adjust the pH to 8 - 8.5 as in step (4).

(11) Partition 3 times with EtOAc (3 x 50 mL). Combine the EtOAc partitions.

(12) Run the EtOAc partition through a bed of Na_2SO_4 (1 g) into a r.b. flask (250 mL).

(13) Remove EtOAc by rotary evaporation and dissolve in MeOH (3 x 2 mL) and transfer into a vial (7 mL).

(14) Remove solvent under N_2 and dissolve sample in 5% MeOH/DCM (100 μL) for TLC analysis.

References

1. Smith, P.; Chang, F.H.; Mackenzie, L. Toxic Phytoplankton and Algal Blooms, Summer 1992/93. *Marine Toxins and New Zealand Shellfish*, **1993**, 11-17. The Royal Society of New Zealand, Wellington, New Zealand.
2. *Toxic Marine Phytoplankton.* Graneli, E.; Sundström, B.; Edler, L.; Anderson, D.M., Eds., **1989**, Elsevier, New York, U.S.A.
3. Till, D.G. Public Health Issues. *Marine Toxins and New Zealand Shellfish*, **1993**, 41-44. The Royal Society of New Zealand, Wellington, New Zealand.
4. Eastaugh, J.; Shepherd, S. Infectious and Toxic Syndromes from Fish and Shellfish Consumption. A Review. *Archives of Internal Medicine*, **1989**, *149*, 1735-1740.
5. Yasumoto, T.; Murata, M. *Chem. Rev.*, **1993**, *93*, 1897-1909.
6. Shimizu, Y. *Chem. Rev.*, **1993**, *93*, 1685-1698.
7. Harada, T.; Oshima, Y.; Yasumoto, T. *Agric. Biol. Chem.*, **1983**, *47*, 191.
8. Carmichael, W.W. The Toxins of Cyanobacteria. *Scientific American*, **1994**, *270(1)*, 68. Diagram re-produced by kind permission of Scientific American, Inc.
9. Laverty, R. Modes of Action of Shellfish Toxins. *Marine Toxins and New Zealand Shellfish*, **1993**, 31-34. The Royal Society of New Zealand, Wellington, New Zealand.
10. Yasumoto, T.; Yasumara, D.; Yotsu, M.; Michishita, T.; Endo, A.; Kotaki, J. *Agric. Biol. Chem.*, **1986**, *50*, 793-795.
11. Simidu, U.; Kita-Tsukamoto, K.; Yasumoto, T.; Yotsu, M. *Int. J. System. Bacteriol.*, **1990**, *40*, 331.
12. Noguchi, T.; Jeon, J.K.; Arakawa, O.; Sugita, H.; Deguchi, Y.; Shida, Y.; Hashimoto, K. *J. Biochem.*, **1986**, *99*, 311-314.

13. Simidu, U.; Noguchi, T.; Hwang, D.F.; Shida, Y.; Hashimoto, K. *Appl. Env. Microbiol.*, **1987**, *53*, 1714-1715.
14. Matsui, T.; Taketsugu, S.; Kodama, K.; Ishii, A.; Yamamori, K.; Shimizu, C. *Nippon Suisan Gakkaishi*, **1989**, *55*, 2199.
15. Yasumoto, T.; Michishita, T. *Agric. Biol. Chem.*, **1985**, *49*, 893.
16. Yotsu, M.; Endo, A.; Yasumoto, T. *Agric. Biol. Chem.*, **1989**, *53*, 893.
17. Davis, C.C. *Bot. Gaz.*, **1947**, *109*, 358-360.
18. Bates, M.; Baker, M.; Wilson, N.; Lane, L.; Handford, S. Epidemiologic Overview of the New Zealand Shellfish Toxicity Outbreak. *Marine Toxins and New Zealand Shellfish.*, **1993**, 35-40. The Royal Society of New Zealand, Wellington, New Zealand.
19. Lin, Y.-Y; Risk, M.; Ray, S.M.; Van Engen, D.; Clardy, J.; Golik, J.; James, J.C.; Nakanishi, K. *J. Am. Chem. Soc.*, **1981**, *103*, 6773-6775.
20. Schreibmayer, W.; Jeglitsch, G. *Biochimica et Biophysica Acta*, **1992**, *1104*, 233-242.
21. Borison H.L.; Ellis, S.; McCarthy, L.E. *British Journal of Pharmacology*, **1980**, *70*, 249-256.
22. Lee, J.S.; Igarashi, T.; Fraga, S.; Dahl, E.; Hovgaard, P.; Yasumoto, T. *J. Appl. Phycol.*, **1989**, *1*, 147.
23. Yasumoto, T.; Murata, M.; Oshima, Y.; Sano, M.; Matsumoto, G.K.; Clardy, J. *Tetrahedron*, **1985**, *41*, 1019-1025.
24. Murata, M.; Kumagai, M.; Lee, J.S.; Yasumoto, T. *Tetrahedron Lett.*, **1987**, *28*, 5869-5872.

25. Mackenzie, L. *Proceedings of the Marine Biotoxin Science Workshop No 7.*, **1997**. Ministry of Agriculture, Wellington, New Zealand (In print).
26. Yasumoto, T.; Oshima, Y.; Yamaguchi, M. *Nippon Suisan Gakkaishi*, **1978**, *44*, 1249.
27. Terao, K.; Ito, E.; Oarada, M.; Murata, M.; Yasumoto, T. *Toxicon*, **1990**, *28*, 1095-1104.
28. Tachibana, K.; Scheuer, P.J.; Tsukitani, Y.; Kikuchi, H.; Van Engen, D.; Clardy, J.; Gopichand, Y.; Schmitz, F.J. *J. Am. Chem. Soc.*, **1981**, *103*, 2469-2471.
29. Murakami, Y.; Oshima, Y.; Yasumoto, T. *Nippon Suisan Gakkaishi*, **1982**, *48*, 69-72.
30. Yasumoto, T.; Oshima, Y.; Sugawara, W.; Fukuyo, Y.; Oguri, H.; Igarashi, T.; Fujita, N. *Nippon Suisan Gakkaishi*, **1980**, *46*, 1405-1411.
31. Satake, M.; Terasawa, K.; Kadowaki, Y.; Yasumoto, T. *Tetrahedron Lett.*, **1996**, *37*, 5955-5958.
32. Takahashi, H.; Kusumi, T.; Kan, Y.; Satake, M.; Yasumoto, T. *Tetrahedron Lett.*, **1996**, *37*, 7087-7090.
33. Yasumoto, T. *Proceedings of the Marine Biotoxin Science Workshop No 7.*, **1997**. Ministry of Agriculture, Wellington, New Zealand (In print).
34. YTX Confirmed In Mussels Harvested from Coromandel Peninsula as Part of This Research Project.
35. YTX Confirmed In Shellfish Harvested from Wedge Point By Fluorescence HPLC. Yasumoto, T. Tohoku University, Japan. *Pers. Comm.*

36. Quilliam, M.A.; Wright, J.L.C. *Analytical Chemistry*, **1989**, *61*, 1053-1060.

37. Takemoto, T.; Daigo, K. *Chem. Pharm. Bull.*, **1958**, *6*, 578-580.

38. Subba Rao, D.V.; Quilliam, M.A.; Pocklington, R. *Can. J. Fisheries Aq. Sci.*, **1988**, *45*, 2076-2079.

39. Bates, S.S.; Bird, C.J.; deFreitas, A.S.W.; Foxall, R.A.; Gilgan, M.; Hanic, L.A.; Johnson, G.E.; McCulloch, A.W.; Odense, P.; Pocklington, R.; Quilliam, M.A.; Sim, P.G.; Smith, J.C.; Subba Rao, D.V.; Todd, E.C.D.; Walter, J.A.; Wright, J.L.C. *Can. J. Fisheries Aq. Sci.*, **1989**, *46*, 1203-1215.

40. Yasumoto, T.; Bagnis, R.; Vernoux, J.P. *Bull. Jpn. Soc. Sci. Fish.*, **1976**, *42*, 359-365.

41. Yasumoto, T.; Nakajima, I.; Ohshima, Y.; Bagnis, R. *Toxic Dinoflagellate Blooms*, Taylor, D.L., Seligner, H., Eds., **1979**, 65. Elsevier, North Holland.

42. Bagnis, R. *Hawaii Med. J.*, **1965**, *28*, 25.

43. (a) Scheuer, P.J.; Takahashi, W.; Tsutsumi, J.; Yoshida, T. *Science*, **1976**, *155*, 1267. (b) Tachibana, K. Ph.D. Thesis, University of Hawaii, **1980**. (c) Nukina, M.; Koyanagi, L.M.; Scheuer, P.J. *Toxicon*, **1984**, *22*, 169-176.

44. (a) Murata, M.; Legrand, A.M.; Ishibashi, Y.; Yasumoto, T. *J. Am. Chem. Soc.*, **1989**, *111*, 8927-8931. (b) Murata, M.; Legrand, A.M.; Ishibashi, Y.; Fukui, M.; Yasumoto, T. *J. Am. Chem. Soc.*, **1990**, *112*, 4380-4386.

45. (a) Lewis, R.J.; Sellin, M.; Poli, M.A.; Norton, R.S.; MacLeod, J.K.; Sheil, M.M. *Toxicon*, **1991**, *29*, 1115-1127. (b) Satake, M.; Murata, M.; Yasumoto, T. *Symposium Papers*, 34th

Symposium On the Chemistry of Natural Products, Tokyo, **1992**, 87. Organizing Committee of the Symposium, Tokyo.

46. Satake, M.; Murata, M.; Yasumoto, T. *Tetrahedron Lett.*, **1993**, *34*, 1975-1978.
47. Li, K.M. *Science*, **1965**, *147*, 1580.
48. Rayner, M.D.; Kosaki, T.I.; Fellmeth, E.L. *Science*, **1968**, *160*, 70.
49. Yokoyama, A.; Murata, M.; Oshima, Y.; Iwashita, T.; Yasumoto, T. *J. Biochem.*, **1988**, *104*, 184-187.
50. Zheng, W.; DeMattei, J.A.; Wu, J.P.; Duan, J.J.W.; Cook, L.R.; Oinuma, H.; Kishi, Y. *J. Am. Chem. Soc.*, **1996**, *118*, 7946-7968.
51. Nonomura, T.; Sasaki, M.; Matsumori, N.; Murata, M.; Tachibana, K.; Yasumoto, T. *Angew. Chem. Int. Ed. Engl.*, **1996**, *35*, 1675-1678.
52. Kosuge T.; Tsuji, K.; Hirai K. *Chem. Pharm. Bull.*, **1982**, *30*, 3255-3259.
53. Kosuge T.; Tsuji, K.; Hirai K.; Fukuyama, T.; Nukaya, H.; Ishida, H. *Chem. Pharm. Bull.*, **1985**, *33*, 2890-2895.
54. Kosuge T.; Tsuji, K.; Hirai K.; Fukuyama, T. *Chem. Pharm. Bull.*, **1985**, *33*, 3059.
55. Kobayashi, J.; Ishibashi, M.; Wälchli, M.R.; Nakamura, H.; Hirata, Y.; Sasaki, T.; Ohizumi, Y. *J. Am. Chem. Soc.*, **1988**, *110*, 490-494.
56. Ishibashi, M.; Kobayashi, J. *Heterocycles*, **1997**, *44*, 543-572.
57. Nakajima, I.; Oshima, Y.; Yasumoto, T. *Nippon Suisan Gakkaishi*, **1981**, *47*, 1029-1033.

58. Paul, G.K.; Matsumori, N.; Murata, M.; Tachibana, K. *Tetrahedron Lett.*, **1995**, *36*, 6279-6282.

59. Murakami, M.; Makabe, K.; Yamaguchi, K.; Konosu, S.; Wälchli, M.R. *Tetrahedron Lett.*, **1988**, *29*, 1149-1152.

60. Torigoe, K.; Murata, M.; Yasumoto, T.; Iwashita, T. *J. Am. Chem. Soc.*, **1988**, *110*, 7876-7877.

61. Hu, T.; deFreitas A.S.W.; Curtis, J.M.; Oshima, Y.; Walter, J.A.; Wright, J.L.C. *J. Nat. Prod.*, **1996**, *59*, 1010-1014.

62. Hu, T.; Curtis, J.M.; Walter, J.A.; Wright, J.L.C. *Tetrahedron Lett.*, **1996**, *37*, 7671-7674.

63. Uemura, D.; Chou, T.; Haino, T.; Nagatsu, A.; Fukuzawa, S.; Zheng, S.; Chen, H. *J. Am. Chem. Soc.*, **1995**, *117*, 1155-1156.

64. Chou, T.; Kamo, O.; Uemura, D. *Tetrahedron Lett.*, **1996**, *37*, 4023-4026.

65. Chou, T.; Haino, T.; Kuramoto, M.; Uemura, D. *Tetrahedron Lett.*, **1996**, *37*, 4027-4030.

66. Hu, T.; Curtis, J.M.; Oshima, Y.; Quilliam, M.A.; Walter, J.A.; Watson-Wright, W.M.; Wright, J.L.C. *J. Chem. Soc. Chem. Commun.*, **1995**, 2159-2161.

67. Seki, T.; Satake, M.; Mackenzie, L.; Kaspar, H.F.; Yasumoto, T. *Tetrahedron Lett.*, **1995**, *36*, 7093-7096.

68. Hannah, D.J.; Till, D.G.; Benseman, B.; Jones, P.D.; Pickston, L.; Walker, N. Toxins and Assay Techniques. *Marine Toxins and New Zealand Shellfish*, **1993**, 28-30. The Royal Society of New Zealand, Wellington, New Zealand.

69. Gardner, T. A Little P, D and NSP. *Proceedings of the Marine Biotoxin Science Workshop No 6.*, **1996**. Ministry of Agriculture, Wellington, New Zealand.

70. Yasumoto, T.; Murata, M.; Oshima, Y.; Matsumoto, G.K.; Clardy, J. *Seafood Toxins.* Ragelis, E.P., Ed., **1984**, 207-214. American Chemical Society, Washington, DC, U.S.A.

71. *Official Methods of Analysis of the Association of Official Analytical Chemists.* Helrich, K. Ed., **1990**, 959-968. AOAC, Washington, DC, U.S.A.

72. Comesanã-Losada, M.; Gago-Martínez, A.; Leao-Martins, J.M.; Rodríguez-Vázquez, J.A. *Analyst*, **1996**, *121*, 1665-1670.

73. Steidinger, K.A.; Joyce, E.A. *Florida Red Tides.*, Educational Series 17, **1973**. State of Florida Department of Natural Resources, U.S.A.

74. Garthwaite, I.; Ross, K.M.; Poli, M.; Towers, N.R. Comparison of Immunoassay, Cellular, and Classical Mouse Bioassay Methods for Detection of Neurotoxic Shellfish Toxins. *Immunoassays for Residue Analysis.* Beier, R.C. and Stanker, L.H. Eds., **1996**, Chapter 32, 404-412. American Chemical Society Symposium Series 621, U.S.A.

75. Hannah, D.J.; Till, D.G.; Deverall, T.; Jones, P.D.; Fry, J.M. *J. Assoc. Off. Anal. Chem.*, **1995**, *78*, 480-483.

76. Ishida, H.; Nozawa, A.; Totoribe, K.; Muramatsu, N.; Nukaya, H.; Tsuji, K.; Yamaguchi, K.; Yasumoto, T.; Kaspar, H.; Berkett, N.; Kosuge, T. *Tetrahedron Lett.*, **1995**, *36*, 725-728.

77. Yasumoto, T. Marine Toxins Occurring in the Oceanian Waters. *Symposium On Oceanian-Japanese Organic Chemistry Synthesis and Natural Products: Socs 12 - Tokushima*, **1996**. Tokushima Bunri University, Japan.

78. Morohashi, A.; Satake, M.; Murata, K.; Naoki, H.; Kaspar, H.F.; Yasumoto, T. *Tetrahedron Lett.*, **1995**, *36*, 8995-8998.

79. Yasumoto, T. Tohoku University, Japan. *Pers. Comm.*

80. Aune, T. Toxicity of Marine and Freshwater Algal Biotoxins Towards Freshly Prepared Hepatocytes. *Mycotoxins and Phycotoxins '88.* Natori S. Et. Al. Eds., **1989**, Pp 461-468. Elsevier, Netherlands.

81. Karplus, M. *J. Am. Chem. Soc.*, **1963**, *85*, 2870-2871.

82. *Encyclopedia of Reagents for Organic Synthesis.* Paquette L.A., Ed-In-Chief, **1995**, 3837-3845 John Wiley & Sons Ltd, England.

83. Miles C. AgResearch, Ruakura, Hamilton, New Zealand. *Pers. Comm.*

84. Mackenzie, L. *Seafood New Zealand*, **1994**, *2*, 47-50.

85. Krebs, K.G.; Heusser, D.; Wimmer, H. *Thin Layer Chromatography, A Laboratory Handbook, 2nd Edition.* Stahl, E. Ed., **1969**, 873-874. Spray Reagent No. 97. Springer-Verlag, New York, U.S.A.

86. Borrell, T. *Marine Biotoxin Science Workshop No 6*, **1996**, Wellington, New Zealand.

87. Falk, M.; Spierenburg, P.F.; Walter, J.A. *J. Comp. Chem.*, **1996**, *17*, 409-417.

88. Ohtani, I.; Kusumi, T.; Kashman, Y.; Kakisawa, H. *J. Org. Chem.*, **1991**, *56*, 1296-1298.

89. Kusumi, T; Fujita, Y.; Ohtani, I.; Kakisawa, H. *Tetrahedron Lett.*, **1991**, *32*, 2923-2926.

90. Blunt J.W. University of Canterbury, New Zealand. *Pers. Comm.*

91. Chem3D™ Version 3.2, **1986-1995**. Cambridgesoft Corporation, Massachusetts, U.S.A.

92. PC Spartan, **1996**. Wavefunction Inc., California, U.S.A.

93. Dewar, M.J.S.; Zoebisch, E.G.; Healy, E.F.; Stewart, J.J.P. *J. Am. Chem. Soc.*, **1985**, *107*, 3902-3909.

94. Basha, A.; Lipton, M.; Weinreb, S.M. *Tetrahedron Lett.*, **1977**, *48*, 4171-4174.

95. *Encyclopedia of Reagents for Organic Synthesis.* Paquette L.A., Ed-In-Chief, **1995**, 2854-2860. John Wiley & Sons Ltd, England.

96. Irwin, N. *Recommended Procedures for the Examination of Seawater and Shellfish*; **1970**, 4th Edition, 61-65 and Table 4.4. American Public Health Association, Inc., U.S.A.

97. Evans, M.B.; Dale, A.D.; Little, C.J. *Chromatographia*, **1980**, *13*, 5-10.

98. *Laboratory Procedures for the Examination of Seawater and Shellfish.* Greenberg & Hunt Eds, 5th Edition, **1985**, American Public Health Association, Inc., U.S.A.

99. Truman, P.; Lake, R.J. *J. Assoc. Off. Anal. Chem. International*, **1996**, *79*, 1130-1133.

Appendix One

Assays

The Mouse Bioassay

Sample extracts were prepared for injection by suspending them in a sterile solution, which contained 1% Tween 60 and 0.85% NaCl in water. Diluent was added to the extract residue to achieve known final concentrations. A one or two mouse system was generally used. Samples were injected into the intraperitoneal cavity (i.p.) of the mice, in known volumes. Mice were observed for symptoms prior to death. For brevetoxin containing samples the symptoms observed were panting and hind leg paralysis leading to a protracted death. For gymnodimine containing samples the symptoms observed were a fast onset of gasping with fits prior to rapid death. Where rapid mouse deaths occurred (within 2 hours), in most cases subsequent dilutions were carried out on a 1 mouse system. Mouse units/mg sample (MU/mg) were calculated from Table A1.[98]

Table A1 is designed for calculation of MU for brevetoxin containing samples. Consequently, gymnodimine containing samples were calculated as the amount of extract required to kill a 20 g mouse (19-21 g).

Table A1 *Relationship of Dose to Death Time and Weight of Mice Injected with Ptychodiscus brevis Toxin(s) Extracted from Shellfish*

		Mouse Weight	Correction
Death Time *min* (20 g mice)	**Mouse units *MU/mL***	**Mouse Weight, *g***	**Correction Factor**
6-7	11.0	15	0.69
8-9	10.0	15.5	0.72
10-11	9.0	16	0.75
12-13	8.0	16.5	0.78
14-15	7.0	17	0.81
16-17	6.0	17.5	0.84
18-19	5.0	18	0.87
20-25	4.5	18.5	0.90
30-34	4.0	19	0.94
38-41.5	3.8	19.5	0.97
45-52.5	3.6	20	1.00
60-71.5	3.4	20.5	1.03
83-94	3.2	21	1.06
105-122.5	3.0	21.5	1.09
140-160	2.8	22	1.12
180-207	2.6	22.5	1.15
234-267	2.4	23	1.18
300-330	2.2	23.5	1.21
360-397.5	2.0	24	1.24
435-487.5	1.8	24.5	1.27
540-592.5	1.6	25	1.30
645-712.5	1.4	25.5	1.33
780-855	1.2	26	1.36
930	1.0		

The P388 Antitumour Assay

The *in vitro* "antitumour" assay used the P388 cell line (murine leukaemia cells) and is extremely sensitive to cytotoxicity effects. Thus the P388 assay is a cytotoxicity-based assay against a specific leukaemia cell type. The IC_{50} result obtained from this assay represented the concentration of the test compound at which the number of viable cells is reduced by fifty per cent relative to the control.

For the P388 assay, a two fold dilution series of the sample was incubated for 72 hours with P388 (Murine Leukaemia) cells. The concentration of sample required to reduce the P388 cell growth by 50% (comparative to control cells) was determined using the absorbance values obtained when the yellow dye [3-(4,5-dimethylthiazol-2-yl]-2,5-diphenyl-2*H*-tetrazolium bromide (MTT) (**65**) was reduced by healthy cells to the purple colour MTT formazan (**66**).

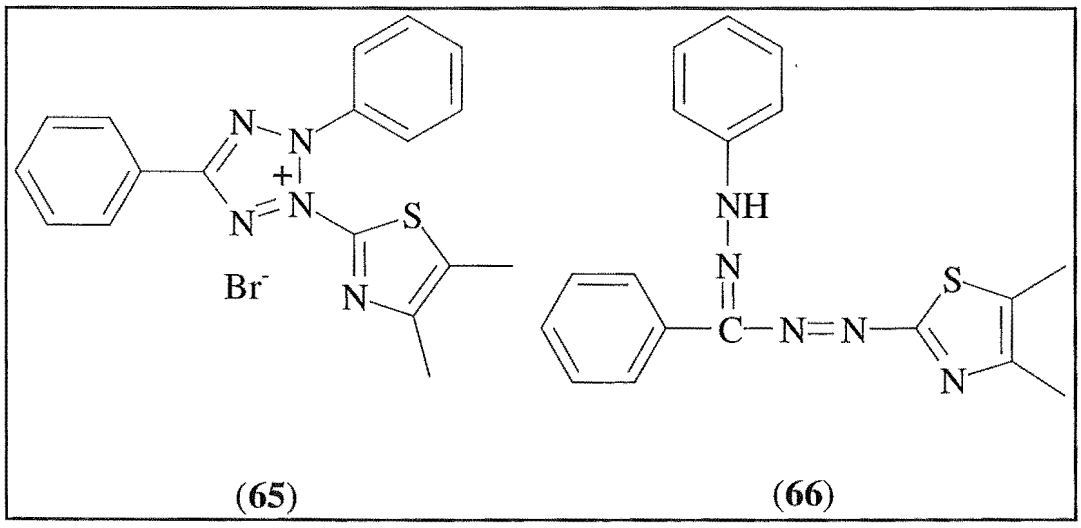

(**65**) (**66**)

The absorbance was expressed as a percentage cell viability relative to the control. This absorbance was plotted against the logarithm of the sample concentration in the well to generate a sample concentration *vs* cell viability curve (Figure A1). The antilogarithm of the concentration producing a fifty per cent reduction in the number of viable cells gave the IC_{50} value. This value was expressed in units of either ng/mL or µg/mL.. Those samples not intersecting the fifty percent line were either too dilute (always above, compound "g") or too concentrated (always below, compounds "c" and "e") to return an IC_{50} value (Figure A1).

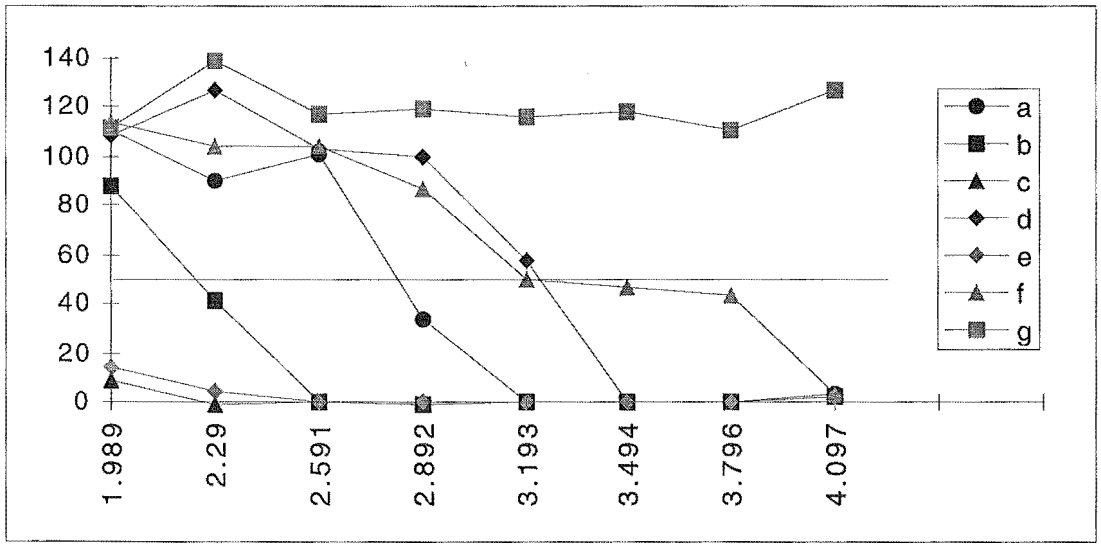

Fig A1 *A Typical Graph Generated From the P388 Assay*

The Neuroblastoma Assay

The neuroblastoma cell culture assay was run at the Communicable Disease Centre, in Porirua, New Zealand. The neuroblastoma assay was run using mouse neuroblastoma cells (Neuro 2A). This assay is designed to detect compounds that exert their toxicity by affecting voltage-gated sodium channels. For this research the assay was designed for brevetoxin detection, as described in Fig A2.

Samples were prepared by suspension in methanol (100 μL). An aliquot (10 μL) of each sample was added to assay medium (0.99 mL). Further dilutions were made from this 1/100 stock. The sample medium used was RPMI 1640 complete medium (Gibco, Grand Island, NY) supplemented with 10% fetal bovin serum, 20 mM Hepes, 25 mM bicarbonate, 1.7 mM glutamine, 1 mM sodium pyruvate and 55 μg gentomicin sulfate/mL.[99]

Cell viability was determined using MTT dye in a similar fashion to the P388 assay.

The results were expressed in "BTX" equivalents as determined by the standard curve for brevetoxin-B (BTX-B).

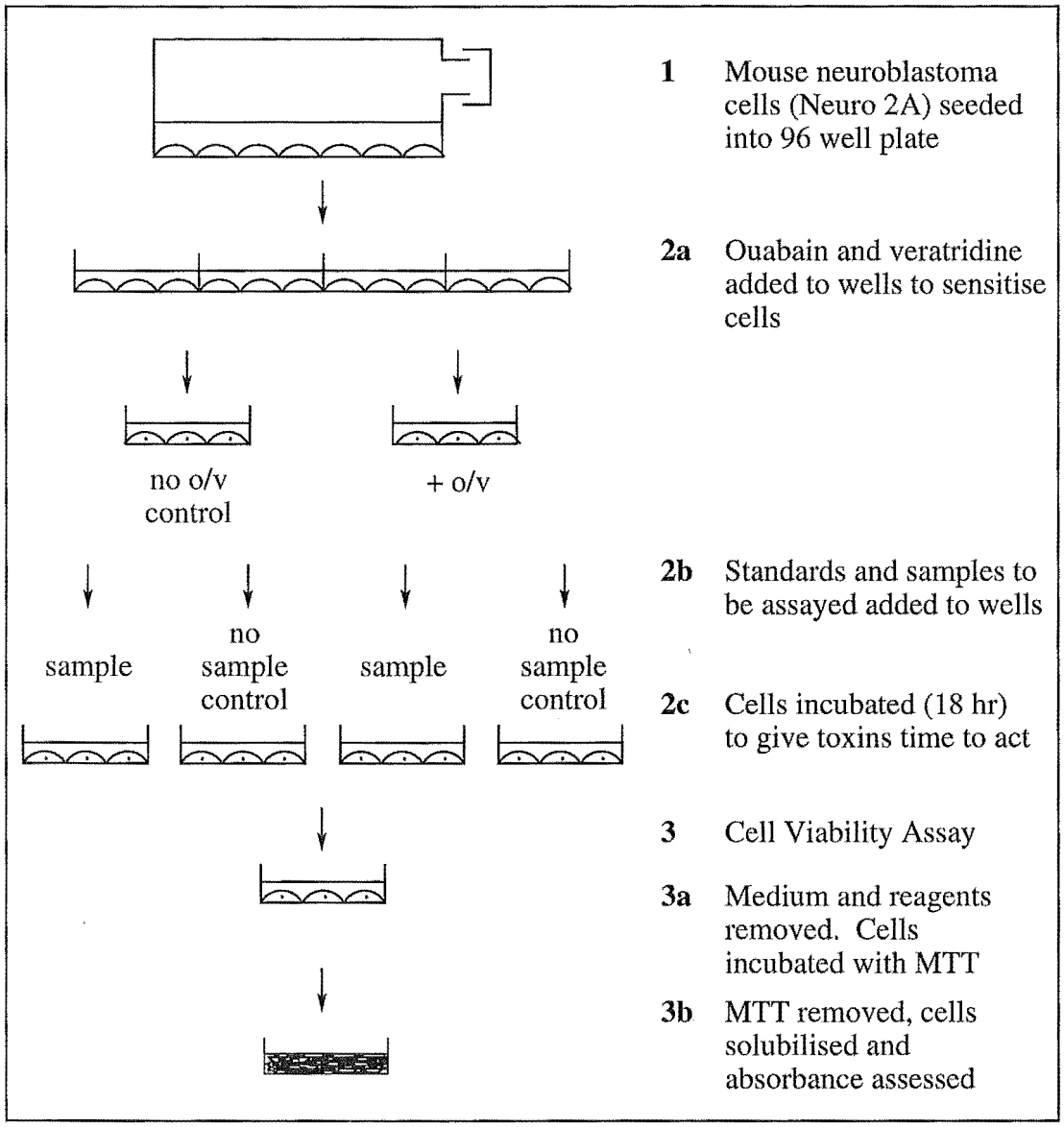

Fig A2 *The Neuroblastoma Assay Protocol*

The Enzyme-Linked Immunosorbent Assay

The competitive ELISA is based on the use of antibodies, specific to a known compound. These antibodies (or antisera) are able to bind to the compound of interest allowing a quantitative measurement of concentration to be made.

At the time of writing either the direct or indirect competitive ELISA was being developed, depending on what was more appropriate for the toxin. A brief overview of each is illustrated in Fig A3. The direct competitive ELISA is described in detail as for the brevetoxin ELISA.[74]

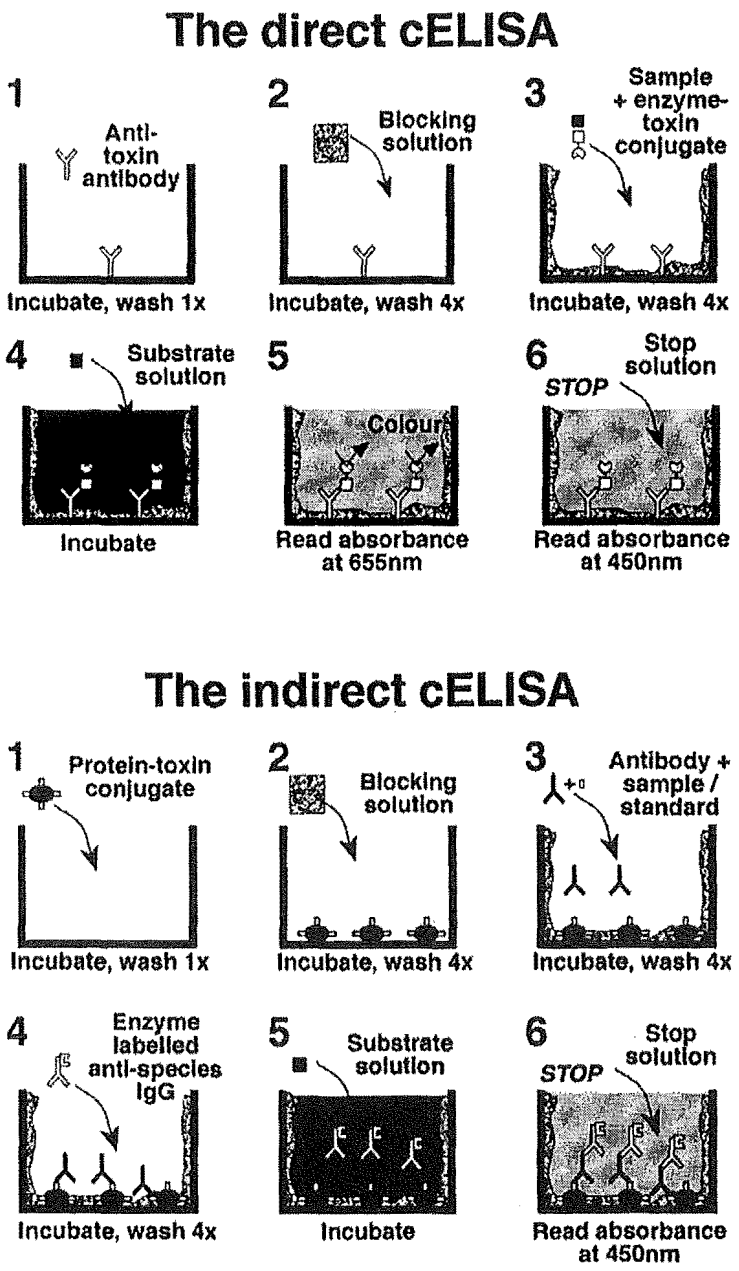

Fig A3 *The Direct and Indirect ELISA Procedures*

Appendix Two

X-Ray Data for Crystal Structure

Table A2.1 *Atomic coordinates (x 10^4) and equivalent isotropic displacement parameters ($Å^2$ x 10^3) for (**56**). U(eq) is defined as one third of the trace of the orthogonalized U_{ij} tensor*

	x	y	z	U(eq)
B r	966(1)	3156(1)	8151(1)	73(1)
O(1)	8171(4)	7129(2)	10514(2)	58(2)
O(4)	9205(4)	7156(2)	9675(2)	42(1)
O(10)	13318(3)	6820(2)	6646(2)	53(1)
C(1)	9035(7)	6859(4)	10210(3)	44(2)
C(2)	9952(6)	6250(4)	10331(3)	44(2)
C(3)	10737(6)	6179(3)	9879(3)	46(2)
C(4)	10309(6)	6733(3)	9427(3)	42(2)
C(5)	9872(6)	6303(3)	8879(3)	34(2)
C(6)	10633(6)	6201(3)	8422(3)	32(2)
C(7)	10247(6)	5692(3)	7902(3)	33(2)
C(8)	10694(5)	6124(3)	7365(2)	24(2)
C(9)	11714(6)	5962(3)	7045(3)	30(2)
C(10)	12061(5)	6495(3)	6558(3)	39(2)
C(11)	12111(5)	6076(3)	5972(3)	43(2)
C(12)	10766(6)	5814(3)	5755(2)	46(2)
C(13)	10869(6)	5375(3)	5184(3)	51(2)
C(14)	9515(6)	5092(3)	4980(3)	50(2)
C(15)	9705(6)	4224(3)	4852(2)	44(2)
C(16)	10804(6)	4004(3)	5248(3)	40(2)
C(17)	10442(6)	3797(3)	5871(3)	35(2)
C(18)	9251(6)	3869(3)	6061(3)	37(2)
C(19)	8840(6)	3818(3)	6676(2)	46(2)
C(20)	9071(6)	4626(3)	6955(2)	35(2)

C(21)	8562(5)	4657(3)	7571(2)	29(2)
N	7188(5)	4470(3)	7594(2)	29(2)
C(32)	6317(5)	5061(3)	7348(2)	35(2)
C(31)	6483(5)	5845(3)	7645(2)	37(2)
C(30)	7909(5)	6084(3)	7662(2)	32(2)
C(22)	8787(5)	5447(3)	7907(3)	26(2)
C(23)	8423(5)	5246(3)	8529(2)	35(2)
C(24)	8550(5)	5943(3)	8935(2)	42(2)
C(25)	9933(6)	5803(3)	10870(2)	71(2)
C(26)	11996(4)	6530(3)	8393(2)	54(2)
C(27)	12659(5)	5315(3)	7158(2)	45(2)
C(28)	10139(5)	4098(3)	4235(2)	69(2)
C(29)	11579(5)	3544(3)	6221(2)	57(2)
O(13)	11655(4)	4682(2)	5248(2)	44(1)
O(1')	7550(4)	3279(2)	7986(2)	63(2)
C(1')	6811(6)	3794(4)	7813(3)	36(2)
C(2')	5355(6)	3654(4)	7889(3)	29(2)
C(3')	4676(7)	3207(4)	7500(3)	52(2)
C(4')	3355(7)	3078(4)	7587(3)	47(2)
C(5')	2756(6)	3351(4)	8047(3)	43(2)
C(6')	3387(7)	3786(4)	8441(3)	64(3)
C(7')	4701(7)	3935(4)	8355(3)	62(3)
C(1")	7696(3)	7070(1)	5282(1)	131(6)
C(2")	6796(3)	6870(1)	5682(1)	112(4)
C(3")	5796(3)	6470(1)	5482(1)	127(5)
C(4")	5596(3)	6270(1)	4882(1)	177(8)
C(5")	6596(3)	6630(1)	4582(1)	146(6)
C(6")	7596(3)	6970(1)	4782(1)	169(7)

Table A2.2 *Bond lengths [Å] for (56)*

	Bond lengths [Å]		Bond lengths [Å]
Br-C(5')	1.911(6)	C(16)-C(17)	1.562(7)
O(1)-C(1)	1.242(7)	C(17)-C(18)	1.325(7)
O(4)-C(1)	1.377(6)	C(17)-C(29)	1.509(7)
O(4)-C(4)	1.483(6)	C(18)-C(19)	1.519(7)
O(10)-C(10)	1.441(6)	C(19)-C(20)	1.560(5)
C(1)-C(2)	1.449(9)	C(20)-C(21)	1.550(7)
C(2)-C(3)	1.352(7)	C(21)-N	1.469(6)
C(2)-C(25)	1.490(7)	C(21)-C(22)	1.595(6)
C(3)-C(4)	1.501(7)	N-C(1')	1.333(6)
C(4)-C(5)	1.559(7)	N-C(32)	1.485(5)
C(5)-C(6)	1.352(7)	C(32)-C(31)	1.534(6)
C(5)-C(24)	1.517(7)	C(31)-C(30)	1.543(6)
C(6)-C(26)	1.532(7)	C(30)-C(22)	1.542(6)
C(6)-C(7)	1.564(7)	C(22)-C(23)	1.556(7)
C(7)-C(8)	1.544(6)	C(23)-C(24)	1.545(6)
C(7)-C(22)	1.579(7)	O(1')-C(1')	1.245(6)
C(8)-C(9)	1.335(7)	C(1')-C(2')	1.548(8)
C(9)-C(27)	1.512(6)	C(2')-C(7')	1.383(8)
C(9)-C(10)	1.515(7)	C(2')-C(3')	1.394(8)
C(10)-C(11)	1.563(7)	C(3')-C(4')	1.409(7)
C(11)-C(12)	1.561(7)	C(4')-C(5')	1.341(8)
C(12)-C(13)	1.549(6)	C(5')-C(6')	1.364(8)
C(13)-O(13)	1.457(6)	C(6')-C(7')	1.408(7)
C(13)-C(14)	1.570(8)	C(1")-C(6")	1.1991
C(14)-C(15)	1.539(6)	C(1")-C(2")	1.3760
C(15)-C(16)	1.527(7)	C(2")-C(3")	1.3362
C(15)-C(28)	1.544(6)	C(3")-C(4")	1.4746
C(16)-O(13)	1.467(6)	C(4")-C(5")	1.4052
		C(5")-C(6")	1.2860

Table A2.3 *Bond angles [°] for (56)*

	Bond angles [°]		Bond angles [°]
C(1)-O(4)-C(4)	106.3(5)	C(29)-C(17)-C(16)	113.1(5)
O(1)-C(1)-O(4)	119.1(7)	C(17)-C(18)-C(19)	125.6(6)
O(1)-C(1)-C(2)	129.5(8)	C(18)-C(19)-C(20)	108.1(4)
O(4)-C(1)-C(2)	111.4(6)	C(21)-C(20)-C(19)	112.1(4)
C(3)-C(2)-C(1)	108.0(7)	N-C(21)-C(20)	111.2(5)
C(3)-C(2)-C(25)	129.6(7)	N-C(21)-C(22)	108.2(5)
C(1)-C(2)-C(25)	122.4(7)	C(20)-C(21)-C(22)	116.6(5)
C(2)-C(3)-C(4)	109.0(6)	C(1')-N-C(21)	119.6(5)
O(4)-C(4)-C(3)	105.2(5)	C(1')-N-C(32)	124.8(5)
O(4)-C(4)-C(5)	109.6(5)	C(21)-N-C(32)	115.5(5)
C(3)-C(4)-C(5)	112.1(5)	N-C(32)-C(31)	110.8(4)
C(6)-C(5)-C(24)	123.3(6)	C(32)-C(31)-C(30)	110.8(4)
C(6)-C(5)-C(4)	123.7(6)	C(22)-C(30)-C(31)	113.0(5)
C(24)-C(5)-C(4)	112.8(6)	C(30)-C(22)-C(23)	111.7(5)
C(5)-C(6)-C(26)	122.1(6)	C(30)-C(22)-C(7)	112.3(5)
C(5)-C(6)-C(7)	123.4(6)	C(23)-C(22)-C(7)	107.6(5)
C(26)-C(6)-C(7)	114.3(5)	C(30)-C(22)-C(21)	109.5(5)
C(8)-C(7)-C(6)	107.3(5)	C(23)-C(22)-C(21)	104.1(5)
C(8)-C(7)-C(22)	115.2(5)	C(7)-C(22)-C(21)	111.4(5)
C(6)-C(7)-C(22)	113.1(5)	C(24)-C(23)-C(22)	113.1(5)
C(9)-C(8)-C(7)	127.3(6)	C(5)-C(24)-C(23)	110.0(5)
C(8)-C(9)-C(27)	124.9(6)	C(13)-O(13)-C(16)	108.2(4)
C(8)-C(9)-C(10)	119.7(6)	O(1')-C(1')-N	124.6(6)
C(27)-C(9)-C(10)	115.2(5)	O(1')-C(1')-C(2')	117.2(6)
O(10)-C(10)-C(9)	110.1(5)	N-C(1')-C(2')	118.1(6)

O(10)-C(10)-C(11)	106.1(5)	C(7')-C(2')-C(3')	118.0(6)
C(9)-C(10)-C(11)	113.7(5)	C(7')-C(2')-C(1')	121.5(7)
C(12)-C(11)-C(10)	113.3(5)	C(3')-C(2')-C(1')	120.5(7)
C(13)-C(12)-C(11)	111.5(6)	C(2')-C(3')-C(4')	119.2(7)
O(13)-C(13)-C(12)	110.4(5)	C(5')-C(4')-C(3')	121.2(7)
O(13)-C(13)-C(14)	106.4(4)	C(4')-C(5')-C(6')	121.5(7)
C(12)-C(13)-C(14)	110.9(6)	C(4')-C(5')-Br	119.8(6)
C(15)-C(14)-C(13)	104.3(5)	C(6')-C(5')-Br	118.7(6)
C(16)-C(15)-C(14)	102.5(5)	C(5')-C(6')-C(7')	118.1(8)
C(16)-C(15)-C(28)	108.9(5)	C(2')-C(7')-C(6')	122.0(8)
C(14)-C(15)-C(28)	111.1(5)	C(6")-C(1")-C(2")	125.6
O(13)-C(16)-C(15)	104.9(5)	C(3")-C(2")-C(1")	114.7
O(13)-C(16)-C(17)	109.2(5)	C(2")-C(3")-C(4")	124.8
C(15)-C(16)-C(17)	117.0(6)	C(5")-C(4")-C(3")	106.1
C(18)-C(17)-C(29)	125.3(7)	C(6")-C(5")-C(4")	128.1
C(18)-C(17)-C(16)	121.6(7)	C(1")-C(6")-C(5")	119.9

Symmetry transformations used to generate equivalent atoms

Table A2.4 *Anisotropic displacement parameters ($Å^2$ x 10^3) for (56). The anisotropic displacement factor exponent takes the form: $-2\pi^2 [h^2 a^{*2} U_{11} + ... + 2hka^*b^*U_{12}]$*

	U_{11}	U_{22}	U_{33}	U_{23}	U_{13}	U_{12}
Br	31(1)	59(1)	129(1)	15(1)	-5(1)	-6(1)
O(1)	47(3)	61(4)	65(4)	-8(3)	11(3)	-1(3)
O(4)	42(3)	37(3)	46(4)	-6(3)	5(4)	3(3)
O(10)	41(2)	41(3)	77(4)	-23(3)	24(3)	-17(3)
C(1)	46(5)	44(5)	41(6)	-12(5)	7(6)	-15(6)
C(2)	30(5)	62(6)	41(6)	7(5)	-9(5)	6(5)
C(3)	41(5)	56(5)	42(5)	4(5)	-18(5)	10(5)
C(4)	33(4)	41(4)	52(5)	-23(5)	5(4)	-9(4)
C(5)	21(4)	37(4)	42(6)	2(4)	-6(4)	-7(4)
C(6)	25(5)	34(4)	37(5)	4(4)	6(4)	-6(4)
C(7)	29(4)	25(4)	45(5)	-16(4)	4(4)	1(3)
C(8)	23(4)	23(4)	25(5)	2(3)	-6(4)	4(4)
C(9)	36(4)	21(4)	35(5)	7(4)	0(4)	3(4)
C(10)	29(4)	27(4)	61(6)	-4(4)	14(5)	-2(4)
C(11)	43(5)	28(4)	57(6)	1(4)	20(5)	0(4)
C(12)	52(6)	37(4)	47(5)	5(4)	5(5)	-1(5)
C(13)	49(5)	47(4)	59(6)	-9(4)	15(6)	0(5)
C(15)	36(5)	61(5)	34(5)	-1(4)	0(4)	-3(4)
C(16)	34(5)	40(4)	47(6)	-10(4)	-1(5)	0(5)
C(17)	31(4)	34(4)	40(5)	-20(4)	-5(5)	1(4)
C(18)	36(5)	44(4)	31(5)	-14(4)	-9(5)	-12(5)
C(19)	52(5)	34(4)	52(5)	-13(4)	14(5)	-2(4)
C(20)	23(4)	38(4)	46(5)	-17(4)	10(5)	-9(4)
C(21)	22(4)	26(4)	38(5)	-3(4)	-5(4)	1(3)
N	23(3)	25(3)	39(4)	7(3)	-7(3)	4(3)

C(32)	17(4)	40(4)	48(5)	0(4)	-5(4)	-6(4)
C(31)	26(4)	28(4)	57(5)	7(4)	-4(4)	11(4)
C(30)	29(4)	39(4)	27(5)	-8(4)	4(4)	-3(4)
C(22)	24(5)	24(4)	30(5)	7(3)	3(4)	5(3)
C(23)	14(4)	37(4)	53(5)	-2(4)	-3(4)	0(4)
C(24)	38(5)	52(5)	36(5)	-5(4)	7(4)	-1(4)
C(25)	63(6)	98(6)	52(6)	17(5)	6(5)	11(5)
C(26)	32(4)	62(5)	67(6)	-32(4)	-7(5)	-13(4)
C(27)	43(5)	38(4)	54(6)	-10(4)	9(5)	13(4)
C(28)	68(6)	90(6)	48(6)	-3(4)	-2(5)	8(5)
C(29)	57(5)	66(5)	47(5)	-14(4)	-10(5)	12(4)
O(13)	45(3)	33(2)	55(3)	-6(3)	3(3)	4(3)
O(1')	39(3)	42(3)	106(5)	32(4)	2(3)	-1(3)
C(1')	37(5)	26(5)	46(6)	0(4)	0(5)	2(4)
C(2')	28(4)	24(4)	35(6)	7(4)	-10(4)	7(4)
C(3')	54(5)	48(5)	53(6)	-6(5)	-7(5)	4(5)
C(4')	33(5)	45(5)	63(7)	-10(5)	-11(5)	-17(5)
C(5')	31(4)	30(5)	67(7)	22(5)	5(5)	-10(4)
C(6')	39(5)	86(7)	67(7)	-13(5)	-1(5)	-19(5)
C(7')	37(5)	84(6)	65(7)	-33(5)	-9(5)	-23(5)
C(1")	84(9)	71(7)	239(17)	37(9)	-49(10)	-11(7)
C(2")	190(12)	80(8)	65(7)	-38(7)	18(8)	13(8)
C(3")	77(8)	71(7)	232(14)	-21(7)	31(10)	34(6)
C(4")	100(10)	96(8)	340(2)	-75(11)	-112(12)	6(7)
C(5")	212(16)	116(10)	108(8)	-32(8)	-114(12)	62(10)
C(6")	171(15)	139(11)	196(17)	86(10)	37(10)	100(10)

Table A2.5 *Hydrogen coordinates (x 10^4) and isotropic displacement parameters ($Å^2$ x 10^3) for (**56**)*

	x	y	z	U(eq)
H(10)	13250	7255	6803	79
H(3)	11446	5835	9852	56
H(4)	11016	7105	9336	50
H(7)	10760	5203	7926	40
H(8)	10186	6553	7250	28
H(10A)	11420	6926	6539	47
H(11A)	12498	6432	5691	51
H(11B)	12674	5616	6003	51
H(12A)	10362	5471	6040	55
H(12B)	10210	6275	5706	55
H(13)	11256	5723	4892	62
H(14A)	8863	5167	5280	60
H(14B)	9242	5376	4637	60
H(15)	8912	3919	4939	52
H(16)	11277	3555	5080	48
H(18)	8598	3961	5788	44
H(19A)	9347	3415	6874	55
H(19B)	7921	3677	6700	55
H(20A)	10002	4740	6955	42
H(20B)	8637	5031	6728	42
H(21)	9020	4241	7786	35
H(32A)	5417	4886	7387	42
H(32B)	6505	5121	6939	42
H(31A)	6147	5810	8036	44
H(31B)	5983	6246	7442	44
H(30A)	8196	6209	7273	38
H(30B)	7998	6560	7894	38
H(23A)	7527	5056	8538	41
H(23B)	8984	4821	8663	41

H(24A)	7887	6335	8845	50
H(24B)	8415	5768	9329	50
H(25A)	9107	5536	10908	106
H(25B)	10052	6158	11189	106
H(25C)	10627	5419	10867	106
H(26A)	12244	6729	8765	81
H(26B)	12024	6953	8116	81
H(26C)	12592	6120	8278	81
H(27A)	12456	5069	7521	67
H(27B)	13530	5529	7172	67
H(27C)	12604	4929	6855	67
H(28A)	10223	3541	4160	103
H(28B)	10969	4352	4175	103
H(28C)	9502	4321	3977	103
H(29A)	11919	3056	6070	85
H(29B)	11309	3467	6614	85
H(29C)	12246	3944	6205	85
H(3')	5098	2990	7181	62
H(4')	2881	2793	7314	57
H(6')	2953	3982	8764	77
H(7')	5152	4238	8626	74
H(1")	8462	7308	5414	157
H(2")	6879	7006	6070	134
H(3")	5167	6302	5746	152
H(4")	4926	5960	4730	213
H(5")	6524	6621	4182	175
H(6")	8254	7142	4534	203

Appendix Three

Publication

Stewart, M.; Blunt, J.W.; Munro, M.H.G.;
Robinson, W.T.; Hannah, D.J.

Tetrahedron Letters, **1997**, *38(27)*, 4889-4890.

The Absolute Stereochemistry of the New Zealand Shellfish Toxin Gymnodimine

Michael Stewart[a], John W Blunt[a*], Murray H G Munro[a*], Ward T Robinson[a] & Donald J Hannah[b]

[a] Department of Chemistry, University of Canterbury, Private Bag 4800, Christchurch, New Zealand

[b] Institute of Environmental Science & Research Ltd, PO Box 30-547, Lower Hutt, New Zealand

Abstract: The absolute stereochemistry of the New Zealand shellfish toxin gymnodimine **1** has been determined by X-ray crystal structure analysis of the *p*-bromobenzamide derivative **3** of gymnodamine **2**.

Commercial oyster beds in Southland, New Zealand were closed in early 1994 due to high levels in the oysters of a biotoxin showing neurotoxic shellfish poisoning (NSP) features in a mouse bioassay.[1] The toxin, named gymnodimine **1**, was isolated and the structure elucidated by NMR spectroscopy.[2] Gymnodimine **1** is structurally related to the pinnatoxins[3] and the spirolides,[4] with the unusual spirocentre and imine functionalities. The pharmacological action of these compounds has not yet been fully defined, although the cyclic imine functionality has been suggested as the pharmacophore of the spirolides.[4] This suggestion has been supported by our observation of the inactivity of the reduced form of **1**, gymnodamine **2**, in the mouse bioassay.[5] A better understanding of the pharmacology of these compounds might be aided by a knowledge of their shape. The relative stereochemistries of only the distantly related pinnatoxins[3] have been reported, while the absolute stereochemistry has not been elucidated for of any of these compounds. We now report the crystal structure and absolute configuration of the *p*-bromobenzamide derivative **3** of gymnodamine **2**, from which the stereochemistry of gymnodimine **1** follows.

Gymnodimine **1** was reisolated from Foveaux Strait oysters,[6] but all attempts at forming crystalline derivatives of **1** at the C10 hydroxyl were impeded by low reactivity at this position. Furthermore, degradation was observed, possibly due to instability of the imine functionality. After reduction of the imine functionality of

gymnodimine **1** the resultant secondary amine gymnodamine **2** was found to be more stable and tractable towards the formation of derivatives. This reduction was achieved stereospecifically with $NaCNBH_3$/MeOH in quantitative yield.[7] Gymnodamine **2** was then converted to the *p*-bromobenzamide **3** by standard methods.[8]

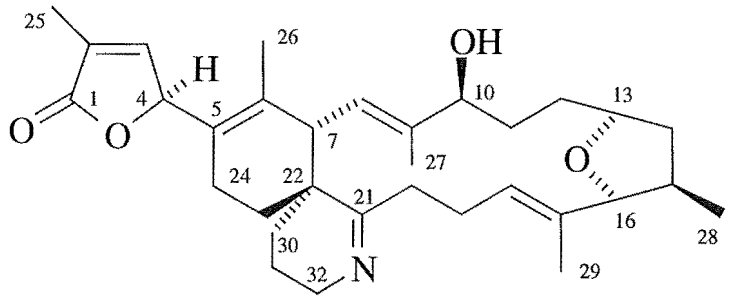

1

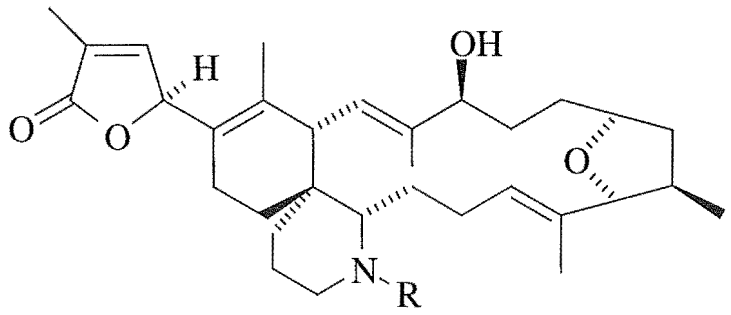

2 R = H
3 R = *p*-BrC_6H_4CO

Recrystallisation of the amide **3** from C_6H_6/CH_2Cl_2 gave irregular shaped, transparent crystals suitable for single crystal X-ray structure analysis. The data were collected using a Siemens P4 diffractometer. The structure of **3** was solved by direct methods (SHELXS-96) and refined by a full-matrix least-squares refinement (SHELXL-96) after being corrected for absorption by using the psi-scan method.[9] The absolute configuration was determined from the anomalous scattering of the bromine atom and stereocentres assigned as 4*S*, 7*S*, 10*S*, 13*R*, 15*R*, 16*R*, 21*S*, 22*R*, as shown in the perspective view (see figure). From this it follows that the absolute stereochemistry of gymnodimine **1** is 4*S*, 7*S*, 10*S*, 13*R*, 15*R*, 16*R*, 22*R*.

The ^1H NMR spectrum of the amide **3** showed doubling of various resonances (3:1 ratio), interpreted as arising from two amide conformations. Comparison of the solution conformation of amide **3** with that in the crystalline state showed good agreement, principally by the observation of NOE interactions (%)

H4/Me26 (2.1), H7/H21 (5.5), H7/Me27 (2.9), H8/H10 (10.1), H16/H15 (2.8), H16/Me28 (1.5), and H18/H15 (10.0), all of which are expected from the parameters derived from the crystal structure. Except for H7/H21, all of these interactions were also observed for imine **1**, together with interactions for H8/H30, H13/Me28 (0.9) and Me29/H16 (4.1). However, additional interactions for H18/H16 (0.7) and H18/Me27 (0.8) in the NOE spectra of the imine **1** suggest the presence in solution of additional conformations for **1**. This is supported by a large change in the chemical shift for H18 (5.00 for **1**, 5.45 for **2** and 5.38 ppm for **3**).

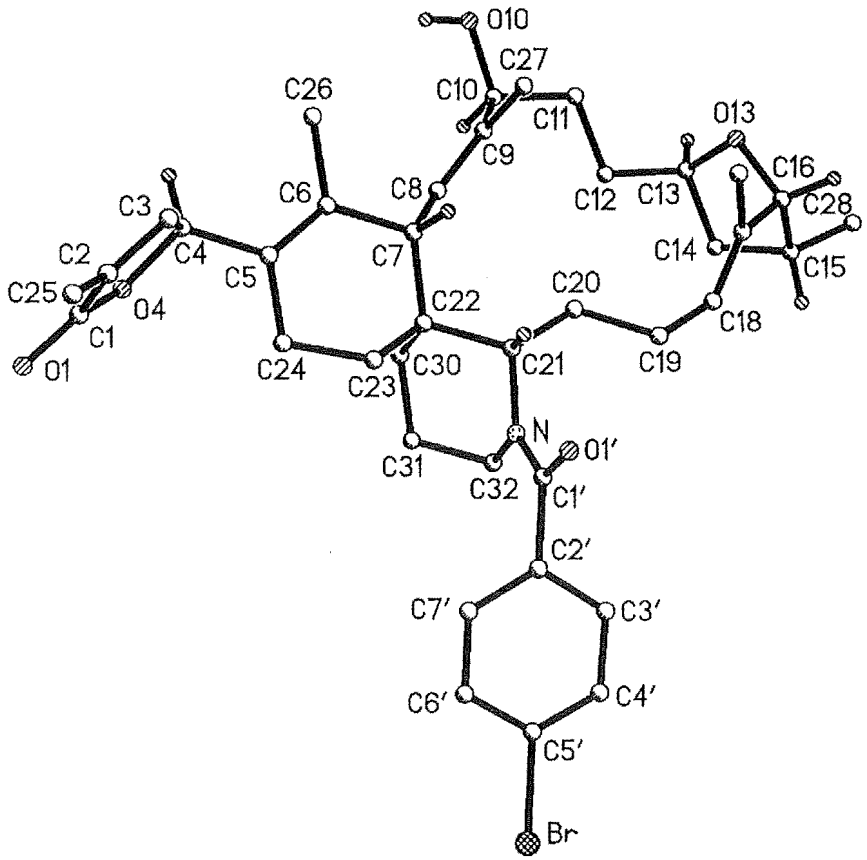

The reactivity of the amine group in **2** is now being utilised to form haptens for the development of an immunoassay for the more sensitive, quantitative and direct detection of gymnodimine **1** in shellfish.

Acknowledgments. We thank Mr B M Clark (UC) for mass spectra and Dr P Truman (ESR) for mouse bioassays.

REFERENCES AND NOTES

1. Mackenzie, L. *Seafood New Zealand* **1994**, *2*, 47-50.
2. Seki, T.; Satake, M.; Mackenzie, L.; Kaspar, H.F.; Yasumoto, T. *Tetrahedron Lett.* **1995**, *36*, 7093-7096.
3. Chou, T.; Haino, T.; Kuramoto, M.; Uemura, D. *Tetrahedron Lett.* **1996** *37*, 4027-4030, and references cited therein.
4. Hu, T.; Curtis, J.M.; Oshima, Y.; Quilliam, M.A.; Walter, J.A.; Watson-Wright, W.M.; Wright, J.L.C. *J. Chem. Soc. Chem. Commun.* **1995**, 2159-2161. Hu, T.; Curtis, J.M.; Walter, J.A.; Wright, J.L.C. *Tetrahedron Lett.* **1996**, *37*, 7671-7674.
5. Minimum Lethal Doses (MLD) (intraperitoneal): gymnodamine **2**, >4040 μg/kg; gymnodimine **1**, 700 μg/kg.
6. Oysters *Tiostrea chilensis* (5 kg), collected at Foveaux Strait, were extracted with 0.1% AcOH/80% MeOH/20% H_2O. After removal of MeOH the extract was neutralised with NH_3, adjusted to pH 8.5 with $NaHCO_3$ and partitioned against CH_2Cl_2. The organic layer was dried *in vacuo* and partitioned between ether and 0.5% aq. AcOH. The aqueous layer was neutralised with NH_3, adjusted to pH 8.5 with $NaHCO_3$ and partitioned against EtOAc. The organic layer was successively chromatographed on DIOL with 3:1 CH_2Cl_2:pet. ether and on AMINO with MeOH to afford gymnodimine **1** (8.4 mg).
7. Gymnodimine **1** (8 mg) was reacted with $NaCNBH_3$ (2 mg) in MeOH (1 mL) and AcOH (5 μL) for 4.5 hr. All solvents were removed *in vacuo* and reaction mixture filtered through a 0.45 μm filter in CH_2Cl_2 (5 x 1 mL) to give gymnodamine **2** (8 mg, 99%) as a colourless oil. HREIMS: $C_{32}H_{47}NO_4$ (M^+ *m/z* 509.3495 Δ -2.01 ppm). All spectral data were consistent with **2**.
8. Gymnodamine **2** (8 mg) was reacted with *p*-bromobenzoyl chloride (4.4 mg) and DMAP (244 μg) in dry CH_2Cl_2 (1 mL) and diisopropylethylamine (3.47 μL) at 0 °C for 30 min. H_2O (10 drops) was added and all solvents removed *in vacuo*. The reaction mixture was partitioned between CH_2Cl_2 and aq. citric acid (10 % w/v) and the organic phase purified on normal phase HPLC (DIOL) in CH_2Cl_2 to give the *p*-bromobenzamide **3** (4.0 mg, 37 %) which was recrystallised from C_6H_6/CH_2Cl_2 to give irregular shaped crystals; mp 251-254 °C; HRFABMS: $C_{39}H_{51}BrNO_5$ (MH^+ *m/z* 692.2971 Δ 2.90 ppm); δ_H ($CDCl_3$) (major conformation) 7.52, d, *J* = 8.8, 2H, H4' H6'; 7.19, d, *J* = 8.3, 2H, H3' H7'; 6.88, bs, 1H, H3; 5.72, bs, 1H, H4; 5.38, t, *J* = 6.3, 7.8, 1H, H18; 5.20, d, *J* = 10.7, 1H, H8; 4.50, dd, *J* = 3.4, 8.8, 2.9, 1H, H21; 4.15, m, 1H, H13; 3.94, obs, 1H, H10; 3.92, bs, 1H, H16; 3.46, dd, *J* = 5.4, 10.3, 1.4, 1H, H32a; 2.99, d, *J* = 11.2, 1H, H7; 2.95, obs, H32b; 2.48, m, 1H, H15; 2.15, m, H19; 2.00, obs, H11a; 1.94, s, 3H, Me25; 1.77, s, 3H, Me27; 1.67, s, 3H, Me29; 1.60, s, 3H, Me26; 1.08, d, *J* = 7.3, 3H, Me28.

9. *Crystal data*: $C_{39}H_{50}BrNO_5 \cdot C_6H_6$, *F.W.* = 770.82, orthorhombic, space group $P2_12_12_1$, a = 10.424(7), b = 17.236(12), c = 23.642(16) Å, $\alpha = 90$, $\beta = 90$, $\gamma = 90$, V = 4248(5) $Å^3$, Z = 4, D_c = 1.205 Mg/m^3, absorption coefficient 1.011 mm^{-1}, minimum and maximum transmission coefficients 0.506, 0.552. Final conventional R factors : [$I>2\sigma(I)$] R_1 = 0.0360, wR_2 = 0.0376. R_1 for inverse stucture = 0.0574.

Appendix Four

Models Created By Spartan

Model GM-1

Heat of Formation: -150.1 kcal/mol

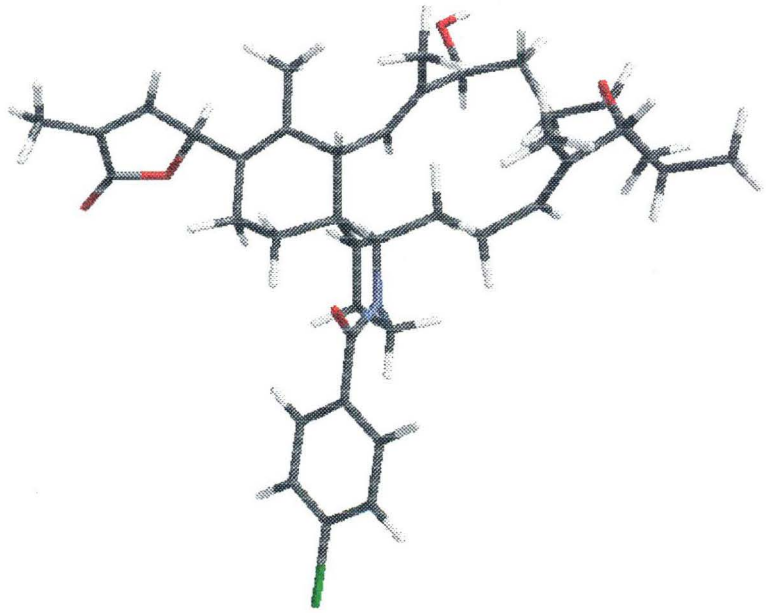

Model GM-2

Heat of Formation: -142.7 kcal/mol

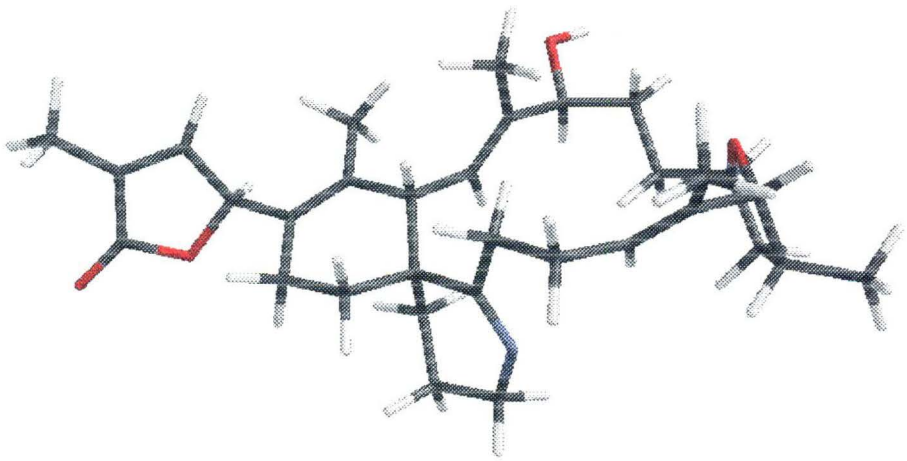

Model GM-3

Heat of Formation: -139.0 kcal/mol

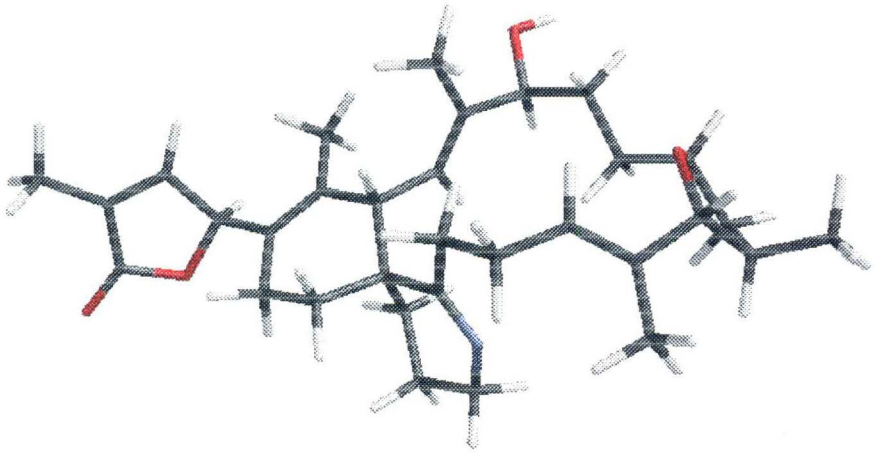

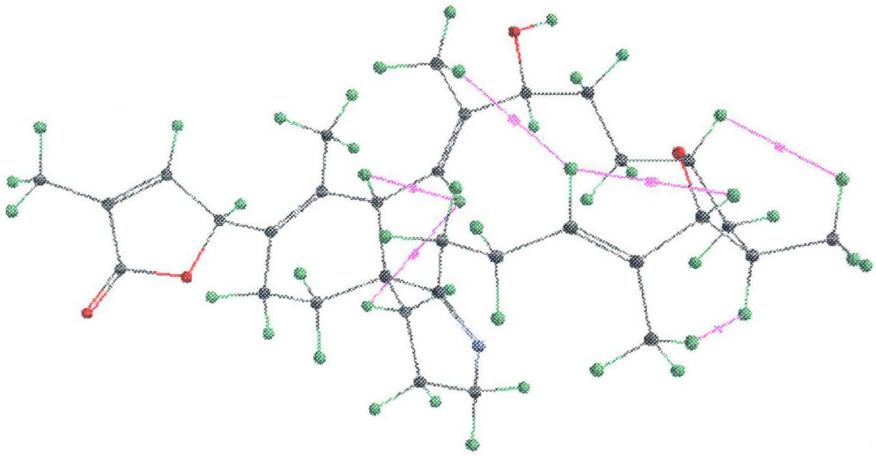

Model GM-3a

Heat of Formation: -143.7 kcal/mol

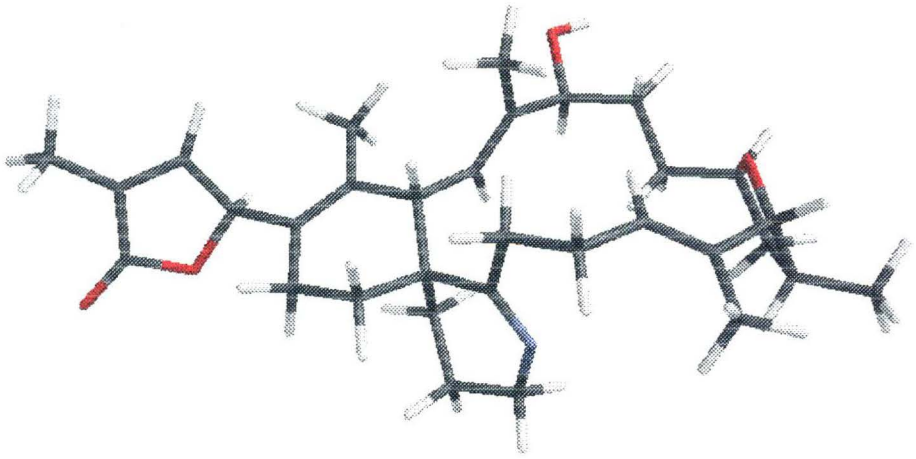

Model GM-4

Strain energy = 45.6579 kcal/mol

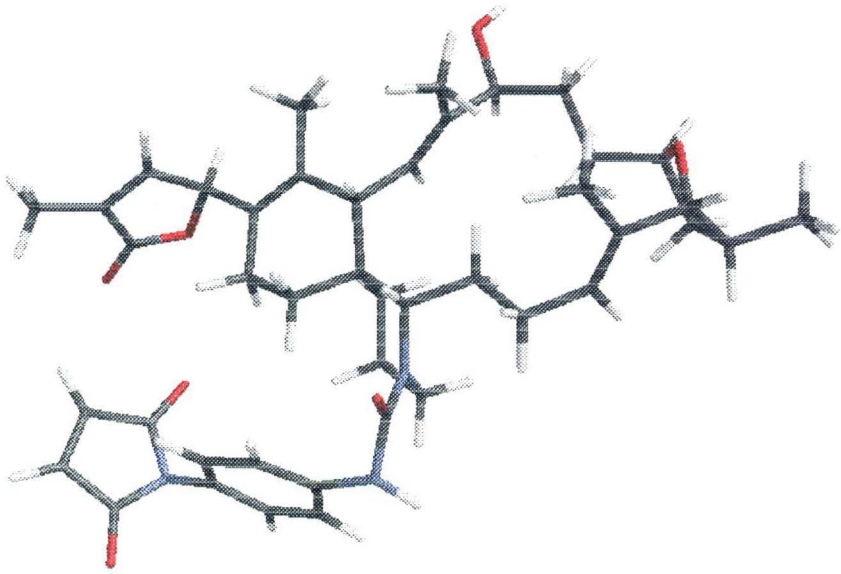

Model GM-5

Heat of Formation: -254.1 kcal/mol

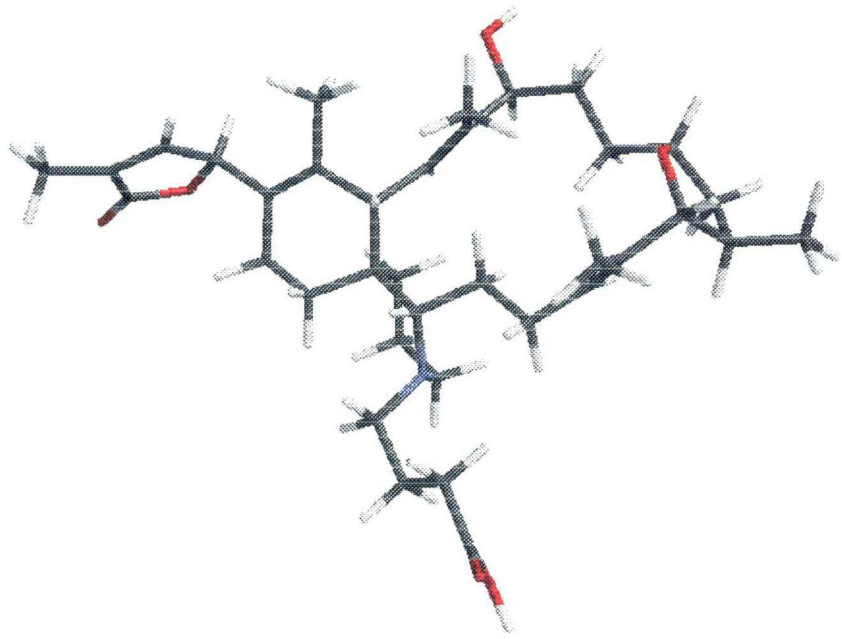

Model GM-6

Heat of Formation: -287.1 kcal/mol